Numerical simulation of finite micromorphic elasticity using FETI-DP domain decomposition methods

Stefanie Vanis

geboren in Gelsenkirchen

Fakultät für Mathematik
Universität Duisburg-Essen
Campus Essen

19. April 2010

Dissertation im Fach Mathematik
zum Erwerb des Dr. rer. nat.
an der Fakultät für Mathematik
der Universität Duisburg-Essen

Erstgutachter:	Prof. Dr. Axel Klawonn Fakultät für Mathematik, Universität Duisburg-Essen
Zweitgutachter:	Prof. Dr. Patrizio Neff Fakultät für Mathematik, Universität Duisburg-Essen

Tag der mündlichen Prüfung: 18.03.2010

Contents

Acknowledgments

I would like to thank my advisor Prof. Axel Klawonn who supervised this work for the encouragement to write this thesis and the time and work he devoted to me and this work. I would also like to thank Prof. Patrizio Neff who also dedicated time and work to me and this thesis. I am thankful to both also for reviewing this work. Furthermore I am happy to express my thanks to Dr. Oliver Rheinbach for many profitable discussions. I would like to thank Prof. Witsch who encouraged me since the beginning of my studies. I am also thankful to my other colleagues from the University of Duisburg-Essen, especially to Andreas Fischle who is one of the colleagues I shared my office with during the last years. I would like to give a special thanks to my whole working group for the good working atmosphere.

Especially I am grateful to my husband Jan for his patience and his encouragement. I would also like to thank my parents who encouraged me very much. Without the help of my family I would not have been able to do this.

Last but not least I would like to thank my mathematics teacher Mr. Zawatzki who already encouraged me to study mathematics during my time at the Schalker Gymnasium and my elementary school teacher Mrs. Sievering who taught me to work independently.

Notation

Here, we will given an overview of the notation used.

$\boldsymbol{\varphi}$	deformation, see, e.g., p. 10, 12
$\mathbf{u}$	displacement, i.e., $\boldsymbol{\varphi}(\mathbf{x}) := \mathbf{x} + \mathbf{u}(\mathbf{x})$, see, e.g., p. 12
F_∇	deformation gradient, i.e., $F_\nabla := \nabla\boldsymbol{\varphi}$, see, e.g., p. 12 Here, we use F_∇ instead of F for the deformation gradient since we denote by F the system matrix of the FETI-DP method.
P	tensorial field, see, e.g., p. 10, 12
λ_e, μ_e	Lamé parameters of standard linear elasticity, see, e.g., p. 12
$\mu_e^{(i)}$	value of μ_e in the subdomain Ω_i, see, e.g., p. 63
h^+	dimensionless hardening like modulus, see, e.g., p. 12
E	Young's modulus, see, e.g., p. 12
ν	Poisson's ratio, see, e.g., p. 12
L_c	positive internal length scale with dimension of a length, see, e.g., p. 12
$\mathrm{GL}^+(3)$	group of all invertible three times three matrices with positive determinant, see, e.g., p. 11
$\mathrm{SO}(3)$	group of all rotations in three dimensions, see, e.g., p. 13
$\mathfrak{so}(3)$	set of three times three skew-symmetric matrices, i.e., $X \in \mathfrak{so}(3) \Leftrightarrow X^T = -X$, see, e.g., p. 23
Id	identity tensor, see, e.g., p. 12
$\mathrm{sym}(X)$	symmetric part of a matrix X, i.e., $\mathrm{sym}(X) := \frac{1}{2}\left(X + X^T\right)$, see, e.g., p. 12
$\mathrm{skew}(X)$	skew-symmetric part of a matrix X, i.e., $\mathrm{skew}(X) := \frac{1}{2}\left(X - X^T\right)$, see, e.g., p. 12
tr(X)	trace of the matrix X, i.e., $\mathrm{tr}(X) := \sum_{i=1}^{n} X_{ii}$, see, e.g., p. 12
$\mathrm{Cof}(X)$	cofactor of an invertible matrix X, i.e., $\mathrm{Cof}(X) := \det(X)X^{-T}$, see, e.g., p. 80

∇X	gradient of a $n \times m$ matrix X, i.e., $\nabla X := \begin{pmatrix} \partial_1 X_{11} & \dots & \partial_n X_{11} \\ & \vdots & \\ \partial_1 X_{1m} & \dots & \partial_n X_{1m} \\ \partial_1 X_{21} & \dots & \partial_n X_{21} \\ & \vdots & \\ \partial_1 X_{nm} & \dots & \partial_n X_{nm} \end{pmatrix}$, see, e.g., p. 12
$\varepsilon(\mathbf{u})$	standard linear elasticity infinitesimal strain tensor, i.e., $\varepsilon(\mathbf{u}) := \mathrm{sym}(\nabla\mathbf{u}) := \mathrm{sym}(F_\nabla - \mathrm{Id})$; see, e.g., p. 20
$\varepsilon_P(\mathbf{u})$	tensor in P-elasticity analogously defined to $\varepsilon(\mathbf{u})$, i.e., $\varepsilon_P(\boldsymbol{\varphi}) := \mathrm{sym}(P^{-1}F_\nabla)$; see, e.g., p. 21
$(X,Y)_F$	Frobenius inner product of two $n \times m$ matrices , i.e., $(X,Y)_F := \mathrm{tr}(X^TY) = \sum_{i=1}^{n}\sum_{j=1}^{m} X_{ij}Y_{ij}$, see, e.g., p. 12
$\Vert X\Vert_F^2$	Frobenius norm, i.e., $\Vert X\Vert_F^2 := (X,X)_F$, see, e.g., p. 12
$(X,Y)_{L_2(\Omega)}$	L_2-inner product, i.e., $(X,Y)_{L_2(\Omega)} := \int_\Omega (X,Y)_F \, d\mathbf{x}$, see, e.g., p. 21
$\Vert X\Vert_{L_2(\Omega)}^2$	L_2-norm, i.e., $\Vert X\Vert_{L_2(\Omega)}^2 := (X,X)_{L_2(\Omega)}$, see, e.g., p. 21
$\Vert X\Vert_{l_2}^2$	Euclidean norm of a vector, i.e., $\Vert X\Vert_{l_2}^2 := \sum_{i=1}^{N} X_i^2$, see, e.g., p. 19
$\vert X\vert_{H^1(\Omega)}^2$	H^1-seminorm, i.e., $\vert X\vert_{H^1(\Omega)}^2 := \int_\Omega \Vert\nabla X\Vert_F^2 \, d\mathbf{x}$, see, e.g., p. 13
$\Vert X\Vert_{H^1(\Omega)}^2$	H^1-norm, i.e., $\Vert X\Vert_{H^1(\Omega)} := \Vert X\Vert_{L_2(\Omega)}^2 + \vert X\vert_{H^1(\Omega)}^2$, see, e.g., p. 13
$\vert u\vert_{H^{1/2}(\partial\Omega)}$	$H^{1/2}$-seminorm, i.e., $\vert u\vert_{H^{1/2}(\partial\Omega)} := \inf_{\substack{v\in H^1(\Omega)\\ v\vert_{\partial\Omega}=u}} \vert v\vert_{H^1(\Omega)}$, see, e.g., p. 82
$\vert\mathbf{u}\vert_{H^{1/2}(\partial\Omega)}^2$	$H^{1/2}$-seminorm for three-dimensional functions, i.e., $\vert\mathbf{u}\vert_{H^{1/2}(\partial\Omega)}^2 := \sum_{i=1}^{3} \vert u_i\vert_{H^{1/2}(\partial\Omega)}^2$, see, e.g., p. 82
$\lambda_{\max}(X)$	maximum eigenvalue of a matrix X, see, e.g., p. 86
$\lambda_{\min}(X)$	minimum eigenvalue of a matrix X, see, e.g., p. 74
$\lambda_{\min,\Omega}(X)$	infimum of minimum eigenvalue of a matrix X over Ω, i.e., $\inf_{x\in\bar\Omega} \lambda_{\min}(X)$, see, e.g., p. 74
$\partial\Omega$	boundary of the domain Ω, see, e.g., p. 13
$\partial\Omega_D$	Dirichlet boundary of the domain Ω, see, e.g., p. 13
$\partial\Omega_N$	Neumann boundary of the domain Ω, see, e.g., p. 13
$L_2(\Omega)$	space of square-summable functions on Ω, i.e., $\{u : \Omega \to \mathbb{R} \vert \int_\Omega \vert u\vert^2 dx < \infty\}$

$H^1(\Omega)$	space of functions on Ω which are square-integrable and have first weak derivatives which are square-summable, i.e., $\{u \in L_2(\Omega) \| D^\alpha u \in L_2(\Omega), 0 \leq \|\alpha\| \leq 1\}$ with a multi index α and D^α denoting the weak derivative, see, e.g., p. 13
$\mathbf{H^1}(\Omega)$	space of three-dimensional H^1-functions on Ω, i.e., $\mathbf{H^1}(\Omega) := (H^1(\Omega))^3$, see, e.g., p. 13
$\mathbf{H^1_0}(\Omega, \partial\Omega_D)$	space of three-dimensional H^1-functions with homogeneous Dirichlet boundary conditions, i.e., $\mathbf{H^1_0}(\Omega, \partial\Omega_D) := \{\mathbf{v} \in \mathbf{H^1}(\Omega) : \mathbf{v} = \mathbf{0} \text{ on } \partial\Omega_D\}$, see, e.g., p. 13
$\mathbf{H^1_0}(\Omega, \Gamma)$	space of three-dimensional H^1-functions with homogeneous boundary conditions on Γ, i.e., $\mathbf{H^1_0}(\Omega, \Gamma) := \{\mathbf{v} \in \mathbf{H^1}(\Omega) : \mathbf{v}\|_\Gamma = \mathbf{0}\}$, see, e.g., p. 72
$H^{1/2}(\partial\Omega)$	$\{u \in L_2(\partial\Omega) \| \\|u\\|_{H^{1/2}(\partial\Omega)} < \infty\}$ with $\\|u\\|^2_{H^{1/2}(\partial\Omega)} := \\|u\\|^2_{L_2(\partial\Omega)} + \|u\|^2_{H^{1/2}(\partial\Omega)}$, see, e.g., p. 82
$\mathbf{H}^{1/2}(\partial\Omega)$	space of three-dimensional functionals in $H^{1/2}(\partial\Omega)$, i.e., $\mathbf{H}^{1/2}(\partial\Omega) := (H^{1/2}(\partial\Omega))^3$, see, e.g., p. 82
$C^0(\bar{\Omega}, \mathbb{R}^{3\times 3})$	space of continuous functions from $\bar{\Omega}$ to $\mathbb{R}^{3\times 3}$, see, e.g., p. 72
$L^\infty(\bar{\Omega}, \mathbb{R}^{3\times 3})$	space of bounded functions from $\bar{\Omega}$ to $\mathbb{R}^{3\times 3}$, see, e.g., p. 72
$C_0^\infty(\bar{\Omega})$	space of arbitrary often differentiable funtions with closed support from $\bar{\Omega}$ to $\bar{\Omega}$, see, e.g., p. 72
$\mathrm{curl}(\mathbf{v})$	curl-operator for a three-dimensional function, i.e., $\mathrm{curl}(\mathbf{v}) := \begin{bmatrix} \partial_2 v_3 - \partial_3 v_2 \\ \partial_3 v_1 - \partial_1 v_3 \\ \partial_1 v_2 - \partial_2 v_1 \end{bmatrix}$, see, e.g., p. 23
$\mathrm{Curl}(\mathbf{v})$	curl-operator for a three times three matrix $X = \begin{bmatrix} x_1 \\ x_2 \\ x_3 \end{bmatrix}$, i.e., $\mathrm{Curl}(X) := \begin{bmatrix} (\mathrm{curl}(x_1^T))^T \\ (\mathrm{curl}(x_2^T))^T \\ (\mathrm{curl}(x_3^T))^T \end{bmatrix}$, see, e.g., p. 23
$\mathbf{W}^h$	space of finite element functions on a triangulation τ_h, i.e., $\mathbf{W}^h := \mathbf{W}^h(\Omega) \subset \mathbf{H^1_0}(\Omega, \partial\Omega_D)$, see, e.g., p. 58
$\mathbf{W}^h(\Omega_i)$	finite element space of continuous, piecewise quadratic functions on the triangulated Ω_i, see, e.g., p. 84
$\mathbf{W}^{(i)}$	trace space $\mathbf{W}^{(i)} := \mathbf{W}^h(\partial\Omega_i \cup \Gamma)$, see, e.g., p. 84
$\mathbf{W}$	product space associated with the trace spaces $\mathbf{W}^{(i)}$, i.e., $\mathbf{W} := \prod_{i=1}^N \mathbf{W}^{(i)}$, see, e.g., p. 84
$\widehat{\mathbf{W}}$	subspace of $\mathbf{W}$ with the finite element approximation of the elliptic problem which is continuous across Γ, see, e.g., p. 85
$\widetilde{\mathbf{W}}$	subspace of partially assembeld finite element functions with an assembly in the primal variables of FETI-DP, i.e., $\widetilde{\mathbf{W}} := \left\{\mathbf{u} : \exists \mathbf{u}^{(i)} \in \mathbf{W}^{(i)}, i = 1, \ldots, N, \text{ such that } \mathbf{u} = \sum_{i=1}^N R^{(i)T}\mathbf{u}^{(i)}\right\}$ see, e.g., p. 85

$\mathcal{N}_x$	set of indices of all subdomains with x in the closure of the subdomain, i.e., $\mathcal{N}_x := \{j \in \{1, \ldots, N\} : x \in \partial\Omega_{j,h}\}$, see, e.g., p. 59
$\mathcal{N}_i$	set of indices of all neighboring subdomains of Ω_i including i, i.e., $\mathcal{N}_i := \{l \in \{1, \ldots, N\}, \partial\Omega_{i,h} \cap \partial\Omega_{l,h} \neq \emptyset\}$, see, e.g., p. 90
$\mathbf{ker}\,(f)$	nullspace of the function f, see, e.g., p. 23
$\lvert\Omega\rvert$	volume of the domain Ω, i.e., $\lvert\Omega\rvert := \int_\Omega 1 d\mathbf{x}$, see, e.g., p. 28
$c_{\nabla P}$	maximum value of the gradient of the tensorial field P, i.e., $c_{\nabla P} := \max\limits_{\mathbf{x}\in\Omega} \max\limits_{i,j,k=1\ldots3} (\partial_k P_{ij})^2$, see, e.g., p. 29
c_P	maximum value of the tensorial field P^{-T}, i.e., $c_P := \max\limits_{\mathbf{x}\in\Omega} \max\limits_{i,j=1\ldots3} (P^{-T})^2_{ij}$, see, e.g., p. 71
Γ	interface obtained by the domain decomposition, i.e., the intersection of the closures of the subdomains $\Gamma := \bigcap\limits_{i=1}^{N} \bar{\Omega}_i$, see, e.g., p. 58
Γ_h	set of nodes on Γ, see, e.g., p. 59
$\partial\Omega_h$	set of nodes on $\partial\Omega$, see, e.g., p. 59
Ω_i	i-th subdomain, see, e.g., p. 58
$\partial\Omega_i$	boundary of the i-th subdomain, see, e.g., p. 59
$\partial\Omega_{i,h}$	set of nodes on $\partial\Omega_i$, see, e.g., p. 59
$\mathcal{F}^{ij}$	face between the subdomains Ω_i and Ω_j, see, e.g., p. 69
$\mathcal{F}^{ij}_h$	set of nodes on $\mathcal{F}^{ij}$ depending on the triangulation τ_h, see, e.g., p. 90
$\theta_{\mathcal{F}^{ij}}$	partition of unity function which is 1 in the nodes on $\mathcal{F}^{ij}_{h/2}$ and 0 everywhere else, see, e.g., p. 90
$\mathcal{E}^{ik}$	edge between the subdomains Ω_i and Ω_k, see, e.g., p. 64
$\mathcal{E}^{ik}_h$	set of nodes on $\mathcal{E}^{ik}$ depending on the triangulation τ_h
$\theta_{\mathcal{E}^{ij}}$	partition of unity function which is 1 in the nodes on $\mathcal{E}^{ik}_{h/2}$ and 0 everywhere else, see, e.g., p. 90
$\mathcal{V}^{jl}$	vertex between the subdomains Ω_j and Ω_l, see, e.g., p. 90
$\theta_{\mathcal{V}^{jl}}$	partition of unity function which is 1 in $\mathcal{V}^{jl}$ and 0 everywhere else, see, e.g., p. 90
τ_h	triangulation with quadratic tetrahedral finite elements, see, e.g., p. 58
$\tau_{h/2}$	triangulation with linear tetrahedral finite elements obtained by naturally splitting the quadratic elements in eight linear elements each, see, e.g., p. 90
M^{-1}	the Dirichlet preconditioner, see, e.g., p. 62
F	FETI-DP system matrix, see, e.g., p. 61
B_*	different jump operators depending on the index, see, e.g., p. 61
R_*	different assembly operators depending on the index, see, e.g., p. 61
$\delta_j^\dagger$	scaling factor for the jump operator, i.e., $\delta_j^\dagger(x) := \frac{(\mu_e^{(j)})^\gamma}{\sum_{k\in\mathcal{N}_x}(\mu_e^{(k)})^\gamma}$, see, e.g., p. 63

Chapter 1

Introduction

Modern life is in many ways influenced by the achievements in physics and engineering. The developments in these sciences are often based on experiments and in recent years more and more on numerical simulations. These simulations are carried out to avoid high costs which arise from experiments, i.e., from the construction of explicit prototypes and from the testing process itself. The latter is often destructive, see, e.g., crash tests in the automotive industry. Such simulations often have to deal with the deformation of bodies under applied forces, a common problem in physics and engineering. The behavior of the bodies under such forces can be modeled with different elasticity formulations. In order to obtain models for the simulations which can be solved with well-known techniques often a linearized elasticity formulation is used. Such formulations are only suitable for infinitesimal deformations. Hence, it is obvious that the standard linear elasticity model has a limited range of application, i.e., it is only correct if the deformation is small. Depending on the application, this might not apply.

A first improvement may be obtained by using nonlinear elasticity models, e.g., the Neo-Hookean or Saint-Venant-Kirchhoff models, which yield a description with a broader range of applications. But standard linear elasticity as well as nonlinear elasticity formulations work with a representation of the body as a cluster of points only and model the displacement of each point, cf. left figure in Figure 1.1. This is a mathematical idealization, the points represent an infinitesimally small volume.

1.1 A micromorphic model

In a realistic physical situation this is not the case. It is not possible to consider the interaction in a given material at any small length scale, e.g., in an atomistic description the mathematical/continuum mechanical representation ceases to be valid beyond the scale of a cluster of atoms, i.e., the material points of the continuum represent always a cluster of atoms, where the classical contin-

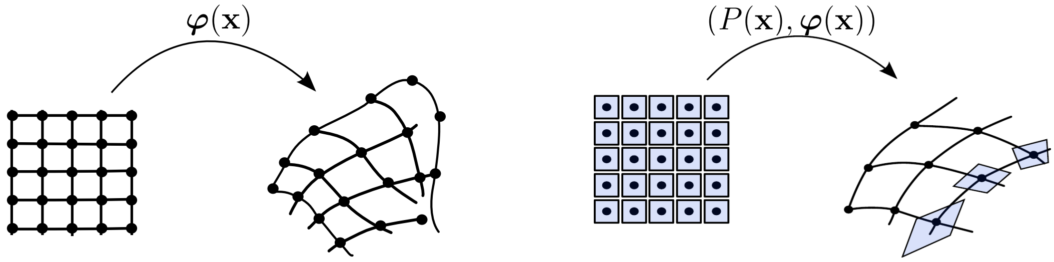

Figure 1.1: *Difference in the description of standard elasticity formulations, i.e., modeling only the deformation φ, (left, deformation of nodal points only) and the micromorphic model with the additional parameter P (right) which includes also an affine mapping of the surrounding structure of the nodes. Moreover, the blue cells interact with each other.*

uum mechanical laws are assumed to be valid. However, the interaction of such clusters with each other cannot be fully described by classical elasticity since the clusters have a finite diameter (length scale) and are not infinitesimally small. In the extended continuum model (micromorphic) one considers directly the finite size of the clusters and their mutual interaction; cf. Figure 1.1 on the right hand side. Here, each grid point represents the center of a cluster. Now the interaction is twofold, the cluster points interact with each other according to (more or less) elasticity (length change/distance change) and the interaction of the neighboring clusters is taken into account by an additional field P. Moreover, the two mechanisms are coupled to each other.

Another problem of all of these descriptions is that they can usually not be solved analytically. Hence, discrete problems are used instead, computing a solution of the problem on a mesh representing the body. Thus, the solution obtained is only an approximation of the solution of the real problem. Here, we have to face two additional problems.

On the one hand, it is well-known that numerical discretizations often have problems with special geometries such as cusps. Models may contain cusps as a result of the geometry or they may occur when cracks are modeled. As a result of singularities of the exact solution, the numerical approximation then exhibits a large local error. Generally, as a remedy, a finer mesh is used around the cusp than in the other areas of the body. Micromorphic elasticity descriptions can be used to obtain a regularization at such crucial points. Thus, the mesh does not need to be refined while the error does not increase as before. For a micromorphic description of cracks, see Mariano [63, 64, 67].

On the other hand, the discretization of the body itself is another challenge which often leads to difficulties. Unfortunately, the reliability and stability of the discrete methods depend on the discretization, i.e., the quality of the mesh. Thus, if the mesh that we use to discretize the body includes very small angles, even in a small area, the convergence rate of the finite element method may deteriorate

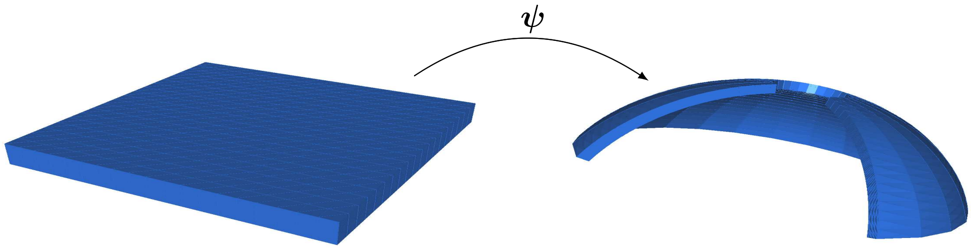

$$\boldsymbol{\psi}(\mathbf{x}) = \begin{pmatrix} ((1-h)+xh)\cos(1.5\pi y)\cos(\alpha+10z)(\beta-\alpha) \\ ((1-h)+xh)\sin(1.5\pi y)\cos(\alpha+10z)(\beta-\alpha) \\ ((1-h)+xh)\sin(\alpha+10z)(\beta-\alpha) \end{pmatrix},$$

Figure 1.2: *Micromorphic description (special gradient case): Predeformation induced by a function $\boldsymbol{\psi}$ and a resulting $P = \nabla\boldsymbol{\psi}$. The parameters α and β represent the angles of the dome and h its thickness. In this way it is possible to model further elastic deformations of the dome with a system of equations given on the flat reference configuration since the geometric information of the dome is encoded in $P = \nabla\boldsymbol{\psi}$.*

or we may obtain difficulties to find a good approximation. Often in physics and engineering the bodies which are deformed have complicated geometries with small bridges, e.g., foams or other porous materials. Such details in the body often lead to finite elements with small angles and a bad aspect ratio. Hence, it would be preferable to model the shape of the body by an additional parameter, i.e., by a predeformation, instead of explicitly discretizing the structure in detail; see Figure 1.2. Furthermore, such predeformations may be used to obtain stress-free descriptions of certain geometries.

These considerations give rise to the idea of considering a micromorphic model for the description of the elastic behavior of a body. Let us therefore assume a body denoted by $\Omega \subset \mathbb{R}^3$ which is Lipschitz, connected, and of diameter 1. We now introduce an additional micromorphic field P. We assume P to be a tensorial field with $P : \Omega \subset \mathbb{R}^3 \to \mathrm{GL}^+(3)$, where $\mathrm{GL}^+(3)$ is the group of all invertible three times three matrices with positive determinant. The matrix $P = P(\mathbf{x}) \in \mathbb{R}^{3\times3}, \mathbf{x} \in \Omega$, is usually not a gradient, i.e., there does not necessarily exist a function $\boldsymbol{\psi}$ such that $P = \nabla\boldsymbol{\psi}$. A case in which a gradient structure for P might be obtained is given when P defines a predeformation as described in Figure 1.2.

We consider an elasticity model with two variables, i.e., the deformation $\boldsymbol{\varphi}$ as in the standard formulations of elasticity and the micromorphic field P. This leads to an alternative minimization problem which occurs in geometrically exact continua models of micromorphic type and is of the form

$$\begin{aligned}\min_{(P,\boldsymbol{\varphi})} E(P,\boldsymbol{\varphi}) := \min_{(P,\boldsymbol{\varphi})} \int_\Omega & \mu_e \|\mathrm{sym}(P^{-1}F_\nabla - \mathrm{Id}\,)\|_F^2 + \mu_c \|\mathrm{skew}(P^{-1}F_\nabla - \mathrm{Id}\,)\|_F^2 \\ & + \frac{\lambda_e}{2}\left(\mathrm{tr}(P^{-1}F_\nabla - \mathrm{Id}\,)\right)^2 \\ & + \mu_e h^+ \|P^T P - \mathrm{Id}\,\|_F^2 + \mu_e\left(\frac{L_c^2}{2}\|\nabla P\|_F^2 + \frac{L_c^q}{q}\|\nabla P\|_F^q\right)\, d\mathbf{x} \\ - \int_\Omega & (f_{\boldsymbol{\varphi}}, \boldsymbol{\varphi})_F + (f_P, P)_F \; d\mathbf{x};\end{aligned}$$

corresponding models can be found in [15, 25, 65, 68]. The special case for $\mu_c = 0$ has been introduced by Neff [72, 73, 76] and is of the form (1.1) below. This and the previous problem admit minimizers which was first shown by Neff in [73], later generalizations have been given by Mariano [66]. The first existence theorem for minimizers in geometrically exact micromorphic elasticity for the case $\mu_c = 0$ has been given by Neff [73]. It is the case $\mu_c = 0$, which we will consider exclusively in this work, i.e., the minimization problem is given in the following form

$$\begin{aligned}\min_{(P,\boldsymbol{\varphi})} E(P,\boldsymbol{\varphi}) := \min_{(P,\boldsymbol{\varphi})} \int_\Omega & \mu_e \|\mathrm{sym}(P^{-1}F_\nabla - \mathrm{Id}\,)\|_F^2 + \frac{\lambda_e}{2}\left(\mathrm{tr}(P^{-1}F_\nabla - \mathrm{Id}\,)\right)^2 \\ & + \mu_e h^+ \|P^T P - \mathrm{Id}\,\|_F^2 + \mu_e\left(\frac{L_c^2}{2}\|\nabla P\|_F^2 + \frac{L_c^q}{q}\|\nabla P\|_F^q\right)\, d\mathbf{x} \qquad (1.1) \\ - \int_\Omega & (f_{\boldsymbol{\varphi}}, \boldsymbol{\varphi})_F + (f_P, P)_F \; d\mathbf{x},\end{aligned}$$

where $\boldsymbol{\varphi} : \Omega \subset \mathbb{R}^3 \to \mathbb{R}^3$ is the deformation and $F_\nabla = \nabla\boldsymbol{\varphi} \in \mathbb{R}^{3\times 3}$ is the deformation gradient. Note that the deformation $\boldsymbol{\varphi}$ is directly related to the displacement $\mathbf{u}(\mathbf{x}) \in \mathbb{R}^3$ since $\boldsymbol{\varphi}(\mathbf{x}) = \mathbf{x} + \mathbf{u}(\mathbf{x})$. With λ_e and μ_e we denote the Lamé parameters of standard linear elasticity if $P = \mathrm{Id}$. They are related to Young's modulus E and Poisson's ratio ν by

$$\mu_e = \frac{E}{2(1+\nu)} \quad \text{and} \quad \lambda_e = \frac{E\nu}{(1+\nu)(1-2\nu)}.$$

With h^+ we denote a kinematic dimensionless hardening like modulus. If we consider (formally) the limit of this kinematic hardening to infinity, i.e., $h^+ \to \infty$, we obtain the constraint $P^T P = \mathrm{Id}$, i.e., a true Cosserat model; see [69, 70]. Furthermore, we introduce an internal length scale $L_c > 0$ which has the dimension of a length. The term including the gradients of P is denoted as the curvature energy and describes the self-interaction of the affine microstructure. By $f_{\boldsymbol{\varphi}}$ and f_P we denote body forces for $\boldsymbol{\varphi}$ and P, respectively, which we assume to be independent of $\boldsymbol{\varphi}$ and P, i.e., we only treat conservative loads, e.g., $f_{\boldsymbol{\varphi}}$ may be gravity.

Furthermore, we have to define boundary conditions for our problem. Therefore, we define a part of the body as Dirichlet boundary denoted by $\partial\Omega_D$ which we provide with homogeneous Dirichlet boundary conditions. The remaining boundary, denoted by $\partial\Omega_N := \partial\Omega \setminus \partial\Omega_D$, is the Neumann boundary and assumed to be subject to a surface force g, i.e., we provide $\partial\Omega_N$ with natural boundary conditions. Here, we assume homogeneous Neumann boundary conditions, i.e, $g = 0$. Note that we may choose different Dirichlet and Neumann boundaries for the two variables, i.e., $\boldsymbol{\varphi}$ and P. In this work we will denote the Dirichlet and Neumann boundary for the displacement by $\partial\Omega_D$ and $\partial\Omega_N$, respectively, and the boundaries for the incremental change of P by $\partial\Omega_{D,P}$ and $\partial\Omega_{N,P}$.

Hence the appropriate space for our variational formulation for the displacement is $\mathbf{H_0^1}(\Omega, \partial\Omega_D) := \{\mathbf{v} \in \mathbf{H^1}(\Omega) : \mathbf{v} = \mathbf{0} \text{ on } \partial\Omega_D\}$. For the incremental change in the micromorphic field, i.e., ΔP, we use the Sobolev space $(H^1(\Omega))^{3\times 3} = (H^1(\Omega))^9$. If we prescribe Dirichlet boundary conditions for P on $\partial\Omega_{D,P}$, i.e., $P|_{\partial\Omega_{D,P}} = P_0 \in \mathrm{GL}^+(3)$, the appropriate space for the incremental change in P, i.e., ΔP contains homogeneous Dirichlet boundary conditions and is given by $(H_0^1(\Omega, \partial\Omega_{D,P}))^9 := \{\mathbf{v} \in (H^1(\Omega))^9 : \mathbf{v} = \mathbf{0} \text{ on } \partial\Omega_{D,P}\}$. We equip $\mathbf{H^1}(\Omega)$ and $(H^1(\Omega))^9$ with the standard Sobolev space norm

$$\|\mathbf{u}\|_{H^1(\Omega)} := (|\mathbf{u}|^2_{H^1(\Omega)} + \|\mathbf{u}\|^2_{L_2(\Omega)})^{1/2},$$

where $\|\mathbf{u}\|^2_{L_2(\Omega)} := \sum_{i=1}^3 \int_\Omega |u_i|^2 d\mathbf{x}$ and $|\mathbf{u}|^2_{H^1(\Omega)} := \sum_{i=1}^3 \|\nabla u_i\|^2_{L_2(\Omega)}$ if $\mathbf{u} \in \mathbf{H^1}(\Omega)$ or $\|\mathbf{u}\|^2_{L_2(\Omega)} := \sum_{i,j=1}^3 \int_\Omega |u_{ij}|^2 d\mathbf{x}$ and $|\mathbf{u}|^2_{H^{1/2}(\partial\Omega)} := \sum_{i,j=1}^3 \|\nabla u_{ij}\|^2_{L_2(\Omega)}$ if $\mathbf{u} \in (H^1(\Omega))^9$. Since the two terms of the H^1-norm scale in a different way under dilation of Ω we introduce the factor $\frac{1}{H^2}$ in front of the squared L_2-norm if the diameter of Ω is H. Thus, we obtain a scaled H^1-norm

$$\|\mathbf{u}\|_{H^1(\Omega)} := (|\mathbf{u}|^2_{H^1(\Omega)} + \frac{1}{H^2}\|\mathbf{u}\|^2_{L_2(\Omega)})^{1/2}.$$

One of the most well-known generalized continuum models is the Cosserat model [15, 21, 25, 36, 37, 38, 39, 40, 41, 70]. As we have seen, it is obtained from our micromorphic model if $P \in \mathrm{SO}(3)$, i.e., P is a rotation with $P^T P = \mathrm{Id}$ and $\det(P) = 1$. The main applications for micromorphic models are the description of cellular materials, metallic foams, material inhomogeneities, eigenstresses and configurational mechanics; see [17, 34, 35, 41, 42, 43, 44, 46, 64, 76, 90, 91]. Small scale material oscillations superposed on the macroscopic deformation $\boldsymbol{\varphi}$ may also be described with the tensorial field P. Additionally, there is a close relationship of our model to plasticity formulations when we consider P as the plastic deformation in a multiplicative decomposition; see [74, 76], and to gradient enhanced continua; cf. [8, 75, 77, 78]. Furthermore, these models have recently received much attention in association with nano-devices and cellular structures since they model size effects in a natural way, i.e., small samples behave comparatively stiffer than larger samples.

We note that in contrast to the model of standard linear elasticity our formulation (1.1) is fully frame indifferent, i.e., the energy is invariant with respect to transformations $(\boldsymbol{\varphi}, P) \to (\bar{Q}\boldsymbol{\varphi}, \bar{Q}P)$ for all constant rotations $\bar{Q} \in \mathrm{SO}(3)$.

1.2 Coupling algorithms - a staggered approach

In our model we have the special situation that of a two-field problem, with a deformation $\boldsymbol{\varphi}$ and a micromorphic field P as unknowns. In general we have two different approaches to handle such problems.

On the one hand, we can solve the minimization problem monolithically, i.e., solving the minimization problem for both variables $\boldsymbol{\varphi}$ and P at the same time. In this case, we obtain a minimization problem with twelve unknowns in each node at a time. Monolithic approaches are, e.g., used by Yoon and Sigmund for electrostatical problems, see [93], Rochus, Rixen and Golinval for electromechanical coupling in micro structures, see [83], and Damanik, Hron, Quazzi and Turek for non-isothermal incompressible flow, see [19]. Furthermore, it is the standard approach in the engineering like treatment of Cosserat models; see [69, 70].

On the other hand, we can treat both fields separately. We refer to this kind of approach as the staggered approach since we solve the problem by solving the minimization problems in an alternating fashion, one after another, several times, i.e., using a fixed point iteration to find the minimizing configuration in $\boldsymbol{\varphi}$ and P. Note, that in P we may not find a minimizer but only a stationary point due to the lack of convexity in P. Hence, we may find only a stationary point for the whole problem which may not be a minimizer. Thus, we obtain two minimization problems in only one variable, i.e., one problem in $\boldsymbol{\varphi}$ and one in P, which are coupled since both variables occur in both problems. If for example $\boldsymbol{\varphi}$ changes we have to compute a new P since the minimization problem for P depends on $\boldsymbol{\varphi}$ and vice versa. Furthermore, we have a reduction in the size of our individual problems since the minimization problem in $\boldsymbol{\varphi}$ leads to three unknowns and the problem in P to nine unknowns in each node. Considering the discretization it is obvious that the staggered approach would be preferable with respect to the memory needed since it leads to two smaller problems which are treated one after another while the monolithic approach leads to one problem of larger size, i.e., for n nodes we obtain in the staggered approach one $3n \times 3n$ matrix and one $9n \times 9n$ matrix while in the monolithic approach we obtain a $12n \times 12n$ matrix in which the matrices from the staggered approach are included. In this work, we will concentrate on the staggered approach and leave the monolithic approach for further research. Our considerations concerning the staggered approach are mainly based on the article by Klawonn, Neff, Rheinbach, and Vanis [48]. Staggered algorithms are a popular approach to solve nonlinear coupled problems in a decomposed fashion. A staggered approach was, e.g., used by Askes, Morata, and Aifantis [2] for a gradient enhanced model in order to obtain two second order problems instead of one fourth order problem. Also similar approaches were used, e.g., by Armero [1] for a solid-fluid coupling, Attouch, Bolte, Redont, and Soubeyran, see [3], for weakly coupled convex minimization problems, or Attouch, Redont, and Soubeyran, see [4], for proximal minimization algorithms.

1.3 FETI domain decomposition methods

In the staggered approach we obtain a strictly convex minimization problem in $\boldsymbol{\varphi}$ which simplifies to linear elasticity when $P = \mathrm{Id}$. Hence, we refer to the this first subproblem as P-elasticity. Since it is known that the **D**ual-**P**rimal **F**inite **E**lement **T**earing and **I**nterconnection (FETI-DP) method works well for standard linear elasticity we introduce this method as an efficient solver for the single P-elasticity problem. Thus, we especially investigate the first part of the problem, i.e., the P-elasticity problem, regarding only $\boldsymbol{\varphi}$ as variable and keeping P fixed. The second problem, i.e., the minimization in P, is a non convex problem which resembles much of a nonlinear Laplacian problem to which we therefore refer to as q-Laplacian problem; see e.g., [84, Section 3.1.3]. This problem is solved by a Newton iteration. The linear system occurring in the Newton iteration is then solved directly by a LU decomposition implemented in MUMPS or in UMFPACK; see [26] and [20], respectively. When we consider the whole problem in the staggered approach, i.e., we minimize the energy alternating for $\boldsymbol{\varphi}$ and P, we also solve the linear system occurring for $\boldsymbol{\varphi}$ with a conjugate gradient method without preconditioning implemented in PETSc [5, 6, 7].

We need to define discrete problems which solve the systems on a grid representing the body. Note, that the discrete systems are approximations of the original problem and that we thus only obtain an approximation of the solution. Furthermore, we linearize the problems, i.e., we solve the minimization problem as a Newton problem to find the root of the first derivative of the corresponding energy functional. Thus, the discretization of such problems lead to large linear systems, i.e., we have to solve matrix vector problems $Ax = b$ with a very large and often sparse matrix A. These systems can easily have several millions of unknowns or even more. Systems of this scale can hardly be solved directly. This is often due to the memory needed or to the fact that direct algorithms can destroy the sparsity of the matrix. Thus, the linear systems are usually solved with iterative methods such as the conjugate gradient method or other Krylov space methods. Here, we again obtain approximations to the solution of the linear system up to a chosen accuracy.

Domain decomposition methods are also often used to solve these linear systems. The domain decomposition methods pursue the idea of dividing the whole global problem into many small local problems by dividing the respective body into small parts. These local problems are then assembled separately without regarding the other problems which makes it possible to work in parallel. Hence, due to the algorithm used it is also possible to solve the local problems in parallel. There remains only a small amount of communication needed to guarantee the continuity of the solution and hence to obtain an appropriate solution on the whole domain. When we use domain decomposition methods, we will concentrate on the FETI-DP method in this work.

The FETI-DP method is a domain decomposition method working on nonoverlapping subdomains. It belongs to the family of FETI methods and was originally introduced by Farhat et al. [27] and extended to three dimensional problems by Farhat, Lesoinne, and Pierson in [28]. For an extensive introduction to different domain decomposition methods, we refer to the monographs by Smith, Bjørstad, and Gropp [88], Toselli and Widlund [89], and Quarteroni and Valli [82].

The continuity of the solutions in the FETI-DP methods is enforced by using Lagrange multipliers and primal variables. Thus, the continuity on the interface is established in two different ways. On the one hand it is established by using Lagrange multipliers which guarantees continuity at convergence of the method. On the other hand we subassemble the values in the primal variables and hence enforce continuity in these nodes already during the solution process. The result of this strategy is a mixed linear system in which the primal variables and the Lagrange multipliers are the unknowns. By eliminating the primal variables the FETI-DP method iterates on the Lagrange multipliers; usually a preconditioned conjugate gradient method is used as Krylov space method. Since the elimination of the primal variables leads to a Schur complement we have to ensure that the local stiffness matrices are invertible. Therefore, the primal constraints are chosen such that these matrices become invertible. Note, that the choice of the primal variables is more elaborate in the case of three dimensional problems than for two dimensional ones. The coupling obtained by the primal variables is also needed such that the algorithm becomes scalable.

The FETI-DP method was first provided with a convergence bound for two dimensional scalar elliptic second order partial differential equations without coefficient jumps in Mandel and Tezaur [62]. Later on in Klawonn and Widlund [55], Klawonn, Widlund, and Dryja [56, 57], and Klawonn and Rheinbach [50] the family of FETI-DP algorithms was extended by different sets of primal variables, e.g., face and edge averages or first order moments for elasticity problems. These new FETI-DP algorithms were furthermore provided with convergence bounds for three dimensional problems; see [55, 56, 57]. Here, we will use several different sets of primal variables, i.e., we will use only vertices as in the beginnings of the FETI-DP methods as well as edge averages and combinations of edge averages and vertices. The work on the FETI-DP method is mainly based on the article by Klawonn, Neff, Rheinbach, and Vanis [47].

Note that the FETI-DP methods descend from the earlier one and two level FETI methods; see Farhat and Roux [33, 32], Farhat, Mandel, and Roux [30], Farhat and Mandel [29], and Farhat, Pierson, and Lesoinne [31]. For the one and two level methods as well as for the FETI-DP methods the Dirichlet preconditioner is used. This preconditioner was first used without scaling; see Farhat, Mandel and Roux [30], and then provided with a scaling to obtain convergence results independent of jumps in the coefficients of the partial differential equation; see Klawonn and Widlund [54, 55], Klawonn, Widlund, and Dryja [56], Klawonn and Rheinbach [51], and Klawonn, Pavarino, and Rheinbach [49]. But also for homogeneous problems, scaling can be important to improve convergence and the condition number estimate, see Madel and Tezaur [61] and Klawonn and Widlund [56].

In this work, FETI-DP methods are only considered for a simple P-elasticity problem. For future work, it would be of interest to apply the FETI-DP solver for the P-elastic subproblems in the staggered approach. Furthermore, the convergence of the Newton iteration for P has turned out to be problematic in the staggered approach depending on the problem. Hence, damping methods for the Newton iteration might be helpful to avoid this problem. In addition we aim to compare the staggered approach for our minimization problem with the results of a monolithic algorithm. Here, we again may have to work with damping strategies in the Newton iteration. The Newton iterations of the monolithic approach require the solution of a much larger linear system which is of a more complicated structure than the q-Laplacian and the P-elasticity problem. Hence an efficient solution of the linear system and a stable convergence of the Newton iteration might be challenging.

Closely related to the FETI-DP algorithms, are the Balancing Domain Decomposition methods by Constraints (BDDC); see Cros [18], Dohrmann [22], Mandel and Dohrmann [59], Mandel, Dohrmann, and Tezaur [60], or Li and Widlund [58].

The remainder of this work is organized as follows. In Chapter 2, the staggered approach for the solution of the coupled minimization problem in $(P, \boldsymbol{\varphi})$ is introduced. Additionally, the continuity of the separate decoupled minimization problems is considered. Furthermore, a basis for the kernel of the bilinear form of P-elasticity is deduced in Section 2.1.2. Chapter 2 concludes with numerical results obtained with the staggered scheme. In Chapter 3, the FETI-DP method is introduced as an efficient solver of the P-elastic subproblem. Following the arguments given by Klawonn and Widlund [55] a condition number estimate for the P-elastic problem is obtained. The selection of primal constraints is considered in Section 3.2 and Korn inequalities needed for the convergence analysis are introduced in Section 3.3. The condition number estimate for P-elasticity is provided in Section 3.4 by using the auxiliary technical lemmas presented in Section 3.5 for piecewise quadratic nodal basis functions. The investigations in the FETI-DP algorithm for the P-elastic problem are concluded by presenting numerical results in Section 3.6.

Chapter 2

Staggered approach

We introduce the algorithm for the solution of the minimization problem (1.1). In the algorithm, problem (1.1) is solved for only one variable, i.e., $\boldsymbol{\varphi}$ or P, at a time. This decoupling leads to a fixed point iteration of the following form

$$\begin{aligned}
&\textit{while } \|\Delta P^{(k)}\|_{l_2} \geq \texttt{tol} \textit{ and } \|\Delta \boldsymbol{\varphi}^{(k)}\|_{l_2} \geq \texttt{tol} \\
&\qquad \textit{solve } \boldsymbol{\varphi}^{(k+1)} := \operatorname{argmin}_{\boldsymbol{\varphi}} E(P^{(k)}, \boldsymbol{\varphi}^{(k)}) \quad \textit{while } P^{(k)} \textit{ is fixed} \\
&\qquad \textit{solve } P^{(k+1)} := \operatorname{argmin}_{P} E(P^{(k)}, \boldsymbol{\varphi}^{(k+1)}) \textit{ while } \boldsymbol{\varphi}^{(k+1)} \textit{ is fixed} \\
&\qquad \textit{update } k = k+1,
\end{aligned} \tag{2.1}$$

for a given tolerance `tol` and with $E(P, \boldsymbol{\varphi})$ being the energy function introduced in (1.1), and $\Delta P^{(k+1)} = P^{(k+1)} - P^{(k)}$ as well as $\Delta \boldsymbol{\varphi}^{(k+1)} = \boldsymbol{\varphi}^{(k+1)} - \boldsymbol{\varphi}^{(k)}$.

We may change the order of the minimization problems in (2.1) and start by minimizing the term for P first and then subsequently for $\boldsymbol{\varphi}$.

This algorithm leads to two different minimization problems each of which exclusively depends on one variable. The minimization for $\boldsymbol{\varphi}$ results in the formulation of standard linear elasticity if P is the identity. A problem similar to the well-known nonlinear q-Laplace problem occurs when we minimize the energy for the variable P. Both problems will be discussed separately in Sections 2.1 and 2.2.

This chapter is based on Klawonn, Neff, Rheinbach and Vanis [48]. Note, that here we give some more details concerning the continuity of the quadratic forms. Some of the considerations concerning the continuity of P-elasticity and its kernel, cf. Sections 2.1.1 and 2.1.2, can be found in Klawonn, Neff, Rheinbach and Vanis [47].

2.1 P-Elasticity

In this section we consider the minimization problem with respect to $\boldsymbol{\varphi}$ with a given field P. Thus, the problem in (1.1) reduces to

$$
\begin{aligned}
\min_{\boldsymbol{\varphi}} \quad & \Big(\int_\Omega \mu_e \|\mathrm{sym}(P^{-1}F_\nabla - \mathrm{Id}\,)\|_F^2 + \frac{\lambda_e}{2}\left(\mathrm{tr}(P^{-1}F_\nabla - \mathrm{Id}\,)\right)^2 \; d\mathbf{x} \\
& - \int_\Omega (f_{\boldsymbol{\varphi}}, \boldsymbol{\varphi})_F \; d\mathbf{x} \Big) .
\end{aligned} \tag{2.2}
$$

For $P = \mathrm{Id}$, (2.2) reduces to the problem of standard linear elasticity, i.e.,

$$
\min_{\boldsymbol{\varphi}} \quad \Big(\int_\Omega \mu_e \|\mathrm{sym}(F_\nabla - \mathrm{Id}\,)\|_F^2 + \frac{\lambda_e}{2}\left(\mathrm{tr}(F_\nabla - \mathrm{Id}\,)\right)^2 \; d\mathbf{x} - \int_\Omega (f_{\boldsymbol{\varphi}}, \boldsymbol{\varphi})_F \; d\mathbf{x} \Big),
$$

written in terms of the deformation $\boldsymbol{\varphi}$ since $\boldsymbol{\varphi} = \mathbf{x} + \mathbf{u}$, $F_\nabla = \mathrm{Id} + \nabla\mathbf{u}$ and $\varepsilon := \mathrm{sym}(\nabla\mathbf{u}) = \mathrm{sym}(F_\nabla - \mathrm{Id}\,)$. Hence, we denote this subproblem as P-elasticity.

In Chapter 3, we introduce the FETI-DP algorithm for this subproblem as an efficient solver. Additionally, we show that the FETI-DP condition number estimate introduced by Klawonn and Widlund for standard linear elasticity, cf. [55], can be extended to the case of P-elasticity under certain assumptions on the matrix P; see Sections 3.3 and 3.4.

We introduce the abbreviation

$$
J_1(P, \boldsymbol{\varphi}) \;\; := \;\; \int_\Omega \mu_e \|\mathrm{sym}(P^{-1}F_\nabla - \mathrm{Id}\,)\|_F^2 + \frac{\lambda_e}{2}\left(\mathrm{tr}(P^{-1}F_\nabla - \mathrm{Id}\,)\right)^2 d\mathbf{x}. \tag{2.3}
$$

The reduced problem (2.2) is formally solved by a Newton iteration, i.e., the problem

Find $\boldsymbol{\varphi}$ such that

$$
\begin{aligned}
\partial_{\boldsymbol{\varphi}} \left(J_1(P, \boldsymbol{\varphi}) - \int_\Omega (f_{\boldsymbol{\varphi}}, \boldsymbol{\varphi}) \, d\mathbf{x} \right) &= 0 \\
\Leftrightarrow \qquad \partial_{\boldsymbol{\varphi}} J_1(P, \boldsymbol{\varphi}) - \int_\Omega f_{\boldsymbol{\varphi}} \; d\mathbf{x} &= 0.
\end{aligned}
$$

is solved by

$$
\begin{aligned}
& \boldsymbol{\varphi}^{(k+1)} = \boldsymbol{\varphi}^{(k)} - (\partial^2_{\boldsymbol{\varphi}} J_1(P, \boldsymbol{\varphi}^{(k)}))^{-1} \Big(\partial_{\boldsymbol{\varphi}} J_1(P, \boldsymbol{\varphi}^{(k)}) - \int_\Omega f_{\boldsymbol{\varphi}} \, d\mathbf{x} \Big) \boldsymbol{\varphi}^{(k)} \\
\Leftrightarrow \;\; & \partial^2_{\boldsymbol{\varphi}} J_1(P, \boldsymbol{\varphi}^{(k)}) \left(\boldsymbol{\varphi}^{(k+1)} - \boldsymbol{\varphi}^{(k)} \right) = \Big(\int_\Omega f_{\boldsymbol{\varphi}} \, d\mathbf{x} - \; \partial_{\boldsymbol{\varphi}} J_1(P, \boldsymbol{\varphi}^{(k)}) \Big) \boldsymbol{\varphi}^{(k)},
\end{aligned} \tag{2.4}
$$

with $\Delta\boldsymbol{\varphi}^{(k+1)} = \boldsymbol{\varphi}^{(k+1)} - \boldsymbol{\varphi}^{(k)} := \mathbf{u}^{(k)}$, where $\mathbf{u}^{(k)}$ is the k-th increment.

From (2.2) it is clear that the problem (2.4) only depends linearly on the deformation $\boldsymbol{\varphi}$. Hence, the unique minimizing solution is obtained in one step and we do not introduce the counter for the Newton iteration; see e.g., (2.20). However, we introduce the Newton algorithm to keep the presentation general enough such that later on we can introduce a nonlinear elasticity formulation.

The formulation obtained by the Newton algorithm is rewritten as the variational problem

Find the k-th increment $\mathbf{u}^{(k)} \in \mathbf{H}_\mathbf{0}^\mathbf{1}(\Omega, \partial\Omega_D)$ *of the elastic body* Ω *such that for all* $\mathbf{v} \in \mathbf{H}_\mathbf{0}^\mathbf{1}(\Omega, \partial\Omega_D)$

$$\int_\Omega 2\mu_e(\varepsilon_P(\mathbf{u}^{(k)}), \varepsilon_P(\mathbf{v}))_F \; d\mathbf{x} + \int_\Omega \lambda_e \; \mathrm{tr}(P^{-1}\nabla \mathbf{u}^{(k)})\mathrm{tr}(P^{-1}\nabla \mathbf{v}) \; d\mathbf{x} = \mathbf{F}_{\boldsymbol{\varphi}}^{(k)}(\mathbf{v}). \quad (2.5)$$

We will refer to the left hand side of (2.5) as $a_{\boldsymbol{\varphi}}^{(k)}(\mathbf{u}^{(k)}, \mathbf{v})$; see (2.7). The right hand side $F_{\boldsymbol{\varphi}}^{(k)}(\mathbf{v})$ is given by

$$\begin{aligned} & \mathbf{F}_{\boldsymbol{\varphi}}^{(k)}(\mathbf{v}) \\ := \; & \int_\Omega (f_{\boldsymbol{\varphi}}, \mathbf{v})_F \; d\mathbf{x} - \int_\Omega \mu_e(P^{-T}(P^{-1}F_\nabla + F_\nabla^T P^{-T} - 2 \cdot \mathrm{Id}\,), \nabla \mathbf{v})_F \; d\mathbf{x} \quad (2.6) \\ & - \int_\Omega \lambda_e \mathrm{tr}(P^{-1}F_\nabla - \mathrm{Id}\,)(P^{-T}, \nabla \mathbf{v})_F \; d\mathbf{x}, \end{aligned}$$

with $F_\nabla = \nabla \boldsymbol{\varphi}^{(k)}$. Here, we define $\varepsilon_P(\mathbf{u})$, analogously to the definition of the symmetric strain tensor $\varepsilon = \mathrm{sym}(\nabla \mathbf{u})$ in standard linear elasticity, as

$$\varepsilon_P(\mathbf{u}) := \mathrm{sym}(P^{-1}\nabla \mathbf{u}) \quad \Rightarrow \quad (\varepsilon_P)_{ij}(\mathbf{u}) := \frac{1}{2}\left(\sum_{k=1}^{3}(P^{-1})_{ik}\frac{\partial u_k}{\partial x_j} + \frac{\partial u_k}{\partial x_i}(P^{-1})_{jk}\right)$$

and we obtain

$$(\varepsilon_P(\mathbf{u}), \varepsilon_P(\mathbf{v}))_F = \sum_{i,j=1}^{3} (\varepsilon_P)_{ij}(\mathbf{u})(\varepsilon_P)_{ij}(\mathbf{v}).$$

We can rewrite the bilinear form $a_{\boldsymbol{\varphi}}^{(k)}(\cdot, \cdot)$ as

$$\begin{aligned} & a_{\boldsymbol{\varphi}}^{(k)}(\mathbf{u}^{(k)}, \mathbf{v}) \\ := \; & 2(\mu_e \varepsilon_P(\mathbf{u}^{(k)}), \varepsilon_P(\mathbf{v}))_{L_2(\Omega)} + (\lambda_e \mathrm{tr}(P^{-1}\nabla \mathbf{u}^{(k)}), \mathrm{tr}(P^{-1}\nabla \mathbf{v}))_{L_2(\Omega)} \quad (2.7) \\ = \; & 2(\mu_e \varepsilon_P(\mathbf{u}^{(k)}), \varepsilon_P(\mathbf{v}))_{L_2(\Omega)} + (\lambda_e \mathrm{tr}(\varepsilon_P(\mathbf{u}^{(k)})), \mathrm{tr}(\varepsilon_P(\mathbf{v})))_{L_2(\Omega)}; \end{aligned}$$

see also the notation on pp. 5 to 8.

2.1.1 Continuity of the bilinear form

In this subsection we will establish continuity of the bilinear form $a_{\boldsymbol{\varphi}}(\cdot, \cdot)$ introduced in (2.7) with respect to the H^1-norm, i.e., $\|\cdot\|_{H^1(\Omega)}$. We can estimate the two terms occurring in (2.7) by assuming that $P, P^{-1} \in C^0(\bar{\Omega})$ and using for $A, B \in \mathrm{I\!R}^{n \times n}$

- the Cauchy-Schwarz inequality: $(A, B)_{L_2(\Omega)} \leq \|A\|_{L_2(\Omega)} \|B\|_{L_2(\Omega)}$,

- the submultiplicativity of the L_2-norm: $\|AB\|_{L_2(\Omega)} \leq \|A\|_{L_2(\Omega)}\|B\|_{L_2(\Omega)}$,
- $\|A^T\|_F = \|A\|_F \Rightarrow \|A^T\|_{L_2(\Omega)} = \|A\|_{L_2(\Omega)}$,
- $(A^T, B)_F = (A, B^T)_F \Rightarrow (A^T, B)_{L_2(\Omega)} = (A, B^T)_{L_2(\Omega)}$,
- $\|\nabla \mathbf{u}\|_{L_2(\Omega)} = |\mathbf{u}|_{H^1(\Omega)}$,
- $|\mathbf{u}|_{H^1(\Omega)} \leq \|\mathbf{u}\|_{H^1(\Omega)}$.

We assume that the Lamé parameters μ_e and λ_e are bounded from above by their maximum value over Ω. Hence, we can neglect the parameters when estimating the terms of the bilinear form $a_{\boldsymbol{\varphi}}(\cdot,\cdot)$ from (2.7).

For the first term in (2.7) this leads to

$$
\begin{aligned}
& (\varepsilon_P(\mathbf{u}), \varepsilon_P(\mathbf{v}))_{L_2(\Omega)} \\
= \; & \frac{1}{4}(P^{-1}\nabla\mathbf{u} + (\nabla\mathbf{u})^T P^{-T}, P^{-1}\nabla\mathbf{v} + (\nabla\mathbf{v})^T P^{-T})_{L_2(\Omega)} \\
= \; & \frac{1}{4}\big[(P^{-1}\nabla\mathbf{u}, P^{-1}\nabla\mathbf{v})_{L_2(\Omega)} + 2(P^{-1}\nabla\mathbf{u}, (\nabla\mathbf{v})^T P^{-T})_{L_2(\Omega)} \\
& \quad + ((\nabla\mathbf{u})^T P^{-T}, (\nabla\mathbf{v})^T P^{-T})_{L_2(\Omega)}\big] \\
\leq \; & \frac{1}{4}\big(\|P^{-1}\nabla\mathbf{u}\|_{L_2(\Omega)}\|P^{-1}\nabla\mathbf{v}\|_{L_2(\Omega)} + 2\|P^{-1}\nabla\mathbf{u}\|_{L_2(\Omega)}\|(\nabla\mathbf{v})^T P^{-T}\|_{L_2(\Omega)} \\
& \quad + \|(\nabla\mathbf{u})^T P^{-T}\|_{L_2(\Omega)}\|(\nabla\mathbf{v})^T P^{-T}\|_{L_2(\Omega)}\big) \\
\leq \; & \|P^{-T}\|^2_{L_2(\Omega)}\|\nabla\mathbf{u}\|_{L_2(\Omega)}\|\nabla\mathbf{v}\|_{L_2(\Omega)} \\
= \; & \|P^{-T}\|^2_{L_2(\Omega)}|\mathbf{u}|_{H^1(\Omega)}|\mathbf{v}|_{H^1(\Omega)} \\
\leq \; & \|P^{-T}\|^2_{L_2(\Omega)}\|\mathbf{u}\|_{H^1(\Omega)}\|\mathbf{v}\|_{H^1(\Omega)}.
\end{aligned} \tag{2.8}
$$

For the second term in (2.7) we consider the following inequality

$$
\begin{aligned}
\operatorname{tr}(A)\operatorname{tr}(B) &= (A, \mathrm{Id}\,)_F(B, \mathrm{Id}\,)_F \\
&\leq |(A, \mathrm{Id}\,)_F|\;|(B, \mathrm{Id}\,)_F| \\
&\leq \|A\|_F\;\|\mathrm{Id}\,\|_F\;\|B\|_F\;\|\mathrm{Id}\,\|_F \\
&\leq \|A\|_F\;n^{1/2}\;\|B\|_F\;n^{1/2} \\
&= n\|A\|_F\|B\|_F
\end{aligned} \tag{2.9}
$$

and obtain for $n = 3$

$$
\begin{aligned}
\int_\Omega \operatorname{tr}(P^{-1}\nabla\mathbf{u})\operatorname{tr}(P^{-1}\nabla\mathbf{v})\;d\mathbf{x} &\leq \int_\Omega 3\,\|P^{-1}\nabla\mathbf{u}\|_F\|P^{-1}\nabla\mathbf{v}\|_F\;d\mathbf{x} \\
&\leq 3\left(\int_\Omega \|P^{-1}\nabla\mathbf{u}\|_F^2\;d\mathbf{x}\right)^{1/2}\left(\int_\Omega \|P^{-1}\nabla\mathbf{v}\|_F^2\;d\mathbf{x}\right)^{1/2} \\
&= 3\,\|P^{-1}\nabla\mathbf{u}\|_{L_2(\Omega)}\|P^{-1}\nabla\mathbf{v}\|_{L_2(\Omega)} \\
&\leq 3\,\|P^{-T}\|^2_{L_2(\Omega)}|\mathbf{u}|_{H^1(\Omega)}|\mathbf{v}|_{H^1(\Omega)} \\
&\leq 3\,\|P^{-T}\|^2_{L_2(\Omega)}\|\mathbf{u}\|_{H^1(\Omega)}\|\mathbf{v}\|_{H^1(\Omega)}.
\end{aligned} \tag{2.10}
$$

By combining (2.8) and (2.10) we obtain

$$a_{\boldsymbol{\varphi}}(\mathbf{u},\mathbf{v}) \le C\|P^{-T}\|^2_{L_2(\Omega)}|\mathbf{u}|_{H^1(\Omega)}|\mathbf{v}|_{H^1(\Omega)} \le C\|P^{-1}\|^2_{L_2(\Omega)}\|\mathbf{u}\|_{H^1(\Omega)}\|\mathbf{v}\|_{H^1(\Omega)}. \quad (2.11)$$

2.1.2 Kernel of the bilinear form $a_{\boldsymbol{\varphi}}(\mathbf{u},\mathbf{v})$

For our condition number estimate of the FETI-DP method, see Section 3.4, we need an explicit representation of the elements $\mathbf{r}$ in the nullspace $\mathbf{ker}\,(\varepsilon_P)$.

From (2.7) we have

$$a_{\boldsymbol{\varphi}}(\mathbf{r},\mathbf{r}) = 0 \quad\Leftrightarrow\quad \|\varepsilon_P(\mathbf{r})\|^2_{L_2(\Omega)} = 0 \,\wedge\, \operatorname{tr}(\varepsilon_P(\mathbf{r}))^2 = 0.$$

Since $\operatorname{tr}(\varepsilon_P(\mathbf{r}))^2 = 0$ if $\|\varepsilon_P(\mathbf{r})\|^2_{L_2(\Omega)} = 0$, we have to consider

$$\begin{array}{rcl} & \|\varepsilon_P(\mathbf{r})\|_F^2 & = 0 \\ \Leftrightarrow & \|P^{-1}\nabla\mathbf{r} + \nabla\mathbf{r}^T P^{-T}\|_F^2 & = 0 \\ \Leftrightarrow & \|P^{-1}(\nabla\mathbf{r} + P\nabla\mathbf{r}^T P^{-T})\|_F^2 & = 0 \\ \Leftrightarrow & \|P^{-1}(\nabla\mathbf{r}P^T + P\nabla\mathbf{r}^T)P^{-T}\|_F^2 & = 0 \\ \Leftrightarrow & \nabla\mathbf{r}P^T + P\nabla\mathbf{r}^T & = 0 \\ \Leftrightarrow & 2\mathrm{sym}(\nabla\mathbf{r}P^T) & = 0 \end{array}$$

From this it follows that $(\nabla\mathbf{r})P^T$ must be a skew symmetric matrix $A(\mathbf{x}) \in \mathfrak{so}(3) := \{X \in \mathbb{R}^{3\times 3} : X^T = -X\}$ and thus we have

$$\nabla\mathbf{r}(\mathbf{x}) = A(\mathbf{x})P^{-T}(\mathbf{x}). \quad (2.12)$$

We use the Curl-operator on both sides of the equation in (2.12), i.e., we use

$$\begin{array}{rccc} \operatorname{curl}: & \mathbb{R}^3 & \to & \mathbb{R}^3 \\ & \begin{bmatrix} y_1 \\ y_2 \\ y_3 \end{bmatrix} & \mapsto & \begin{bmatrix} \partial_2 y_3 - \partial_3 y_2 \\ \partial_3 y_1 - \partial_1 y_3 \\ \partial_1 y_2 - \partial_2 y_1 \end{bmatrix}. \end{array}$$

and since we have matrices on both sides of the equation, we define the Curl of a matrix as the curl of its rows.

If we apply Curl to the left hand side of the second equation in (2.12), we get the curl of the divergence of a potential in all three rows. Thus, $\operatorname{Curl}(\nabla\mathbf{r}) = 0$ under the assumption that $\mathbf{r}$ is twice continuously differentiable. We will now apply the Curl to the right hand side of the second equality in (2.12). For convenience we introduce $a_i(\mathbf{x})$ as the rows of the matrix $A(\mathbf{x})$ and $p_i(\mathbf{x})$ as the columns of the matrix $P^{-T}(\mathbf{x})$ and get

$$A(\mathbf{x})P^{-T}(\mathbf{x}) = \begin{bmatrix} a_1(\mathbf{x})p_1(\mathbf{x}) & a_1(\mathbf{x})p_2(\mathbf{x}) & a_1(\mathbf{x})p_3(\mathbf{x}) \\ a_2(\mathbf{x})p_1(\mathbf{x}) & a_2(\mathbf{x})p_2(\mathbf{x}) & a_2(\mathbf{x})p_3(\mathbf{x}) \\ a_3(\mathbf{x})p_1(\mathbf{x}) & a_3(\mathbf{x})p_2(\mathbf{x}) & a_3(\mathbf{x})p_3(\mathbf{x}) \end{bmatrix}. \quad (2.13)$$

We will now calculate the curl of the rows $j \in \{1, 2, 3\}$ explicitly. Therefore we use the abbreviation ∂_k instead of $\frac{\partial}{\partial x_k}$ and with $\partial_k a_m$ we denote the component-by-component partial derivative of the row a_m, i.e.,

$$\partial_k a_m = (\partial_k a_{m1}, \partial_k a_{m2}, \partial_k a_{m3});$$

an analogous notation is used for the column p_m. We obtain

$$\begin{aligned} \operatorname{curl} \begin{bmatrix} a_j p_1 \\ a_j p_2 \\ a_j p_3 \end{bmatrix} &= \begin{bmatrix} \partial_2(a_j p_3) - \partial_3(a_j p_2) \\ \partial_3(a_j p_1) - \partial_1(a_j p_3) \\ \partial_1(a_j p_2) - \partial_2(a_j p_1) \end{bmatrix} \\ &= \begin{bmatrix} (\partial_2 a_j) p_3 - (\partial_3 a_j) p_2 \\ (\partial_3 a_j) p_1 - (\partial_1 a_j) p_3 \\ (\partial_1 a_j) p_2 - (\partial_2 a_j) p_1 \end{bmatrix} + \begin{bmatrix} a_j(\partial_2 p_3 - \partial_3 p_2) \\ a_j(\partial_3 p_1 - \partial_1 p_3) \\ a_j(\partial_1 p_2 - \partial_2 p_1) \end{bmatrix}. \end{aligned}$$

Here, we dropped the explicit dependence on $\mathbf{x}$ in our notation. We now denote by p_{ij} the entry in the i-th row and the j-th column of P^{-T} and obtain

$$\begin{aligned} \operatorname{Curl}(AP^{-T}) &= \begin{bmatrix} (\partial_2 a_1)p_3 - (\partial_3 a_1)p_2 & (\partial_3 a_1)p_1 - (\partial_1 a_1)p_3 & (\partial_1 a_1)p_2 - (\partial_2 a_1)p_1 \\ (\partial_2 a_2)p_3 - (\partial_3 a_2)p_2 & (\partial_3 a_2)p_1 - (\partial_1 a_2)p_3 & (\partial_1 a_2)p_2 - (\partial_2 a_2)p_1 \\ (\partial_2 a_3)p_3 - (\partial_3 a_3)p_2 & (\partial_3 a_3)p_1 - (\partial_1 a_3)p_3 & (\partial_1 a_3)p_2 - (\partial_2 a_3)p_1 \end{bmatrix} \\ &\quad + \begin{bmatrix} a_1(\partial_2 p_3 - \partial_3 p_2) & a_1(\partial_3 p_1 - \partial_1 p_3) & a_1(\partial_1 p_2 - \partial_2 p_1) \\ a_2(\partial_2 p_3 - \partial_3 p_2) & a_2(\partial_3 p_1 - \partial_1 p_3) & a_2(\partial_1 p_2 - \partial_2 p_1) \\ a_3(\partial_2 p_3 - \partial_3 p_2) & a_3(\partial_3 p_1 - \partial_1 p_3) & a_3(\partial_1 p_2 - \partial_2 p_1) \end{bmatrix} \\ &= \underbrace{\begin{bmatrix} \partial_1 a_1 & \partial_2 a_1 & \partial_3 a_1 \\ \partial_1 a_2 & \partial_2 a_2 & \partial_3 a_2 \\ \partial_1 a_3 & \partial_2 a_3 & \partial_3 a_3 \end{bmatrix}}_{\in M^{3\times 9}} \cdot \underbrace{\begin{bmatrix} 0 & -p_3 & p_2 \\ p_3 & 0 & -p_1 \\ -p_2 & p_1 & 0 \end{bmatrix}}_{\in M^{9\times 3}} \\ &\quad + \begin{bmatrix} a_1 \\ a_2 \\ a_3 \end{bmatrix} \cdot \begin{bmatrix} \partial_2 p_{13} - \partial_3 p_{12} & \partial_3 p_{11} - \partial_1 p_{13} & \partial_1 p_{12} - \partial_2 p_{11} \\ \partial_2 p_{23} - \partial_3 p_{22} & \partial_3 p_{21} - \partial_1 p_{23} & \partial_1 p_{22} - \partial_2 p_{21} \\ \partial_2 p_{33} - \partial_3 p_{32} & \partial_3 p_{31} - \partial_1 p_{33} & \partial_1 p_{32} - \partial_2 p_{31} \end{bmatrix} \\ &= L_{P^{-T}}(D_{\mathbf{x}} A) + A \cdot \operatorname{Curl}(P^{-T}). \end{aligned} \tag{2.14}$$

Here, $L_{P^{-T}}(D_{\mathbf{x}} A(\mathbf{x}))$ denotes the linear operator in P^{-T} applied to the derivative of $A(\mathbf{x})$ defined by the first matrix product. Combining these results we have

$$\begin{aligned} \operatorname{Curl}(\nabla \mathbf{r}(\mathbf{x})) &= \operatorname{Curl}(A(\mathbf{x}) P^{-T}(\mathbf{x})) \\ \Leftrightarrow \qquad 0 &= L_{P^{-T}}(D_{\mathbf{x}} A(\mathbf{x})) + A(\mathbf{x}) \operatorname{Curl}(P^{-T}(\mathbf{x})). \end{aligned} \tag{2.15}$$

If we assume that the matrix P^{-T} is a gradient, i.e., there exists a function $\boldsymbol{\psi} : \mathbb{R}^3 \to \mathbb{R}^3$ such that $P^{-T}(\mathbf{x}) = \nabla \boldsymbol{\psi}(\mathbf{x})$ with $\boldsymbol{\psi}$ twice continuously differentiable, it follows that $\operatorname{Curl}(P^{-T}(\mathbf{x})) = 0$. Thus, it is necessary that $L_{P^{-T}}(D_{\mathbf{x}} A(\mathbf{x})) = 0$.

Since $L_{P^{-T}}$ is a linear operator and invertible if and only if $\det(P^{-T}) \neq 0$, cf. [71, Lemma 3.7], the condition $L_{P^{-T}}(D_{\mathbf{x}}A(\mathbf{x})) = 0$ is satisfied if and only if $D_{\mathbf{x}}A(\mathbf{x}) = 0$ which means that $A(\mathbf{x}) = \text{const} = \bar{A}$. From this follows

$$\nabla\mathbf{r} = \bar{A}P^{-T} = \bar{A}\nabla\boldsymbol{\psi}(\mathbf{x}) \quad \Rightarrow \quad \mathbf{r}(\mathbf{x}) = \bar{A}\boldsymbol{\psi}(\mathbf{x}) + \bar{b}$$

with a constant translation vector $\bar{b} \in \mathrm{IR}^3$ and a constant skew-symmetric matrix $\bar{A} \in \mathfrak{so}\,(3)$. Thus, we have

$$\bar{A} = \begin{bmatrix} 0 & \alpha & -\beta \\ -\alpha & 0 & \gamma \\ \beta & -\gamma & 0 \end{bmatrix} \quad , \quad \bar{b} = \begin{bmatrix} a \\ b \\ c \end{bmatrix},$$

with suitable constants $\alpha, \beta, \gamma, a, b, c \in \mathrm{IR}$, and can write $\mathbf{r}(\mathbf{x})$ as

$$\begin{aligned} \mathbf{r}(\mathbf{x}) &= \bar{A}\nabla\boldsymbol{\psi}(\mathbf{x}) + \bar{b} \\ &= \begin{bmatrix} \alpha\psi^{(2)}(\mathbf{x}) - \beta\psi^{(3)}(\mathbf{x}) + a \\ -\alpha\psi^{(1)}(\mathbf{x}) + \gamma\psi^{(3)}(\mathbf{x}) + b \\ \beta\psi^{(1)}(\mathbf{x}) - \gamma\psi^{(2)}(\mathbf{x}) + c \end{bmatrix} \\ &= \alpha \begin{bmatrix} \psi^{(2)}(\mathbf{x}) \\ -\psi^{(1)}(\mathbf{x}) \\ 0 \end{bmatrix} + \beta \begin{bmatrix} -\psi^{(3)}(\mathbf{x}) \\ 0 \\ \psi^{(1)}(\mathbf{x}) \end{bmatrix} + \gamma \begin{bmatrix} 0 \\ \psi^{(3)}(\mathbf{x}) \\ -\psi^{(2)}(\mathbf{x}) \end{bmatrix} \\ &\quad + a \begin{bmatrix} 1 \\ 0 \\ 0 \end{bmatrix} + b \begin{bmatrix} 0 \\ 1 \\ 0 \end{bmatrix} + c \begin{bmatrix} 0 \\ 0 \\ 1 \end{bmatrix}. \end{aligned}$$

From this representation we obtain the following basis of $\mathbf{ker}\,(\varepsilon_P)$

$$\begin{aligned} &\mathbf{r}_1 := \begin{bmatrix} 1 \\ 0 \\ 0 \end{bmatrix}, \ \mathbf{r}_2 := \begin{bmatrix} 0 \\ 1 \\ 0 \end{bmatrix}, \ \mathbf{r}_3 := \begin{bmatrix} 0 \\ 0 \\ 1 \end{bmatrix}, \\ &\mathbf{r}_4(\mathbf{x}) := \begin{bmatrix} \psi^{(2)}(\mathbf{x}) \\ -\psi^{(1)}(\mathbf{x}) \\ 0 \end{bmatrix}, \ \mathbf{r}_5(\mathbf{x}) := \begin{bmatrix} -\psi^{(3)}(\mathbf{x}) \\ 0 \\ \psi^{(1)}(\mathbf{x}) \end{bmatrix}, \ \mathbf{r}_6(\mathbf{x}) := \begin{bmatrix} 0 \\ \psi^{(3)}(\mathbf{x}) \\ -\psi^{(2)}(\mathbf{x}) \end{bmatrix}. \end{aligned} \tag{2.16}$$

Clearly, we obtain the basis elements for the nullspace of standard linear elasticity if $\boldsymbol{\psi}(\mathbf{x}) = \mathbf{x}$, i.e., $P = \mathrm{Id}$. Later on, in our analysis of the FETI-DP method, cf.

Chapter 3, for $\mathbf{r}_l, l = 4, 5, 6$, we have to consider shifted versions

$$\begin{aligned}
\mathbf{r}_4(\mathbf{x}) &:= \frac{1}{H_{\boldsymbol{\psi}}} \begin{bmatrix} \psi^{(2)}(\mathbf{x}) - \psi^{(2)}(\hat{\mathbf{x}}) \\ -\psi^{(1)}(\mathbf{x}) + \psi^{(1)}(\hat{\mathbf{x}}) \\ 0 \end{bmatrix}, \\
\mathbf{r}_5(\mathbf{x}) &:= \frac{1}{H_{\boldsymbol{\psi}}} \begin{bmatrix} -\psi^{(3)}(\mathbf{x}) + \psi^{(3)}(\hat{\mathbf{x}}) \\ 0 \\ \psi^{(1)}(\mathbf{x}) - \psi^{(1)}(\hat{\mathbf{x}}) \end{bmatrix}, \\
\mathbf{r}_6(\mathbf{x}) &:= \frac{1}{H_{\boldsymbol{\psi}}} \begin{bmatrix} 0 \\ \psi^{(3)}(\mathbf{x}) - \psi^{(3)}(\hat{\mathbf{x}}) \\ -\psi^{(2)}(\mathbf{x}) + \psi^{(2)}(\hat{\mathbf{x}}) \end{bmatrix},
\end{aligned} \tag{2.17}$$

where $H_{\boldsymbol{\psi}}$ is the diameter of the transformed domain $\boldsymbol{\psi}(\Omega)$, i.e., $H_{\boldsymbol{\psi}} := \operatorname{diam}(\boldsymbol{\psi}(\Omega))$, and $\hat{\mathbf{x}}$ is a shift parameter such that $\psi^{(j)}(\mathbf{x}) - \psi^{(j)}(\hat{\mathbf{x}})$ can be estimated by a constant times $H_{\boldsymbol{\psi}}$, i.e., $(\psi^{(j)}(\mathbf{x}) - \psi^{(j)}(\hat{\mathbf{x}}))^2 \le C H_{\boldsymbol{\psi}}^2$.

2.2 The q-Laplace problem

The second decoupled problem is nonlinear and non convex. We again use the abbreviation J_1, cf. Section 2.1, (2.3), and further introduce

$$J_2(P) := \int_\Omega \mu_e h^+ \|P^T P - \operatorname{Id}\|_F^2 + \mu_e \left(\frac{L_c^2}{2} \|\nabla P\|_F^2 + \frac{L_c^q}{q} \|\nabla P\|_F^q \right) d\mathbf{x}. \tag{2.18}$$

Hence, we consider the minimization problem

$$\min_P \left(J_1(P, \boldsymbol{\varphi}) + J_2(P) - \int_\Omega (f_P, P)\, d\mathbf{x} \right) \tag{2.19}$$

which again will be solved with a Newton iteration, i.e.,

$$\begin{aligned}
&\partial_P^2 (J_1(P_{n-1}^{(k+1)}, \boldsymbol{\varphi}) + J_2(P_{n-1}^{(k+1)})) \Delta P_n^{(k+1)} \\
= \; &\Big(\int_\Omega f_P \, d\mathbf{x} - \; \partial_P (J_1(P_{n-1}^{(k+1)}, \boldsymbol{\varphi}) + J_2(P_{n-1}^{(k+1)})) \Big) P_{n-1}^{(k+1)},
\end{aligned} \tag{2.20}$$

with n denoting the n-th Newton iteration step, i.e., for $n = 1, 2, \ldots$, we have $\Delta P_n^{(k+1)} := P_n^{(k+1)} - P_{n-1}^{(k+1)}$ and $P_0^{(k+1)} = P^{(k)}$. Hence, we obtain the new iterate $P_n^{(k+1)} = P_{n-1}^{(k+1)} + \Delta P_n^{(k+1)}$. This Newton iteration has to be solved every time we compute the minimizer for the micromorphic field P. Again we discretize the linear system (2.20) and obtain the following problem

Find the n-th Newton increment $\Delta P_n^{(k+1)} := Q \in (H^1(\Omega))^{3\times 3} = (H^1(\Omega))^9$ *such that for all* $R \in (H^1(\Omega))^9$

$$a_{P,n}^{(k)}(Q, R) = \mathbf{F}_{P,n}^{(k)}(R).$$

Here, we use $(H^1(\Omega))^9$ when we have pure homogeneous Neumann boundary conditions and replace $(H^1(\Omega))^9$ by $(H^1_0(\Omega, \partial\Omega_{D,P}))^9$ when we introduce Dirichlet boundary conditions on $\partial\Omega_{D,P}$. The choice of the appropriate space is due to the problem we consider. Note that in the Newton iteration we $P + \Delta P \in \mathrm{GL}^+(3)$ is not explicitely enforced.

The abbreviations $a^{(k)}_{P,n}(Q, R)$ and $\mathbf{F}^{(k)}_{P,n}(R)$ are used for

$$\begin{aligned} a^{(k)}_{P,n}(Q,R) \ := \ & \int_\Omega 2\mu_e \big((\mathrm{sym}(P^{-1}QP^{-1}F_\nabla), P^{-1}RP^{-1}F_\nabla)_F \\ & \quad + (\mathrm{sym}(P^{-1}F_\nabla - \mathrm{Id}\,), P^{-1}(QP^{-1}R + RP^{-1}Q)P^{-1}F_\nabla)_F\big) \ d\mathbf{x} \\ & + \int_\Omega \lambda_e \big(\ \mathrm{tr}(P^{-1}QP^{-1}F_\nabla)\mathrm{tr}(P^{-1}RP^{-1}F_\nabla) \\ & + \mathrm{tr}(P^{-1}F_\nabla - \mathrm{Id}\,)\mathrm{tr}(P^{-1}(QP^{-1}R + RP^{-1}Q)P^{-1}F_\nabla)\big) \ d\mathbf{x} \\ & + \int_\Omega 4\mu_e h^+(PP^TQ + PQ^TP + QP^TP - Q, R)_F \ d\mathbf{x} \\ & + \int_\Omega \mu_e \big(\ (L_c^2 + L_c^q \|\nabla P\|_F{}^{q-2})(\nabla Q, \nabla R)_F \\ & \qquad + (q-2)L_c^q \|\nabla P\|_F{}^{q-4}(\nabla P, \nabla Q)_F(\nabla P, \nabla R)_F\big) \ d\mathbf{x} \end{aligned} \tag{2.21}$$

and

$$\begin{aligned} \mathbf{F}^{(k)}_{P,n}(R) \ := \ & \int_\Omega f_P^T \mathbf{v} \ d\mathbf{x} \\ & + \int_\Omega 2\mu_e (\mathrm{sym}(P^{-1}F_\nabla - \mathrm{Id}\,), P^{-1}RP^{-1}F_\nabla)_F \ d\mathbf{x} \\ & + \int_\Omega \lambda_e \mathrm{tr}(P^{-1}F_\nabla - \mathrm{Id}\,)\mathrm{tr}(P^{-1}RP^{-1}F_\nabla) \ d\mathbf{x} \\ & + \int_\Omega 4\mu_e h^+(P^TP - \mathrm{Id}\,, P^TR)_F \ d\mathbf{x} \\ & - \int_\Omega \mu_e \big(\ (L_c^2 + L_c^q \|\nabla P\|_F^{q-2})(\nabla P, R)_F\big) \ d\mathbf{x}\ , \end{aligned} \tag{2.22}$$

with $P := P^{(k+1)}_{n-1}, Q := \Delta P^{(k+1)}_n$, and $F_\nabla = \nabla\boldsymbol{\varphi}$.

As in the case of P-elasticity we show in the next section that the quadratic form $a_P(\cdot,\cdot)$ is continuous with respect to the H^1-norm. Due to the presence of $\|P^TP - \mathrm{Id}\,\|^2$ in J_2 and since P^{-1} appears in J_1 the problem is not convex with respect to P but strictly convex with respect to the highest derivative appearing in P.

2.2.1 Continuity of the quadratic form $a_P(Q, R)$

In this section we establish the continuity of the quadratic form $a_P(\cdot,\cdot)$ introduced in (2.21) with respect to the H^1-norm. We again assume that the parameters μ_e,

λ_e, h^+, and L_c can be bounded by their maximum values over the domain Ω such that we can neglect them in the further considerations.

We consider every term in (2.21) separately. We use the Cauchy-Schwarz-inequality and the other tools introduced in Section 2.1.1 and obtain for the first integral in (2.21) the following two estimates

$$
\begin{aligned}
&\int_\Omega (\mathrm{sym}(P^{-1}QP^{-1}F_\nabla), P^{-1}RP^{-1}F_\nabla)_F \; d\mathbf{x} \\
= \; & \frac{1}{2} \int_\Omega (P^{-1}QP^{-1}F_\nabla, P^{-1}RP^{-1}F_\nabla)_F \; d\mathbf{x} + \int_\Omega (F_\nabla^T P^{-T} Q^T P^{-T}, P^{-1}RP^{-1}F_\nabla)_F \; d\mathbf{x} \\
= \; & \frac{1}{2} \big((P^{-1}QP^{-1}F_\nabla, P^{-1}RP^{-1}F_\nabla)_{L_2(\Omega)} + (F_\nabla^T P^{-T} Q^T P^{-T}, P^{-1}RP^{-1}F_\nabla)_{L_2(\Omega)} \big) \\
\le \; & \|P^{-1}QP^{-1}F_\nabla\|_{L_2(\Omega)} \|P^{-1}RP^{-1}F_\nabla\|_{L_2(\Omega)} \\
\le \; & \|P^{-1}\|^4_{L_2(\Omega)} \|F_\nabla\|^2_{L_2(\Omega)} \|R\|_{L_2(\Omega)} \|Q\|_{L_2(\Omega)} \\
\le \; & \|P^{-1}\|^4_{L_2(\Omega)} \|F_\nabla\|^2_{L_2(\Omega)} \|R\|_{H^1(\Omega)} \|Q\|_{H^1(\Omega)}
\end{aligned}
$$

and

$$
\begin{aligned}
&\int_\Omega (\mathrm{sym}(P^{-1}F_\nabla - \mathrm{Id}\,), P^{-1}(QP^{-1}R + RP^{-1}Q)P^{-1}F_\nabla)_F \; d\mathbf{x} \\
\le \; & \|\mathrm{sym}(P^{-1}F_\nabla - \mathrm{Id}\,)\|_{L_2(\Omega)} \|P^{-1}QP^{-1}RP^{-1}F_\nabla + P^{-1}RP^{-1}QP^{-1}F_\nabla\|_{L_2(\Omega)} \\
\le \; & \frac{1}{2} \|P^{-1}F_\nabla + F_\nabla^T P^{-1} - 2 \cdot \mathrm{Id}\,\|_{L_2(\Omega)} (\|P^{-1}QP^{-1}RP^{-1}F_\nabla\|_{L_2(\Omega)} \\
& \qquad\qquad\qquad\qquad + \|P^{-1}RP^{-1}QP^{-1}F_\nabla\|_{L_2(\Omega)}) \\
\le \; & (\|P^{-1}F_\nabla\|_{L_2(\Omega)} + \|\mathrm{Id}\,\|_{L_2(\Omega)})(2\|P^{-1}\|^3_{L_2(\Omega)} \|F_\nabla\|_{L_2(\Omega)} \|Q\|_{L_2(\Omega)} \|R\|_{L_2(\Omega)}) \\
\le \; & 2(\, \|P^{-1}\|_{L_2(\Omega)} \|F_\nabla\|_{L_2(\Omega)} + 3|\Omega| \,) \|P^{-1}\|^3_{L_2(\Omega)} \|F_\nabla\|_{L_2(\Omega)} \|Q\|_{H^1(\Omega)} \|R\|_{H^1(\Omega)},
\end{aligned}
$$

with $|\Omega|$ being the volume of the domain Ω, i.e., $|\Omega| = \int_\Omega 1 \; d\mathbf{x}$. The second integral of (2.21) again contains products of traces. Thus, we use (2.9) and get

$$
\begin{aligned}
&\int_\Omega \mathrm{tr}(P^{-1}QP^{-1}F_\nabla)\mathrm{tr}(P^{-1}RP^{-1}F_\nabla) \; d\mathbf{x} \\
\le \; & 3 \int_\Omega \|P^{-1}QP^{-1}F_\nabla\|_F \|P^{-1}RP^{-1}F_\nabla\|_F \; d\mathbf{x} \\
\le \; & 3\|P^{-1}QP^{-1}F_\nabla\|_{L_2(\Omega)} \|P^{-1}RP^{-1}F_\nabla\|_{L_2(\Omega)} \\
\le \; & 3\|P^{-1}\|^4_{L_2(\Omega)} \|F_\nabla\|^2_{L_2(\Omega)} \|Q\|_{L_2(\Omega)} \|R\|_{L_2(\Omega)} \\
\le \; & 3\|P^{-1}\|^4_{L_2(\Omega)} \|F_\nabla\|^2_{L_2(\Omega)} \|Q\|_{H^1(\Omega)} \|R\|_{H^1(\Omega)}
\end{aligned}
$$

and

$$\begin{aligned}
&\int_\Omega \mathrm{tr}(P^{-1}F_\nabla - \mathrm{Id}\,)\mathrm{tr}(P^{-1}(QP^{-1}R + RP^{-1}Q)P^{-1}F_\nabla)\ d\mathbf{x}\\
\leq\ & 3\int_\Omega \|P^{-1}F_\nabla - \mathrm{Id}\,\|_F\|P^{-1}QP^{-1}RP^{-1}F_\nabla + P^{-1}RP^{-1}QP^{-1}F_\nabla\|_F\ d\mathbf{x}\\
\leq\ & 3\|P^{-1}F_\nabla - \mathrm{Id}\,\|_{L_2(\Omega)}\|P^{-1}QP^{-1}RP^{-1}F_\nabla + P^{-1}RP^{-1}QP^{-1}F_\nabla\|_{L_2(\Omega)}\\
\leq\ & 3(\|P^{-1}F_\nabla\|_{L_2(\Omega)} + \|\mathrm{Id}\,\|_{L_2(\Omega)})(\|P^{-1}QP^{-1}RP^{-1}F_\nabla\|_{L_2(\Omega)} + \|P^{-1}RP^{-1}QP^{-1}F_\nabla\|_{L_2(\Omega)})\\
\leq\ & 3(\ \|P^{-1}\|_{L_2(\Omega)}\|F_\nabla\|_{L_2(\Omega)} + 3|\Omega|\ )(2\|P^{-1}\|^3_{L_2(\Omega)}\|F_\nabla\|_{L_2(\Omega)}\|Q\|_{L_2(\Omega)}\|R\|_{L_2(\Omega)})\\
\leq\ & 6(\ \|P^{-1}\|_{L_2(\Omega)}\|F_\nabla\|_{L_2(\Omega)} + 3|\Omega|\ )\|P^{-1}\|^3_{L_2(\Omega)}\|F_\nabla\|_{L_2(\Omega)}\|Q\|_{H^1(\Omega)}\|R\|_{H^1(\Omega)}.
\end{aligned}$$

Now we consider the third integral arising from $\|P^TP - \mathrm{Id}\,\|^2$

$$\begin{aligned}
&\int_\Omega (PP^TQ + PQ^TP + QP^TP - Q, R)_F\ d\mathbf{x}\\
&\quad\leq\ \|PP^TQ + PQ^TP + QP^TP - Q\|_{L_2(\Omega)}\|R\|_{L_2(\Omega)}\\
&\quad\leq\ \big(\|PP^TQ + PQ^TP + QP^TP\|_{L_2(\Omega)} + \|Q\|_{L_2(\Omega)}\big)\,\|R\|_{L_2(\Omega)}\\
&\quad\leq\ \big(\|P\|^2_{L_2(\Omega)} + 1\big)\,\|Q\|_{L_2(\Omega)}\|R\|_{L_2(\Omega)}\\
&\quad\leq\ \big(\|P\|^2_{L_2(\Omega)} + 1\big)\,\|Q\|_{H^1(\Omega)}\|R\|_{H^1(\Omega)}.
\end{aligned}$$

Before we estimate the last integral, we consider the inner product between the gradients occurring in the integral separately

$$\int_\Omega (\nabla Q, \nabla R)_F\ d\mathbf{x} = (\nabla Q, \nabla R)_{L_2(\Omega)} \leq \|\nabla Q\|_{L_2(\Omega)}\|\nabla R\|_{L_2(\Omega)} \leq \|Q\|_{H^1(\Omega)}\|R\|_{H^1(\Omega)}.$$

Additionally, we define the maximum value of the gradient of P, i.e., ∇P, by

$$c_{\nabla P} := \max_{\mathbf{x}\in\Omega}\ \max_{i,j,k=1\ldots3} (\partial_k P_{ij})^2.$$

Thus, we obtain

$$\begin{aligned}
\int_\Omega \|\nabla P\|_F^{q-2}(\nabla Q, \nabla R)_F\ d\mathbf{x}\ &=\ \int_\Omega (\sum_{i,j,k=1}^{3}(\partial_k P_{ij})^2)^{q-2}(\nabla Q, \nabla R)_F\ d\mathbf{x}\\
&\leq\ \int_\Omega (27\max_{i,j,k=1\ldots3}(\partial_k P_{ij})^2)^{q-2}(\nabla Q, \nabla R)_F\ d\mathbf{x}\\
&\leq\ 27c_{\nabla P}^{q-2}\int_\Omega (\nabla Q, \nabla R)_F\ d\mathbf{x}\\
&\leq\ 27c_{\nabla P}^{q-2}\|Q\|_{H^1(\Omega)}\|R\|_{H^1(\Omega)}
\end{aligned}$$

and

$$\begin{aligned}
\int_\Omega \|\nabla P\|_F^{q-4}(\nabla P, \nabla Q)_F(\nabla P, \nabla R)_F\ d\mathbf{x}\ &\leq\ \int_\Omega \|\nabla P\|_F^{q-2}\|\nabla Q\|_F\|\nabla R\|_F\ d\mathbf{x}\\
&\leq\ 27c_{\nabla P}^{q-2}\|\nabla Q\|_{L_2(\Omega)}\|\nabla R\|_{L_2(\Omega)}\\
&\leq\ 27c_{\nabla P}^{q-2}\|Q\|_{H^1(\Omega)}\|R\|_{H^1(\Omega)}.
\end{aligned}$$

Hence, we have shown that the quadratic form $a_P(\cdot,\cdot)$, cf. (2.21), is continuous with respect to the H^1-norm, i.e.,

$$a_P(Q,R) \le C(P)\ \|Q\|_{H^1(\Omega)}\|R\|_{H^1(\Omega)}.$$

2.3 Numerical results for the staggered scheme

In this chapter we present results from computations with our staggered algorithm. We consider three different test computations. In Section 2.3.1 we present results for computations with predetermined solutions P and $\boldsymbol{\varphi}$. In Sections 2.3.2 and 2.3.3 the results for the computation of a torsion up to an angle of $\frac{\pi}{2}$ are presented. Section 2.3.2 uses the micromorphic model as presented in (1.1) in Chapter 1. In Section 2.3.3 we use a modified micromorphic model where the volumetric response is governed by a determinant term instead of a trace term as in Section 2.3.2. This modified model is more realistic for large volumetric stretch. The computations are carried out on a computer with an Intel Core i7 quad core processor with 2.67 GHz and 12 GB memory.

It is common to all calculations that the linear systems occurring in the Newton iterations for $\boldsymbol{\varphi}$ and P, respectively, were solved by using PETSc [7, 5, 6]. We solve the P-elastic system with a conjugate gradient solver without using a preconditioner. For the system occurring in the subproblem for the micromorphic field P, i.e., the q-Laplacian problem, we use a direct LU decomposition from UMFPACK [20] or MUMPS [26]. Let us note that none of the computations was performed in parallel. For the P-elastic problem we later introduce the FETI-DP algorithm and thus obtain a more efficient solver; cf. Chapter 3. Note, that we have by now not implemented the parallel FETI-DP solver in the staggered approach.

All of our computations are tested for the unit cube, i.e., $\Omega = \Omega_{\text{c}} = [0,1]^3$. Additionally, in Sections 2.3.2 and 2.3.3, we consider a cylindrical geometry with height 2 and diameter 1, i.e., $\Omega = \Omega_{\text{cyl}} = \{(x,y,z)^T = \mathbf{x} \in \mathbb{R}^3 : \sqrt{x^2+y^2} \le 0.5 \wedge z \in [0,2]\}$. The meshes for the cylinder are generated with Netgen; cf. [87, 86]. In contrast to the cylinder we discretize the unit cube in a regular way. Therefore, we first decompose Ω_{c} into hexahedra. These are decomposed into tetrahedra by introducing one additional point in the center of each hexahedron. We connect this midpoint with each vertex of the related hexahedron. This results in 6 pyramids with square bases. By splitting each base into two triangles we obtain 12 tetrahedra for each hexahedron; cf. Figure 2.1. Since we use quadratic elements, we have to introduce additional points on the edges of the tetrahedra. The number of degrees of freedom for a mesh of the unit cube can be computed from h by

$$3\left(\left(2\cdot\frac{1}{h}\right)^3 + \left(2\cdot\frac{1}{h}+1\right)^3\right).$$

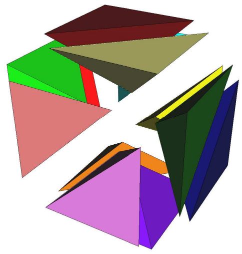

Figure 2.1: Decomposition of a hexahedron into 12 tetrahedra.

The material parameters are $E = 210$ kN/mm^2 and $\nu = 0.29$, which correspond to $\mu_e \approx 81.4$ kN/mm^2 and $\lambda_e \approx 112.4$ kN/mm^2. Furthermore, we choose $L_c = 1, h^+ = 0.1$, and $q = 4$. We choose the tolerance `tol` in (2.1) as $\texttt{tol} = 10^{-7}$, i.e., we stop the fixed point iteration if $\|\Delta P^{(k)}\|_{l_2}$ and $\|\Delta \boldsymbol{\varphi}^{(k)}\|_{l_2}$ are both smaller than 10^{-7}. The Newton iterations are carried out up to an accuracy of 10^{-5}.

In Sections 2.3.2 and 2.3.3 we choose the Dirichlet boundary for the P-elastic subproblem as the lower face of either the cube or the cylinder, i.e., $\partial\Omega_D := \{\mathbf{x} \in \Omega | z = 0\}$. Note, that we work with pure homogeneous Neumann boundary conditions in Sections 2.3.2 and 2.3.3 for the q-Laplacian problem, i.e., $\partial\Omega_{D,P} = \emptyset$. Otherwise, in Section 2.3.1 we have Dirichlet boundary for the P-elasticity and the q-Laplacian problem. There we provide both subproblems with homogeneous Dirichlet boundary conditions on the whole surface of the unit cube, i.e., $\partial\Omega_D = \partial\Omega_{D,P} = \{\mathbf{x} \in \Omega_c | x \in \{0,1\} \vee y \in \{0,1\} \vee z \in \{0,1\}\}$.

2.3.1 Computations with P and φ given

The first tests are carried out for a reduced minimization problem, i.e.,

$$
\begin{aligned}
\min_{(P,\boldsymbol{\varphi})} \int_\Omega & \mu_e \|\mathrm{sym}(P^{-1}F_\nabla - \mathrm{Id}\,)\|_F^2 + \frac{\lambda_e}{2}\left(\mathrm{tr}(P^{-1}F_\nabla - \mathrm{Id}\,)\right)^2 \\
& + \mu_e \left(\frac{L_c^2}{2}\|\nabla P\|_F^2 + \frac{L_c^q}{q}\|\nabla P\|_F^q \right) \, d\mathbf{x} \\
& - \int_\Omega (f_{\boldsymbol{\varphi}}, \boldsymbol{\varphi})_F + (f_P, P)_F \, d\mathbf{x},
\end{aligned}
$$

where we have left out the term $\mu_e h^+ \|P^T P - \mathrm{Id}\,\|_F^2$ which penalizes the perturbation from P to a rotation. With these tests, we want to confirm that our staggered approach converges to a given solution. Hence, we choose a pair of variable $(P, \boldsymbol{\varphi})$. For such a pair $(P, \boldsymbol{\varphi})$ we compute $f_{\boldsymbol{\varphi}}$ and f_P such that the right hand side of the Newton algorithm becomes zero for $(P, \boldsymbol{\varphi})$. Thus, we know that the pair $(P, \boldsymbol{\varphi})$ is a stationary point of our problem.

We start the staggered scheme with an initial guess $(P^{(0)}, \boldsymbol{\varphi}^{(0)})$. This initial guess equals the chosen solution on the Dirichlet boundary, i.e., $(P^{(0)}(\mathbf{x}), \boldsymbol{\varphi}^{(0)}(\mathbf{x})) = (P(\mathbf{x}), \boldsymbol{\varphi}(\mathbf{x}))$ for $\mathbf{x} \in \{\mathbf{x} \in \Omega_c : x \in \{0,1\} \vee y \in \{0,1\} \vee z \in \{0,1\}\}$. In the other points of the cube we perturb the solution $(P, \boldsymbol{\varphi})$ to obtain an initial guess.

We consider two different sets of given a deformation $\boldsymbol{\varphi}$ and a micromorphic field P. We will denote these different sets as $\boldsymbol{\varphi}_i$ and P_i with $i \in \{1,2,3\}$. The initial guesses we will refer to as $\boldsymbol{\varphi}_i^{(0)}$ and $P_i^{(0)}$, respectively.

Example 1: As first setup we choose a linear function for the deformation $\boldsymbol{\varphi}_1$. P_1 is in accordance to $\boldsymbol{\varphi}_1$ chosen as its gradient $P = \nabla\boldsymbol{\varphi}_1$, i.e.,

$$\begin{aligned}
\boldsymbol{\varphi}_1 : \mathbb{R}^3 \to \mathbb{R}^3 \quad &; \quad \mathbf{x} \mapsto \begin{pmatrix} x - z \\ -2x + y + 3z \\ -y - 2z \end{pmatrix}, \\
P_1 : \mathbb{R}^3 \to \mathbb{R}^{3\times 3} \quad &; \quad \mathbf{x} \mapsto \begin{pmatrix} 1 & 0 & -1 \\ -1 & 1 & 3 \\ 0 & -1 & -2 \end{pmatrix}.
\end{aligned}$$

Thus, we have $\nabla P_1 = 0$ and $P_1^{-1} F_{\nabla,1} = P_1^{-1}\nabla\boldsymbol{\varphi}_1 = \mathrm{Id}$. Hence, we know in advance that the minimum energy must be zero. Furthermore, the body forces $f_{\boldsymbol{\varphi}}$ and f_P are zero.

Example 2: For the second setup we again choose $P_2 = \nabla\varphi_2$. The deformation $\boldsymbol{\varphi}_2$ is chosen as a quadratic function. Hence, we can represent $\boldsymbol{\varphi}_2$ exactly with our implementation since we work with piecewise quadratic nodal basis functions, i.e.,

$$\begin{aligned}
\boldsymbol{\varphi}_2 : \mathbb{R}^3 \to \mathbb{R}^3 \quad &; \quad \mathbf{x} \mapsto \begin{pmatrix} (x+1)(z+1) \\ (x+1)(y+1) \\ (y+1)(z+1) \end{pmatrix}, \\
P_2 : \mathbb{R}^3 \to \mathbb{R}^{3\times 3} \quad &; \quad \mathbf{x} \mapsto \begin{pmatrix} (z+1) & 0 & (x+1) \\ (y+1) & (x+1) & 0 \\ 0 & (z+1) & (y+1) \end{pmatrix}.
\end{aligned}$$

P_2 is linear, due to the choice as the gradient of the deformation. Hence, it can also be represented exactly by our nodal basis functions. Since ∇P_2 is non zero we obtain a minimizing energy of $12\mu_e$. Again the body forces are computed to be equal to zero, i.e., $f_{\boldsymbol{\varphi}} = 0$ and $f_P = 0$.

All calculations lead to the correct solution if the fixed point iteration converges. For both examples we observe that they converge even for strong perturbations. As we would expect the fixed point iteration converges for both examples within one step if we only perturb one variable in the initial guess and start our staggered algorithm by minimizing the energy with respect to the perturbed variable.

Comparing Example 1 and Example 2 we notice that Example 2 is more stable with respect to the perturbations in the initial guess than the first one, i.e., in Example 2 we can even start with the identities $P^{(0)} = \mathrm{Id}$ and $\boldsymbol{\varphi}^{(0)} = \mathbf{x}$ outside the Dirichlet boundary and obtain a convergent fixed point iteration. The problem within the fixed point iteration for Example 1 and Example 2 lies in the convergence of the Newton iteration for the micromorphic field, i.e., the minimization step for the variable P. We observe that the Newton iterations for P sometimes do not converge and hence also the fixed point iteration does not converge. These problems in the convergence of the Newton iteration occur earlier with respect to the perturbations of the initial guess if we start with the minimization problem in P rather than starting with the one in $\boldsymbol{\varphi}$. Even the number of fixed point iteration steps is slightly smaller if we start with the minimization for $\boldsymbol{\varphi}$ than if we start with the one in P. Hence, we concluded that it might be always better to start with the minimization problem in $\boldsymbol{\varphi}$. Furthermore, these observations give rise to the idea to investigate the effects of damped Newton iterations for the minimization problem in P in future research.

If the fixed point iteration converges, the Euclidean norms of the fixed point iteration increments $\Delta\boldsymbol{\varphi}^{(k)}$ and $\Delta P^{(k)}$ converge to zero with a convergence rate of order 1; cf. Figures 2.2, 2.3, 2.4, and 2.5, in which the logarithm of the increments is displayed versus the number of fixed point iteration steps. Note, that the calculations for Example 2 need less fixed point iteration steps than the ones for Example 1.

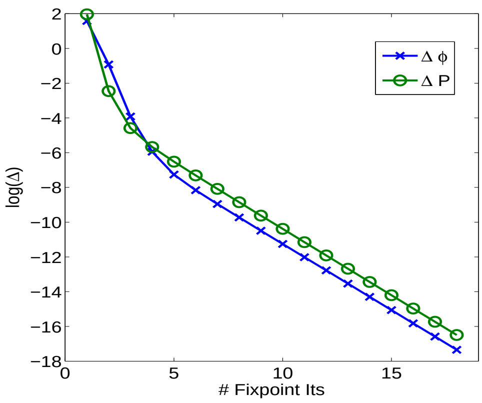

Figure 2.2: *Example 1, mesh with 1241 nodes, i.e., $h = 0.25$, first minimization in $\boldsymbol{\varphi}$ then in P. Initial guess:*
$\boldsymbol{\varphi}_1^{(0)} = (0.9\varphi_{1,1}, \varphi_{1,2}, 0.9\varphi_{1,3})^T$ *and*
$P_1^{(0)} = ((P_{1,11}, P_{1,12}, 0.9P_{1,13}), (0.9P_{1,21}, P_{1,22}, P_{1,23}), (P_{1,31}, 0.9P_{1,32}, P_{1,33}))^T$.

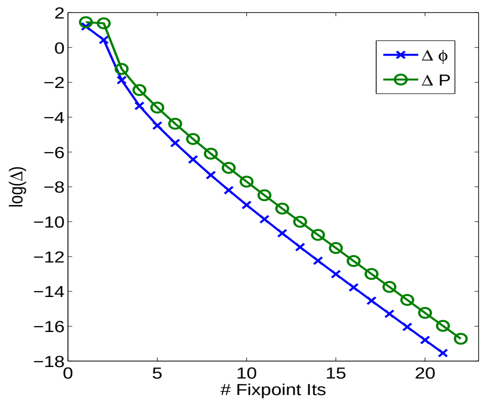

Figure 2.3: *Example 1, mesh with 9009 nodes, i.e., $h = 0.125$, first minimization in P then in $\boldsymbol{\varphi}$. Initial guess:*
$\boldsymbol{\varphi}_1^{(0)} = (0.9\varphi_{1,1}, \varphi_{1,2}, \varphi_{1,3})^T$ *and*
$P_1^{(0)} = P_1 - 0.1\,\mathrm{Id}$.

The convergence of the Newton iteration for P in Example 2 is monotone and quadratic with respect to the Euclidean norm of the correction term, i.e.,

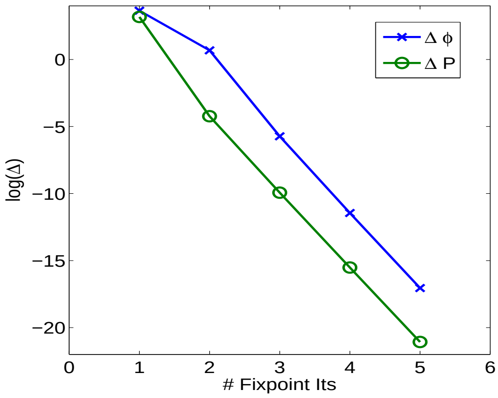

Figure 2.4: *Example 2, mesh with 1241 nodes, i.e.,* $h = 0.25$, *first minimization in* P *then in* $\boldsymbol{\varphi}$. *Initial guess:* $\boldsymbol{\varphi}_2^{(0)} = (0.8\varphi_{2,1}, \varphi_{2,2} - z, y\ \varphi_{2,3})^T$ *and* $P_2^{(0)} = ((P_{2,11}, P_{2,12} + y, P_{2,13}), (0.9P_{2,21}, P_{2,22}, P_{2,23}), (P_{2,31}, P_{2,32}, P_{2,33} - x))^T$.

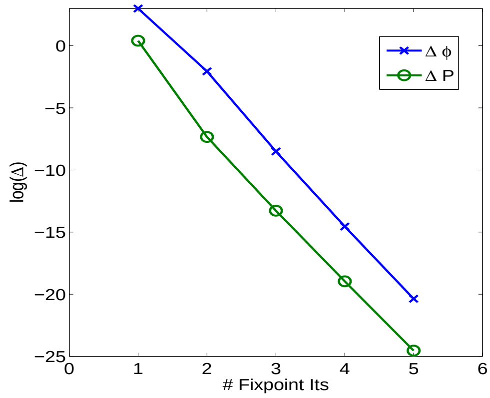

Figure 2.5: *Example 2, mesh with 9009 nodes, i.e.,* $h = 0.125$, *first minimization in* $\boldsymbol{\varphi}$ *then in* P. *Initial guess:* $\boldsymbol{\varphi}_2^{(0)} = (0.9\varphi_{2,1}, \varphi_{2,2}, \varphi_{2,3})^T$ *and* $P_2^{(0)} = P_2 - 0.1\,\mathrm{Id}$.

$\|\Delta P_n^{(k+1)}\|_{l_2}$, and with respect to the Euclidean norm of the residuum. For Example 1 we observe monotone and quadratic convergence for $\|\Delta P_n^{(k+1)}\|_{l_2}$ and the residuum if we start our fixed point iteration with the minimization problem in $\boldsymbol{\varphi}$ as displayed in (2.1). Instead, if we start with the problem in P in our fixed point iteration, we observe monotone but not quadratic convergence with respect to $\|\Delta P_n^{(k+1)}\|_{l_2}$ and the residuum. Note that with respect to the residuum we also observe quadratic convergence but not with respect to $\|\Delta P_n^{(k+1)}\|_{l_2}$. These observations confirm us in the idea always to start with the minimization in $\boldsymbol{\varphi}$. This idea was implemented in the torsion calculations presented in Sections 2.3.2 and 2.3.2.

2.3.2 Torsion with linear volumetric term

In this section, we present numerical results for the torsion of the unit cube and the cylinder as described before. Since we set the body forces f_P and $f_{\boldsymbol{\varphi}}$ to zero we consider the following energy for our minimization problem

$$\begin{aligned} E(P, \boldsymbol{\varphi}) \quad := \quad & \int_\Omega \mu_e \|\mathrm{sym}(P^{-1}F_\nabla - \mathrm{Id}\,)\|_F^2 + \frac{\lambda_e}{2}\left(\mathrm{tr}(P^{-1}F_\nabla - \mathrm{Id}\,)\right)^2 \\ & + \mu_e h^+ \|P^T P - \mathrm{Id}\,\|_F^2 + \mu_e \left(\frac{L_c^2}{2}\|\nabla P\|_F^2 + \frac{L_c^q}{q}\|\nabla P\|_F^q\right)\, d\mathbf{x} \end{aligned}$$

with $F_\nabla = \nabla\boldsymbol{\varphi}$ as before. Note, that here the P-elasticity problem is linear (notably in the volumetric term $\frac{\lambda_e}{2}\left(\operatorname{tr}(P^{-1}F_\nabla - \mathrm{Id}\,)\right)^2)$; see the definition of the bilinear form in (2.7).

In the case of the unit cube we consider meshes with different mesh widths h. For the cylinder we use two meshes, i.e., one mesh with 876 nodes and a finer mesh with 3852 nodes. For the cube we choose the torsion axis in z-direction through the middle of the x-y-plane, i.e., $\{\mathbf{x} \in \Omega_\mathrm{c} : x = 0.5 \wedge y = 0.5 \wedge z \in [0,1]\}$. We choose the torsion axis in the same way for the cylinder, i.e., $\{\mathbf{x} \in \Omega_\mathrm{cyl} : x = 0 \wedge y = 0 \wedge z \in [0,2]\}$. We obtain the torsion of our geometry by using Dirichlet boundary conditions, i.e., in each load step we use the displacement between the configuration of the current load step and the contorted configuration of the next load step as boundary value on the upper face of the body in the P-elasticity subproblem for $\boldsymbol{\varphi}$. As upper faces we define $\{\mathbf{x} \in \Omega_\mathrm{c} : z = 1\}$ and $\{\mathbf{x} \in \Omega_\mathrm{cyl} : z = 2\}$ for the cube and the cylinder, respectively. As mentioned before, we use homogeneous Dirichlet boundary conditions for the displacement on the lower face of either the cube or the cylinder, i.e., $\{\mathbf{x} \in \Omega : z = 0\}$. These homogeneous Dirichlet boundary conditions keep the lower face of the body fixed.

For the minimization problem in P we assume pure homogeneous Neumann boundary conditions. However, in a large neighborhood of $P = \mathrm{Id}$ we obtain an invertible tangent matrix by introducing $h^+\|P^TP - \mathrm{Id}\,\|_F^2$.

The overall torsion of $\frac{\pi}{2}$ is applied in steps of $\frac{\pi}{64}$ and the system is solved using a fixed point iteration in every step. Every fixed point iteration is started with the deformation $\boldsymbol{\varphi}$ and the micromorphic field P obtained in the last step. The start values for the first fixed point iteration are $\boldsymbol{\varphi}(\mathbf{x}) = \mathbf{x}$ and $P = \mathrm{Id}\,$.

In our numerical experiments, the Newton iterations for P converge monotonously independent of the geometry, the mesh size or the overall torsion angle. At most we need 6 Newton iterations for the unit cube and 5 for the cylinder. The number of Newton iterations decreases within each fixed point iteration. Moreover, the maximum number of Newton iterations needed, decreases with higher overall angle. For both geometries we observe that the finer we choose our mesh the earlier we obtain quadratic convergence in the Newton iteration with respect to the Euclidean norm of $\Delta P_n^{(k)}$.

The number of fixed point iteration steps needed, increases monotonously with the overall angle if we consider the unit cube. The behavior for the cylindric geometry is slightly different. There, we first observe a decrease of fixed point iteration steps before the number of iterations increases. Furthermore, the finer our mesh is chosen, the more fixed point iteration steps we need independently of the geometry. Note that the minimum number of fixed point iteration steps needed for the cylinder is higher than the maximum number needed for the cube in our experiments.

The Euclidean norms of the fixed point iteration increments $\Delta\boldsymbol{\varphi}^{(k)}$ and $\Delta P^{(k)}$ converge to zero with a convergence rate of order 1; cf Figures 2.6, 2.7, 2.8, 2.9, 2.10, 2.11, 2.12 and 2.13 in which the logarithm of the increments is displayed versus the number of fixed point iteration steps. These results are nearly completely independent of the geometry and the overall torsion angle.

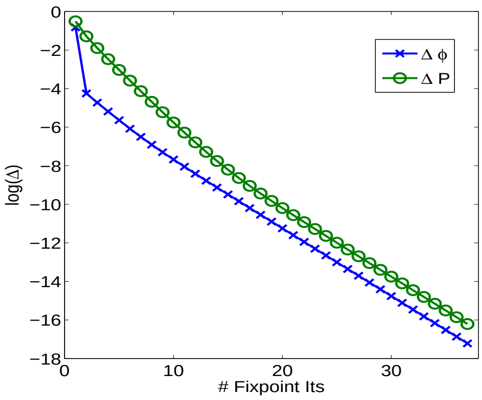

Figure 2.6: *Overall angle* $\frac{5\pi}{32}$*, mesh of the unit cube with 1241 nodes, i.e.,* $h = 0.25$*.*

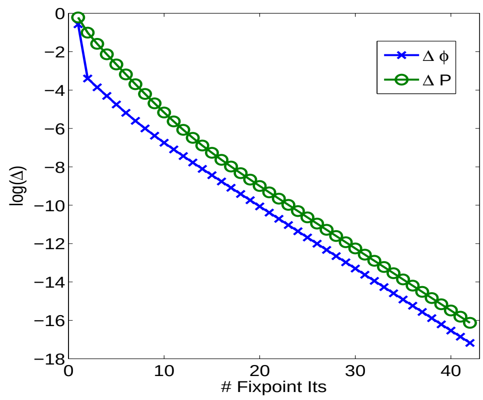

Figure 2.7: *Overall angle* $\frac{9\pi}{32}$*, mesh of the unit cube with 2331 nodes, i.e.,* $h = 0.2$*.*

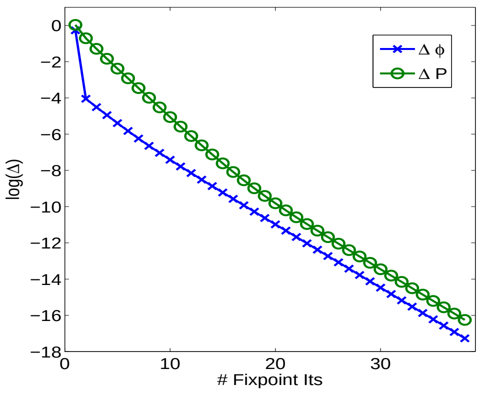

Figure 2.8: *Overall angle* $\frac{7\pi}{32}$*, mesh of the unit cube with 3925 nodes, i.e.,* $h = \frac{1}{6}$*.*

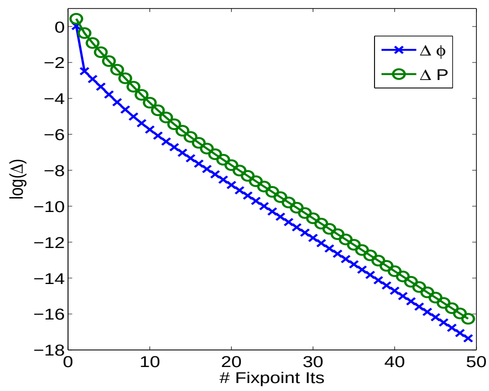

Figure 2.9: *Overall angle* $\frac{3\pi}{8}$*, mesh of the unit cube with 9009 nodes, i.e.,* $h = 0.125$*.*

Only in the case of the first loadstep for the cylinder we observe that the decrease is slower in the beginning than in the further fixed point iteration. Asymptotically, we observe the same behavior as before; see Figures 2.14 and 2.15.

In Figures 2.16 and 2.17, 2.18 and 2.19, 2.20 and 2.21, 2.22 and 2.23, 2.24 and 2.25, 2.26 and 2.27, 2.28 and 2.29, 2.30 and 2.31, 2.32 and 2.33, we present results for the unit cube. Here, we compare the results for our new model with the ones for standard linear elasticity for three different mesh sizes and different overall angles. The results for standard linear elasticity are obtained by setting

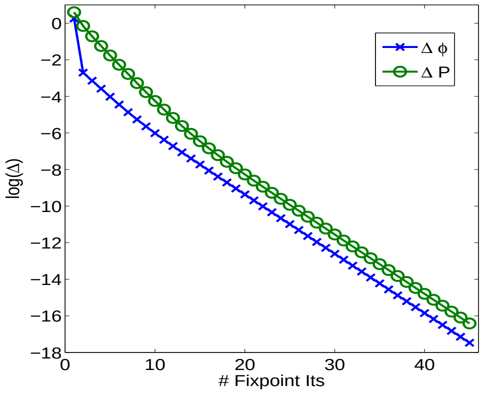

Figure 2.10: *Overall angle $\frac{\pi}{4}$, mesh of the unit cube with 12691 nodes, i.e., $h = \frac{1}{9}$.*

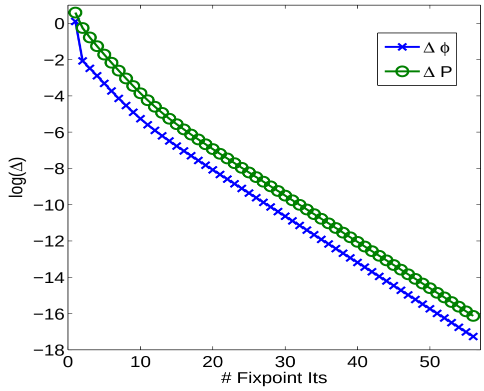

Figure 2.11: *Overall anlge $\frac{\pi}{2}$, mesh of the unit cube with 12691 nodes, i.e., $h = \frac{1}{9}$.*

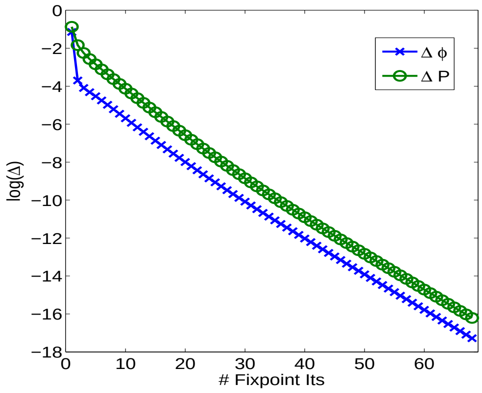

Figure 2.12: *Overall angle $\frac{25\pi}{64}$, mesh of the cylinder with 876 nodes.*

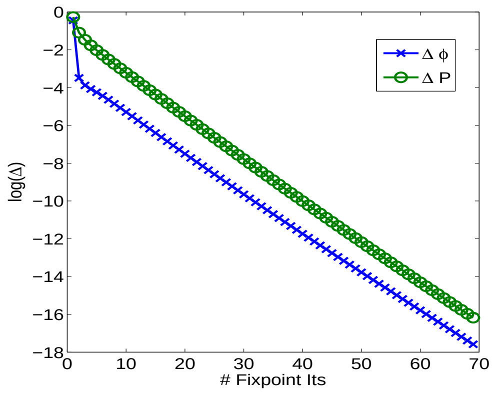

Figure 2.13: *Overall angle $\frac{17\pi}{64}$, mesh of the cylinder with 3852 nodes.*

$P = \mathrm{Id}$ throughout the whole torsion process. Furthermore, we present results for larger overall angles in Figures 2.34, 2.35, and 2.36.

Additionally considering the figures that we obtain for finer meshes of the unit cube, we observe an obvious influence of the mesh size on the accuracy of the solution; cf. Figures 2.34, 2.35, 2.36, 2.37, and 2.38.

Furthermore, we present cross sections of the contorted cubes. In addition to the figures presented before, the cross sections contain the values of $\|P^T P - \mathrm{Id}\,\|_F$ in each node. The quantity $\|P^T P - \mathrm{Id}\,\|_F$ measures the distance of the matrix P to a rotation. We observe that the values obtained for $\|P^T P - \mathrm{Id}\,\|_F$ decrease with a finer mesh and increase with an increasing overall angle. Considering the definition of the Frobenius norm, we record that we seem to obtain matrices very close to rotations; see Figures 2.39, 2.40, 2.41, 2.42, 2.43, 2.44, 2.45, and 2.46.

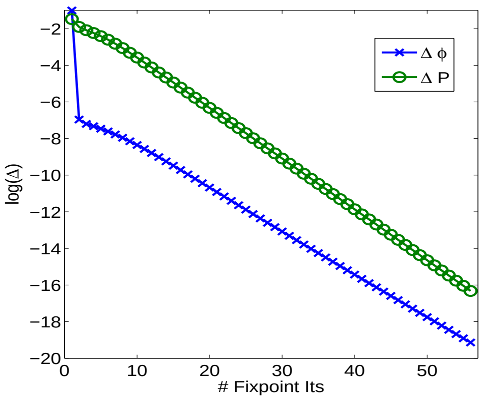

Figure 2.14: *First fixed point iteration for a mesh of the cylinder with 876 nodes.*

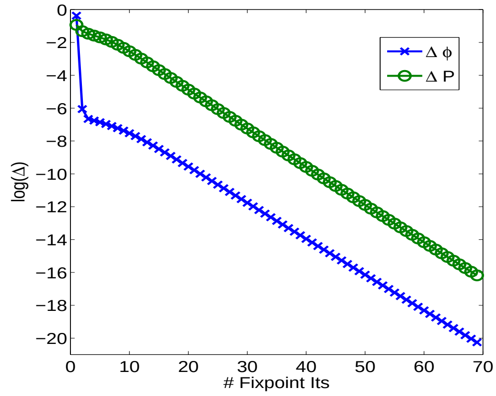

Figure 2.15: *First fixed point iteration for a mesh of the cylinder with 3852 nodes.*

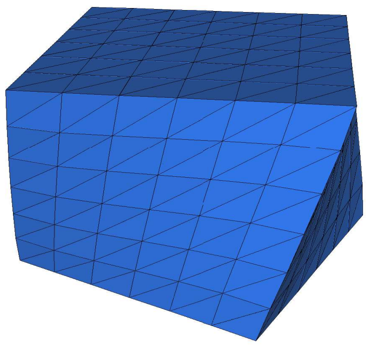

Figure 2.16: *Overall angle* $\frac{\pi}{8}$*, mesh of the unit cube with 3925 nodes.*

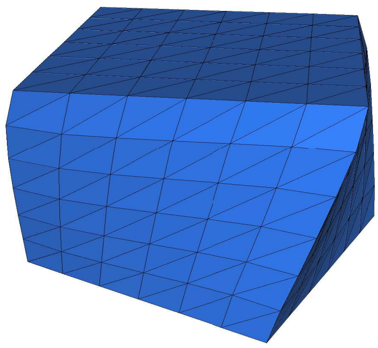

Figure 2.17: *Overall angle* $\frac{\pi}{8}$ *, mesh of the unit cube with 3925 nodes, standard linear elasticity* ($P = \mathrm{Id}$).

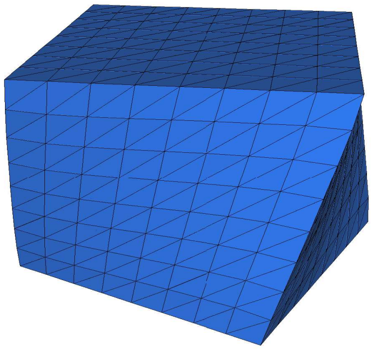

Figure 2.18: *Overall angle* $\frac{\pi}{8}$, *mesh of the unit cube with 9009 nodes.*

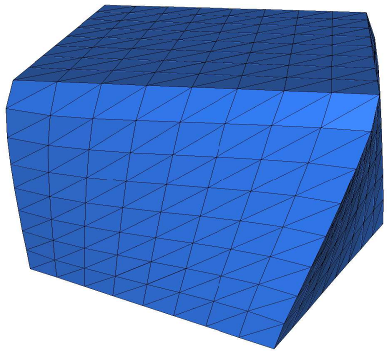

Figure 2.19: *Overall angle* $\frac{\pi}{8}$, *mesh of the unit cube with 9009 nodes, standard linear elasticity* ($P = \mathrm{Id}$).

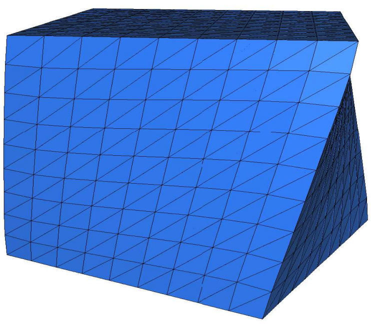

Figure 2.20: *Overall angle* $\frac{\pi}{8}$, *mesh of the unit cube with 12691 nodes.*

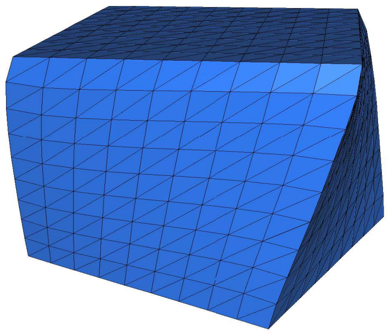

Figure 2.21: *Overall angle* $\frac{\pi}{8}$, *mesh of the unit cube with 12691 nodes, standard linear elasticity* ($P = \mathrm{Id}$).

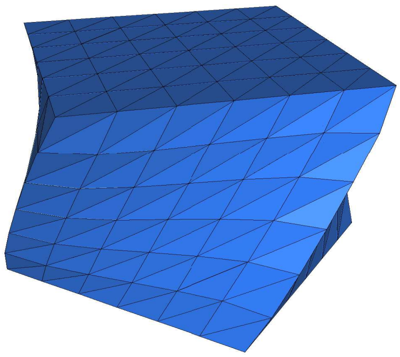

Figure 2.22: *Overall angle* $\frac{\pi}{4}$*, mesh of the unit cube with 3925 nodes.*

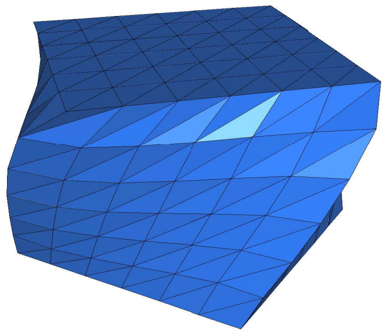

Figure 2.23: *Overall angle* $\frac{\pi}{4}$*, mesh of the unit cube with 3925 nodes, standard linear elasticity* $(P = \mathrm{Id}\,)$*.*

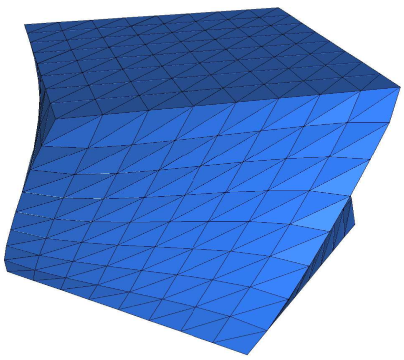

Figure 2.24: *Overall angle* $\frac{\pi}{4}$*, mesh of the unit cube with 9009 nodes.*

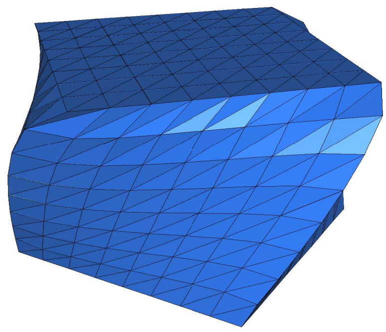

Figure 2.25: *Overall angle* $\frac{\pi}{4}$*, mesh of the unit cube with 9009 nodes, standard linear elasticity* $(P = \mathrm{Id}\,)$*.*

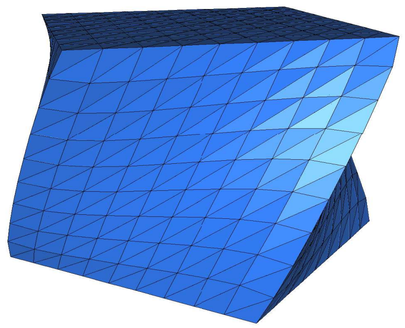

Figure 2.26: *Overall angle* $\frac{\pi}{4}$*, mesh of the unit cube with 12691 nodes.*

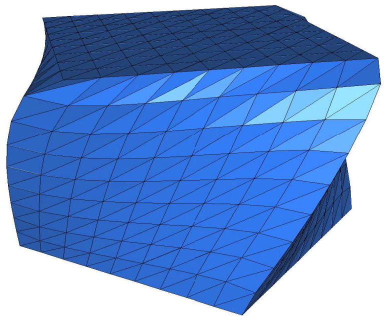

Figure 2.27: *Overall angle* $\frac{\pi}{4}$ *, mesh of the unit cube with 12691 nodes, standard linear elasticity (*$P = \mathrm{Id}$ *).*

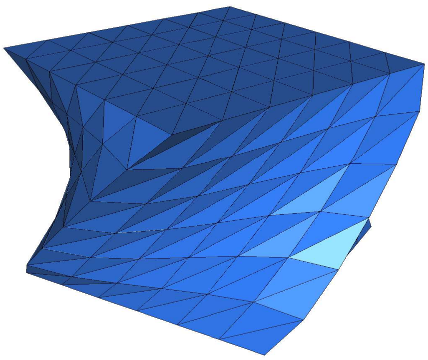

Figure 2.28: *Overall angle* $\frac{3\pi}{8}$*, mesh of the unit cube with 3925 nodes.*

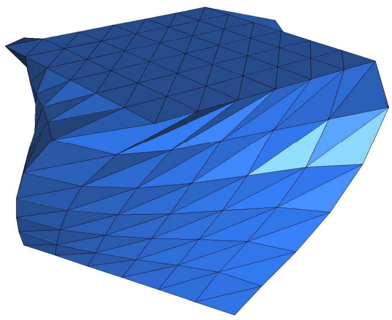

Figure 2.29: *Overall angle* $\frac{3\pi}{8}$*, mesh of the unit cube with 3925 nodes, standard linear elasticity (*$P = \mathrm{Id}$ *).*

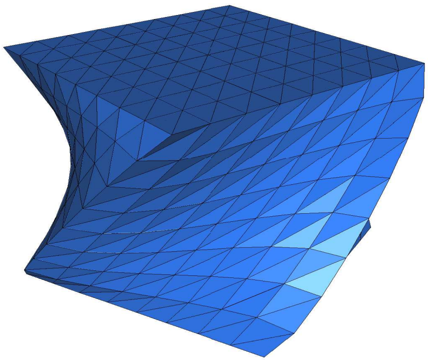

Figure 2.30: *Overall angle* $\frac{3\pi}{8}$*, mesh of the unit cube with 9009 nodes.*

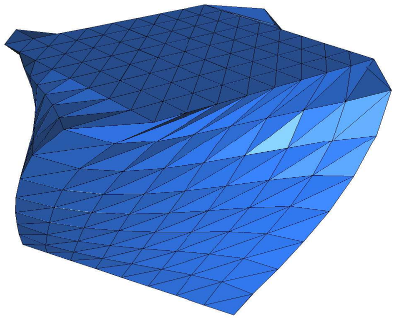

Figure 2.31: *Overall angle* $\frac{3\pi}{8}$ *, mesh of the unit cube with 9009 nodes, standard linear elasticity (*$P = \mathrm{Id}$ *).*

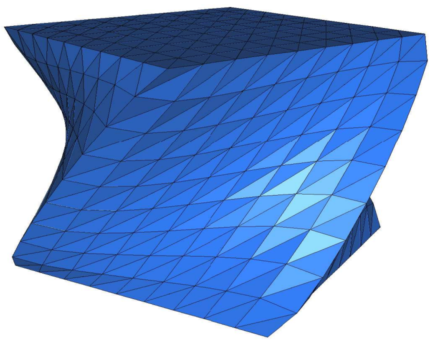

Figure 2.32: *Overall angle* $\frac{3\pi}{8}$*, mesh of the unit cube with 12691 nodes.*

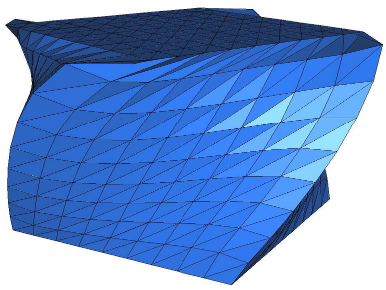

Figure 2.33: *Overall angle* $\frac{3\pi}{8}$ *, mesh of the unit cube with 12691 nodes, standard linear elasticity (*$P = \mathrm{Id}$ *).*

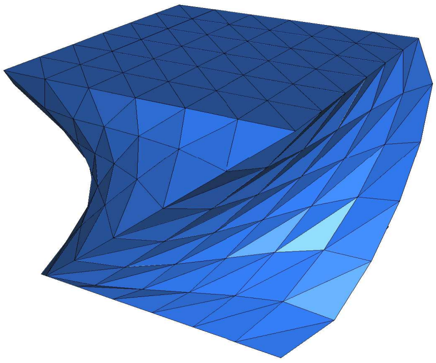

Figure 2.34: *Overall angle* $\frac{\pi}{2}$, *mesh of the unit cube with 3925 nodes.*

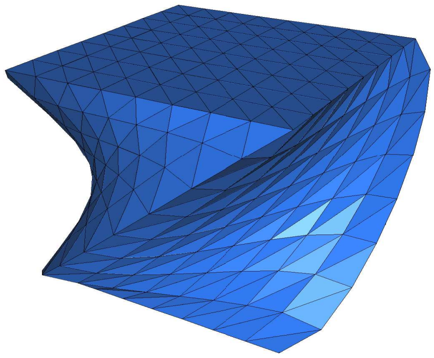

Figure 2.35: *Overall angle* $\frac{\pi}{2}$, *mesh of the unit cube with 9009 nodes.*

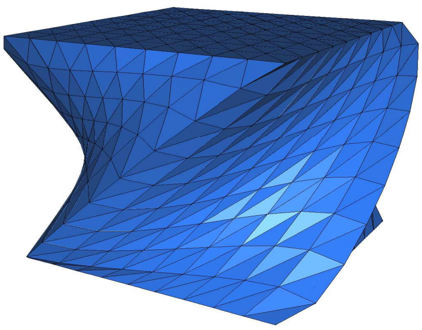

Figure 2.36: *Overall angle* $\frac{\pi}{2}$, *mesh of the unit cube with 12691 nodes.*

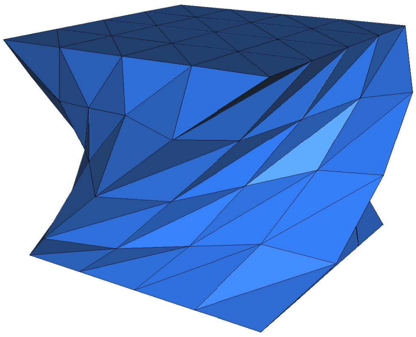

Figure 2.37: *Overall angle $\frac{\pi}{2}$, mesh of the unit cube with 1241 nodes.*

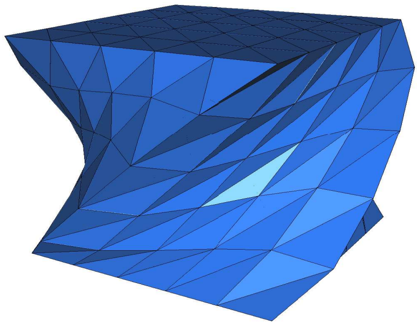

Figure 2.38: *Overall angle $\frac{\pi}{2}$, mesh of the unit cube with 2331 nodes.*

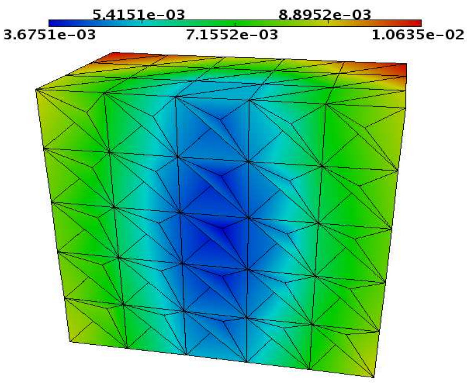

Figure 2.39: *Uncontorted mesh of the unit cube with 2331 nodes, with values of $\|P^T P - \mathrm{Id}\,\|_F$ for an overall angle of $\frac{\pi}{4}$.*

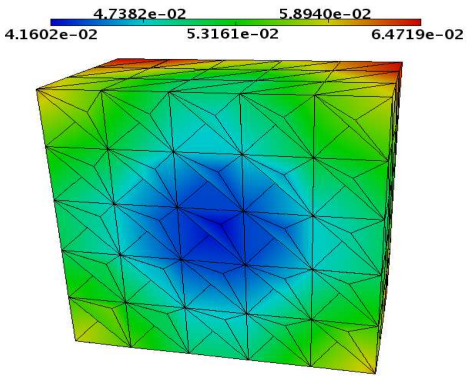

Figure 2.40: *Uncontorted mesh of the unit cube with 2331 nodes, with values of $\|P^T P - \mathrm{Id}\,\|_F$ for an overall angle of $\frac{\pi}{2}$.*

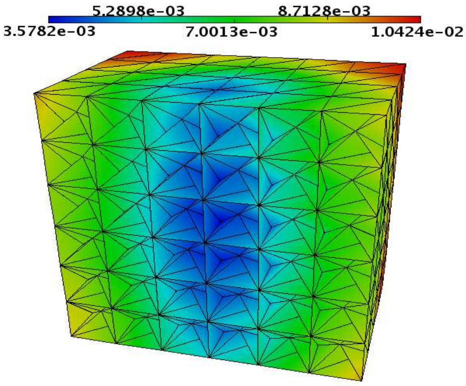

Figure 2.41: *Uncontorted mesh of the unit cube with 3925 nodes, with values of* $\|P^T P - \mathrm{Id}\,\|_F$ *for an overall angle of* $\frac{\pi}{4}$.

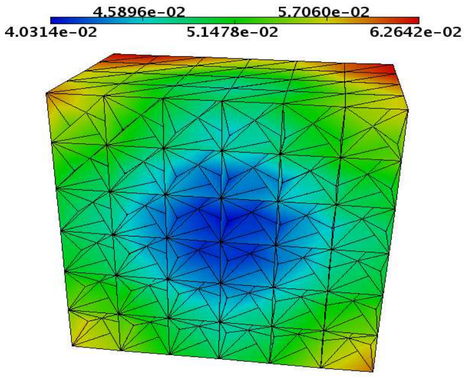

Figure 2.42: *Uncontorted mesh of the unit cube with 3925 nodes, with values of* $\|P^T P - \mathrm{Id}\,\|_F$ *for an overall angle of* $\frac{\pi}{2}$.

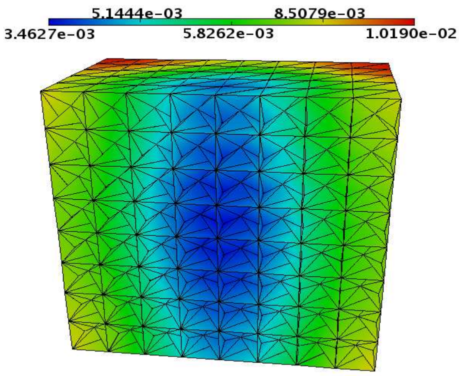

Figure 2.43: *Uncontorted mesh of the unit cube with 9009 nodes, with values of* $\|P^T P - \mathrm{Id}\,\|_F$ *for an overall angle of* $\frac{\pi}{4}$.

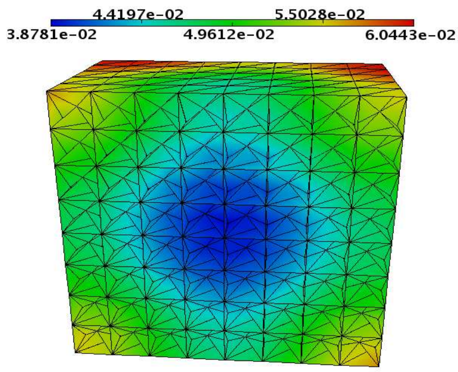

Figure 2.44: *Uncontorted mesh of the unit cube with 9009 nodes, with values of* $\|P^T P - \mathrm{Id}\,\|_F$ *for an overall angle of* $\frac{\pi}{2}$.

We present results for the cylinder in the Figures 2.47, 2.48, 2.49, 2.50, 2.51, 2.52, 2.53, and 2.54. The figures show contorted meshes of the cylinder of different mesh size and different overall angle. We again present two different types of figures. On the one hand we have figures showing the contorted cylinder itself; see Figures 2.47, 2.49, 2.51, and 2.53. On the other hand the cross sections introduced before are presented; cf. Figures 2.48, 2.50, 2.52, and 2.54. There, we observe that the values obtained for $\|P^T P - \mathrm{Id}\,\|_F$ decrease with a finer mesh and increase with an increasing overall angle as for the meshes of the unit cube.

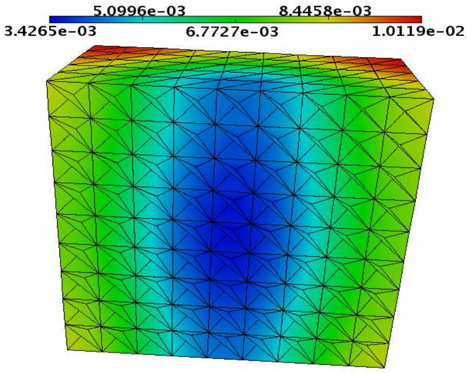

Figure 2.45: *Uncontorted mesh of the unit cube with 12691 nodes, with values of* $\|P^T P - \mathrm{Id}\,\|_F$ *for an overall angle of* $\frac{\pi}{4}$.

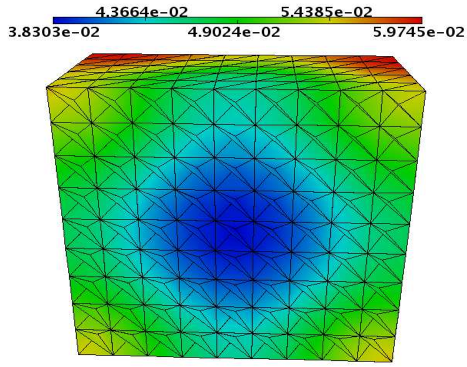

Figure 2.46: *Uncontorted mesh of the unit cube with 12691 nodes, with values of* $\|P^T P - \mathrm{Id}\,\|_F$ *for an overall angle of* $\frac{\pi}{2}$.

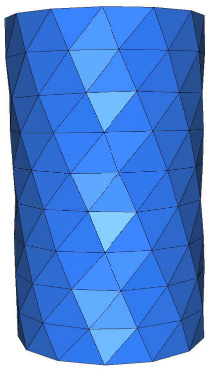

Figure 2.47: *Overall angle* $\frac{\pi}{4}$, *mesh of the cylinder with 876 nodes.*

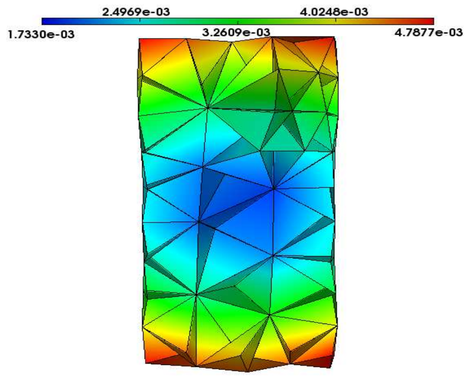

Figure 2.48: *Overall angle* $\frac{\pi}{4}$, *mesh of the cylinder with 876 nodes, with values of* $\|P^T P - \mathrm{Id}\,\|_F$.

In Figures 2.51 and 2.53 we observe a slight volumetric increase in the upper and lower part of the cylinder. Furthermore, we have a constriction in the middle of the geometry. These effects are due to using a quadratic energy to control the volumetric deformation, i.e., using

$$\frac{\lambda_e}{2}\left(\mathrm{tr}(P^{-1}F_{\nabla} - \mathrm{Id}\,)\right)^2$$

Hence, as an alternative, we also considered a more elaborate, nonlinear elasticity model which will be described in detail in Section 2.3.3.

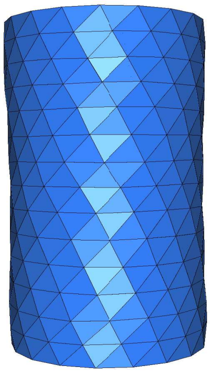

Figure 2.49: *Overall angle* $\frac{\pi}{4}$*, mesh of the cylinder with 3852 nodes.*

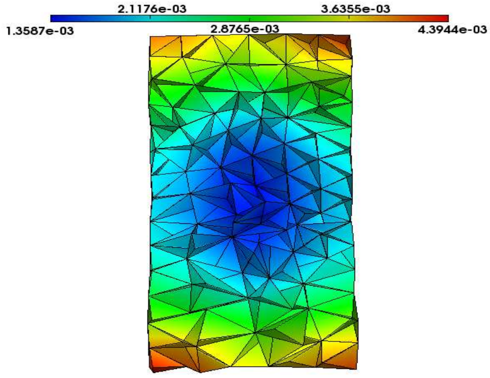

Figure 2.50: *Overall angle* $\frac{\pi}{4}$*, mesh of the cylinder with 3852 nodes, with values of* $\|P^T P - \mathrm{Id}\,\|_F$.

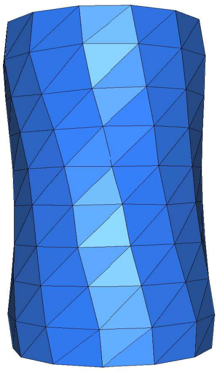

Figure 2.51: *Overall angle* $\frac{\pi}{2}$*, mesh of the cylinder with 876 nodes.*

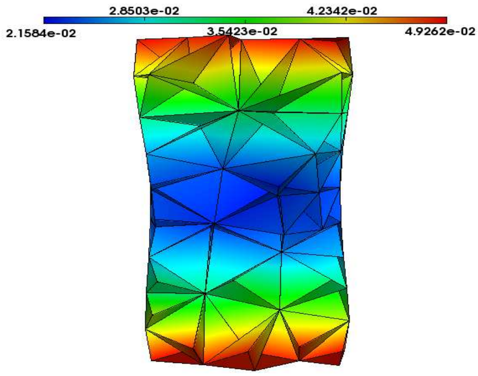

Figure 2.52: *Overall angle* $\frac{\pi}{2}$*, mesh of the cylinder with 876 nodes, with values of* $\|P^T P - \mathrm{Id}\,\|_F$.

2.3.3 Torsion with nonlinear volumetric term

Here, we present results for a torsion with a nonlinear elasticity formulation which we use to avoid the volumetric increase observed for the linearized model. We consider the same setting as in Section 2.3.2 but we make a slight change in the energy formulation. Therefore, we replace the quadratic volumetric term

$$\frac{\lambda_e}{2}\left(\mathrm{tr}(P^{-1}F_\nabla - \mathrm{Id}\,)\right)^2$$

by the general nonlinear volumetric term

$$\frac{\lambda_e}{4}\left((\det(F_\nabla) - 1)^2 + \left(\frac{1}{\det(F_\nabla)} - 1\right)^2\right).$$

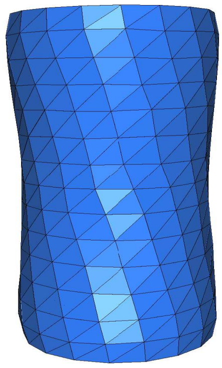

Figure 2.53: *Overall angle $\frac{\pi}{2}$, mesh of the cylinder with 3852 nodes.*

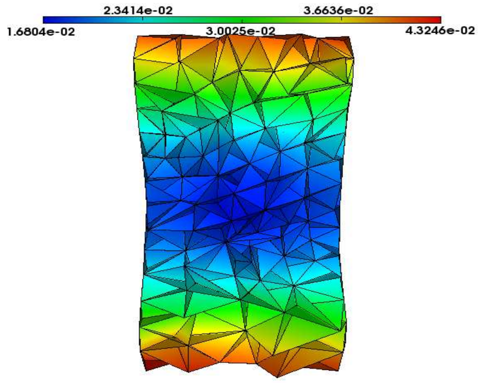

Figure 2.54: *Overall angle $\frac{\pi}{2}$, mesh of the cylinder with 3852 nodes, with values of $\|P^T P - \mathrm{Id}\,\|_F$.*

Both terms are linearization equivalent in $\boldsymbol{\varphi} = \mathbf{x}$, $P = \mathrm{Id}$, i.e., they lead to the same linearized formulations when $\boldsymbol{\varphi} = \mathbf{x}$, $P = \mathrm{Id}$. By this change we obtain a nonlinear P-elasticity formulation which has to be solved with several Newton iteration steps. Thus, we have to reformulate our Newton iteration introduced in Section 2.1 (2.4) as for the q-Laplacian problem; cf. (2.20), into

$$\partial^2_{\boldsymbol{\varphi}} J_1(P, \boldsymbol{\varphi}_{n-1}^{(k+1)}) \left(\boldsymbol{\varphi}_n^{(k+1)} - \boldsymbol{\varphi}_{n-1}^{(k+1)}\right) = -\left(\partial_{\boldsymbol{\varphi}} J_1(P, \boldsymbol{\varphi}_{n-1}^{(k+1)})\right) \boldsymbol{\varphi}_{n-1}^{(k+1)},$$

with n denoting the n-th Newton iteration step, i.e., for $n = 1, 2, \ldots$, we have $\Delta\boldsymbol{\varphi}_n^{(k+1)} := \boldsymbol{\varphi}_n^{(k+1)} - \boldsymbol{\varphi}_{n-1}^{(k+1)} =: \mathbf{u}_n^{(k)}$ and $\boldsymbol{\varphi}_0^{(k+1)} = \boldsymbol{\varphi}^{(k)}$. Hence, we obtain the new iterate $\boldsymbol{\varphi}_n^{(k+1)} = \boldsymbol{\varphi}_{n-1}^{(k+1)} + \Delta\boldsymbol{\varphi}_n^{(k+1)}$. Furthermore, we obtain a new quadratic form $a^{(k)}_{\boldsymbol{\varphi},n}(\cdot,\cdot)$ and right hand side $\mathbf{F}^{(k)}_{\boldsymbol{\varphi},n}(\mathbf{v})$ when we discretize the Newton iteration as in Section 2.2, i.e.,

$$\begin{aligned}
& a^{(k)}_{\boldsymbol{\varphi},n}(\mathbf{u}_n^{(k)}, \mathbf{v}) \\
:= & \int_\Omega 2\mu_e(\varepsilon_P(\mathbf{u}_n^{(k)}), \varepsilon_P(\mathbf{v}))_F \\
& + \frac{\lambda_e}{2}\left[\mathrm{tr}((\nabla\mathbf{u}_n^{(k)})F_\nabla^{-1})\mathrm{tr}((\nabla\mathbf{v})F_\nabla^{-1})\left(2\det(F_\nabla)^2 - \det(F_\nabla) - \frac{1}{\det(F_\nabla)} + \frac{2}{\det(F_\nabla)^2}\right)\right. \\
& \left. - \,\mathrm{tr}((\nabla\mathbf{u}_n^{(k)})F_\nabla^{-1}(\nabla\mathbf{v})F_\nabla^{-1})\left((\det(F_\nabla) - 1)\left(\det(F_\nabla) + \frac{1}{\det(F_\nabla)^2}\right)\right)\right]\, d\mathbf{x}
\end{aligned}$$

and

$$\begin{aligned}
&\mathbf{F}^{(k)}_{\boldsymbol{\varphi},n}(\mathbf{v}) \\
:= \quad & -\int_\Omega \mu_e (P^{-T}(P^{-1}F_\nabla + F_\nabla^T P^{-T} - 2\cdot \mathrm{Id}\,), \nabla \mathbf{v})_F \\
& -\frac{\lambda_e}{2}\mathrm{tr}((\nabla \mathbf{v})F_\nabla^{-1}) \left((\det(F_\nabla) - 1) \left(\det(F_\nabla) + \frac{1}{\det(F_\nabla)^2} \right) \right) \, d\mathbf{x},
\end{aligned}$$

with $F_\nabla = \nabla \boldsymbol{\varphi}^{(k+1)}_{n-1}$. Note that for $F_\nabla = \mathrm{Id}$ we obtain the same bilinear form as introduced in (2.7) which is consistent with the linearization of the volumetric term.

Since the new term does no longer depend on P our minimization problem in P reduces to

$$\begin{aligned}
\min_P \int_\Omega & \mu_e \|\mathrm{sym}(P^{-1}F_\nabla - \mathrm{Id}\,)\|_F^2 + \mu_e \left(\frac{L_c^2}{2}\|\nabla P\|_F^2 + \frac{L_c^q}{q}\|\nabla P\|_F^q \right) \\
& + \mu_e h^+ \|P^T P - \mathrm{Id}\,\|_F^2 \, d\mathbf{x}.
\end{aligned}$$

Hence, we obtain the same quadratic form as in Section 2.2, (2.21), without the trace terms. The same holds for the right hand side of the discretized q-Laplacian problem in (2.22). There are no more changes necessary in the q-Laplacian problem when we change the terms as described.

When we analyze the results for this nonlinear formulation we observe that for the cubic geometry the number of fixed point iteration steps needed in each single load step is much smaller than in the linear formulation, i.e., we need about half as many fixed point iteration steps in the beginning. Furthermore, the number of fixed point iteration steps needed increases only very slowly in contrast to the linear formulation. Hence, in the last load step we need less than half as many fixed point iteration steps in the nonlinear case than in the linear case. For the cylinder we again observe that the number of fixed point iteration steps needed first decreases and than increases with an increasing overall angle. As in the case for the cubic geometry the number of fixed point iterations needed is much smaller than in the linear case. For the linear formulation we observe that the maximum number of fixed point iteration steps needed for the meshes of the unit cube is smaller than the minimum number of fixed point iteration steps needed for the meshes of the cylinder. Here, we observe that for the coarser mesh of the cylinder, i.e., the mesh with 876 nodes, the minimum number is slightly smaller than the maximum number for the fine meshes of the unit cube, i.e., the meshes with 9009 and 12961 nodes. The observations concerning the increase of the fixed point iteration steps needed when we use finer meshes can as well be made for the nonlinear case.

The Newton iterations for the deformation $\boldsymbol{\varphi}$ are quadratically convergent with respect to the Euclidean norm of the residual as well as with respect to the

Euclidean norm of the correction, i.e., $\|\Delta\boldsymbol{\varphi}_n^{(k)}\|_{l_2}$ for fixed k, independent of the geometry, the mesh size and the overall angle. We need at most three Newton iteration steps in the case of the cubic geometry and at most four in the case of the cylinder.

Note that the Newton iteration for the field P behaves in the same way as in the linear formulation; see Section 2.3.2. The only difference we observe, is in the number of Newton iteration steps. Here, we have a slight increase in the maximum number of iteration steps, i.e., we need at most six or seven steps for both geometries depending on the mesh size.

The convergence behavior of the Euclidean norm of the increments $\Delta\boldsymbol{\varphi}^{(k)}$ and $\Delta P^{(k)}$ is also comparable to the one for the linear formulation. In contrast to the linear formulation we do not observe a change in the gradient in the figures for $\Delta P^{(k)}$ for the cubic geometry; see Figures 2.55, 2.56, 2.57, 2.58, and 2.59. However, in the case of the cylindric geometry this change is more obvious than in the linear case for the finer mesh; see Figure 2.61, and vanishes for an increasing overall angle for the coarser cylindric grid; Figure 2.60. Note, that we do not obtain an exception as for the first load step in the linear formulation for the cylinder any longer; see Figures 2.62 and 2.63.

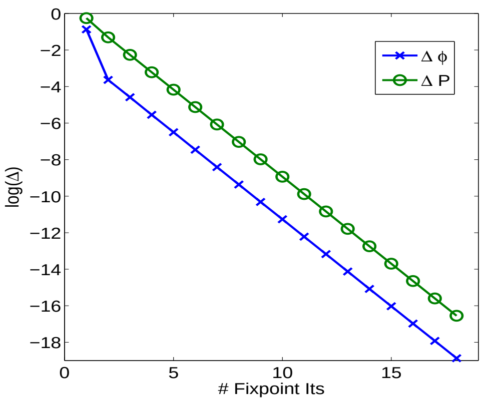

Figure 2.55: *Overall angle* $\frac{9\pi}{32}$*, mesh of the unit cube with 1241 nodes, i.e.,* $h = 0.25$.

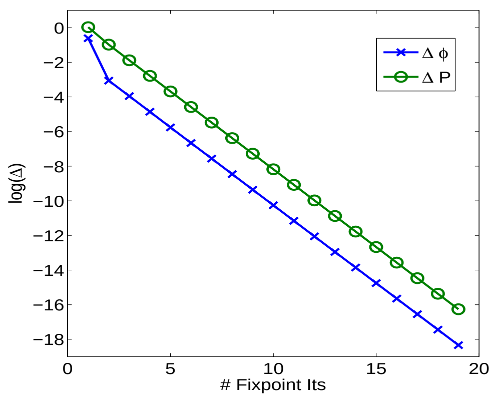

Figure 2.56: *Overall angle* $\frac{23\pi}{64}$*, mesh of the unit cube with 2331 nodes, i.e.,* $h = 0.2$.

In Figures 2.64 and 2.65 it is shown, that the volumetric increase due to the linearization we observed for the cylinder is avoided with the nonlinear formulation.

Furthermore we observe a slight increase in the values of $\|P^TP - \mathrm{Id}\,\|_F$; see Figures 2.66, 2.67, 2.68 and 2.69.

As for the cylinder we observe an increase of the values of $\|P^TP - \mathrm{Id}\,\|_F$ for the meshes of the unit cube in comparison to the values obtained for the linear formulation; see Figures 2.71, 2.73, 2.75, 2.77, and 2.79. Additionally, we present figures showing the contorted cube which do not obviously differ from the ones

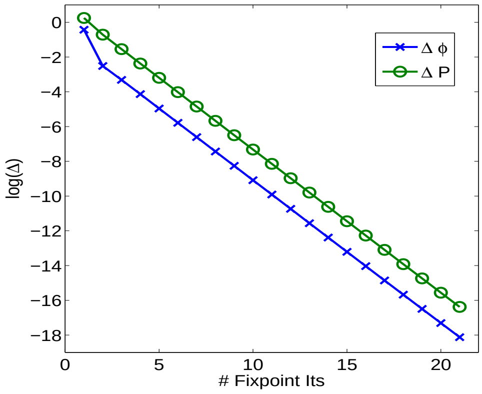

Figure 2.57: *Overall angle* $\frac{15\pi}{32}$*, mesh of the unit cube with 3925 nodes, i.e.,* $h = \frac{1}{6}$.

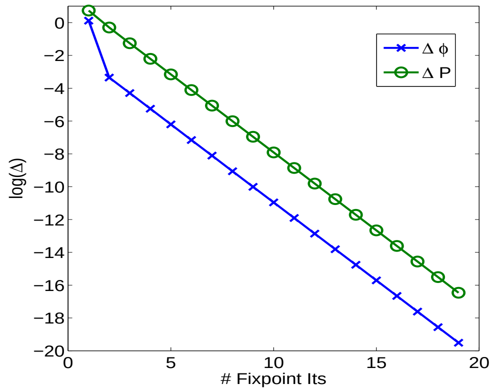

Figure 2.58: *Overall angle* $\frac{5\pi}{32}$*, mesh of the unit cube with 9009 nodes, i.e.,* $h = 0.125$.

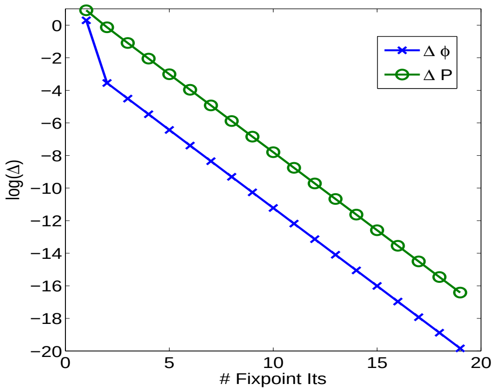

Figure 2.59: *Overall angle* $\frac{7\pi}{64}$*, mesh of the unit cube with 12691 nodes, i.e.,* $h = \frac{1}{9}$.

obtained for the linear formulation; see Figures 2.70, 2.72, 2.74, 2.76, and 2.78.

From these observation it seems that although we would have expected the computations with a nonlinear elasticity formulation to be more expensive than these with a linear elasticity formulation that the expense seems to reduce. Since we need less fixed point iteration steps we also have a decrease of minimization problems in P. But the minimization problems in P are much more expensive to solve than the P-elastic problems in $\boldsymbol{\varphi}$. The increase in the amount of work for the P-elasticity problem due to more steps than in the linear formulation is in comparison to the decrease due to the less needed q-Laplacian problems neglectable. The small increase in the number of Newton iteration steps in the q-Laplacian problem also does not make up the decrease in the overall number

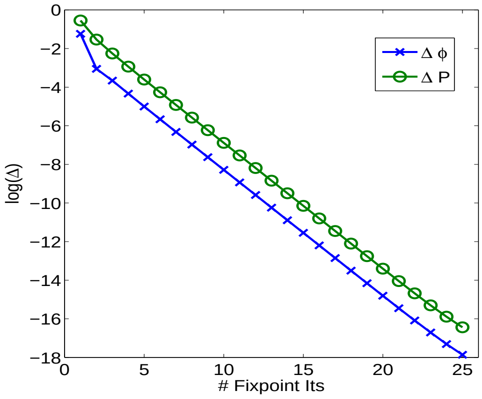

Figure 2.60: *Overall angle* $\frac{23\pi}{64}$, *mesh of the cylinder with 876 nodes.*

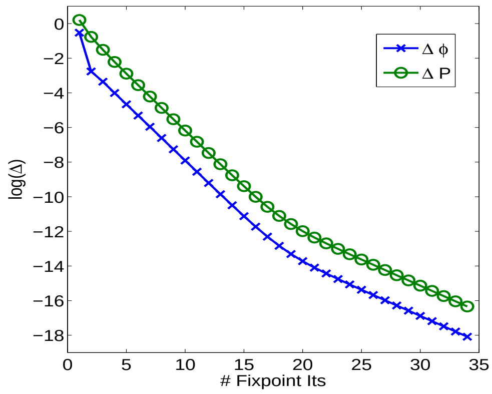

Figure 2.61: *Overall angle* $\frac{\pi}{4}$, *mesh of the cylinder with 3852 nodes.*

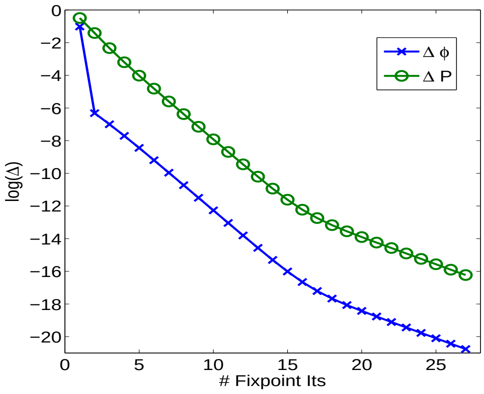

Figure 2.62: *Overall angle* $\frac{\pi}{64}$, *mesh of the cylinder with 876 nodes.*

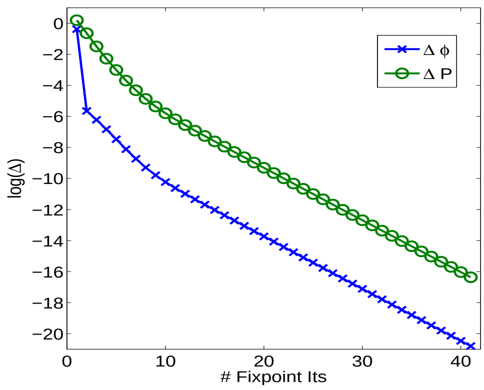

Figure 2.63: *Overall angle* $\frac{\pi}{64}$, *mesh of the cylinder with 3852 nodes.*

of fixed point iteration steps. Furthermore, we observed only a slight increase in the values of $\|P^T P - \mathrm{Id}\,\|_F$ which seems not to be problematic. Hence, we may conclude from these first observations that the nonlinear elasticity formulation seems to lead to better results and is less expensive than the linearized approach for the torsion.

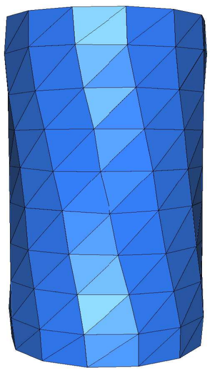

Figure 2.64: *Overall angle $\frac{\pi}{2}$, mesh of the cylinder with 876 nodes, compare with 2.51.*

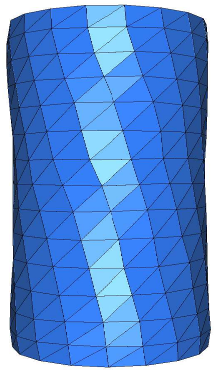

Figure 2.65: *Overall angle $\frac{\pi}{2}$, mesh of the cylinder with 3852 nodes, compare with 2.53.*

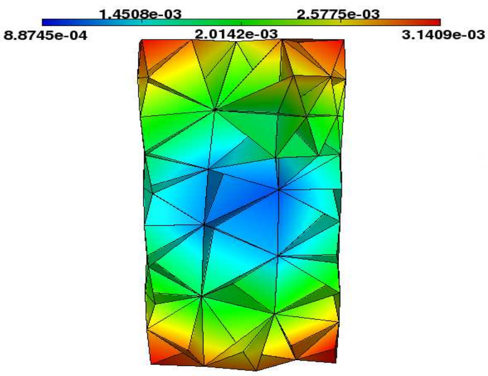

Figure 2.66: *Overall angle $\frac{\pi}{4}$, mesh of the cylinder with 876 nodes, with values of $\|P^TP - \mathrm{Id}\|_F$, compare with 2.48.*

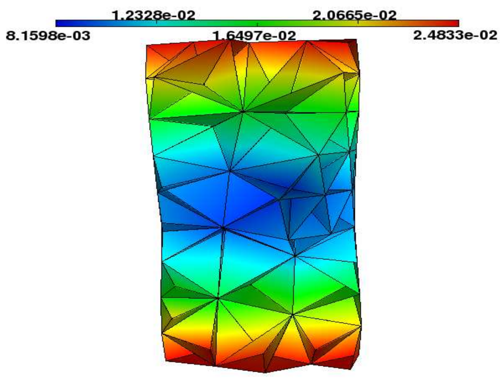

Figure 2.67: *Overall angle $\frac{\pi}{2}$, mesh of the cylinder with 876 nodes, with values of $\|P^TP - \mathrm{Id}\|_F$, compare with 2.52.*

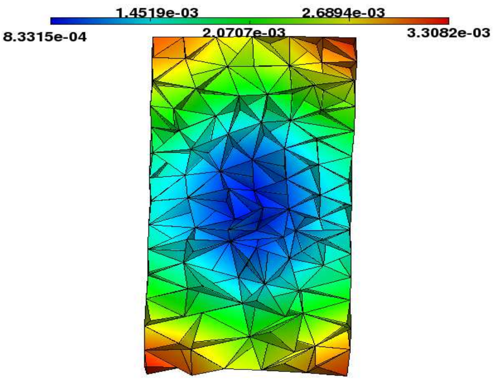

Figure 2.68: *Overall angle $\frac{\pi}{4}$, mesh of the cylinder with 3852 nodes, with values of $\|P^T P - \mathrm{Id}\,\|_F$, compare with 2.50.*

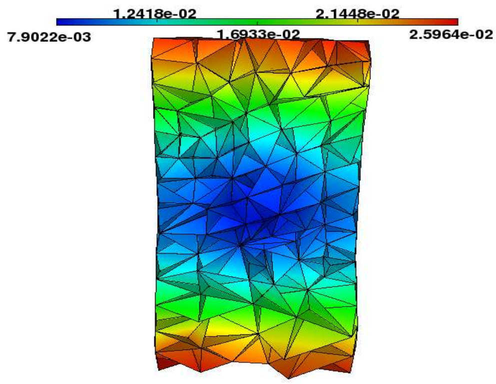

Figure 2.69: *Overall angle $\frac{\pi}{2}$, mesh of the cylinder with 3852 nodes, with values of $\|P^T P - \mathrm{Id}\,\|_F$, compare with 2.54.*

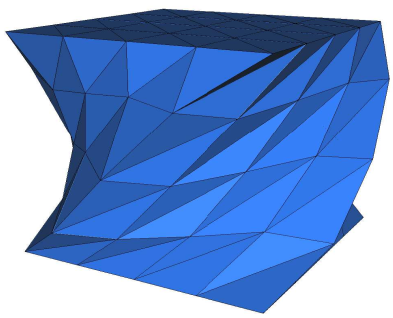

Figure 2.70: *Overall angle $\frac{\pi}{2}$, mesh of the unit cube with 1241 nodes.*

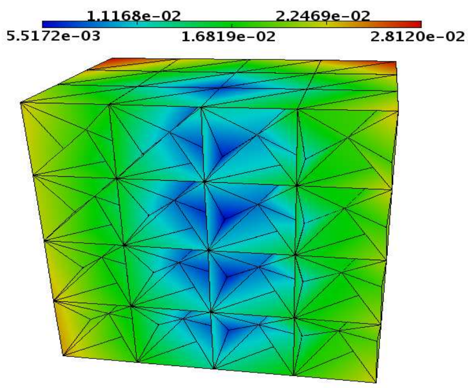

Figure 2.71: *Uncontorted mesh of the unit cube with 1241 nodes, with values of $\|P^T P - \mathrm{Id}\,\|_F$ for an overall angle of $\frac{\pi}{2}$.*

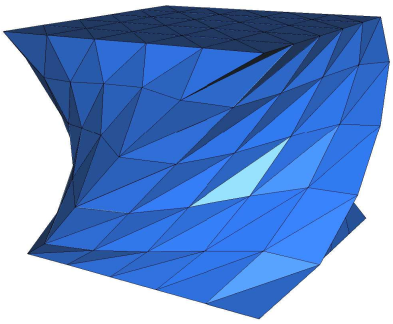

Figure 2.72: *Overall angle* $\frac{\pi}{2}$*, mesh of the unit cube with 2331 nodes.*

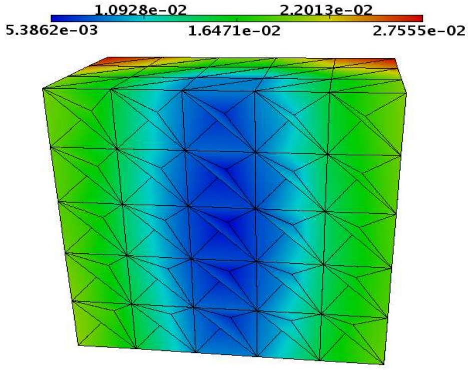

Figure 2.73: *Uncontorted mesh of the unit cube with 2331 nodes, with values of* $\|P^T P - \mathrm{Id}\,\|_F$ *for an overall angle of* $\frac{\pi}{2}$.

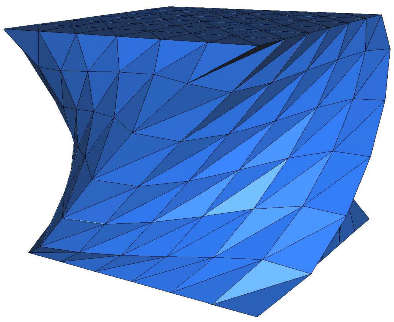

Figure 2.74: *Overall angle* $\frac{\pi}{2}$*, mesh of the unit cube with 3925 nodes.*

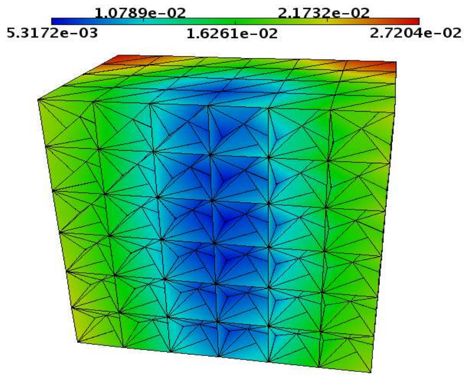

Figure 2.75: *Uncontorted mesh of the unit cube with 3925 nodes, with values of* $\|P^T P - \mathrm{Id}\,\|_F$ *for an overall angle of* $\frac{\pi}{2}$.

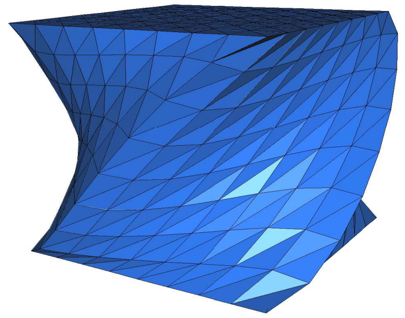

Figure 2.76: *Overall angle $\frac{\pi}{2}$, mesh of the unit cube with 9009 nodes.*

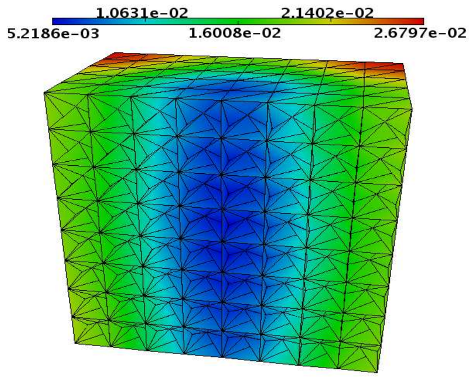

Figure 2.77: *Uncontorted mesh of the unit cube with 9009 nodes, with values of $\|P^T P - \mathrm{Id}\,\|_F$ for an overall angle of $\frac{\pi}{2}$.*

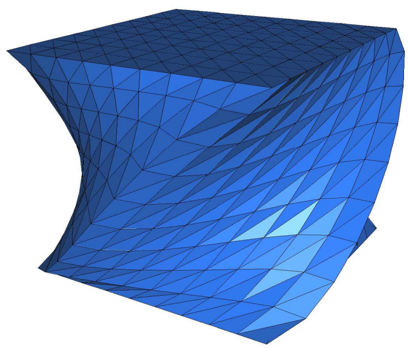

Figure 2.78: *Overall angle $\frac{\pi}{2}$, mesh of the unit cube with 12691 nodes.*

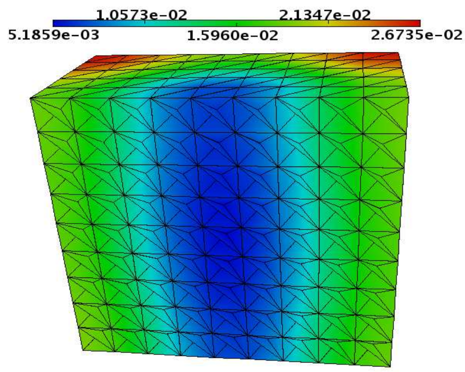

Figure 2.79: *Uncontorted mesh of the unit cube with 12691 nodes, with values of $\|P^T P - \mathrm{Id}\,\|_F$ for an overall angle of $\frac{\pi}{2}$.*

Chapter 3

Efficient solution of P-elasticity with FETI-DP

The FETI-DP method has proven to be an efficient domain decomposition method to solve large linear systems arising for example in elasticity problems. Since our P-elastic subproblem changes to a standard linear elasticity problem when we chose $P = \mathrm{Id}$ we consider the FETI-DP approach also for the P-elastic problem.

In this chapter we will first give a short introduction to the FETI-DP method; see Section 3.1. In Section 3.2, we will establish the constraints used in the FETI-DP method for the case of P-elasticity. The Korn inequalities needed to guarantee uniform ellipticity are established for the P-elasticity problem in Section 3.3. In Section 3.4 we establish the condition number estimate for the preconditioned FETI-DP system. Some of the technical tools needed in our analysis will be presented in Section 3.5 with proofs for piecewise quadratic nodal basis functions. To complete this chapter, we present numerical results for the P-elasticity problem solved with the FETI-DP algorithm in Section 3.6. In this chapter we will mainly follow the arguments given in Klawonn and Widlund [55].

This chapter is based on Klawonn, Neff, Rheinbach, and Vanis [47]. For the convenience of the reader we repeat the arguments and outline some proofs in a more detailed fashion.

3.1 The Dual-Primal FETI Method

In this section, we will give an algorithmic description of the dual-primal FETI (**F**inite **E**lement **T**earing and **I**nterconnecting) domain decomposition method for P-elasticity. For related FETI-DP algorithms for linear elasticity problems, see [50, 52, 55].

In FETI methods the computational domain is partitioned into nonoverlapping subdomains and the continuity of the solution across subdomain boundaries is enforced by Lagrange multipliers. The dual problem is then solved iteratively by a preconditioned Krylov subspace method. As a result, the FETI iterates are in general discontinuous across the subdomain boundaries before convergence.

In dual-primal FETI methods, the variables on the subdomain boundaries are divided into two classes, the primal and the dual variables. As primal variables, labeled with Π, we refer to variables which are assembled before the iteration and in which continuity is enforced in each iteration step. For dual variables, labeled with Δ, the continuity is established weakly by the introduction of Lagrange multipliers thus enforcing continuity only at convergence. The primal variables also form a globally coupled problem. This global problem is necessary to obtain numerical scalability, i.e., independence on the number of subdomains, but should be kept as small as possible.

3.1.1 Triangulation of Ω

The FETI methods work on discrete spaces as numerical methods do in general. A triangulation τ_h of the domain Ω is assumed to be given. The elements of τ_h are supposed to be shape regular and to have a typical diameter h. We assume that the domain Ω can be represented exactly as union of tetrahedral finite elements. The corresponding conforming finite element space of finite element functions is denoted by $\mathbf{W}^h := \mathbf{W}^h(\Omega) \subset \mathbf{H}^1_0(\Omega, \partial\Omega_D)$. Then we obtain a discrete form of the problem

Find $\mathbf{u}_h \in \mathbf{W}^h(\Omega)$ *such that*

$$a(\mathbf{u}_h, \mathbf{v}_h) = \mathbf{F}(\mathbf{v}_h) \quad \forall \mathbf{v}_h \in \mathbf{W}^h. \tag{3.1}$$

When there is no risk of confusion, we drop the subscript h from now on.

We will work with piecewise quadratic nodal basis functions for the problem of P-elasticity. Hence, we have one additional node on each edge of each tetrahedron belonging to the triangulation τ_h. With these additional nodes we can split each tetrahedron in a natural way in eight smaller tetrahedrons, cf. Figure 3.1 The triangulation we obtain by this further splitting will be denoted by $\tau_{h/2}$. We will use this triangulation exclusively to define linear finite element functions in the theoretical analysis; see Section 3.4, (3.56).

3.1.2 Decomposition of Ω

We assume a Lipschitz domain Ω partitioned into N subdomains Ω_i, $i = 1, \ldots, N$, each of which is the union of finite elements with matching finite element nodes on the boundaries of neighboring subdomains across the interface Γ. The interface Γ is the union of three different groups of open sets, namely, subdomain faces, edges, and vertices. Here, we follow the presentation given in Klawonn and Rheinbach [50, Section 2]; see also Klawonn and Widlund [55]. We denote individual faces, edges and vertices by $\mathcal{F}, \mathcal{E}$, and $\mathcal{V}$, respectively. To define faces, edges, and

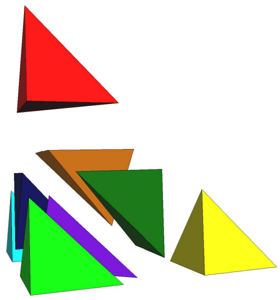

Figure 3.1: Decomposition of one 10 node tetrahedra into eight 4 node tetrahedra.

vertices, we introduce certain equivalence classes. Let us denote the sets of nodes on $\partial\Omega, \partial\Omega_i$, and Γ by $\partial\Omega_h, \partial\Omega_{i,h}$, and Γ_h, respectively. For any interface nodal point $x \in \Gamma_h$, we define

$$\mathcal{N}_x := \{j \in \{1, \dots, N\} : x \in \partial\Omega_{j,h}\},$$

i.e., $\mathcal{N}_x$ is the set of indices of all subdomains with x in the closure of the subdomain. For a node x we define the multiplicity as $|\mathcal{N}_x|$.

Associated with the nodes of the finite element mesh, we have a graph, the nodal graph, which represents the node-to-node adjacency. For a given node $x \in \Gamma_h$, we denote by $\mathcal{C}_{\text{con}}(x)$ the connected component of the nodal subgraph, defined by $\mathcal{N}_x$, to which x belongs. For two interface points $x, y \in \Gamma_h$, we introduce an equivalence relation by

$$x \sim y :\Leftrightarrow \mathcal{N}_x = \mathcal{N}_y \quad \text{and} \quad y \in \mathcal{C}_{\text{con}}(x).$$

We can now describe faces, edges and vertices using their equivalence classes. Here, $|G|$ denotes the cardinality of the set G. We define the following.

Definition 1

$$\begin{aligned} x \in \mathcal{F} \quad &:\Leftrightarrow \quad |\mathcal{N}_x| = 2. \\ x \in \mathcal{E} \quad &:\Leftrightarrow \quad |\mathcal{N}_x| \geq 3 \ \text{ and } \ \exists y \in \Gamma_h, y \neq x, \ \text{ such that } \ y \sim x. \\ x \in \mathcal{V} \quad &:\Leftrightarrow \quad |\mathcal{N}_x| \geq 3 \ \text{ and } \ \nexists y \in \Gamma_h, y \neq x, \ \text{ such that } \ y \sim x. \end{aligned}$$

In the case of a decomposition into regular substructures, e.g., cubes or tetrahedra, our definition of faces, edges, and vertices conforms to our basic geometric intuition. On the other hand, for subdomains generated by an automatic mesh partitioner, the situation can be quite complicated. We can, e.g., have several edges with the same index set $\mathcal{N}_x$ or an edge and a vertex with the same $\mathcal{N}_x$. In practice, we can also have situations when there are not enough edges and potential edge constraints for some subdomains. Then we have to use constraints on some extra edges on $\partial\Omega_N$, which otherwise would be regarded as part of a face. A similar problem might occur for flat structures for which additional constraints might be required for each subdomain. Therefore, we introduce an alternative definition of edges.

Definition 2 *An edge is the largest connected set of nodes with the same index set $\mathcal{N}_x$, where $\mathcal{N}_x \geq 3$ or $\mathcal{N}_x \geq 2$ and x is on $\partial\Omega_N$.*

If needed, we will increase the number of edges in unstructured cases by switching locally from definition of edges given in Definition 1 to Definition 2 and by splitting edges into several edges.

3.1.3 The basic algorithm

In this section we will give an algorithmic description of the basic FETI-DP method. Let us therefore assume that Ω is given and decomposed as described in Section 3.1.2. For each subdomain we need the local stiffness matrix $K^{(i)}$, the local load vector $\mathbf{f}^{(i)}$, and the vector of the local nodal values $\mathbf{u}^{(i)}$. We distinguish between interior nodes and interface nodes, denoted by I and Γ, respectively. Additionally, we distinguish between dual and primal nodes on the interface, denoted by an index Δ or Π, respectively. In the primal variables we will establish the continuity by assembling before the iteration. In the dual nodes the continuity is established by an additional constraint which is established by using a vector of the Lagrange multipliers. This vector of the Lagrange multipliers will be denoted by λ. Thus, we have

$$K^{(i)} = \begin{bmatrix} K_{II}^{(i)} & K_{\Delta I}^{(i)T} & K_{\Pi I}^{(i)T} \\ K_{\Delta I}^{(i)} & K_{\Delta\Delta}^{(i)} & K_{\Pi\Delta}^{(i)T} \\ K_{\Pi I}^{(i)} & K_{\Pi\Delta}^{(i)} & K_{\Pi\Pi}^{(i)} \end{bmatrix}, \quad \mathbf{u}^{(i)} = \begin{bmatrix} \mathbf{u}_I^{(i)} \\ \mathbf{u}_\Delta^{(i)} \\ \mathbf{u}_\Pi^{(i)} \end{bmatrix} \quad \text{and} \quad \mathbf{f}^{(i)} = \begin{bmatrix} \mathbf{f}_I^{(i)} \\ \mathbf{f}_\Delta^{(i)} \\ \mathbf{f}_\Pi^{(i)} \end{bmatrix}.$$

Introducing

$$\mathbf{u}_B = \begin{bmatrix} \mathbf{u}_I \\ \mathbf{u}_\Delta \end{bmatrix}, \quad \mathbf{f}_B = \begin{bmatrix} \mathbf{f}_I \\ \mathbf{f}_\Delta \end{bmatrix}, \quad \mathbf{u}_B^{(i)} = \begin{bmatrix} \mathbf{u}_I^{(i)} \\ \mathbf{u}_\Delta^{(i)} \end{bmatrix}, \quad \mathbf{f}_B^{(i)} = \begin{bmatrix} \mathbf{f}_I^{(i)} \\ \mathbf{f}_\Delta^{(i)} \end{bmatrix}.$$

yields

$$K_{BB} = \operatorname{diag}(K_{BB}^{(i)}) \quad \text{with} \quad K_{BB}^{(i)} = \begin{bmatrix} K_{II}^{(i)} & K_{\Delta I}^{(i)T} \\ K_{\Delta I}^{(i)} & K_{\Delta\Delta}^{(i)} \end{bmatrix}$$

as well as

$$K_{\Pi B} = \left[K_{\Pi B}^{(1)}, \ldots, K_{\Pi B}^{(N)}\right] \quad \text{with} \quad K_{\Pi B}^{(i)} = \left[K_{\Pi I}^{(i)} K_{\Pi\Delta}^{(i)}\right].$$

Next, we assemble the primal variables, indicating the assembled variables by a tilde. This yields

$$\widetilde{K} = \begin{bmatrix} K_{BB} & \widetilde{K}_{\Pi B}^T \\ \widetilde{K}_{\Pi B} & \widetilde{K}_{\Pi\Pi} \end{bmatrix},$$

with $\widetilde{K}_{\Pi B} = \left[\widetilde{K}_{\Pi B}^{(1)}, \ldots, \widetilde{K}_{\Pi B}^{(N)}\right]$.

The assembly process can be described using restriction operators $R_\Pi^{(i)}$ with

$$\begin{aligned} \widetilde{K}_{\Pi B}^{(i)} &= R_\Pi^{(i)T} K_{\Pi B}^{(i)} \qquad\qquad \forall i = 1, \ldots, N \\ \widetilde{K}_{BB} &= \sum_{i=1}^{N} R_\Pi^{(i)T} K_{\Pi\Pi}^{(i)} R_\Pi^{(i)}. \end{aligned}$$

The matrices $R_\Pi^{(i)}$ only have entries 0 or 1, the global number of columns equals the number of primal variables, and the number of rows equals the number of primal variables belonging to the subdomain Ω_i. The entry in the i-th column and the j-th row of $R_\Pi^{(i)}$ is set to 1 if the j-th primal node in the subdomain Ω_i equals the i-th primal node in the global problem.

In order to obtain a continuous $\mathbf{u}_\Delta$ we introduce a discrete jump operator $B = [0 \ B_\Delta]$. The operator B_Δ is constructed with entries $-1, 0,$ or 1, in such a way that it will enforce continuity for matching nodes across the interface, i.e., $\mathbf{u}_B$ is continuous if $B\mathbf{u}_B = 0 = B_\Delta \mathbf{u}_\Delta$.

This leads to a new formulation of our problem

Find $\mathbf{u}$ *such that*

$$K\mathbf{u} = \mathbf{f} \quad \text{and} \quad B\mathbf{u}_B = 0$$

and with λ being the vector of the Lagrange multipliers we obtain

$$\begin{bmatrix} K_{BB} & \widetilde{K}_{\Pi B}^T & B^T \\ \widetilde{K}_{\Pi B} & \widetilde{K}_{\Pi\Pi} & 0 \\ B & 0 & 0 \end{bmatrix} \begin{bmatrix} \mathbf{u}_B \\ \tilde{\mathbf{u}}_\Pi \\ \lambda \end{bmatrix} = \begin{bmatrix} \mathbf{f}_B \\ \tilde{\mathbf{f}}_\Pi \\ \mathbf{0} \end{bmatrix}. \tag{3.2}$$

In a next step, the variables $\mathbf{u}_B$ and $\tilde{\mathbf{u}}_\Pi$ are eliminated by two block Gaussian eliminations which leads to

$$F\lambda = \mathbf{d}.$$

With the first block Gaussian elimination we eliminate the interior and dual variables, i.e., $\mathbf{u}_B$.

$$\begin{aligned} &\begin{bmatrix} K_{BB} & \widetilde{K}_{\Pi B}^T & B^T \\ 0 & \widetilde{K}_{\Pi\Pi} - \widetilde{K}_{\Pi B} K_{BB}^{-1} \widetilde{K}_{\Pi B}^T & -\widetilde{K}_{\Pi B} K_{BB}^{-1} B^T \\ 0 & -B K_{BB}^{-1} \widetilde{K}_{\Pi B}^T & -B K_{BB}^{-1} B^T \end{bmatrix} \begin{bmatrix} \mathbf{u}_B \\ \tilde{\mathbf{u}}_\Pi \\ \lambda \end{bmatrix} \\ &\qquad = \begin{bmatrix} \mathbf{f}_B \\ \tilde{\mathbf{f}}_\Pi - \widetilde{K}_{\Pi B} K_{BB}^{-1} \mathbf{f}_B \\ -B K_{BB}^{-1} \mathbf{f}_B \end{bmatrix} \end{aligned}$$

Introducing $\widetilde{S}_{\Pi\Pi} := \widetilde{K}_{\Pi\Pi} - \widetilde{K}_{\Pi B} K_{BB}^{-1} \widetilde{K}_{\Pi B}^T$ and eliminating in a second step the subassembled primal variables, i.e., $\tilde{\mathbf{u}}_\Pi$, leads to

$$\begin{bmatrix} K_{BB} & \widetilde{K}_{\Pi B}^T & B^T \\ 0 & \widetilde{S}_{\Pi\Pi} & -\widetilde{K}_{\Pi B} K_{BB}^{-1} B^T \\ 0 & 0 & -BK_{BB}^{-1}B^T - BK_{BB}^{-1}\widetilde{K}_{\Pi B}^T \widetilde{S}_{\Pi\Pi} \widetilde{K}_{\Pi B} K_{BB}^{-1} B^T \end{bmatrix} \begin{bmatrix} \mathbf{u}_B \\ \tilde{\mathbf{u}}_\Pi \\ \lambda \end{bmatrix}$$
$$= \begin{bmatrix} \mathbf{f}_B \\ \tilde{\mathbf{f}}_\Pi - \widetilde{K}_{\Pi B} K_{BB}^{-1} \mathbf{f}_B \\ -BK_{BB}^{-1}\mathbf{f}_B + BK_{BB}^{-1}\widetilde{K}_{\Pi B}^T \widetilde{S}_{\Pi\Pi} \left(\tilde{\mathbf{f}}_\Pi - \widetilde{K}_{\Pi B} K_{BB}^{-1} \mathbf{f}_B \right) \end{bmatrix}.$$

Hence, we have $F\lambda = \mathbf{d}$ with

$$\begin{aligned} F &= BK_{BB}^{-1}B^T + BK_{BB}^{-1}\widetilde{K}_{\Pi B}^T \widetilde{S}_{\Pi\Pi}^{-1} \widetilde{K}_{\Pi B} K_{BB}^{-1} B^T, \\ d &= BK_{BB}^{-1}\mathbf{f}_B - BK_{BB}^{-1}\widetilde{K}_{\Pi B}^T \widetilde{S}_{\Pi\Pi}^{-1} (\mathbf{f}_\Pi - \widetilde{K}_{\Pi B} K_{BB}^{-1} \mathbf{f}_B). \end{aligned}$$

Before we are going to construct our preconditioner, we give an alternative representation of F which is used in our convergence analysis in Section 3.4. We describe F in terms of the Schur complement $\widetilde{S}_\varepsilon$, which we obtain by eliminating only the interior variables in $\widetilde{K}$, i.e.,

$$\widetilde{S}_\varepsilon = \begin{bmatrix} K_{\Delta\Delta} - K_{\Delta I} K_{II}^{-1} K_{\Delta I}^T & \widetilde{K}_{\Pi\Delta}^T - K_{\Delta I} K_{II}^{-1} \widetilde{K}_{\Pi I}^T \\ \widetilde{K}_{\Pi\Delta} - \widetilde{K}_{\Pi I} K_{II}^{-1} K_{\Delta I}^T & \widetilde{K}_{\Pi\Pi} - \widetilde{K}_{\Pi I} K_{II}^{-1} \widetilde{K}_{\Pi I}^T \end{bmatrix}.$$

With this Schur complement we obtain the system

$$\widetilde{S}_\varepsilon \begin{bmatrix} \mathbf{u}_\Delta \\ \tilde{\mathbf{u}}_\Pi \end{bmatrix} = \begin{bmatrix} \mathbf{f}_\Delta - K_{\Delta I} K_{II}^{-1} \mathbf{f}_I \\ \tilde{\mathbf{f}}_\Pi - \widetilde{K}_{\Pi I} K_{II}^{-1} \mathbf{f}_I \end{bmatrix}.$$

To use $\widetilde{S}_\varepsilon$ for the definition of F, we need another restriction operator $\widetilde{R}_{\Delta\Gamma}$ which restricts partially assembled interface variables to their dual displacement part, i.e., such that

$$\widetilde{R}_{\Delta\Gamma}\mathbf{u}_\Gamma = \mathbf{u}_\Delta \ \text{ with } \ \mathbf{u}_\Gamma = [\mathbf{u}_\Delta, \tilde{\mathbf{u}}_\Pi]^T.$$

With

$$B_\Gamma = B_\Delta \widetilde{R}_{\Delta\Gamma},$$

we have

$$F = B_\Gamma \widetilde{S}_\varepsilon^{-1} B_\Gamma^T. \tag{3.3}$$

To define the standard FETI-DP Dirichlet preconditioner M^{-1}, we introduce a scaled jump operator $B_{D,\Delta} := [B_{D,\Delta}^{(1)}, \ldots, B_{D,\Delta}^{(N)}]$. It is constructed by scaling the submatrices of B_Δ, i.e., $B_\Delta^{(i)}$, as follows. Each row of $B_\Delta^{(i)}$ with a nonzero entry corresponding to a Lagrange multiplier connecting a subdomain Ω_i with a neighboring subdomain Ω_j at a point $x \in \partial\Omega_{i,h} \cup \partial\Omega_{j,h}$ is multiplied with the scalar factor

$$\delta_j^\dagger(x) := \frac{(\mu_e^{(j)})^\gamma}{\sum_{k\in\mathcal{N}_x}(\mu_e^{(k)})^\gamma}, \tag{3.4}$$

where $\mathcal{N}_x$ is the set of all subdomain indices of subdomains which have x on their boundary, i.e., $\mathcal{N}_x := \{i \in \{1,\ldots,N\} : x \in \partial\Omega_i\}$, and $\gamma \in [\frac{1}{2}, \infty)$.

Finally, we introduce a block-diagonal Schur complement matrix $S_\varepsilon := \mathrm{diag}(S_\varepsilon^{(i)})$ with $S_\varepsilon^{(i)}$ being the Schur complement which we obtain by eliminating the interior variables from $K^{(i)}$, i.e.,

$$S_\varepsilon^{(i)} = K_{\Gamma\Gamma}^{(i)} - K_{\Gamma I}^{(i)}(K_{II}^{(i)})^{-1}(K_{\Gamma I}^{(i)})^T.$$

Then

$$M^{-1} = B_{D,\Delta}R_{\Delta\Gamma}S_\varepsilon R_{\Delta\Gamma}^T B_{D,\Delta}^T = \sum_{i=1}^N B_{D,\Delta}^{(i)} R_{\Delta\Gamma}^{(i)} S_\varepsilon^{(i)} R_{\Delta\Gamma}^{(i)T} B_{D,\Delta}^{(i)T}. \tag{3.5}$$

Here, the $R_{\Delta\Gamma}^{(i)}$ are restriction matrices such that

$$R_{\Delta\Gamma}^{(i)} \begin{bmatrix} \mathbf{u}_\Delta^{(i)} \\ \mathbf{u}_\Pi^{(i)} \end{bmatrix} = \mathbf{u}_\Delta^{(i)}$$

and

$$R_{\Delta\Gamma} = \mathrm{diag}_{i=1}^N(R_{\Delta\Gamma}^{(i)}).$$

We note that the application of the preconditioner M^{-1} to a vector only requires the solution of local Dirichlet problems.

We can also express the preconditioner M^{-1} in terms of $\widetilde{S}_\varepsilon$ using a local assembly operator $R^{(i)}$

$$R^{(i)T} = \begin{bmatrix} R_\Delta^{(i)T} & 0 \\ 0 & R_\Pi^{(i)T} \end{bmatrix},$$

with

$$R_\Delta^{(i)T}\mathbf{u}_\Delta^{(i)} = \begin{bmatrix} \mathbf{v}_\Delta^{(1)} \\ \vdots \\ \mathbf{v}_\Delta^{(N)} \end{bmatrix} \quad \text{and} \quad \mathbf{v}_\Delta^{(i)} := \begin{cases} \mathbf{0}_\Delta^{(j)}, & i \neq j \\ \mathbf{u}_\Delta^{(j)}, & i = j \end{cases}$$

cf. Klawonn and Widlund [55], Klawonn, Pavarino, and Rheinbach [49], and Li and Widlund [58]. This leads to the relationship

$$\widetilde{S}_\varepsilon = \sum_{i=1}^N R^{(i)T} S_\varepsilon^{(i)} R^{(i)} = R^T S_\varepsilon R, \tag{3.6}$$

with $R^T = [R^{(1)T} \dots R^{(N)T}]$.

Relation (3.6) combined with

$$B_{D,\Gamma} = B_{D,\Delta}\widetilde{R}_{\Delta\Gamma} \quad \text{and} \quad \widetilde{R}_{\Delta\Gamma}R^T = R_{\Delta\Gamma},$$

leads to another representation of the preconditioner M^{-1}

$$M^{-1} = B_{D,\Gamma}R^T S_\varepsilon R B_{D,\Gamma}^T = B_{D,\Gamma}\widetilde{S}_\varepsilon B_{D,\Gamma}^T. \tag{3.7}$$

For more detailed information, see, e.g., Klawonn and Widlund [55].

3.2 Selection of constraints

In order to obtain a scalable FETI-DP algorithm for P-elasticity in three dimensions, we need to select an appropriate number of primal constraints. It is well-known that choosing only vertex constraints, i.e., subassembling only in the vertices of the subdomains, leads to an algorithm which has a condition number estimate of the order of $O(H/h)$; see, e.g., Klawonn, Widlund, and Dryja [56], Klawonn, Rheinbach, and Widlund [53], and Farhat, Lesoinne, and Pierson [28]. To improve the algorithms, in addition or instead of the vertex constraints, certain averages and first order moments over edges or faces were introduced as primal constraints for the case of linear elasticity; see Klawonn and Widlund [55], Klawonn and Rheinbach [50] and Farhat, Lesoinne, and Pierson [28]. Here, we follow the approach of edge averages and first order moments; see Klawonn and Widlund [55], and Klawonn and Rheinbach [50] and generalize it to the case of P-elasticity. In order to control the kernel of the subdomain stiffness matrices $K^{(i)}$, we have to control the elements of $\mathbf{ker}\,(\varepsilon_P)$ and thus we need at least six constraints. As in [50, 51, 52, 55] for linear elasticity, we will work with edge average constraints of the form

$$g_n(\mathbf{w}^{(i)}) := \frac{\int_{\mathcal{E}^{ik}} w_l^{(i)}\, d\mathbf{x}}{\int_{\mathcal{E}^{ik}} 1\, d\mathbf{x}} \quad , \quad n = 1, \dots, 6\,. \tag{3.8}$$

These constraints can be interpreted as averages over the edge $\mathcal{E}^{ik}$ of the function $w_l^{(i)}, l \in \{1,2,3\}, i \in \{1,\dots,N\}$ which is the l-th component of $\mathbf{w}^{(i)} = (w_1^{(i)}, w_2^{(i)}, w_3^{(i)}) \in \mathbf{W}^{(i)}$.

Definition 3 *An edge $\mathcal{E}^{ik}$ is called a primal edge if at least one of its displacement components is provided with a constraint.*

Such a constraint belongs to a face $\mathcal{F}^{ij}$ if $\mathcal{E}^{ik}$ is a part of the boundary of this face. To define a fully primal face; cf. Definition 4, we introduce six constraints such constraints which have to be linearly independent on the $\mathbf{ker}\,(\varepsilon_P)$, i.e.,

$$\forall \mathbf{r} \in \mathbf{ker}\,(\varepsilon_P) \quad : \quad \sum_{n=1}^{6} g_n(\mathbf{r})^2 = 0 \quad \Leftrightarrow \quad \mathbf{r} = 0 \tag{3.9}$$

Clearly, this is equivalent to

$$g_n(\mathbf{r}) = 0 \quad \forall n = 1, \ldots, 6 \quad \Leftrightarrow \quad \mathbf{r} = 0\,.$$

We can obtain six such functionals by choosing at least three edges which belong to the boundary of the face $\mathcal{F}^{ij}$.

Lemma 1 *Let $P^{-T} = \nabla\boldsymbol{\psi}$ and $\boldsymbol{\psi}$ be a $\mathcal{C}^1$-diffeomorphism with $\det(\nabla\boldsymbol{\psi})$ being bounded from below and above, i.e., $0 < c \leq |\det(\nabla\boldsymbol{\psi})| \leq C < \infty$. Then, for every subdomain face and for the standard case, cf. Assumption 1 in Section 3.4, we can always find six edge averages of the displacement components that are linearly independent when restricted to the space $\mathbf{ker}\,(\varepsilon_P)$.*

Proof: First we will consider the elements $\mathbf{r}_4, \mathbf{r}_5$, and $\mathbf{r}_6$ of $\mathbf{ker}\,(\varepsilon_P)$, cf. (2.17). For $\mathbf{w} = (w^{(j)})_{j=1,2,3}$ we consider

$$g(\mathbf{w}) = \frac{\int_{\mathcal{E}^{ik}} w^{(j)}(\mathbf{x})\; d\mathbf{x}}{\int_{\mathcal{E}^{ik}} 1 \; d\mathbf{x}}.$$

Since we want to control the basis elements of $\mathbf{ker}\,(\varepsilon_P)$ we have to evaluate g for these elements

$$g(\mathbf{r}_n) = \frac{\int_{\mathcal{E}^{ik}} \mathbf{r}_n^{(j)}(\mathbf{x})\; d\mathbf{x}}{\int_{\mathcal{E}^{ik}} 1 \; d\mathbf{x}} \quad \text{for } n = 4, 5, 6.$$

Because $\boldsymbol{\psi}$ is a $\mathcal{C}^1$-diffeomorphism, we can carry out a change of variables

$$\boldsymbol{\psi} : \Omega_i \to \widehat{\Omega}_i \;\;,\;\; \mathbf{x} \mapsto \boldsymbol{\xi} := \boldsymbol{\psi}(\mathbf{x}).$$

By using the transformation formula, cf. Lemma 2, we obtain

$$g(\mathbf{r}_n) = \frac{\int_{\boldsymbol{\xi} \in \boldsymbol{\psi}(\mathcal{E}^{ik})} \mathbf{r}_n^{(j)}(\boldsymbol{\psi}^{-1}(\boldsymbol{\xi}))\, |\det(\nabla\boldsymbol{\psi}^{-1}(\boldsymbol{\xi}))|\; d\boldsymbol{\xi}}{\int_{\boldsymbol{\xi} \in \boldsymbol{\psi}(\mathcal{E}^{ik})} |\det(\nabla\boldsymbol{\psi}^{-1}(\boldsymbol{\xi}))|\; d\boldsymbol{\xi}}$$

and by using the special form of $\mathbf{r}$ introduced in Section 2.1.2, we have

$$\mathbf{r}_4(\boldsymbol{\psi}^{-1}(\boldsymbol{\xi})) = \begin{bmatrix} \psi^{(2)}(\boldsymbol{\psi}^{-1}(\boldsymbol{\xi})) - \psi^{(2)}(\boldsymbol{\psi}^{-1}(\hat{\boldsymbol{\xi}})) \\ -\psi^{(1)}(\boldsymbol{\psi}^{-1}(\boldsymbol{\xi})) + \psi^{(1)}(\boldsymbol{\psi}^{-1}(\hat{\boldsymbol{\xi}})) \\ 0 \end{bmatrix} = \begin{bmatrix} \xi_2 - \hat{\xi}_2 \\ -\xi_1 + \hat{\xi}_1 \\ 0 \end{bmatrix} =: \tilde{\mathbf{r}}_4(\boldsymbol{\xi}). \quad (3.10)$$

For $n = 5, 6$, we obtain analogously

$$\tilde{\mathbf{r}}_5(\boldsymbol{\xi}) := \begin{bmatrix} -\xi_3 + \hat{\xi}_3 \\ 0 \\ \xi_1 - \hat{\xi}_1 \end{bmatrix} \quad , \quad \tilde{\mathbf{r}}_6(\boldsymbol{\xi}) := \begin{bmatrix} 0 \\ \xi_3 - \hat{\xi}_3 \\ -\xi_2 + \hat{\xi}_2 \end{bmatrix}. \qquad (3.11)$$

For $n = 4, 5, 6$, we have

$$g(\mathbf{r}_n) = \frac{\int_{\boldsymbol{\xi}\in\boldsymbol{\psi}(\mathcal{E}^{ik})} \tilde{\mathbf{r}}_n^{(j)}(\boldsymbol{\xi})\,|\det(\nabla\boldsymbol{\psi}^{-1}(\boldsymbol{\xi}))|\;d\boldsymbol{\xi}}{\int_{\boldsymbol{\xi}\in\boldsymbol{\psi}(\mathcal{E}^{ik})} |\det(\nabla\boldsymbol{\psi}^{-1}(\boldsymbol{\xi}))|\;d\boldsymbol{\xi}}.$$

Since the entries in $\mathbf{r}_n$ are constant for $n = 1, 2, 3$ it is obvious that we obtain

$$\mathbf{r}_n(\mathbf{x}) = \tilde{\mathbf{r}}_n(\boldsymbol{\xi}) \quad n = 1, 2, 3. \tag{3.12}$$

The functions $\tilde{\mathbf{r}}_n$, $n = 1, \ldots, 6$, have the form of the standard basis of the space of rigid body modes from linear elasticity. Since we have assumed that the determinant of P^{-T} is bounded from below and above we obtain

$$\frac{c}{C}\;\underbrace{\frac{\int_{\boldsymbol{\xi}\in\boldsymbol{\psi}(\mathcal{E}^{ik})} \tilde{\mathbf{r}}_n^{(j)}(\boldsymbol{\xi})\;d\boldsymbol{\xi}}{\int_{\boldsymbol{\xi}\in\boldsymbol{\psi}(\mathcal{E}^{ik})} 1\;d\boldsymbol{\xi}}}_{=:\tilde{g}(\tilde{\mathbf{r}}_n)} \;\le\; g(\mathbf{r}_n) \;\le\; \frac{C}{c}\;\underbrace{\frac{\int_{\boldsymbol{\xi}\in\boldsymbol{\psi}(\mathcal{E}^{ik})} \tilde{\mathbf{r}}_n^{(j)}(\boldsymbol{\xi})\;d\boldsymbol{\xi}}{\int_{\boldsymbol{\xi}\in\boldsymbol{\psi}(\mathcal{E}^{ik})} 1\;d\boldsymbol{\xi}}}_{=\tilde{g}(\tilde{\mathbf{r}}_n)}. \tag{3.13}$$

It was shown by Klawonn and Widlund [55, Proposition 5.1], that the lemma holds for the rigid body modes $\tilde{\mathbf{r}}_n$ of standard linear elasticity and the related functionals $\tilde{g}$.

From (3.13) also follows that six linear independent functionals g_n exist. Let therefore $g_n(\mathbf{r}) = 0$ hold $\forall n = 1, \ldots, 6$. Then (3.13) implies that $\tilde{g}_n(\tilde{\mathbf{r}}) = 0$ holds $\forall n = 1, \ldots, 6$. But since the lemma is true for the $\tilde{g}_n$ it follows that $\tilde{\mathbf{r}} = 0$. Because the transformation only affects the basis vectors but not the coefficients we obtain that $\mathbf{r} = 0$. Hence, the lemma also holds for the case of P-elasticity when P^{-T} is a gradient. $\square$

Note that the selection of a linearly independent set of constraints for a fully primal face can be automated quite simply by using a QR factorization with column pivoting. For the details we refer to e.g. Klawonn and Widlund [55, Section 5].

The linear functionals $g_1, \ldots, g_6$ yield a basis for $\mathbf{ker}\,(\varepsilon_P)'$. Then there exists a dual basis of $\mathbf{ker}\,(\varepsilon_P)'$ spanned by possibly other linear functionals $f_1, \ldots, f_6$ which satisfy $f_m(\mathbf{r}_n) = \delta_{nm}, n, m = 1, \ldots, 6$, where the $\mathbf{r}_n$ denote the basis elements of $\mathbf{ker}\,(\varepsilon_P)$. Thus, we can show that there exists a set of scalar values β_{mn} such that

$$f_m(\mathbf{w}) = \sum_{n=1}^{6} \beta_{mn} g_n(\mathbf{w}) \qquad \forall \mathbf{w} \in \mathbf{W}^{(i)}\;,\; \forall m = 1, \ldots, 6\,. \tag{3.14}$$

That these coefficients are benign is known for standard linear elasticity; see [55]. As we have other basis elements for P-elasticity than for standard linear elasticity we have to show that the β_{mn} in the case of P-elasticity are again benign; this is shown under the assumption that the upper and lower bound of the determinant of $\nabla\boldsymbol{\psi}$ are sufficiently close to each other. For standard linear elasticity we have with sufficiently small $\tilde{\beta}_{ml}$

$$\tilde{f}_m(\tilde{\mathbf{r}}_n) = \sum_{l=1}^{6} \tilde{\beta}_{ml}\tilde{g}_l(\tilde{\mathbf{r}}_n) = \delta_{mn},$$

where the $\tilde{g}_n$ are the same functionals as defined in the proof of Lemma 1, cf. (3.13). Let us now define the functional

$$\hat{f}_m(\mathbf{w}) = \sum_{l=1}^{6} \tilde{\beta}_{ml} g_l(\mathbf{w}).$$

Then, we have for $\mathbf{r}_n \in \mathbf{ker}\,(\varepsilon_P)$ that

$$\hat{f}_m(\mathbf{r}_n) = \sum_{l=1}^{6} \tilde{\beta}_{ml} g_l(\mathbf{r}_n).$$

We transform the $g_l(\mathbf{r}_n)$ as in the proof of Lemma 1 and obtain

$$\begin{aligned}
\hat{f}_m(\mathbf{r}_n) &= \sum_{l=1}^{6} \tilde{\beta}_{ml} g_l(\mathbf{r}_n) \\
&= \sum_{l=1}^{6} \tilde{\beta}_{ml} \frac{\int_{\mathcal{E}^{ik}} r_n^{(j)}(\mathbf{x})\; d\mathbf{x}}{\int_{\mathcal{E}^{ik}} 1\; d\mathbf{x}} \\
&= \sum_{l=1}^{6} \tilde{\beta}_{ml} \frac{\int_{\boldsymbol{\xi}\in\boldsymbol{\psi}(\mathcal{E}^{ik})} \tilde{\mathbf{r}}_n^{(j)}(\boldsymbol{\xi})\, |\det(\nabla\boldsymbol{\psi}^{-1}(\boldsymbol{\xi}))|\; d\boldsymbol{\xi}}{\int_{\boldsymbol{\xi}\in\boldsymbol{\psi}(\mathcal{E}^{ik})} |\det(\nabla\boldsymbol{\psi}^{-1}(\boldsymbol{\xi}))|\; d\boldsymbol{\xi}}.
\end{aligned}$$

With the same bounds as in Lemma 1 we get

$$\frac{c}{C}\sum_{l=1}^{6} \tilde{\beta}_{ml}\tilde{g}_l(\tilde{\mathbf{r}}_n) \le \hat{f}_m(\mathbf{r}_n) \le \frac{C}{c}\sum_{l=1}^{6} \tilde{\beta}_{ml}\tilde{g}_l(\tilde{\mathbf{r}}_n)$$

which gives us

$$\frac{c}{C}\tilde{f}_m(\tilde{\mathbf{r}}_n) \le \hat{f}_m(\mathbf{r}_n) \le \frac{C}{c}\tilde{f}_m(\tilde{\mathbf{r}}_n)$$

and hence we obtain for $m \neq n$

$$0 \le \hat{f}_m(\mathbf{r}_n) \le 0 \quad \Leftrightarrow \quad \hat{f}_m(\mathbf{r}_n) = 0.$$

Furthermore, for $m = n$ we get

$$\frac{c}{C} \le \hat{f}_m(\mathbf{r}_m) \le \frac{C}{c}.$$

Thus, there exists a constant $C_f \in [\frac{c}{C}, \frac{C}{c}]$ such that

$$\hat{f}_m(\mathbf{r}_m) = C_f.$$

Obviously, we also have

$$\hat{f}_m(\mathbf{r}_n) = 0.$$

Next, we define $\beta_{mn} := \frac{1}{C_f}\tilde{\beta}_{mn}$ and we have

$$f_m(\mathbf{r}_n) \;=\; \sum_{l=1}^{6} \frac{1}{C_f}\tilde{\beta}_{ml} g_l(\mathbf{r}_n) \;=\; \frac{1}{C_f}\hat{f}_m(\mathbf{r}_n) \;=\; \delta_{mn}. \tag{3.15}$$

These β_{mn} are suitable coefficients as long as the constants c and C are sufficiently close to each other.

The constructions in (3.14) and (3.15) leads to an alternative basis. For an arbitrary $\mathbf{r} \in \mathbf{ker}\,(\varepsilon_P)$ and $m = 1, \ldots 6$, $f_m(\mathbf{r}_l) = \delta_{ml}$ implies

$$0 = f_m(\mathbf{r}) = f_m\left(\sum_{l=1}^{6} \alpha_l \mathbf{r}_l\right) = \sum_{l=1}^{6} \alpha_l f_m(\mathbf{r}_l) = \sum_{l=1}^{6} \alpha_l \delta_{ml} = \alpha_m \tag{3.16}$$

$$\Rightarrow \mathbf{r} = \sum_{l=1}^{6} \alpha_l \mathbf{r}_l = 0.$$

Furthermore, we obtain

$$\begin{aligned}
|g_m(\mathbf{w}^{(i)})|^2 \;&=\; \left| \frac{\int_{\mathcal{E}^{ik}} w_l^{(i)}\; d\mathbf{x}}{\int_{\mathcal{E}^{ik}} 1\; d\mathbf{x}} \right|^2 \\
&\leq\; \frac{\left| \left(\int_{\mathcal{E}^{ik}} (w_l^{(i)})^2\; d\mathbf{x}\right)^{1/2} \left(\int_{\mathcal{E}^{ik}} 1^2\; d\mathbf{x}\right)^{1/2} \right|^2}{\left|\int_{\mathcal{E}^{ik}} 1\; d\mathbf{x}\right|^2} \\
&\leq\; \frac{\left|\int_{\mathcal{E}^{ik}} (w_l^{(i)})^2\; d\mathbf{x}\right|}{\left|\int_{\mathcal{E}^{ik}} 1\; d\mathbf{x}\right|} \;\leq\; C H_i^{-1} ||w_l^{(i)}||^2_{L_2(\mathcal{E}^{ik})}.
\end{aligned}$$

In the last inequality we have used that the length of $\mathcal{E}^{ik}$ is on the order of H_i. With Lemma 14, we obtain

$$||\mathbf{w}^{(i)}||^2_{L_2(\mathcal{E}^{ik})} \leq C\left(1 + \log\left(\frac{H_i}{h_i}\right)\right)\left(|\mathbf{w}^{(i)}|^2_{H^{1/2}(\mathcal{F}^{ij})} + \frac{1}{H_i}||\mathbf{w}^{(i)}||^2_{L_2(\mathcal{F}^{ij})}\right).$$

This motivates the following definition of a fully primal face, cf. also Klawonn and Widlund [55].

Definition 4 *(Fully primal face) A face $\mathcal{F}^{ij}$ is fully primal if, in the space of primal constraints over $\mathcal{F}^{ij}$, there exists a set f_m , $m = 1, \ldots, 6$, of linear functionals on $\mathbf{W}^{(i)}$ with the following properties:*

1. $|f_m(\mathbf{w}^{(i)})|^2 \leq CH_i^{-1}\left(1 + \log\left(\frac{H_i}{h_i}\right)\right)\left(|\mathbf{w}^{(i)}|^2_{H^{1/2}(\mathcal{F}^{ij})} + \frac{1}{H_i}||\mathbf{w}^{(i)}||^2_{L_2(\mathcal{F}^{ij})}\right)$,
2. $f_m(\mathbf{r}_l) = \delta_{ml} \quad \forall m, l = 1, \ldots, 6, \quad \mathbf{r}_l \in \mathbf{ker}\,(\varepsilon_P)$.

Let us note that the largest of the constants C, over all fully primal faces, enters the final bound of the condition number of the iterative method.

3.3 Equivalence of norms

Since unique solvability follows from the $\mathbf{H}^1$-continuity (2.11) and $\mathbf{H}^1$-ellipticity we have to establish both for our bilinear form. Thus, we are left with showing that $a(\cdot, \cdot)$ can be bounded from below by $|\cdot|^2_{H^1(\Omega)}$.

The upper bound was already established as a byproduct of the continuity considerations in Section 2.1.1, i.e., we have

$$a_{\boldsymbol{\varphi}}(\mathbf{u}, \mathbf{u}) \leq C\|P^{-T}\|^2_{L_2(\Omega)}|\mathbf{u}|^2_{H^1(\Omega)}.$$

This lower bound can be achieved by a suitable generalized Korn inequality, cf. Section 3.3.1, Theorems 1 and 3, since

$$\begin{aligned} a_{\boldsymbol{\varphi}}(\mathbf{u}, \mathbf{u}) &= \mu_e(\varepsilon_P(\mathbf{u}), \varepsilon_P(\mathbf{u}))_{L_2(\Omega)} + \frac{\lambda_e}{2}(\mathrm{tr}(P^{-1}\nabla\mathbf{u}), \mathrm{tr}(P^{-1}\nabla\mathbf{u}))_{L_2(\Omega)} \\ &\geq \mu_e(\varepsilon_P(\mathbf{u}), \varepsilon_P(\mathbf{u}))_{L_2(\Omega)}. \end{aligned}$$

3.3.1 Korn inequalities

In this section, we discuss different Korn inequalities which are needed in our convergence analysis in Section 3.4.

The results needed can partly be found in Neff [71]. Since we are interested in the influence of the structural parameter P in the constants obtained, we will outline the proofs here. In Neff [71], an upper estimate for the expression

$$\|(\nabla\phi)P^T(\mathbf{x}) + P(\mathbf{x})(\nabla\phi)^T\|^2_{L_2(\Omega)} = \int_\Omega \|(\nabla\phi)P^T(\mathbf{x}) + P(\mathbf{x})(\nabla\phi)^T\|^2_F \, d\mathbf{x} \quad (3.17)$$

is derived. Here, we have

$$(\varepsilon_P(\mathbf{u}), \varepsilon_P(\mathbf{u}))_{L_2(\Omega)} = \|P^{-1}\nabla\mathbf{u} + (\nabla\mathbf{u})^T P^{-T}\|^2_{L_2(\Omega)} = \int_\Omega \|P^{-1}\nabla\mathbf{u} + (\nabla\mathbf{u})^T P^{-T}\|^2_F \, d\mathbf{x},$$

which can also be represented as

$$\|P^{-1}\nabla\mathbf{u} + (\nabla\mathbf{u})P^{-T}\|^2_{L_2(\Omega)} = \|P^{-1}((\nabla\mathbf{u})P^T + P(\nabla\mathbf{u})^T)P^{-T}\|^2_{L_2(\Omega)}. \quad (3.18)$$

If we are able to ensure that the following norm equivalence holds

$$\begin{array}{rl} \exists\, 0 < c, C < \infty : & c\|(\nabla \mathbf{u})P^T + P(\nabla \mathbf{u})^T\|_{L_2(\Omega)} \\ \leq & \|P^{-1}((\nabla \mathbf{u})P^T + P(\nabla \mathbf{u})^T)P^{-T}\|_{L_2(\Omega)} \\ \leq & C\|(\nabla \mathbf{u})P^T + P(\nabla \mathbf{u})^T\|_{L_2(\Omega)}, \end{array}$$

we can use the estimates given in Neff [71] for (3.17) again for (3.18). Note, that we are also interested to know how the constants c and C depend on P.

Since we know that the L_2-norm is submultiplicative we have

$$\begin{array}{rl} & \|P^{-1}((\nabla \mathbf{u})P^T + P(\nabla \mathbf{u})^T)P^{-T}\|_{L_2(\Omega)} \\ \leq & \|P^{-1}\|_{L_2(\Omega)} \;\; \|(\nabla \mathbf{u})P^T + P(\nabla \mathbf{u})^T\|_{L_2(\Omega)} \;\; \|P^{-T}\|_{L_2(\Omega)} \\ = & \|P^{-T}\|^2_{L_2(\Omega)} \;\; \|(\nabla \mathbf{u})P^T + P(\nabla \mathbf{u})^T\|_{L_2(\Omega)}. \end{array} \tag{3.19}$$

To obtain the lower estimate we use that the spectral norm of a matrix, i.e., $\|\cdot\|_2$, is equivalent to the Frobenius matrix norm, i.e., $\|\cdot\|_F$, on the space of real, finite dimensional $m \times n$ matrices, i.e., $\mathbb{R}^{m\times n}$, with $m, n < \infty$. For $N \in \mathbb{R}^{n\times n}$ we obtain

$$\begin{array}{rcccl} \frac{1}{\sqrt{n}}\|N\|_F & \leq & \|N\|_2 & \leq & \|N\|_F, \\ \|N\|_2 & \leq & \|N\|_F & \leq & \sqrt{n}\|N\|_2. \end{array} \tag{3.20}$$

For a proof of this estimate we refer to Bunse-Gerstner [14, Lemma 1.8.3].

Now we derive a lower bound for $\|LNL^T\|_2$ with $L := P^{-1}$ and $N := (\nabla \mathbf{u})P^T + P(\nabla \mathbf{u})^T$. Since N is symmetric we have

$$\begin{array}{rcl} \|LNL^T\|_2 & = & \sup\limits_{\substack{x\in\mathbb{R}^3 \\ x\neq 0}} \left| \frac{< LNL^T x, x >}{< x, x >} \right| \\ & = & \sup\limits_{\substack{x\in\mathbb{R}^3 \\ x\neq 0}} \left| \frac{< NL^T x, L^T x >}{< x, x >} \right| \\ & = & \sup\limits_{\substack{y\in\mathbb{R}^3 \\ L^{-T}y\neq 0}} \left| \frac{< Ny, y >}{< L^{-T}y, L^{-T}y >} \right| \end{array}$$

Using that N is symmetric, $\|L^{-T}y\|_2 \leq \|L^{-T}\|_2\|y\|_2$, and the lower estimate of the first part of (3.20), we obtain

$$\begin{array}{rcl} \sup\limits_{\substack{y\in\mathbb{R}^3 \\ L^{-T}y\neq 0}} \left| \frac{< Ny, y >}{< L^{-T}y, L^{-T}y >} \right| & \geq & \frac{1}{\|L^{-T}\|_2^2} \sup\limits_{\substack{y\in\mathbb{R}^3 \\ y\neq 0}} \left| \frac{< Ny, y >}{< y, y >} \right| \\ & = & \frac{1}{\|L^{-T}\|_2^2} \cdot \|N\|_2 \geq \frac{1}{\|L^{-T}\|_F^2} \cdot \|N\|_2, \end{array}$$

Thus with $n = 3$, we obtain the following estimate

$$\begin{aligned}
\|P^{-1}((\nabla\mathbf{u})P^T + P(\nabla\mathbf{u})^T)P^{-T}\|_F &\geq \|P^{-1}((\nabla\mathbf{u})P^T + P(\nabla\mathbf{u})^T)P^{-T}\|_2 \\
&\geq \frac{1}{\|P^{-T}\|_F^2}\|(\nabla\mathbf{u})P^T + P(\nabla\mathbf{u})^T\|_2 \\
&\geq \frac{1}{\sqrt{n}\|P^{-T}\|_F^2}\|(\nabla\mathbf{u})P^T + P(\nabla\mathbf{u})^T\|_F \qquad (3.21)\\
&= \frac{1}{\sqrt{3}\|P^{-T}\|_F^2}\|(\nabla\mathbf{u})P^T + P(\nabla\mathbf{u})^T\|_F.
\end{aligned}$$

Next, we consider

$$\begin{aligned}
\|\varepsilon_P(\mathbf{u})\|_{L_2(\Omega)}^2 &= \|P^{-1}((\nabla\mathbf{u})P^T + P(\nabla\mathbf{u})^T)P^{-T}\|_{L_2(\Omega)}^2 \\
&= \int_\Omega \|P^{-1}((\nabla\mathbf{u})P^T + P(\nabla\mathbf{u})^T)P^{-T}\|_F^2 \, d\mathbf{x} \qquad (3.22)\\
&\geq \int_\Omega \frac{1}{3\|P^{-T}\|_F^4}\cdot\|(\nabla\mathbf{u})P^T + P(\nabla\mathbf{u})^T\|_F^2 \, d\mathbf{x}.
\end{aligned}$$

We also have

$$\begin{aligned}
\frac{1}{\|P^{-T}\|_F^2} &= \frac{1}{\left(\sum_{i,j=1}^{n}(P^{-T})_{ij}^2(\mathbf{x})\right)} \geq \frac{1}{\left(\sum_{i,j=1}^{3}(\max_{\mathbf{x}\in\Omega}(P^{-T})_{ij}(\mathbf{x}))^2\right)} \\
&\geq \frac{1}{\left(\sum_{i,j=1}^{3}(\max_{i,j=1,2,3}\max_{\mathbf{x}\in\Omega}(P^{-T})_{ij}(\mathbf{x}))^2\right)} \qquad (3.23)\\
&\geq \frac{1}{\left(3^2\underbrace{(\max_{i,j=1\ldots n}\max_{\mathbf{x}\in\Omega}(P^{-T})_{ij}(\mathbf{x}))^2}_{=:c_P^2}\right)} = \frac{1}{9c_P^2}.
\end{aligned}$$

Combining (3.23) with (3.22), (3.21), and (3.19) leads to the inequality

$$\begin{aligned}
\frac{1}{n^{5/2}c_P^2}\|(\nabla\mathbf{u})P^T + P(\nabla\mathbf{u})^T\|_{L_2(\Omega)} &\leq \left(\int_\Omega (\frac{1}{n^{1/2}\|P^{-T}\|_F^2}\|(\nabla\mathbf{u})P^T + P(\nabla\mathbf{u})^T\|_F)^2 \, d\mathbf{x}\right)^{1/2} \\
&\leq \left(\int_\Omega \|P^{-1}((\nabla\mathbf{u})P^T + P(\nabla\mathbf{u})^T)P^{-T}\|_F^2 \, d\mathbf{x}\right)^{1/2} \\
&= \|\varepsilon_P(\mathbf{u})\|_{L_2(\Omega)} \qquad (3.24)\\
&= \|P^{-1}((\nabla\mathbf{u})P^T + P(\nabla\mathbf{u})^T)P^{-T}\|_{L_2(\Omega)} \\
&\leq \|P^{-T}\|_{L_2(\Omega)}^2\|(\nabla\mathbf{u})P^T + P(\nabla\mathbf{u})^T\|_{L_2(\Omega)} \\
&\leq 9c_P^2|\Omega|\|(\nabla\mathbf{u})P^T + P(\nabla\mathbf{u})^T\|_{L_2(\Omega)},
\end{aligned}$$

with $|\Omega| := \int_\Omega 1 \, d\mathbf{x}$.

Let us now consider the Korn inequalities needed for our convergence analysis. Since we work with domain decomposition methods, we may have subdomains Ω_i with homogeneous Dirichlet boundary conditions on part of their boundaries and we can use Korn's first inequality on $\mathbf{H}^1_0(\Omega_i, \partial\Omega_D \cap \partial\Omega_i)$. But, in general, we also have subdomains with only natural boundary conditions such that we need Korn's second inequality. First we consider the following theorem given in Neff [71] and generalized by Pompe [80].

Theorem 1 *(Generalized Korn's first inequality)*
Let $\Omega \subset \mathbb{R}^3$ be a bounded Lipschitz domain and let $\Sigma \subset \partial\Omega$ be a smooth part of the boundary with nonvanishing two-dimensional Lebesgue measure. Let

$$\mathbf{H}^1_0(\Omega, \Gamma) := \{\boldsymbol{\phi} \in \mathbf{H}^1(\Omega) \mid \boldsymbol{\phi}_{|\Gamma} = 0\}$$

and let $P^{-T} = \nabla\boldsymbol{\psi} \in C^0(\bar{\Omega}, \mathbb{R}^{3\times3}) \subset L^\infty(\bar{\Omega}, \mathbb{R}^{3\times3})$ be given with a positive constant α^+ such that $\det P^T \geq \alpha^+$ and let $\boldsymbol{\psi} : \bar{\Omega} \subset \mathbb{R}^3 \mapsto \mathbb{R}^3$ be a C^1-diffeomorphism. Then there exists a constant $c^+ > 0$ such that

$$\|(\nabla\boldsymbol{\phi})P^T(\mathbf{x}) + P(\mathbf{x})(\nabla\boldsymbol{\phi})^T\|^2_{L_2(\Omega)} \geq c^+\|\boldsymbol{\phi}\|^2_{H^1(\Omega)} \quad \forall\boldsymbol{\phi} \in \mathbf{H}^1_0(\Omega, \Gamma) \ .$$

This theorem combined with the equivalence relation (3.24) leads to

$$\|\varepsilon_P(\mathbf{u})\|^2_{L_2(\Omega)} \ \geq \ \frac{1}{n^5 c_P^4}\|(\nabla\mathbf{u})P^T + P(\nabla\mathbf{u})^T\|^2_{L_2(\Omega)} \ \geq \ \frac{c^+}{3^5 c_P^4}\|\mathbf{u}\|^2_{H^1(\Omega)} \ \geq \ \frac{c^+}{243 c_P^4}|\mathbf{u}|^2_{H^1(\Omega)}$$

for all $\mathbf{u} \in \mathbf{H}^1_0(\Omega_i, \partial\Omega_D \cap \partial\Omega_i)$.

Proof: The proof given here can be found in [71]; for the convenience of the reader, it is repeated using our notation and working out the dependence of the constants on P.

Since $\boldsymbol{\psi}$ is assumed to be a diffeomorphism, we interprete it as a transformation of variables and define $\boldsymbol{\xi} := \boldsymbol{\psi}(\mathbf{x})$, cf. Section 3.2 proof of Lemma 1.

As $C_0^\infty(\Omega, \Gamma)$ is dense in $\mathbf{H}^1_0(\Omega, \Gamma)$, we can assume that $\boldsymbol{\phi} \in C_0^\infty(\Omega, \Gamma)$ and we achieve the estimate for $\mathbf{H}^1_0(\Omega, \Gamma)$ by a density argument. With $\boldsymbol{\phi}$ we construct another function $\boldsymbol{\phi}_e$

$$\boldsymbol{\phi}_e(\boldsymbol{\psi}(\mathbf{x})) = \boldsymbol{\phi}_e(\boldsymbol{\xi}) := \boldsymbol{\phi}(\boldsymbol{\psi}^{-1}(\boldsymbol{\xi})) = \boldsymbol{\phi}(\boldsymbol{\psi}^{-1}(\boldsymbol{\psi}(\mathbf{x}))) = \boldsymbol{\phi}(\mathbf{x}).$$

This function $\boldsymbol{\phi}_e$ is differentiable with a gradient

$$\begin{aligned} \nabla_{\mathbf{x}}\boldsymbol{\phi}(\mathbf{x}) \ &= \ \nabla_{\mathbf{x}}\left(\boldsymbol{\phi}_e(\boldsymbol{\xi})\right) \ = \ \left(\nabla_{\boldsymbol{\xi}}\boldsymbol{\phi}_e(\boldsymbol{\xi})\right)\left(\nabla_{\mathbf{x}}\boldsymbol{\psi}(\mathbf{x})\right) \\ \Leftrightarrow \left(\nabla_{\mathbf{x}}\boldsymbol{\phi}(\mathbf{x})\right)\left(\nabla_{\mathbf{x}}\boldsymbol{\psi}(\mathbf{x})\right)^{-1} \ &= \ \nabla_{\boldsymbol{\xi}}\boldsymbol{\phi}_e(\boldsymbol{\xi}) \ = \ \left(\nabla_{\mathbf{x}}\boldsymbol{\phi}(\mathbf{x})\right)P^T \\ \Leftrightarrow \ \left(\nabla_{\mathbf{x}}\boldsymbol{\phi}(\mathbf{x})\right)\left(\nabla_{\boldsymbol{\xi}}\boldsymbol{\psi}^{-1}(\boldsymbol{\xi})\right) \ &= \ \nabla_{\boldsymbol{\xi}}\boldsymbol{\phi}_e(\boldsymbol{\xi}). \end{aligned} \tag{3.25}$$

Here, we obtain the last equivalence either from

$$\begin{array}{rcl}\mathbb{1} = \nabla_{\mathbf{x}}(\mathbf{x}) & = \nabla_{\mathbf{x}}(\boldsymbol{\psi}^{-1}(\boldsymbol{\psi}(\mathbf{x}))) & = (\nabla_{\boldsymbol{\xi}}\boldsymbol{\psi}^{-1}(\boldsymbol{\xi}))(\nabla_{\mathbf{x}}\boldsymbol{\psi}(\mathbf{x})) \\ \Leftrightarrow & (\nabla_{\mathbf{x}}\boldsymbol{\psi}(\mathbf{x}))^{-1} & = (\nabla_{\boldsymbol{\xi}}\boldsymbol{\psi}^{-1}(\boldsymbol{\xi})),\end{array}$$

or from

$$\nabla_{\boldsymbol{\xi}}\boldsymbol{\phi}_e(\boldsymbol{\xi}) = \nabla_{\boldsymbol{\xi}}\boldsymbol{\phi}(\boldsymbol{\psi}^{-1}(\boldsymbol{\xi})) = (\nabla_{\mathbf{x}}\boldsymbol{\phi}(\mathbf{x}))\left(\nabla_{\boldsymbol{\xi}}\boldsymbol{\psi}^{-1}(\boldsymbol{\xi})\right).$$

Instead of the given L_2-norm, we consider the expression in terms of $\boldsymbol{\phi}_e$ and use the standard first Korn inequality on the transformed domain $\boldsymbol{\psi}(\Omega)$; cf. Ciarlet [16], [55, Lemma 2.1]. Note that the constant depends on $\boldsymbol{\psi}(\Omega)$ and on $\boldsymbol{\psi}(\Gamma) \subset \boldsymbol{\psi}(\partial\Omega)$, i.e., $C := C(\boldsymbol{\psi}(\Omega), \boldsymbol{\psi}(\Gamma))$.

$$\int_{\boldsymbol{\xi}\in\boldsymbol{\psi}(\Omega)} \|\nabla_{\boldsymbol{\xi}}\boldsymbol{\phi}_e(\boldsymbol{\xi}) + (\nabla_{\boldsymbol{\xi}}\boldsymbol{\phi}_e(\boldsymbol{\xi}))^T\|_F^2 \, d\boldsymbol{\xi} \;\geq\; C \int_{\boldsymbol{\xi}\in\boldsymbol{\psi}(\Omega)} \|\nabla_{\boldsymbol{\xi}}\boldsymbol{\phi}_e(\boldsymbol{\xi})\|_F^2 \, d\boldsymbol{\xi}. \quad (3.26)$$

With the transformation formula, cf. Lemma 2, we achieve for (3.26)

$$\begin{aligned}&\int_{\boldsymbol{\xi}\in\boldsymbol{\psi}(\Omega)} \|\nabla_{\boldsymbol{\xi}}\boldsymbol{\phi}_e(\boldsymbol{\xi}) + (\nabla_{\boldsymbol{\xi}}\boldsymbol{\phi}_e(\boldsymbol{\xi}))^T\|_F^2 \, d\boldsymbol{\xi} \\ = &\int_{\boldsymbol{\xi}\in\boldsymbol{\psi}(\Omega)} \|\nabla_{\boldsymbol{\xi}}\boldsymbol{\phi}_e(\boldsymbol{\psi}(\mathbf{x})) + (\nabla_{\boldsymbol{\xi}}\boldsymbol{\phi}_e(\boldsymbol{\psi}(\mathbf{x})))^T\|_F^2 \, d\boldsymbol{\xi} \qquad (3.27) \\ = &\int_{\Omega} \|\nabla_{\boldsymbol{\xi}}\boldsymbol{\phi}_e(\boldsymbol{\psi}(\mathbf{x})) + (\nabla_{\boldsymbol{\xi}}\boldsymbol{\phi}_e(\boldsymbol{\psi}(\mathbf{x})))^T\|_F^2 \, |\det(\nabla\boldsymbol{\psi}(\mathbf{x}))| \, d\mathbf{x}\end{aligned}$$

and

$$\int_{\boldsymbol{\xi}\in\boldsymbol{\psi}(\Omega)} \||\nabla\boldsymbol{\phi}_e(\boldsymbol{\xi})\|_F^2 \, d\boldsymbol{\xi} = \int_{\Omega} \|\nabla\boldsymbol{\phi}_e(\boldsymbol{\psi}(\mathbf{x}))\|_F^2 \, |\det(\nabla\boldsymbol{\psi}(\mathbf{x}))| \, d\mathbf{x}. \qquad (3.28)$$

Since we have

$$\begin{aligned}1 = \det(\mathrm{Id}\,) = \det((\nabla\boldsymbol{\psi}(\mathbf{x})) \cdot (\nabla\boldsymbol{\psi}(\mathbf{x}))^{-1}) = \det(\nabla\boldsymbol{\psi}(\mathbf{x})) \cdot \det(P^T) \\ \Leftrightarrow \quad 0 \leq \frac{1}{\det(P^T)} = \det((\nabla\boldsymbol{\psi}(\mathbf{x})) \leq \frac{1}{\alpha^+},\end{aligned}$$

we can estimate $\det(\nabla\boldsymbol{\psi}(\mathbf{x}))$ by its maximum over all $\mathbf{x} \in \Omega$ in (3.27), i.e., the left hand side, and by its minimum in (3.28), i.e., the right hand side. Combining these results we obtain

$$\int_{\Omega} \|\nabla_{\boldsymbol{\xi}}\boldsymbol{\phi}_e(\boldsymbol{\psi}(\mathbf{x})) + (\nabla_{\boldsymbol{\xi}}\boldsymbol{\phi}_e(\boldsymbol{\psi}(\mathbf{x})))^T\|_F^2 \, d\mathbf{x} \geq C \, \frac{\min_{\mathbf{x}\in\Omega} \det(\nabla\boldsymbol{\psi}(\mathbf{x}))}{\max_{\mathbf{x}\in\Omega} \det(\nabla\boldsymbol{\psi}(\mathbf{x}))} \int_{\Omega} \|\nabla\boldsymbol{\phi}_e(\boldsymbol{\psi}(\mathbf{x}))\|_F^2 \, d\mathbf{x}.$$

Using (3.25) yields

$$\|\nabla_{\mathbf{x}}(\boldsymbol{\phi}(\mathbf{x}))P^T + P(\nabla_{\mathbf{x}}\boldsymbol{\phi}(\mathbf{x}))^T\|_{L_2(\Omega)}^2 \geq C\frac{\min_{\mathbf{x}\in\Omega} \det(\nabla\boldsymbol{\psi}(\mathbf{x}))}{\max_{\mathbf{x}\in\Omega} \det(\nabla\boldsymbol{\psi}(\mathbf{x}))}\|\nabla_{\mathbf{x}}\boldsymbol{\phi}(\mathbf{x})P^T\|_{L_2(\Omega)}^2. \quad (3.29)$$

As we aim to obtain an upper estimate for $\|\boldsymbol{\phi}\|_{H^1(\Omega)}$, we have to examine $\|\nabla_{\mathbf{x}}\boldsymbol{\phi}(\mathbf{x})P^T\|_{L_2(\Omega)}$ more closely.

$$\begin{aligned}
\|(\nabla\boldsymbol{\phi})P^T(\mathbf{x})\|^2_{L_2(\Omega)} &= \int_\Omega \operatorname{tr}(((\nabla\boldsymbol{\phi})P^T(\mathbf{x}))((\nabla\boldsymbol{\phi})P^T(\mathbf{x}))^T)\ d\mathbf{x} \\
&= \int_\Omega \operatorname{tr}(\underbrace{(\nabla\boldsymbol{\phi})}_{:=L}\underbrace{(P^T(\mathbf{x})P(\mathbf{x}))}_{:=N}(\nabla\boldsymbol{\phi})^T)\ d\mathbf{x} \\
&= \int_\Omega \sum_{k=1}^3 \Big(\sum_{i,j=1}^3 l_{ki}n_{ij}l_{kj}\Big)\ d\mathbf{x}.
\end{aligned}$$

With l_k being the k-th row of L, we have, since N is symmetric,

$$\sum_{i,j=1}^3 l_{ki}n_{ij}l_{kj} \;=\; l_kNl_k^T \;=\; < Nl_k^T, l_k^T > . \tag{3.30}$$

We use a Rayleigh quotient argument for the smallest eigenvalue of N and obtain

$$\lambda_{\min}(N) \;=\; \min_{\substack{\mathbf{x}\in\mathbb{R}^3\\ \mathbf{x}\neq 0}} \frac{< N\mathbf{x},\mathbf{x} >}{< \mathbf{x},\mathbf{x} >} \;\leq\; \frac{< Nl_k^T, l_k^T >}{< l_k^T, l_k^T >}. \tag{3.31}$$

It follows that

$$\lambda_{\min}(N)\Big(\sum_{i=1}^3 l_{ki}^2\Big) = \lambda_{\min}(N) < l_k^T, l_k^T > \;\leq\; < Nl_k^T, l_k^T > = \sum_{i,j=1}^3 l_{ki}n_{ij}l_{kj}.$$

To obtain a constant which is independent of $\mathbf{x}$, we define $\lambda_{\min,\Omega}(N)$ as $\inf_{\mathbf{x}\in\overline{\Omega}}(\lambda_{\min}(N))(\mathbf{x})$. This leads to

$$\begin{aligned}
\|(\nabla\boldsymbol{\phi})P^T(\mathbf{x})\|^2_{L_2(\Omega)} &\geq \lambda_{\min,\Omega}(P^TP)\int_\Omega \sum_{k=1}^3(\sum_{i=1}^3(\partial_k\boldsymbol{\phi}_i)^2)\ d\mathbf{x} \\
&= \lambda_{\min,\Omega}(P^TP)\int_\Omega \operatorname{tr}((\nabla\boldsymbol{\phi})(\nabla\boldsymbol{\phi})^T)\ d\mathbf{x} \qquad (3.32)\\
&= \lambda_{\min,\Omega}(P^TP)\|\nabla\boldsymbol{\phi}\|^2_{L_2(\Omega)} \;=\; \lambda_{\min,\Omega}(P^TP)|\boldsymbol{\phi}|^2_{H^1(\Omega)}.
\end{aligned}$$

We combine (3.33) with (3.29) and obtain

$$\|\nabla_{\mathbf{x}}\boldsymbol{\phi}(\mathbf{x})P^T + P(\nabla_{\mathbf{x}}\boldsymbol{\phi}(\mathbf{x}))^T\|^2_{L_2(\Omega)} \geq C\,\frac{\min_{\mathbf{x}\in\Omega}\det(P^{-T}(\mathbf{x}))}{\max_{\mathbf{x}\in\Omega}\det(P^{-T}(\mathbf{x}))}\lambda_{\min,\Omega}(P^TP)|\boldsymbol{\phi}|^2_{H^1(\Omega)}.$$

Since Ω is a bounded Lipschitz domain and we have Dirichlet boundary conditions, we can use a standard Poincaré-Friedrichs inequality; see Theorem 2. The desired inequality follows by a density argument. $\square$

Theorem 2 *(Poincaré-Friedrichs inequality)*
Let $\Omega \subset \mathbb{R}^d$ be a Lipschitz domain and let $\Gamma_0 \subset \partial\Omega$ have positive measure. Then

$$\exists c := c(\Omega) > 0 : \|u\|_{H^1(\Omega)} \leq c|u|_{H^1(\Omega)}$$

for all $u \in H^1_{\Gamma_0}(\Omega) := \{u \in H^1(\Omega) : u_{|\Gamma_0} = 0\}$.

Theorem 2 can, e.g., be found in Toselli and Widlund [89, Lemma A.14].

Lemma 2 *(Transformation formula)*
Let $\Omega, \hat{\Omega} \subset \mathbb{R}^d$ be open and $\boldsymbol{\phi} : \hat{\Omega} \to \Omega$ be a diffeomorphism. Then

$$v : \Omega \to \mathbb{R}$$

is integrable over Ω if and only if

$$(v \circ \boldsymbol{\phi})|\det \nabla\boldsymbol{\phi}| : \hat{\Omega} \to \mathbb{R}$$

is integrable over $\hat{\Omega}$. In this case one obtains

$$\int_\Omega v(y)\ dy = \int_{\hat{\Omega}} f(\boldsymbol{\phi}(x))|\det \nabla\boldsymbol{\phi}(x)|\ dx.$$

This lemma can, e.g., be found in Rudin [85, 8.27].

In the case of a subdomain which intersects the Dirichlet boundary with homogeneous boundary conditions we now obtain the H^1-ellipticity of $a_{\boldsymbol{\varphi}}(\cdot,\cdot)$ by using Theorem 1.

Theorem 3 *(Korn's second inequality)*
Let us consider the same assumptions as in Theorem 1. Then, there exists a constant $c^+ > 0$ such that

$$\|(\nabla\boldsymbol{\phi})P^T(\mathbf{x}) + P(\mathbf{x})(\nabla\boldsymbol{\phi})^T\|^2_{L_2(\Omega)} + \|\boldsymbol{\phi}\|^2_{L_2(\Omega)} \geq c^+\|\boldsymbol{\phi}\|^2_{H^1(\Omega)} \quad \forall\boldsymbol{\phi} \in \mathbf{H^1}(\Omega),$$

where c^+ is a constant depending on $\boldsymbol{\psi}(\Omega)$.

Using (3.24) we obtain the H^1-ellipticity of $a_\varphi(\cdot,\cdot)$ with Theorem 3 since

$$\begin{aligned}
& \|\varepsilon_P(\mathbf{u})\|^2_{L_2(\Omega)} + \|\mathbf{u}\|^2_{L_2(\Omega)} \\
\geq\ & \frac{1}{n^5 c_P^4}\|(\nabla\mathbf{u})P^T + P(\nabla\mathbf{u})^T\|^2_{L_2(\Omega)} + \|\mathbf{u}\|^2_{L_2(\Omega)} \\
\geq\ & \min\left\{\frac{1}{3^5 c_P^4}, 1\right\}\left(\|(\nabla\mathbf{u})P^T + P(\nabla\mathbf{u})^T\|^2_{L_2(\Omega)} + \|\mathbf{u}\|^2_{L_2(\Omega)}\right) \\
\geq\ & \min\left\{\frac{1}{243 c_P^4}, 1\right\}c^+\|\mathbf{u}\|^2_{H^1(\Omega)} \\
\geq\ & \min\left\{\frac{1}{243 c_P^4}, 1\right\}c^+|\mathbf{u}|^2_{H^1(\Omega)}.
\end{aligned}$$

Proof: We can proceed in nearly the same way as in the proof of Theorem 1.

Since $C^\infty(\bar{\Omega})$ is dense in $\mathbf{H^1}(\Omega)$, we choose $\boldsymbol{\phi} \in C^\infty(\bar{\Omega})$. Then, we can complete our proof with a standard density argument. The function $\boldsymbol{\phi}_e$ may also be defined as before. Hence, we can also adopt the considerations concerning $\boldsymbol{\phi}_e$. Here, we will use the standard second Korn inequality on the transformed domain $\boldsymbol{\psi}(\Omega)$; cf. Nitsche [79], and obtain

$$\int_{\boldsymbol{\xi}\in\boldsymbol{\psi}(\Omega)} \|\nabla_{\boldsymbol{\xi}}\boldsymbol{\phi}_e(\boldsymbol{\xi}) + \nabla_{\boldsymbol{\xi}}\boldsymbol{\phi}_e(\boldsymbol{\xi})\|_F^2 \, d\boldsymbol{\xi} + \|\boldsymbol{\phi}_e\|^2_{L_2(\boldsymbol{\psi}(\Omega))} \;\geq\; c(\boldsymbol{\psi}(\Omega))\|\boldsymbol{\phi}_e\|^2_{H^1(\boldsymbol{\psi}(\Omega))}, \tag{3.33}$$

which can also be written in the following way

$$\int_{\boldsymbol{\xi}\in\boldsymbol{\psi}(\Omega)} \|\nabla_{\boldsymbol{\xi}}\boldsymbol{\phi}_e(\boldsymbol{\xi}) + \nabla_{\boldsymbol{\xi}}\boldsymbol{\phi}_e(\boldsymbol{\xi})\|_F^2 \, d\boldsymbol{\xi} + \int_{\boldsymbol{\xi}\in\boldsymbol{\psi}(\Omega)} \|\boldsymbol{\phi}_e(\boldsymbol{\xi})\|_F^2 \, d\boldsymbol{\xi} \geq c(\boldsymbol{\psi}(\Omega)) \int_{\boldsymbol{\xi}\in\boldsymbol{\psi}(\Omega)} \|\nabla_{\boldsymbol{\xi}}\boldsymbol{\phi}_e(\boldsymbol{\xi})\|_F^2 + \|\boldsymbol{\phi}_e(\boldsymbol{\xi})\|_F^2 \, d\boldsymbol{\xi},$$

where now a constant $c := c(\boldsymbol{\psi}(\Omega))$ occurs, depending on the shape of the transformed domain. We use the transformation formula of integrals and estimate the determinant as before to obtain

$$\begin{aligned}
& \int_\Omega \|(\nabla_{\mathbf{x}}\boldsymbol{\phi})P^T(\mathbf{x}) + P(\mathbf{x})(\nabla_{\mathbf{x}}\boldsymbol{\phi})^T\|_F^2 + \|\boldsymbol{\phi}\|_F^2 \, d\mathbf{x} \\
\geq\ & c(\boldsymbol{\psi}(\Omega))\frac{\min_{\mathbf{x}\in\Omega}\det(\nabla\boldsymbol{\psi}(\mathbf{x}))}{\max_{\mathbf{x}\in\Omega}\det(\nabla\boldsymbol{\psi}(\mathbf{x}))} \int_\Omega \|(\nabla_{\mathbf{x}}\boldsymbol{\phi})P^T\|_F^2 + \|\boldsymbol{\phi}\|_F^2 \, d\mathbf{x} \\
\geq\ & c(\boldsymbol{\psi}(\Omega))\frac{\min_{\mathbf{x}\in\Omega}\det(\nabla\boldsymbol{\psi}(\mathbf{x}))}{\max_{\mathbf{x}\in\Omega}\det(\nabla\boldsymbol{\psi}(\mathbf{x}))} \left(\lambda_{\min,\Omega}(P^TP)\|\nabla_{\mathbf{x}}\boldsymbol{\phi}\|^2_{L_2(\Omega)} + \|\boldsymbol{\phi}\|^2_{L_2(\Omega)}\right) \\
\geq\ & c(\boldsymbol{\psi}(\Omega))\frac{\min_{\mathbf{x}\in\Omega}\det(\nabla\boldsymbol{\psi}(\mathbf{x}))}{\max_{\mathbf{x}\in\Omega}\det(\nabla\boldsymbol{\psi}(\mathbf{x}))} \min\{\lambda_{\min,\Omega}(P^TP), 1\} \left(\|\nabla_{\mathbf{x}}\boldsymbol{\phi}\|^2_{L_2(\Omega)} + \|\boldsymbol{\phi}\|^2_{L_2(\Omega)}\right) \\
=\ & c(\boldsymbol{\psi}(\Omega))\frac{\min_{\mathbf{x}\in\Omega}\det(P^{-T}(\mathbf{x}))}{\max_{\mathbf{x}\in\Omega}\det(P^{-T}(\mathbf{x}))} \min\{\lambda_{\min,\Omega}(P^TP), 1\} \; \|\boldsymbol{\phi}\|^2_{H^1(\Omega)}. \qquad \square
\end{aligned}$$

If the subdomain boundary does not intersect the Dirichlet boundary, as in Theorem 3, we follow the line of arguments given in Klawonn and Widlund [55].

Therefore, we introduce two alternative inner products on $\mathbf{H^1}(\Omega)$ for a region of diameter 1

$$\begin{aligned}
(\mathbf{u}, \mathbf{v})_{E_1} &:= (\varepsilon_P(\mathbf{u}), \varepsilon_P(\mathbf{v}))_{L_2(\Omega)} + (\mathbf{u}, \mathbf{v})_{L_2(\Omega)}, \\
(\mathbf{u}, \mathbf{v})_{E_2} &:= (\varepsilon_P(\mathbf{u}), \varepsilon_P(\mathbf{v}))_{L_2(\Omega)} + \sum_{i=1}^{6} (\mathbf{u}, \mathbf{r}_i)_{L_2(\Sigma)} (\mathbf{v}, \mathbf{r}_i)_{L_2(\Sigma)}, \\
\text{with} \quad (\mathbf{u}, \mathbf{r}_i)_{L_2(\Sigma)} &= \int_\Sigma \mathbf{u}^T \mathbf{r}_i \, ds\,.
\end{aligned}$$

Here, $\Sigma \subset \partial\Omega$ is assumed to have positive two dimensional Hausdorff measure.

Lemma 3 *$\|\cdot\|_{E_1}$ and $\|\cdot\|_{E_2}$ which we obtain by defining $\|\mathbf{u}\|_{E_j}^2 := (\mathbf{u},\mathbf{u})_{E_j}$ for $j = 1, 2$, i.e.,*

$$\begin{aligned}
\|\mathbf{u}\|_{E_1}^2 &= \|\varepsilon_P(\mathbf{u})\|_{L_2(\Omega)}^2 + \|\mathbf{u}\|_{L_2(\Omega)}^2, \\
\|\mathbf{u}\|_{E_2}^2 &= \|\varepsilon_P(\mathbf{u})\|_{L_2(\Omega)}^2 + \sum_{i=1}^{6}(\mathbf{u},\mathbf{r}_i)_{L_2(\Sigma)}^2
\end{aligned}$$

are norms on $\mathbf{H^1}(\Omega)$.

Proof: To show that $\|\cdot\|_{E_j}$ define norms for $j \in \{1, 2\}$ we have to prove that

1. $\|\mathbf{u}\|_{E_j} = 0 \Leftrightarrow \mathbf{u} = 0 \quad \forall \mathbf{u} \in \mathbf{H^1}(\Omega)$,
2. $\|\lambda\mathbf{u}\|_{E_j} = |\lambda|\|\mathbf{u}\|_{E_j} \quad \forall \lambda \in \mathbb{R}, \mathbf{u} \in \mathbf{H^1}(\Omega)$,
3. $\|\mathbf{u}+\mathbf{v}\|_{E_j} \leq \|\mathbf{u}\|_{E_j} + \|\mathbf{v}\|_{E_j} \quad \forall \mathbf{u},\mathbf{v} \in \mathbf{H^1}(\Omega)$.

The implication $\mathbf{u} = 0 \Rightarrow \|\mathbf{u}\|_{E_j} = 0$ is obvious.

For $j = 1$ we obtain the other implication by using Theorem 3.

$$0 = \|\mathbf{u}\|_{E_1}^2 = (\varepsilon_P(\mathbf{u}), \varepsilon_P(\mathbf{u}))_{L_2(\Omega)} + (\mathbf{u},\mathbf{u})_{L_2(\Omega)} \geq c\|\mathbf{u}\|_{H^1(\Omega)}^2 \geq 0$$

$$\Rightarrow \quad \|\mathbf{u}\|_{H^1(\Omega)} = 0 \quad \Leftrightarrow \quad \mathbf{u} = 0.$$

For $j = 2$ we have

$$\begin{aligned}
0 = \|\mathbf{u}\|_{E_2}^2 \;&\Leftrightarrow\; \|\varepsilon_P(\mathbf{u})\|_{L_2(\Omega)}^2 + \sum_{i=1}^{6}\left(\int_\Sigma \mathbf{u}^T\mathbf{r}_i \; ds\right)^2 = 0 \\
&\Leftrightarrow\; \|\varepsilon_P(\mathbf{u})\|_{L_2(\Omega)}^2 = 0 \;\wedge\; \int_\Sigma \mathbf{u}^T\mathbf{r}_i \; ds = 0 \; \forall\, i = 1, \ldots, 6. \qquad (3.34)
\end{aligned}$$

From the second equality in (3.34) follows

$$(\mathbf{u},\mathbf{v})_{L_2(\Sigma)} = 0 \quad \forall \mathbf{v} := \sum_{i=1}^{6} \alpha_i\mathbf{r}_i \in \mathbf{ker}\,(\varepsilon_P).$$

From the first equality in (3.34) follows that $\mathbf{u} \in \mathbf{ker}\,(\varepsilon_P)$. Hence, we can test with $\mathbf{v} = \mathbf{u}$ and obtain

$$(\mathbf{u},\mathbf{u})_{L_2(\Sigma)} = 0 \quad \Leftrightarrow \quad \|\mathbf{u}\|_{L_2(\Sigma)}^2 = 0 \quad \Leftrightarrow \quad \mathbf{u} = 0.$$

Since the $\mathbf{r}_i$ are linear independent on Σ we obtain that $\mathbf{u} = 0$ on Ω and not only on Σ since the α_i are zero.

That the second item holds for $j = 1, 2$ is obvious.

We are left to prove the triangle inequality for $j = 1, 2$. Therefore, we use

$$\begin{aligned}
\varepsilon_P(\mathbf{u}+\mathbf{v}) &= \mathrm{sym}(P^{-1}\nabla(\mathbf{u}+\mathbf{v})) \\
&= \frac{1}{2}(P^{-1}(\nabla\mathbf{u}+\nabla\mathbf{v}) + (\nabla\mathbf{u}+\nabla\mathbf{v})^T P^{-T}) \\
&= \frac{1}{2}(P^{-1}(\nabla\mathbf{u}) + (\nabla\mathbf{u})^T P^{-T} + P^{-1}(\nabla\mathbf{v}) + (\nabla\mathbf{v})^T P^{-T}) \\
&= \mathrm{sym}(P^{-1}\nabla\mathbf{u}) + \mathrm{sym}(P^{-1}\nabla\mathbf{v}) \\
&= \varepsilon_P(\mathbf{u}) + \varepsilon_P(\mathbf{v})
\end{aligned}$$

and hence obtain

$$\begin{aligned}
\|\varepsilon_P(\mathbf{u}+\mathbf{v})\|^2_{L_2(\Omega)} &= \|\varepsilon_P(\mathbf{u}) + \varepsilon_P(\mathbf{v})\|^2_{L_2(\Omega)} \\
&\leq (\|\varepsilon_P(\mathbf{u})\|_{L_2(\Omega)} + \|\varepsilon_P(\mathbf{v})\|_{L_2(\Omega)})^2 \qquad (3.35) \\
&= \|\varepsilon_P(\mathbf{u})\|^2_{L_2(\Omega)} + 2\|\varepsilon_P(\mathbf{u})\|_{L_2(\Omega)}\|\varepsilon_P(\mathbf{v})\|_{L_2(\Omega)} + \|\varepsilon_P(\mathbf{v})\|^2_{L_2(\Omega)}.
\end{aligned}$$

For $j = 1$ equation (3.35) yields

$$\begin{aligned}
\|\mathbf{u}+\mathbf{v}\|^2_{E_1} &= \|\varepsilon_P(\mathbf{u}+\mathbf{v})\|^2_{L_2(\Omega)} + \|\mathbf{u}+\mathbf{v}\|^2_{L_2(\Omega)} \\
&\leq \|\varepsilon_P(\mathbf{u})\|^2_{L_2(\Omega)} + \|\mathbf{u}\|^2_{L_2(\Omega)} + \|\varepsilon_P(\mathbf{v})\|^2_{L_2(\Omega)} + \|\mathbf{v}\|^2_{L_2(\Omega)} \\
&\quad +2\left(\|\varepsilon_P(\mathbf{u})\|_{L_2(\Omega)}\|\varepsilon_P(\mathbf{v})\|_{L_2(\Omega)} + \|\mathbf{u}\|_{L_2(\Omega)}\|\mathbf{v}\|_{L_2(\Omega)}\right) \\
&\leq \|\mathbf{u}\|^2_{E_1} + \|\mathbf{v}\|^2_{E_1} \\
&\quad +2\left[(\|\varepsilon_P(\mathbf{u})\|^2_{L_2(\Omega)} + \|\mathbf{u}\|^2_{L_2(\Omega)})(\|\varepsilon_P(\mathbf{v})\|^2_{L_2(\Omega)} + \|\mathbf{v}\|^2_{L_2(\Omega)})\right]^{1/2} \\
&= \|\mathbf{u}\|^2_{E_1} + \|\mathbf{v}\|^2_{E_1} + 2\|\mathbf{u}\|_{E_1}\|\mathbf{v}\|_{E_1} \\
&= (\|\mathbf{u}\|_{E_1} + \|\mathbf{v}\|_{E_1})^2
\end{aligned}$$

and for $j = 2$ we obtain

$$\begin{aligned}
\|\mathbf{u}+\mathbf{v}\|^2_{E_2} &= \|\varepsilon_P(\mathbf{u}+\mathbf{v})\|^2_{L_2(\Omega)} + \sum_{i=1}^{6}(\mathbf{u}+\mathbf{v}, \mathbf{r}_i)^2_{L_2(\Sigma)} \\
&\leq \|\varepsilon_P(\mathbf{u})\|^2_{L_2(\Omega)} + 2\|\varepsilon_P(\mathbf{u})\|_{L_2(\Omega)}\|\varepsilon_P(\mathbf{v})\|_{L_2(\Omega)} + \|\varepsilon_P(\mathbf{v})\|^2_{L_2(\Omega)} \\
&\quad + \sum_{i=1}^{6}((\mathbf{u}, \mathbf{r}_i)_{L_2(\Sigma)} + (\mathbf{v}, \mathbf{r}_i)_{L_2(\Sigma)})^2 \\
&= \|\varepsilon_P(\mathbf{u})\|^2_{L_2(\Omega)} + 2\|\varepsilon_P(\mathbf{u})\|_{L_2(\Omega)}\|\varepsilon_P(\mathbf{v})\|_{L_2(\Omega)} + \|\varepsilon_P(\mathbf{v})\|^2_{L_2(\Omega)} \\
&\quad + \sum_{i=1}^{6}\left((\mathbf{u}, \mathbf{r}_i)^2_{L_2(\Sigma)} + 2(\mathbf{u}, \mathbf{r}_i)_{L_2(\Sigma)}(\mathbf{v}, \mathbf{r}_i)_{L_2(\Sigma)} + (\mathbf{v}, \mathbf{r}_i)^2_{L_2(\Sigma)}\right) \\
&\leq \|\varepsilon_P(\mathbf{u})\|^2_{L_2(\Omega)} + \sum_{i=1}^{6}(\mathbf{u}, \mathbf{r}_i)^2_{L_2(\Sigma)} + \|\varepsilon_P(\mathbf{v})\|^2_{L_2(\Omega)} + \sum_{i=1}^{6}(\mathbf{v}, \mathbf{r}_i)^2_{L_2(\Sigma)} \\
&\quad +2\left(\|\varepsilon_P(\mathbf{u})\|_{L_2(\Omega)}\|\varepsilon_P(\mathbf{v})\|_{L_2(\Omega)} + \sum_{i=1}^{6}(\mathbf{u}, \mathbf{r}_i)_{L_2(\Sigma)}(\mathbf{v}, \mathbf{r}_i)_{L_2(\Sigma)}\right)
\end{aligned}$$

$$
\begin{aligned}
&= \|\mathbf{u}\|_{E_2}^2 + \|\mathbf{v}\|_{E_2}^2 + 2\left(\left(\|\varepsilon_P(\mathbf{u})\|_{L_2(\Omega)}^2 + \sum_{i=1}^{6}(\mathbf{u},\mathbf{r}_i)_{L_2(\Sigma)}^2\right)\right. \\
&\qquad\qquad \left.\left(\|\varepsilon_P(\mathbf{v})\|_{L_2(\Omega)}^2 + \sum_{i=1}^{6}(\mathbf{v},\mathbf{r}_i)_{L_2(\Sigma)}^2\right)\right)^{1/2} \\
&= \|\mathbf{u}\|_{E_2}^2 + \|\mathbf{v}\|_{E_2}^2 + 2\|\mathbf{u}\|_{E_2}\|\mathbf{v}\|_{E_2} \\
&= (\|\mathbf{u}\|_{E_2} + \|\mathbf{v}\|_{E_2})^2.
\end{aligned}
$$

Hence, $\|\cdot\|_{E_1}$ and $\|\cdot\|_{E_2}$ are norms. □

These norms are equivalent.

Lemma 4 *Let $\Omega \subset \mathbb{R}^3$ be a Lipschitz domain of diameter 1 and let $\Sigma \subset \partial\Omega$ be of positive measure. Then, there exist constants $0 < c \leq C < \infty$ such that*

$$
c||\mathbf{u}||_{E_1} \leq ||\mathbf{u}||_{E_2} \leq C||\mathbf{u}||_{E_1} \quad \forall \mathbf{u} \in \mathbf{H^1}(\Omega)\,.
$$

Proof: We first prove the right inequality. Using the Cauchy-Schwarz inequality, Theorem 3, and a trace theorem, we obtain

$$
\begin{aligned}
\|\mathbf{u}\|_{E_2}^2 &\leq \|\varepsilon_P(\mathbf{u})\|_{L_2(\Omega)}^2 + \Big(\sum_{i=1}^{6}(\mathbf{r}_i,\mathbf{r}_i)_{L_2(\Sigma)}\Big)\|\mathbf{u}\|_{L_2(\Omega)}^2 \\
&\leq \|\varepsilon_P(\mathbf{u})\|_{L_2(\Omega)}^2 + C(\boldsymbol{\psi}(\Omega))\left(\|\varepsilon_P(\mathbf{u})\|_{L_2(\Omega)}^2 + \|\mathbf{u}\|_{L_2(\Omega)}^2\right) \\
&\leq (1 + C(\boldsymbol{\psi}(\Omega)))\,\|\mathbf{u}\|_{E_1}^2.
\end{aligned}
$$

To show the left inequality we return to the case of linear elasticity. Therefore we consider that the elements $\mathbf{r} \in \mathbf{ker}\,(\varepsilon_P)$ are in fact transformed to the elements $\tilde{\mathbf{r}} \in \mathbf{ker}\,(\varepsilon)$ of standard linear elasticity, cf., proof of Lemma 1. We then know from Klawonn and Widlund [55, Lemma 6.2] that

$$
\begin{aligned}
&\int_{\boldsymbol{\xi}\in\boldsymbol{\psi}(\Omega)} \|\nabla_{\boldsymbol{\xi}}\mathbf{u}_e(\boldsymbol{\xi}) + (\nabla_{\boldsymbol{\xi}}\mathbf{u}_e(\boldsymbol{\xi}))^T\|_F \, d\boldsymbol{\xi} \; + \; \sum_{i=1}^{6}\int_{\boldsymbol{\xi}\in\boldsymbol{\psi}(\Sigma)} (\mathbf{u}_e(\boldsymbol{\xi}), \tilde{\mathbf{r}}_i(\boldsymbol{\xi}))_F^2 \, d\boldsymbol{\xi} \\
\geq \; & C\|\mathbf{u}_e(\boldsymbol{\xi})\|_{E_1(\boldsymbol{\psi}(\Omega))}^2.
\end{aligned}
\tag{3.36}
$$

Here, the notation from the proof of Theorem 1 are used. The constant C depends on the domains over which we integrate and hence we write $C(\boldsymbol{\psi}(\Omega), \boldsymbol{\psi}(\Sigma))$. This results from the use of Rellich's theorem in the proof for of standard linear elasticity and apparently cannot be avoided. The first term on the left hand side of (3.36) can be treated as already done in the proof of Theorem 1, i.e.,

$$
\|\mathrm{sym}(\nabla_{\boldsymbol{\xi}}\mathbf{u}_e(\boldsymbol{\xi}))\|_{L_2(\boldsymbol{\psi}(\Omega))}^2 \leq \underbrace{\max_{\mathbf{x}\in\Omega} |\det(P^{-T}(\mathbf{x}))|}_{=:\, c_{\det}} \;\; \|\mathrm{sym}(\nabla_{\mathbf{x}}\mathbf{u}(\mathbf{x})P^T)\|_{L_2(\Omega)}^2.
$$

For the second term, for $i = 1, \dots, 6$, we obtain

$$\begin{aligned}\int_{\boldsymbol{\xi}\in\boldsymbol{\psi}(\Sigma)} (\mathbf{u}_e(\boldsymbol{\xi}), \tilde{\mathbf{r}}_i(\boldsymbol{\xi}))_F^2 \, d\boldsymbol{\xi} &= \int_\Sigma (\mathbf{u}_e(\boldsymbol{\psi}(\mathbf{x})), \tilde{\mathbf{r}}_i(\boldsymbol{\psi}(\mathbf{x})))_F^2 \, \|\operatorname{Cof}(P^{-T}(\mathbf{x})) \cdot \mathbf{n}\| \, d\mathbf{x} \\ &\le \underbrace{\max_{\mathbf{x}\in\Sigma} \|\operatorname{Cof}(P^{-T}(\mathbf{x}))\|}_{=:\, c_{\text{cof}}} \int_\Sigma (\mathbf{u}(\mathbf{x}), \mathbf{r}_i(\mathbf{x}))_F^2 d\mathbf{x},\end{aligned}$$

where the cofactor of an invertible matrix A is given by $\operatorname{Cof}(A) = \det(A)A^{-T}$. Furthermore, we use Nanson's relation, cf., [45, (2.55)], i.e.,

$$d\mathbf{s} = \det(A)A^{-T} d\mathbf{S}$$

which gives the relation of the vector elements between the infinitesimal areas $d\mathbf{s}$ and $d\mathbf{S}$ on the current and the reference configuration, respectively. Here, the submultiplicativity and the fact that $\mathbf{n}$ is a unit normal surface vector are used. Combining these results, we obtain

$$\begin{aligned}\|\mathbf{u}(\mathbf{x})\|_{E_2(\Omega)}^2 &\ge \min\left(\frac{1}{c_{\text{cof}}}, \frac{1}{c_{\text{det}}}\right) \|\mathbf{u}_e(\boldsymbol{\xi})\|_{E_2(\boldsymbol{\psi}(\Omega))}^2 \\ &\ge C(\boldsymbol{\psi}(\Omega), \boldsymbol{\psi}(\Sigma)) \min\left(\frac{1}{c_{\text{cof}}}, \frac{1}{c_{\text{det}}}\right) \|\mathbf{u}_e(\boldsymbol{\xi})\|_{E_1(\boldsymbol{\psi}(\Omega))}^2 \\ &\ge C(\boldsymbol{\psi}(\Omega), \boldsymbol{\psi}(\Sigma)) \min\left(\frac{1}{c_{\text{cof}}}, \frac{1}{c_{\text{det}}}\right) \min_{\mathbf{x}\in\Omega} |\det(P^{-T}(\mathbf{x}))| \;\; \|\mathbf{u}_e(\boldsymbol{\xi})\|_{E_1(\boldsymbol{\psi}(\Omega))}^2.\end{aligned}$$

The last inequality can be obtained by the using the transformation formula, cf. Lemma 2. □

Lemma 5 *(trace theorem)*
Let $\Omega \subset \mathbb{R}^d$ be Lipschitz. Then there exists a bounded linear mapping

$$\gamma : H^1(\Omega) \to L_2(\partial\Omega)$$

with

$$(\gamma u)(\mathbf{x}) = u(\mathbf{x}) \quad \forall \mathbf{x} \in \Omega$$

for all $u \in C^1(\bar{\Omega})$ and since γ is continuous further there exists a constant $C \ge 0$ such that

$$\|\gamma u\|_{L_2(\partial\Omega)} \le C\|u\|_{H^1(\Omega)} \quad \forall u \in H^1(\Omega).$$

See, e.g., Braess [10, 3.1 Spursatz].

Using these results, we obtain the following lemma.

Lemma 6 *Let $\Omega \subset \mathbb{R}^3$ be a Lipschitz domain of diameter 1, and let $\Sigma \subset \partial\Omega$ be of positive measure. Then, there exists a positive constant $C > 0$ such that*

$$|\mathbf{u}|_{H^1(\Omega)}^2 + \|\mathbf{u}\|_{L_2(\Sigma)}^2 \le C\Big((\varepsilon_P(\mathbf{u}), \varepsilon_P(\mathbf{u}))_{L_2(\Omega)} + \|\mathbf{u}\|_{L_2(\Sigma)}^2\Big) \quad \forall \mathbf{u} \in \mathbf{H}^1(\Omega).$$

Proof: By using the standard inequality between norm and seminorm, the expression obtained by Theorem 3, and Lemma 4, we obtain

$$\begin{aligned}
& |\mathbf{u}|^2_{H^1(\Omega)} + \|\mathbf{u}\|^2_{L_2(\Sigma)} \\
\leq \quad & \|\mathbf{u}\|^2_{H^1(\Omega)} + \|\mathbf{u}\|^2_{L_2(\Sigma)} \\
\leq \quad & \frac{1}{c^+} \max\{n^5 c_P^4, 1\}(\varepsilon_P(\mathbf{u}), \varepsilon_P(\mathbf{u}))_{L_2(\Omega)} + \|\mathbf{u}\|^2_{L_2(\Omega)}\Big) + \|\mathbf{u}\|^2_{L_2(\Sigma)} \\
= \quad & \frac{1}{c^+} \max\{3^5 c_P^4, 1\}\|\mathbf{u}\|^2_{E_1} + \|\mathbf{u}\|^2_{L_2(\Sigma)} \\
\leq \quad & \frac{c}{c^+} \max\{243 c_P^4, 1\}\Big((\varepsilon_P(\mathbf{u}), \varepsilon_P(\mathbf{u}))_{L_2(\Omega)} + \sum_{i=1}^{6} (\mathbf{u}, \mathbf{r}_i)^2_{L_2(\Sigma)}\Big) + \|\mathbf{u}\|^2_{L_2(\Sigma)}.
\end{aligned}$$

By using the Cauchy-Schwarz inequality, we obtain

$$\begin{aligned}
|\mathbf{u}|^2_{H^1(\Omega)} + \|\mathbf{u}\|^2_{L_2(\Sigma)} \quad & \leq \quad C_1(\varepsilon_P(\mathbf{u}), \varepsilon_P(\mathbf{u}))_{L_2(\Omega)} + C_2\|\mathbf{u}\|^2_{L_2(\Sigma)} \\
& \leq \quad \max\{C_1, C_2\}\Big((\varepsilon_P(\mathbf{u}), \varepsilon_P(\mathbf{u}))_{L_2(\Omega)} + \|\mathbf{u}\|^2_{L_2(\Sigma)}\Big),
\end{aligned}$$

where the positive constants C_1, C_2 both depend in different ways on c_P. □

We obtain a new generalized Korn inequality by combining the results obtained so far.

Lemma 7 *Let $\Omega \subset \mathbb{R}^3$ be a Lipschitz domain and let $P^{-T} = \nabla\boldsymbol{\psi}$ with $\nabla\boldsymbol{\psi} \in C^0(\bar{\Omega}, \mathbb{R}^{3\times 3}) \subset C^\infty(\bar{\Omega}, \mathbb{R}^{3\times 3})$ be given with $\det(P^{-T}) \geq \alpha^+ > 0$ and let $\boldsymbol{\psi} : \bar{\Omega} \subset \mathbb{R}^3 \to \mathbb{R}^3$ be a $\mathcal{C}^1$-diffeomorphism. Then there exist constants $C, c > 0$, invariant under dilation, such that*

$$c|\mathbf{u}|_{H^1(\Omega)} \leq \|\varepsilon_P(\mathbf{u})\|_{L_2(\Omega)} \leq C|\mathbf{u}|_{H^1(\Omega)},$$

where $\mathbf{u} \in \{\mathbf{v} \in \mathbf{H^1}(\Omega) : (\mathbf{v}, \mathbf{r})_{L_2(\Sigma)} = 0 \ \forall \mathbf{r} \in \mathbf{ker}\,(\varepsilon_P)\}$.

Proof: The right inequality was proven in Section 2.1.1. There it was shown that

$$\|\varepsilon_P(\mathbf{u})\|_{L_2(\Omega)} \leq C\|P^{-1}\|^2_{L_2(\Omega)}|\mathbf{u}|_{H^1(\Omega)}.$$

There remains to prove the left inequality. We obtain

$$\begin{aligned}
\|\varepsilon_P(\mathbf{u})\|^2_{L_2(\Omega)} \quad & = \quad \|\varepsilon_P(\mathbf{u})\|^2_{L_2(\Omega)} + \sum_{i=1}^{6} (\mathbf{u}, \mathbf{r}_i)^2_{L_2(\Sigma)} \\
& \geq \quad c\left(\|\varepsilon_P(\mathbf{u})\|^2_{L_2(\Omega)} + \|\mathbf{u}\|^2_{L_2(\Omega)}\right) \\
& \geq \quad c^+ \min\left\{\frac{1}{3^6 c_P^4}, 1\right\}|\mathbf{u}|^2_{H^1(\Omega)}.
\end{aligned}$$

Here, we used that $(\mathbf{u}, \mathbf{r}_i)_{L_2(\Sigma)} = 0$ for all $i = 1, \ldots, 6$, as well as Lemma 4 and Theorem 3. The invariance under dilation can easily be seen by using the transformation formula for a dilation of a domain with diameter H. □

At this point, we have completed our proof of the H^1-ellipticity not only for $\mathbf{u} \in \mathbf{H_0^1}(\Omega)$ but also for $\mathbf{u} \in \big\{\mathbf{v} \in \mathbf{H^1}(\Omega) : (\mathbf{v}, \mathbf{r})_{L_2(\Sigma)} = 0 \ \forall \mathbf{r} \in \mathbf{ker}\,(\varepsilon_P)\big\}$.

3.3.2 Trace spaces, harmonic and P-elastic extensions

In the following, we will make extensive use of trace spaces equipped with trace norms. We will recall some definitions in the scalar valued case which can be extended to the three dimensional case by summing over the components. Let Σ again be a subset of $\partial\Omega$ with positive measure as before. The norms on the Sobolev space $H^{1/2}(\partial\Omega)$ and $\mathbf{H}^{1/2}(\partial\Omega) := (H^{1/2}(\partial\Omega))^3$ can be defined as

$$
\begin{aligned}
|u|_{H^{1/2}(\partial\Omega)} &:= \inf_{\substack{v\in H^1(\Omega)\\ v|_{\partial\Omega}=u}} |v|_{H^1(\Omega)} \quad \text{for} \quad v \in H^{1/2}(\partial\Omega), && (3.37)\\
|\mathbf{u}|^2_{H^{1/2}(\partial\Omega)} &:= \sum_{i=1}^{3} |u_i|^2_{H^{1/2}(\partial\Omega)} \quad \text{for} \quad \mathbf{u} \in \mathbf{H^{1/2}}(\partial\Omega). && (3.38)
\end{aligned}
$$

Another useful seminorm on $\mathbf{H}^{1/2}(\partial\Omega)$, is given by

$$
|\mathbf{u}|^2_{E_P(\partial\Omega)} := \inf_{\substack{\mathbf{v}\in \mathbf{H^1}(\Omega)\\ \mathbf{v}|_{\partial\Omega}=\mathbf{u}}} \|\varepsilon_P(\mathbf{u})\|^2_{L_2(\Omega)}. \tag{3.39}
$$

These seminorms motivate the definitions of the harmonic and P-elastic extensions of a function $\mathbf{u} \in \mathbf{H}^{1/2}(\partial\Omega)$ denoted by $(\mathbf{u}_{\text{harm}})$ and $(\mathbf{u}_{\text{P}-\text{elast}})$, respectively. These extensions belong to the space $\{\mathbf{v} \in \mathbf{H^1}(\Omega) : \mathbf{v}|_{\partial\Omega} = \mathbf{u}\}$ and are defined as

$$
\begin{aligned}
|\mathbf{u}_{\text{harm}}|_{H^1(\Omega)} &:= |\mathbf{u}|_{H^{1/2}(\partial\Omega)},\\
\|\varepsilon_P(\mathbf{u}_{\text{P}-\text{elast}})\|_{L_2(\Omega)} &:= |\mathbf{u}|_{E_P(\partial\Omega)}.
\end{aligned} \tag{3.40}
$$

Note that the harmonic and elastic extensions minimize the energies defined by the respective seminorms.

By using Lemma 6 and the fact that the $H^{1/2}$-seminorm of a function $\mathbf{u}$ is smaller or equal to the H^1-seminorm of any function which equals $\mathbf{u}$ on $\partial\Omega$, e.g., $\mathbf{u}_{\text{P}-\text{elast}}$, we obtain for $\mathbf{u} \in \mathbf{H}^{1/2}(\partial\Omega)$

$$
\begin{aligned}
|\mathbf{u}|^2_{H^{1/2}(\partial\Omega)} &= |\mathbf{u}_{\text{harm}}|^2_{H^1(\Omega)} \leq |\mathbf{u}_{\text{P}-\text{elast}}|^2_{H^1(\Omega)}\\
&\leq C\|\varepsilon_P(\mathbf{u}_{\text{P}-\text{elast}})\|^2_{L_2(\Omega)} = C|\mathbf{u}|^2_{E_P(\partial\Omega)}
\end{aligned} \tag{3.41}
$$

Combining (3.41) with a standard scaling argument, we also have two inequalities similar to the Korn inequalities on the trace space $\mathbf{H}^{1/2}(\partial\Omega)$.

Lemma 8 *Let $\Omega \subset \mathbb{R}^3$ be a Lipschitz domain of diameter H and $\Sigma \subset \partial\Omega$ an open subset with positive surface measure. Then there exists a constant $C > 0$, invariant under dilation, such that*

$$
|\mathbf{u}|^2_{H^{1/2}(\Sigma)} + \frac{1}{H}\|\mathbf{u}\|^2_{L_2(\Sigma)} \leq C\left(|\mathbf{u}|^2_{E_P(\Sigma)} + \frac{1}{H}\|\mathbf{u}\|^2_{L_2(\Sigma)}\right),
$$

where $\mathbf{u} \in \mathbf{H^{1/2}}(\Sigma)$.

We also have an additional Korn inequality.

Lemma 9 *Let $\Omega \subset \mathbb{R}^3$ be a Lipschitz domain of diameter H. Furthermore, let $P^{-T} = \nabla\boldsymbol{\psi} \in C^0(\bar{\Omega}, \mathbb{R}^{3\times 3}) \subset L^\infty(\bar{\Omega}, \mathbb{R}^{3\times 3})$ be given with $\det P^T \geq \alpha^+ > 0$ and let $\boldsymbol{\psi} : \bar{\Omega} \subset \mathbb{R}^3 \mapsto \mathbb{R}^3$ be a C^1-diffeomorphism. Then there exists a positive constant C, independent of H, such that*

$$\inf_{\mathbf{r}\in\mathbf{ker}\,(\varepsilon_P)} \|\mathbf{u}-\mathbf{r}\|^2_{L_2(\partial\Omega)} \leq CH|\mathbf{u}|^2_{E_P(\partial\Omega)} \quad \forall \mathbf{u} \in \mathbf{H}^{1/2}(\partial\Omega).$$

Proof: We can prove the lemma for a domain Ω of unit diameter and then extend it to a domain with diameter H by a standard scaling argument.

Let $\mathbf{u} \in \mathbf{H}^{1/2}(\partial\Omega)$ be arbitrary but fixed and define $\mathbf{r} \in \mathbf{ker}\,(\varepsilon_P)$ to be the minimizing element for which $(\mathbf{u}-\mathbf{r}, \mathbf{r}_i)_{L_2(\Omega)} = 0$ holds for all $i \in \{1, \ldots, 6\}$. From the standard trace theorem, cf. Lemma 5, with the P-elastic extension we get

$$\begin{aligned}
\|\mathbf{u}-\mathbf{r}\|^2_{L_2(\partial\Omega)} &\leq C\Big(|(\mathbf{u}-\mathbf{r})_{\mathrm{P-elast}}|^2_{H^1(\Omega)} + \|(\mathbf{u}-\mathbf{r})_{\mathrm{P-elast}}\|^2_{L_2(\Omega)}\Big) \\
&\leq C\Big(\|\varepsilon_P\big((\mathbf{u}-\mathbf{r})_{\mathrm{P-elast}}\big)\|^2_{L_2(\Omega)} + \|(\mathbf{u}-\mathbf{r})_{\mathrm{P-elast}}\|^2_{L_2(\Omega)}\Big) \\
&\leq C\left(\|\varepsilon_P\big((\mathbf{u}-\mathbf{r})_{\mathrm{P-elast}}\big)\|^2_{L_2(\Omega)} + \sum_{i=1}^{6}((\mathbf{u}-\mathbf{r})_{\mathrm{P-elast}}, \mathbf{r}_i)^2_{L_2(\partial\Omega)}\right) \\
&= C\Big(|\mathbf{u}-\mathbf{r}|^2_{E_P(\partial\Omega)} + \sum_{i=1}^{6}(\mathbf{u}-\mathbf{r}, \mathbf{r}_i)^2_{L_2(\partial\Omega)}\Big) \\
&= C|\mathbf{u}-\mathbf{r}|^2_{E_P(\partial\Omega)},
\end{aligned}$$

by using Lemma 4 and the second Korn inequality, cf. Theorem 3. We also have

$$|\mathbf{u}-\mathbf{r}|_{E_P(\partial\Omega)} = \|\varepsilon_P(\mathbf{u}-\mathbf{r})\|_{L_2(\Omega)} = \|\varepsilon_P(\mathbf{u}) - \varepsilon_P(\mathbf{r})\|_{L_2(\Omega)}$$

and since $\mathbf{r} \in \mathbf{ker}\,(\varepsilon_P)$ we obtain

$$|\mathbf{u}-\mathbf{r}|_{E_P(\partial\Omega)} = \|\varepsilon_P(\mathbf{u})\|_{L_2(\Omega)} = |\mathbf{u}|_{E_P(\partial\Omega)}. \tag{3.42}$$

Combining (3.42) with the estimate above leads to

$$\|\mathbf{u}-\mathbf{r}\|^2_{L_2(\partial\Omega)} \leq C|\mathbf{u}|^2_{E_P(\partial\Omega)}.$$

Since we use Theorem 3 the constant depends on P. □

In our convergence analysis in Section 3.4 we use the Schur complement S which is obtained from the discretization of a vector-valued Laplace operator scaled by $\mu_e := \max_i \mu_e^{(i)}$. As in the case of P-elasticity, we get local Schur complements $S_\varepsilon^{(i)}$ and $S^{(i)}$ by eliminating the interior variables. Since S is block-diagonal with blocks $S^{(i)}$, we work with the norm $|\mathbf{u}|^2_S := \sum_{i=1}^N |u^{(i)}|^2_{S^{(i)}}$, where $|u^{(i)}|^2_{S^{(i)}} := (S^{(i)}u^{(i)}, u^{(i)})_F$.

A proof of the equivalence of the $S^{(i)}$- and the $H^{1/2}(\partial\Omega_i)$-seminorms of elements of $W^{(i)}$ and for floating subdomains Ω_i can be found already in [9] for the case of piecewise linear elements in two dimensions, and the tools necessary to extend this result to more general finite elements are provided in [92]; see also [89, Section 4.4]. In our case, we of course have to multiply $|u^{(i)}|^2_{H^{1/2}(\partial\Omega_i)}$ by the factor $\mu_e^{(i)}$. The extension to boundary subdomains is also immediate.

Thus we have to consider the relation between S and S_ε. Since we consider in the basic assumption, cf. Assumption 1, that the values $\mu_e^{(i)}$ and $\lambda_e^{(i)}$ are constant on the subdomains we can consider the norm scaled by μ_e and obtain

$$|\mathbf{u}|^2_{S_\varepsilon} \leq 9c_P^2 \max_i (1 + \frac{\lambda_e^{(i)}}{\mu_e}) |\mathbf{u}|^2_S \quad \forall \mathbf{w} \in \mathbf{W}^h. \tag{3.43}$$

To complete our notation, we introduce for $\mathbf{u} \in \widetilde{\mathbf{W}}$ a norm

$$|\mathbf{u}|_{\widetilde{S}_\varepsilon} := (\widetilde{S}_\varepsilon \mathbf{u}, \mathbf{u})_F^{1/2}. \tag{3.44}$$

And for $\mathbf{u} \in \widetilde{\mathbf{W}}$ we get, by using (3.6), the relation

$$|\mathbf{u}|_{\widetilde{S}_\varepsilon} = |R\mathbf{u}|_{S_\varepsilon}, \tag{3.45}$$

where $R\mathbf{u} \in \mathbf{W}$.

3.4 Convergence analysis

In this section, we provide an analysis of the convergence of our FETI-DP algorithms. We first present an abstract theoretical framework that almost exclusively uses algebraic arguments except for one condition, which requires the analytic tools of Sections 3.3.1 and 3.5. Then we establish this condition for a special configuration of primal constraints.

We first review the abstract theory developed in Klawonn and Widlund [55], which provides a condition number estimate for the preconditioned FETI-DP matrix $M^{-1}F$. We will work with the representations of F and M^{-1} given in (3.3) and (3.7), respectively. We note that the proof of Lemma 11 is new and generalizes Lemma 8.5 from [55] to the case of P-elasticity. In contrast to the results in [55], here we use piecewise quadratic finite element functions. The technical lemmas needed for our analysis, cf. Section 3.5, are extended to this case and the proofs are new.

Let us repeat the notation of spaces usually used in the analysis of FETI-DP methods. We denote by $\mathbf{W} := \prod_{i=1}^N \mathbf{W}^{(i)}$ the product space associated with the trace spaces $\mathbf{W}^{(i)}$, i.e., $\mathbf{W}^{(i)} := \mathbf{W}^h(\partial\Omega_i \cup \Gamma)$ where $\mathbf{W}^h(\Omega_i)$ denotes the finite element space of continuous, piecewise quadratic functions. Note, that the elements in $\mathbf{W}$ might be discontinuous across the interface. The finite element approximation of the elliptic problem is continuous across Γ, and we denote the corresponding subspace of $\mathbf{W}$ by $\widehat{\mathbf{W}}$. Furthermore, we define

$$\widetilde{\mathbf{W}} := \left\{ \mathbf{u} : \exists \mathbf{u}^{(i)} \in \mathbf{W}^{(i)}, i = 1, \dots, N, \text{ such that } \mathbf{u} = \sum_{i=1}^{N} R^{(i)T} \mathbf{u}^{(i)} \right\}.$$

as the subspace of partially assembled finite element functions with an assembly in the primal variables of FETI-DP.

As indicated before, we let $\mathbf{V} := \mathbf{range}\,(M^{-1}) \subset \mathbf{range}\,(B_{D,\Gamma})$ be the space of Lagrange multipliers. If we choose the initial guess $\lambda^{(0)}$ in the conjugate gradient algorithm in $\mathbf{V}$, e.g., $\lambda^{(0)} = 0$, then all iterates $\lambda^{(k)}$ will remain in $\mathbf{V}$. As in [54, Section 5], we introduce a projection

$$P_D : \widetilde{\mathbf{W}} \longrightarrow \widetilde{\mathbf{W}}, \quad P_D := B_{D,\Gamma}^T B_\Gamma.$$

A simple computation shows that P_D preserves the jump of any function $\mathbf{u} \in \widetilde{\mathbf{W}}$ with respect to the jump operator B_Γ, i.e.,

$$B_\Gamma P_D \mathbf{u} = B_\Gamma \mathbf{u} \quad \forall \mathbf{u} \in \widetilde{\mathbf{W}}. \tag{3.46}$$

Similarly, the transpose P_D^T preserves the scaled jump, i.e.,

$$B_{D,\Gamma} P_D^T \mathbf{u} = B_{D,\Gamma} \mathbf{u}. \tag{3.47}$$

Since the elements of $\widehat{\mathbf{W}}$ take common values across the interface we have $P_D \mathbf{u} = 0$ for all $\mathbf{u} \in \widetilde{\mathbf{W}}$.

Let $\mathbf{w} \in \widetilde{\mathbf{W}}$, then we have

$$(R^{(i)} P_D \mathbf{w})(\mathbf{x}) = \sum_{j \in \mathcal{N}_\mathbf{x}} \delta_j^\dagger ((R^{(i)} \mathbf{w})(\mathbf{x}) - (R^{(j)} \mathbf{w})(\mathbf{x})), \quad \mathbf{x} \in \partial\Omega_{i,h} \cap \Gamma_h, \tag{3.48}$$

see [55, (8.3)] and [54, (4.4)]. Here, $\mathcal{N}_\mathbf{x} := \left\{ j \in \{1, \dots N\} : \mathbf{x} \in \partial\Omega_{j,h} \right\}$ denotes the set of the indices of the subdomains which have $\mathbf{x}$ on their boundary. Furthermore, $\delta_j^\dagger$ is the scalar factor introduced in (3.4). We note that formula (3.48) is independent of the particular choice of B_Γ.

To show our condition number estimate, we require the operator P_D to satisfy the following stability condition; see also Lemma 11.

Condition 1 *For all* $\mathbf{w} \in \widetilde{\mathbf{W}}$, *we have*

$$|P_D \mathbf{w}|_{\widetilde{S}_\varepsilon}^2 \leq C \left(1 + \log\left(\frac{H}{h}\right) \right)^2 |\mathbf{w}|_{\widetilde{S}_\varepsilon}^2,$$

with $\frac{H}{h} := \max_i \left(\frac{H_i}{h_i}\right)$, *$H_i$ being the subdomain diameter of and h_i the typical element diameter in the subdomain Ω_i.*

This condition will be shown for a particular set of primal variables in this section. When this condition holds for a set of primal constraints we obtain the following condition number estimate. Note that the proof is taken from [55, Theorem 8.2] and only repeated for the convenience of the reader.

Theorem 4 *The condition number of the preconditioned FETI-DP matrix satisfies*

$$\kappa(M^{-1}F) \leq C\left(1+\log\left(\frac{H}{h}\right)\right)^2.$$

Here, C is independent of h, H, γ and the values of μ_e and λ_e but it depends on $P^{-T} = \nabla\boldsymbol{\psi}$.

Proof: Since

$$\kappa(M^{-1}F) = \frac{\lambda_{\max}(M^{-1}F)}{\lambda_{\min}(M^{-1}F)}$$

we obtain an upper estimate of the condition number by using an upper estimate for $\lambda_{\max}$ and a lower estimate for $\lambda_{\min}$. We use a standard Rayleigh quotient argument to characterize the eigenvalues as follows

$$\begin{aligned} \lambda_{\max}(M^{-1}F) &= \max_{\substack{\mathbf{v}\in\mathbf{V}\\ \mathbf{v}\neq 0}} \frac{\langle M^{-1}F\mathbf{v},\mathbf{v}\rangle_F}{\langle \mathbf{v},\mathbf{v}\rangle_F} \\ \text{and} \qquad \lambda_{\min}(M^{-1}F) &= \min_{\substack{\mathbf{v}\in\mathbf{V}\\ \mathbf{v}\neq 0}} \frac{\langle M^{-1}F\mathbf{v},\mathbf{v}\rangle_F}{\langle \mathbf{v},\mathbf{v}\rangle_F}, \end{aligned}$$

where $\langle \mathbf{v},\mathbf{v}\rangle_F := \mathbf{v}^T F\mathbf{v}$. Obviously it is sufficient to prove

$$\forall \mathbf{v}\in\mathbf{V} : \langle \mathbf{v},\mathbf{v}\rangle_F \;\leq\; \langle M^{-1}F\mathbf{v},\mathbf{v}\rangle_F \;\leq\; C\left(1+\log\left(\frac{H}{h}\right)\right)^2 \langle \mathbf{v},\mathbf{v}\rangle_F, \tag{3.49}$$

With (3.49) we obtain the estimates

$$\lambda_{\max}(M^{-1}F) = \max_{\substack{\mathbf{v}\in\mathbf{V}\\ \mathbf{v}\neq 0}} \frac{\langle M^{-1}F\mathbf{v},\mathbf{v}\rangle_F}{\langle \mathbf{v},\mathbf{v}\rangle_F} \leq C\left(1+\log\left(\frac{H}{h}\right)\right)^2, \tag{3.50}$$

$$\lambda_{\min}(M^{-1}F) = \min_{\substack{\mathbf{v}\in\mathbf{V}\\ \mathbf{v}\neq 0}} \frac{\langle M^{-1}F\mathbf{v},\mathbf{v}\rangle_F}{\langle \mathbf{v},\mathbf{v}\rangle_F} \geq \min_{\substack{\mathbf{v}\in\mathbf{V}\\ \mathbf{v}\neq 0}} \frac{\langle \mathbf{v},\mathbf{v}\rangle_F}{\langle \mathbf{v},\mathbf{v}\rangle_F} = 1. \tag{3.51}$$

From (3.50) and (3.51) follows directly the estimate for $\kappa(M^{-1}F)$.

$$\kappa(M^{-1}F) = \frac{\lambda_{\max}(M^{-1}F)}{\lambda_{\min}(M^{-1}F)} \leq C\left(1+\log\left(\frac{H}{h}\right)\right)^2.$$

It remains to prove the bounds introduced in (3.49). Remind that $\mathbf{V} = \mathbf{range}\,(M^{-1}) \subset \mathbf{range}\,(B_{D,\Gamma})$.

Lower bound. For all $\mathbf{v} \in \mathbf{V} \subset \mathbf{range}\,(B_{D,\Gamma})$ exists a $\boldsymbol{\nu}$ such that $B_{D,\Gamma}\boldsymbol{\nu} = \mathbf{v}$. With (3.47) we have

$$\mathbf{v} = B_{D,\Gamma}\boldsymbol{\nu} \;\; = B_{D,\Gamma}P_D^T\boldsymbol{\nu} \;\; = B_{D,\Gamma}B_\Gamma^T B_{D,\Gamma}\boldsymbol{\nu} \;\; = B_{D,\Gamma}B_\Gamma^T\mathbf{v}\,.$$

Using the definitions of M^{-1} and F; see (3.7) and (3.3), respectively, we obtain together with the Cauchy-Schwarz inequality

$$\begin{aligned}
\langle \mathbf{v},\mathbf{v}\rangle_F^2 &= \langle \mathbf{v}, B_{D,\Gamma}B_\Gamma^T\mathbf{v}\rangle_F^2 \\
&= \langle F\mathbf{v}, B_{D,\Gamma}\widetilde{S}_\varepsilon^{1/2}\widetilde{S}_\varepsilon^{-1/2}B_\Gamma^T\mathbf{v}\rangle^2 \\
&= \langle \widetilde{S}_\varepsilon^{1/2}B_{D,\Gamma}^T F\mathbf{v}, \widetilde{S}_\varepsilon^{-1/2}B_\Gamma^T\mathbf{v}\rangle^2 \\
&\leq \langle \widetilde{S}_\varepsilon^{1/2}B_{D,\Gamma}^T F\mathbf{v}, \widetilde{S}_\varepsilon^{1/2}B_{D,\Gamma}^T F\mathbf{v}\rangle\langle \widetilde{S}_\varepsilon^{-1/2}B_\Gamma^T\mathbf{v}, \widetilde{S}_\varepsilon^{-1/2}B_\Gamma^T\mathbf{v}\rangle \\
&= \langle B_{D,\Gamma}\widetilde{S}_\varepsilon B_{D,\Gamma}^T F\mathbf{v}, F\mathbf{v}\rangle\langle B_\Gamma\widetilde{S}_\varepsilon^{-1}B_\Gamma^T\mathbf{v},\mathbf{v}\rangle \\
&= \langle M^{-1}F\mathbf{v},\mathbf{v}\rangle_F\langle \mathbf{v},\mathbf{v}\rangle_F.
\end{aligned}$$

Cancelling the common factor $\langle \mathbf{v},\mathbf{v}\rangle_F$ gives the lower bound.

Upper bound. For $\mathbf{v} \in \mathbf{V}$ holds $\widetilde{S}_\varepsilon^{-1}B_\Gamma^T\mathbf{v} \in \widetilde{\mathbf{W}}$. By using Condition 1 and again the definitions of M^{-1} and F we obtain for all $\mathbf{v} \in \mathbf{V}$

$$\begin{aligned}
\langle M^{-1}F\mathbf{v},\mathbf{v}\rangle_F &= \langle B_{D,\Gamma}\widetilde{S}_\varepsilon B_{D,\Gamma}^T B_\Gamma\widetilde{S}_\varepsilon^{-1}B_\Gamma^T\mathbf{v}, B_\Gamma\widetilde{S}_\varepsilon^{-1}B_\Gamma^T\mathbf{v}\rangle \\
&= \langle \widetilde{S}_\varepsilon(B_{D,\Gamma}^T B_\Gamma)\widetilde{S}_\varepsilon^{-1}B_\Gamma^T\mathbf{v}, (B_{D,\Gamma}^T B_\Gamma)\widetilde{S}_\varepsilon^{-1}B_\Gamma^T\mathbf{v}\rangle \\
&= |P_D(\widetilde{S}_\varepsilon^{-1}B_\Gamma^T\mathbf{v})|_{\widetilde{S}_\varepsilon}^2 \\
&\leq C\left(1+\log\left(\frac{H}{h}\right)\right)^2 |\widetilde{S}_\varepsilon^{-1}B_\Gamma^T\mathbf{v}|_{\widetilde{S}_\varepsilon}^2 \\
&\leq C\left(1+\log\left(\frac{H}{h}\right)\right)^2 \langle \widetilde{S}_\varepsilon\widetilde{S}_\varepsilon^{-1}B_\Gamma^T\mathbf{v}, \widetilde{S}_\varepsilon^{-1}B_\Gamma^T\mathbf{v}\rangle \\
&= C\left(1+\log\left(\frac{H}{h}\right)\right)^2 \langle B_\Gamma\widetilde{S}_\varepsilon^{-1}B_\Gamma^T\mathbf{v},\mathbf{v}\rangle \\
&= C\left(1+\log\left(\frac{H}{h}\right)\right)^2 \langle \mathbf{v},\mathbf{v}\rangle_F.
\end{aligned}$$

Thus, we have the upper bound of (3.49). □

We will now give a proof of the condition number estimate, i.e., of Condition 1. We follow the structure of the proof in Klawonn and Widlund [55] and give the full details for a special case, see [55, Section 8.1] and Assumption 2. The other cases considered in Klawonn and Widlund [55, Sections 8.3, 8.4] can be treated analogously.

As in [55], Condition 1 will be established under the following assumptions; cf. [55, Assumption 3.3, Assumption 8.3]

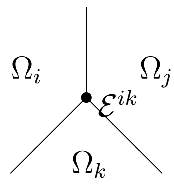

Figure 3.2: Planar cut of three domains sharing an edge.

Assumption 1 *(1) Each subdomain Ω_i is the union of a number of shape regular tetrahedral coarse elements, the number of which is uniformly bounded, and all the edges of Ω_i are straight line segments.*

(2) Each face has a boundary that is a closed curve formed by at least three edges except when part of the boundary of the face belongs to $\partial\Omega_D$. In the latter case the part of the boundary that belongs to the interface Γ_h is the union of edges and vertices. We will refer to them as the standard and the Dirichlet case, respectively.

(3) The Lamé constants do not vary inside one subdomain, and the triangulation of each subdomain is quasi-uniform.

Assumption 2 *In the decomposition of Ω into subdomains, no more than three subdomains are common to any edge and with each of the three subdomains sharing a face with the other two; see Figure 3.2. Furthermore, all subdomain vertices are primal and all faces are fully primal; cf. Definition 4.*

Considering Assumption 2, we know that each face $\mathcal{F}^{ij}$ which is common to two subdomains Ω_i and Ω_j has six linear functionals $f_m(\cdot)$ which satisfy the conditions of Definition 4. In addition, for all $\mathbf{w} \in \widetilde{\mathbf{W}}$, the f_m share the same values on the face $\mathcal{F}^{ij}$, i.e.,

$$f_m(\mathbf{w}^{(i)}) = f_m(\mathbf{w}^{(j)}) \quad \text{where} \;\; \mathbf{w}^{(i)} = R^{(i)}\mathbf{w} \;, \quad \mathbf{w}^{(j)} = R^{(j)}\mathbf{w}.$$

With these assumptions we can prove Condition 1; see Lemma 11.

In order to obtain our estimate, we need a relation between the coefficients $\mu_e^{(i)}, \mu_e^{(k)}$, and the functions $\delta_k^\dagger$. Note that again the proof is taken from [55, Lemma 8.4] and only repeated for the convenience of the reader.

Lemma 10 *For $\gamma \geq \frac{1}{2}$ holds*

$$\mu_e^{(i)}(\delta_j^\dagger)^2 \leq \min(\mu_e^{(i)}, \mu_e^{(j)}).$$

Proof: For this proof we recall the definition of $\delta_k^\dagger$ in (3.4)

$$\delta_j^\dagger(x) := \frac{(\mu_e^{(j)})^\gamma}{\sum_{k\in\mathcal{N}_x}(\mu_e^{(k)})^\gamma}.$$

Since $\mu_e^{(l)} > 0$ for all $l \in \{1, \dots, N\}$ and $\{i, j\} \subset \mathcal{N}_x$, we can estimate the denominator of $\delta_j^\dagger$ from below by

$$\sum_{k \in \mathcal{N}_x} (\mu_e^{(k)})^\gamma \geq (\mu_e^{(i)})^\gamma + (\mu_e^{(j)})^\gamma = (\mu_e^{(j)})^\gamma \left(1 + \left(\frac{\mu_e^{(i)}}{\mu_e^{(j)}}\right)^\gamma\right).$$

Hence, we have

$$\begin{aligned} \frac{\mu_e^{(i)} (\delta_j^\dagger)^2}{\min(\mu_e^{(i)}, \mu_e^{(j)})} &\leq \frac{\mu_e^{(i)}}{\min(\mu_e^{(i)}, \mu_e^{(j)})} \frac{(\mu_e^{(j)})^{2\gamma}}{(\mu_e^{(j)})^{2\gamma} \left(1 + \left(\frac{\mu_e^{(i)}}{\mu_e^{(j)}}\right)^\gamma\right)^2} \\ &= \frac{\mu_e^{(i)}}{\min(\mu_e^{(i)}, \mu_e^{(j)})} \frac{1}{\left(1 + \left(\frac{\mu_e^{(i)}}{\mu_e^{(j)}}\right)^\gamma\right)^2}. \end{aligned} \tag{3.52}$$

We now consider separately the two possible cases $\mu_e^{(j)} = \min(\mu_e^{(i)}, \mu_e^{(j)})$ and $\mu_e^{(i)} = \min(\mu_e^{(i)}, \mu_e^{(j)})$.

Let us first assume that $\mu_e^{(j)} = \min(\mu_e^{(i)}, \mu_e^{(j)})$, i.e., $\mu_e^{(j)} \leq \mu_e^{(i)}$. Hence, $x := \frac{\mu_e^{(i)}}{\mu_e^{(j)}} \geq 1$ and

$$x \geq 1 \Rightarrow x^p \geq x^q \text{ for } p \geq q.$$

From $\gamma \geq \frac{1}{2}$ now follows

$$x^\gamma \geq x^{\frac{1}{2}}.$$

Inserting the substitution $x = \frac{\mu_e^{(i)}}{\mu_e^{(j)}}$ and the result obtained in (3.52) gives

$$\frac{\mu_e^{(i)}}{\mu_e^{(j)}} \frac{1}{\left(1 + \left(\frac{\mu_e^{(i)}}{\mu_e^{(j)}}\right)^\gamma\right)^2} = \frac{x}{(1 + x^\gamma)^2} \leq \frac{x}{(1 + \sqrt{x})^2} = \frac{x}{1 + x + 2\sqrt{x}} \tag{3.53}$$

Hence, the inequality holds since

$$\frac{x}{1 + x + 2\sqrt{x}} \leq 1 \quad \Leftrightarrow \quad 0 \leq 1 + 2\sqrt{x}.$$

In the other case, i.e., $\mu_e^{(i)} \leq \mu_e^{(j)}$, we use $x := \frac{\mu_e^{(i)}}{\mu_e^{(j)}} \in (0, 1]$. And since $\mu_e^{(i)} = \min(\mu_e^{(i)}, \mu_e^{(j)})$ equation (3.52) reduces to

$$\frac{1}{(1 + x^\gamma)^2} \leq 1 \quad \Leftrightarrow \quad 1 \leq (1 + x^\gamma)^2,$$

which holds since $x^\gamma \geq 0$. $\square$

Now we can prove that Condition 1 is satisfied.

Lemma 11 *Given the Assumptions 1 and 2, we have for all* $\mathbf{w} \in \widetilde{\mathbf{W}}$

$$|P_D \mathbf{w}|^2_{\widetilde{S}_\varepsilon} \leq C \left(1 + \log\left(\frac{H}{h}\right)\right)^2 |\mathbf{w}|^2_{\widetilde{S}_\varepsilon}.$$

Proof: Let $\mathbf{w} \in \widetilde{\mathbf{W}}$ be arbitrary. Considering (3.45) we have

$$|P_D \mathbf{w}|_{\widetilde{S}_\varepsilon} = |R P_D \mathbf{w}|_{S_\varepsilon} \quad \text{and} \quad |\mathbf{w}|_{\widetilde{S}_\varepsilon} = |R\mathbf{w}|_{S_\varepsilon}. \tag{3.54}$$

Hence with (3.43) and $\mathbf{v}^{(i)} := R^{(i)} P_D \mathbf{w}$ it is sufficient to show that

$$\sum_{i=1}^{N} |\mathbf{v}^{(i)}|^2_{S^{(i)}} = |R P_D \mathbf{w}|^2_S \leq C \left(1 + \log\left(\frac{H}{h}\right)\right)^2 |R\mathbf{w}|^2_{S_\varepsilon}.$$

Since $R\mathbf{w} = [R^{(1)}\mathbf{w}, \ldots, R^{(N)}\mathbf{w}] = [\mathbf{w}^{(1)}, \ldots, \mathbf{w}^{(N)}] \in \mathbf{W}$ it is sufficient to prove for each $i = 1, \ldots N$

$$|\mathbf{v}^{(i)}|^2_{S^{(i)}} \leq C \left(1 + \log\left(\frac{H}{h}\right)\right)^2 \sum_{j \in \mathcal{N}_i} |\mathbf{w}^{(j)}|^2_{S^{(j)}_\varepsilon}, \tag{3.55}$$

where $\mathcal{N}_i$ is the set of the indices of neighboring subdomains of Ω_i including i itself, i.e., $\mathcal{N}_i := \{l \in \{1, \ldots, N\}, \partial\Omega_{i,h} \cap \partial\Omega_{l,h} \neq \emptyset\}$.

To prove the estimate, we introduce partition-of-unity functions $\theta_{\mathcal{F}^{ij}}, \theta_{\mathcal{E}^{ik}}$, and $\theta_{\mathcal{V}^{il}}$ associated with the decomposition of the interface Γ into faces, edges, and vertices, cf. Definition 1, Section 3.1.3. These functions are finite element functions on the decomposition $\tau_{h/2}$. Here, $\tau_{h/2}$ denotes the decompositon which is obtained when we split each tetrahedron naturally into eight new tetrahedra by using the midpoints of the edges of the quadratic elements as new vertices. The functions $\theta_{\mathcal{F}^{ij}}$, $\theta_{\mathcal{E}^{ik}}$, and $\theta_{\mathcal{V}^{il}}$ are supposed to be piecewise linear finite element functions on $\tau_{h/2}$ taking the value 1 in each point of the respective sets of interface nodes and vanishing elsewhere, e.g.,

$$\theta_{\mathcal{F}^{ij}}(\mathbf{x}) = \begin{cases} 1 & \text{if } \mathbf{x} \in \mathcal{F}^{ij}_{h/2} \\ 0 & \text{if } \mathbf{x} \notin \mathcal{F}^{ij}_{h/2} \end{cases}. \tag{3.56}$$

With these functions, we can write $\mathbf{v}^{(i)}$ as

$$\mathbf{v}^{(i)} = \sum_{\mathcal{F}^{ij} \subset \partial\Omega_i} I^h(\theta_{\mathcal{F}^{ij}} \mathbf{v}^{(i)}) + \sum_{\mathcal{E}^{ik} \subset \partial\Omega_i} I^h(\theta_{\mathcal{E}^{ik}} \mathbf{v}^{(i)}) + \sum_{\mathcal{V}^{il} \in \partial\Omega_i} \theta_{\mathcal{V}^{il}} \mathbf{v}^{(i)}(\mathcal{V}^{il}). \tag{3.57}$$

Since all vertices are primal, cf. Assumption 2, we see from (3.48) that $\mathbf{v}^{(i)}$ vanishes at all vertices and

$$\mathbf{v}^{(i)} = \sum_{\mathcal{F}^{ij} \subset \partial\Omega_i} I^h(\theta_{\mathcal{F}^{ij}} \mathbf{v}^{(i)}) + \sum_{\mathcal{E}^{ik} \subset \partial\Omega_i} I^h(\theta_{\mathcal{E}^{ik}} \mathbf{v}^{(i)}). \tag{3.58}$$

Face Terms. Since the faces $\mathcal{F}^{ij}$ are shared by the two subdomains Ω_i and Ω_j, there remains only one term in (3.48)

$$I^h(\theta_{\mathcal{F}^{ij}}\delta_j^\dagger(\mathbf{w}^{(i)} - \mathbf{w}^{(j)})). \tag{3.59}$$

All faces are chosen to be fully primal, cf. Assumption 2, and thus we have six linear functionals $f_m^{\mathcal{F}^{ij}}(\cdot) = f_m(\cdot)$ on $\mathcal{F}^{ij}$ which satisfy $f_m^{\mathcal{F}^{ij}}(\mathbf{w}^{(i)}) = f_m^{\mathcal{F}^{ij}}(\mathbf{w}^{(j)})$ for $m = 1, \ldots, 6$. Next, we consider

$$\mathbf{w}^{(i)} - \mathbf{w}^{(j)} = \left(\mathbf{w}^{(i)} - \sum_{m=1}^{6} f_m^{\mathcal{F}^{ij}}(\mathbf{w}^{(i)})\mathbf{r}_m\right) - \left(\mathbf{w}^{(j)} - \sum_{m=1}^{6} f_m^{\mathcal{F}^{ij}}(\mathbf{w}^{(j)})\mathbf{r}_m\right). \tag{3.60}$$

From Defintion 4 follows for the basis elements of $\mathbf{ker}\,(\varepsilon_P)$

$$f_m^{\mathcal{F}^{ij}}(\mathbf{r}_n) = \delta_{mn} \quad \forall m, n = 1, \ldots 6.$$

Using the representation of an arbitrary element $\mathbf{r}^{(i)} \in \mathbf{ker}\,\varepsilon_P$, with $\mathbf{r}^{(i)} \in \mathbf{W}^{(i)}$, in terms of the basis $(\mathbf{r}_m)_{m=1,\ldots,6}$, we obtain

$$\begin{aligned} \mathbf{r}^{(i)} = \sum_{n=1}^{6} \alpha_n \mathbf{r}_n &= \sum_{n=1}^{6}(\sum_{m=1}^{6} \alpha_m f_n^{\mathcal{F}ij}(\mathbf{r}_m))\mathbf{r}_n \\ &= \sum_{n=1}^{6} f_n^{\mathcal{F}^{ij}}(\sum_{m=1}^{6} \alpha_m \mathbf{r}_m)\mathbf{r}_n = \sum_{n=1}^{6} f_n^{\mathcal{F}^{ij}}(\mathbf{r}^{(i)})\mathbf{r}_n. \end{aligned} \tag{3.61}$$

We extend the first term of the right hand side in (3.60) by using (3.61)

$$\mathbf{w}^{(i)} - \sum_{m=1}^{6} f_m^{\mathcal{F}^{ij}}(\mathbf{w}^{(i)})\mathbf{r}_m = (\mathbf{w}^{(i)} - \mathbf{r}^{(i)}) - \sum_{m=1}^{6} f_m^{\mathcal{F}^{ij}}(\mathbf{w}^{(i)} - \mathbf{r}^{(i)})\mathbf{r}_m. \tag{3.62}$$

We can estimate the first term on the right hand side in (3.62) by using Lemmas 16 and 7

$$\begin{aligned} & |I^h(\theta_{\mathcal{F}^{ij}}(\mathbf{w}^{(i)} - \mathbf{r}^{(i)}))|^2_{H^{1/2}(\partial\Omega_i)} \\ \leq\ & C\left(1 + \log\left(\frac{H_i}{h_i}\right)\right)^2 \left(|\mathbf{w}^{(i)} - \mathbf{r}^{(i)}|^2_{H^{1/2}(\partial\Omega_i)} + \frac{1}{H_i}\|\mathbf{w}^{(i)} - \mathbf{r}^{(i)}\|^2_{L_2(\partial\Omega_i)}\right) \\ \leq\ & C\left(1 + \log\left(\frac{H_i}{h_i}\right)\right)^2 \left(|\mathbf{w}^{(i)} - \mathbf{r}^{(i)}|^2_{E_P(\partial\Omega_i)} + \frac{1}{H_i}\|\mathbf{w}^{(i)} - \mathbf{r}^{(i)}\|^2_{L_2(\partial\Omega_i)}\right) \\ \leq\ & C\left(1 + \log\left(\frac{H_i}{h_i}\right)\right)^2 \left(|\mathbf{w}^{(i)}|^2_{E_P(\partial\Omega_i)} + \frac{1}{H_i}\|\mathbf{w}^{(i)} - \mathbf{r}^{(i)}\|^2_{L_2(\partial\Omega_i)}\right). \end{aligned} \tag{3.63}$$

To estimate the second part in (3.62), we need two auxiliary inequalities. By using Lemma 12 and considering that $\|\mathbf{r}_m\|_\infty < C$ we obtain

$$|I^h(\theta_{\mathcal{F}^{ij}}\mathbf{r}_m)|^2_{H^{1/2}(\partial\Omega_i)} \leq CH_i\left(1 + \log\left(\frac{H_i}{h_i}\right)\right). \tag{3.64}$$

By using Definition 4 and Lemma 8 we get

$$\begin{aligned}
&|f_m^{\mathcal{F}^{ij}}(\mathbf{w}^{(i)} - \mathbf{r}^{(i)})|^2 \\
\leq\ & CH_i^{-1}\left(1+\log\left(\frac{H_i}{h_i}\right)\right)\left(|\mathbf{w}^{(i)} - \mathbf{r}^{(i)}|^2_{H^{1/2}(\partial\Omega_i)} + \frac{1}{H_i}\|\mathbf{w}^{(i)} - \mathbf{r}^{(i)}\|^2_{L_2(\partial\Omega_i)}\right) \\
\leq\ & CH_i^{-1}\left(1+\log\left(\frac{H_i}{h_i}\right)\right)\left(|\mathbf{w}^{(i)} - \mathbf{r}^{(i)}|^2_{E_P(\partial\Omega_i)} + \frac{1}{H_i}\|\mathbf{w}^{(i)} - \mathbf{r}^{(i)}\|^2_{L_2(\partial\Omega_i)}\right) \qquad (3.65)\\
\leq\ & CH_i^{-1}\left(1+\log\left(\frac{H_i}{h_i}\right)\right)\left(|\mathbf{w}^{(i)}|^2_{E_P(\partial\Omega_i)} + \frac{1}{H_i}\|\mathbf{w}^{(i)} - \mathbf{r}^{(i)}\|^2_{L_2(\partial\Omega_i)}\right).
\end{aligned}$$

Hence, we have

$$\begin{aligned}
&\left| I^h\Big(\theta_{\mathcal{F}^{ij}}\Big(\sum_{m=1}^{6} f_m^{\mathcal{F}^{ij}}(\mathbf{w}^{(i)} - \mathbf{r}^{(i)})\mathbf{r}_m\Big)\Big)\right|^2_{H^{1/2}(\partial\Omega_i)} \\
\leq\ & \sum_{m=1}^{6} |f_m^{\mathcal{F}^{ij}}(\mathbf{w}^{(i)} - \mathbf{r}^{(i)})|^2 |I^h(\theta_{\mathcal{F}^{ij}}\mathbf{r}_m)|^2_{H^{1/2}(\partial\Omega_i)} \qquad (3.66)\\
\leq\ & C\left(1+\log\left(\frac{H_i}{h_i}\right)\right)^2\left(|\mathbf{w}^{(i)}|^2_{E_P(\partial\Omega_i)} + \frac{1}{H_i}\|\mathbf{w}^{(i)} - \mathbf{r}^{(i)}\|^2_{L_2(\partial\Omega_i)}\right).
\end{aligned}$$

Combining the results of (3.63) and (3.66) with the triangle inequality for (3.62), we obtain the estimate

$$\begin{aligned}
& \mu_e^{(i)}\left| I^h\left(\theta_{\mathcal{F}^{ij}}\left(\mathbf{w}^{(i)} - \sum_{m=1}^{6} f_m^{\mathcal{F}^{ij}}(\mathbf{w}^{(i)})\mathbf{r}_m\right)\right)\right|^2_{H^{1/2}(\partial\Omega_i)} \\
=\ & \mu_e^{(i)}\left| I^h\left(\theta_{\mathcal{F}^{ij}}\left((\mathbf{w}^{(i)} - \mathbf{r}^{(i)}) - \sum_{m=1}^{6} f_m^{\mathcal{F}^{ij}}(\mathbf{w}^{(i)} - \mathbf{r}^{(i)})\mathbf{r}_m\right)\right)\right|^2_{H^{1/2}(\partial\Omega_i)} \\
\leq\ & 2\mu_e^{(i)}|I^h(\theta_{\mathcal{F}^{ij}}(\mathbf{w}^{(i)} - \mathbf{r}^{(i)}))|^2_{H^{1/2}(\partial\Omega_i)} \qquad (3.67)\\
& +2\mu_e^{(i)}\left| I^h\left(\theta_{\mathcal{F}^{ij}}\left(\sum_{m=1}^{6} f_m^{\mathcal{F}^{ij}}(\mathbf{w}^{(i)} - \mathbf{r}^{(i)})\mathbf{r}_m\right)\right)\right|^2_{H^{1/2}(\partial\Omega_i)} \\
\leq\ & C\left(1+\log\left(\frac{H_i}{h_i}\right)\right)^2 \mu_e^{(i)}\left(|\mathbf{w}^{(i)}|^2_{E_P(\partial\Omega_i)} + \frac{1}{H_i}\|\mathbf{w}^{(i)} - \mathbf{r}^{(i)}\|^2_{L_2(\partial\Omega_i)}\right).
\end{aligned}$$

Since $\mathbf{r}^{(i)} \in \mathbf{W}^{(i)}$ is arbitrary, we can assume that we have chosen the minimizing $\mathbf{r}^{(i)}$, as in Lemma 9 and obtain

$$\|\mathbf{w}^{(i)} - \mathbf{r}^{(i)}\|^2_{L_2(\partial\Omega_i)} \leq CH_i|\mathbf{w}^{(i)}|^2_{E_P(\partial\Omega_i)}.$$

This yields

$$\mu_e^{(i)} \left| I^h \left(\theta_{\mathcal{F}^{ij}} \left(\mathbf{w}^{(i)} - \sum_{m=1}^{6} f_m^{\mathcal{F}^{ij}}(\mathbf{w}^{(i)})\mathbf{r}_m \right) \right) \right|^2_{H^{1/2}(\partial\Omega_i)} \leq C \left(1 + \log\left(\frac{H_i}{h_i}\right)\right)^2 \mu_e^{(i)} |\mathbf{w}^{(i)}|^2_{E_P(\partial\Omega_i)}. \quad (3.68)$$

We can proceed in the same way for the second term of the right hand side in (3.60) and obtain

$$\mu_e^{(j)} \left| I^h \left(\theta_{\mathcal{F}^{ij}} \left(\mathbf{w}^{(j)} - \sum_{m=1}^{6} f_m^{\mathcal{F}^{ij}}(\mathbf{w}^{(j)})\mathbf{r}_m \right) \right) \right|^2_{H^{1/2}(\partial\Omega_i)} \leq C \left(1 + \log\left(\frac{H_j}{h_j}\right)\right)^2 \mu_e^{(j)} |\mathbf{w}^{(j)}|^2_{E_P(\partial\Omega_j)}. \quad (3.69)$$

The estimates (3.68) and (3.69) together with the triangle inequality, (3.60), and Lemma 10 yield

$$\begin{aligned}
& \mu_e^{(i)} |I^h(\theta_{\mathcal{F}^{ij}} \delta_j^\dagger (\mathbf{w}^{(i)} - \mathbf{w}^{(j)}))|^2_{H_{00}^{1/2}(\mathcal{F}^{ij})} \\
= \; & \mu_e^{(i)} \left| \delta_j^\dagger I^h \left(\theta_{\mathcal{F}^{ij}} \left(\left(\mathbf{w}^{(i)} - \sum_{m=1}^{6} f_m^{\mathcal{F}^{ij}}(\mathbf{w}^{(i)})\mathbf{r}_m \right) - \left(\mathbf{w}^{(j)} - \sum_{m=1}^{6} f_m^{\mathcal{F}^{ij}}(\mathbf{w}^{(j)})\mathbf{r}_m \right) \right) \right) \right|^2_{H_{00}^{1/2}(\mathcal{F}^{ij})} \\
\leq \; & \min(\mu_e^{(i)}, \mu_e^{(j)}) \left(\left| I^h \theta_{\mathcal{F}^{ij}} \left(\left(\mathbf{w}^{(i)} - \sum_{m=1}^{6} f_m^{\mathcal{F}^{ij}}(\mathbf{w}^{(i)})\mathbf{r}_m \right) \right) \right|^2_{H^{1/2}(\partial\Omega_i)} \right. \\
& \qquad \left. + \left| I^h \theta_{\mathcal{F}^{ij}} \left(\left(\mathbf{w}^{(j)} - \sum_{m=1}^{6} f_m^{\mathcal{F}^{ij}}(\mathbf{w}^{(j)})\mathbf{r}_m \right) \right) \right|^2_{H^{1/2}(\partial\Omega_j)} \right) \\
\leq \; & \mu_e^{(i)} \left| I^h \theta_{\mathcal{F}^{ij}} \left(\left(\mathbf{w}^{(i)} - \sum_{m=1}^{6} f_m^{\mathcal{F}^{ij}}(\mathbf{w}^{(i)})\mathbf{r}_m \right) \right) \right|^2_{H^{1/2}(\partial\Omega_i)} \\
& + \mu_e^{(j)} \left| I^h \theta_{\mathcal{F}^{ij}} \left(\left(\mathbf{w}^{(j)} - \sum_{m=1}^{6} f_m^{\mathcal{F}^{ij}}(\mathbf{w}^{(j)})\mathbf{r}_m \right) \right) \right|^2_{H^{1/2}(\partial\Omega_j)} \\
\leq \; & C \left(1 + \log\left(\frac{H_i}{h_i}\right)\right)^2 \mu_e^{(i)} |\mathbf{w}^{(i)}|^2_{E_P(\partial\Omega_i)} + C \left(1 + \log\left(\frac{H_j}{h_j}\right)\right)^2 \mu_e^{(j)} |\mathbf{w}^{(j)}|^2_{E_P(\partial\Omega_j)}.
\end{aligned}$$

Edge Terms. Since we assume that at most three subdomains are common to a single edge, cf. Assumption 2, two subdomains sharing an edge also share a face. Thus, we can reduce our edge estimates to estimates on the corresponding faces using Lemma 14 and the results obtained in this section so far.

From (3.48), we see, by using Lemma 13, that we have to estimate

$$\mu_e^{(i)} \|\delta_j^\dagger (\mathbf{w}^{(i)} - \mathbf{w}^{(j)})\|^2_{L_2(\mathcal{E}^{ik})} + \mu_e^{(i)} \|\delta_k^\dagger (\mathbf{w}^{(i)} - \mathbf{w}^{(k)})\|^2_{L_2(\mathcal{E}^{ik})}.$$

The analysis for the first term will be carried out in detail. The second term can then be treated in an analogous way.

Let us assume that the edge $\mathcal{E}^{ik}$ belongs to the boundary of the face $\mathcal{F}^{ij}$ common to Ω_i and Ω_j. Using Lemma 10, (3.60), and the triangle inequality we obtain

$$\begin{aligned}
&\mu_e^{(i)}\|\delta_j^\dagger(\mathbf{w}^{(i)}-\mathbf{w}^{(j)})\|^2_{L_2(\mathcal{E}^{ik})} \\
\leq\ & \min(\mu_e^{(i)},\mu_e^{(j)})\|\mathbf{w}^{(i)}-\mathbf{w}^{(j)}\|^2_{L_2(\mathcal{E}^{ik})} \qquad (3.70)\\
\leq\ & 2\mu_e^{(i)}\left\|\mathbf{w}^{(i)}-\sum_{l=1}^{6} f_l^{\mathcal{F}^{ij}}(\mathbf{w}^{(i)})\mathbf{r}_l\right\|^2_{L_2(\mathcal{E}^{ik})}+2\mu_e^{(j)}\left\|\mathbf{w}^{(j)}-\sum_{l=1}^{6} f_l^{\mathcal{F}^{ij}}(\mathbf{w}^{(j)})\mathbf{r}_l\right\|^2_{L_2(\mathcal{E}^{ik})}.
\end{aligned}$$

To estimate the first term, we use the identity (3.62) and choose $\mathbf{r}^{(i)}\in\mathbf{W}^{(i)}$ arbitrarily. Combining this with the triangle inequality and Lemma 14, we obtain

$$\begin{aligned}
&2\mu_e^{(i)}\left\|\mathbf{w}^{(i)}-\sum_{l=1}^{6} f_l^{\mathcal{F}^{ij}}(\mathbf{w}^{(i)})\mathbf{r}_l\right\|^2_{L_2(\mathcal{E}^{ik})}\\
\leq\ & 4\mu_e^{(i)}\|\mathbf{w}^{(i)}-\mathbf{r}^{(i)}\|^2_{L_2(\mathcal{E}^{ik})}+4\mu_e^{(i)}\left\|\sum_{l=1}^{6} f_l^{\mathcal{F}^{ij}}(\mathbf{w}^{(i)}-\mathbf{r}^{(i)})\mathbf{r}_l\right\|^2_{L_2(\mathcal{E}^{ik})}\\
\leq\ & C\left(1+\log\left(\frac{H_i}{h_i}\right)\right)\mu_e^{(i)}\left(|\mathbf{w}^{(i)}-\mathbf{r}^{(i)}|^2_{H^{1/2}(\partial\Omega_i)}+\frac{1}{H_i}\|\mathbf{w}^{(i)}-\mathbf{r}^{(i)}\|^2_{L_2(\partial\Omega_i)}\right)\\
&+C\mu_e^{(i)}\sum_{l=1}^{6}|f_l^{\mathcal{F}^{ij}}(\mathbf{w}^{(i)}-\mathbf{r}^{(i)})|^2\|\mathbf{r}_l\|^2_{L_2(\mathcal{E}^{ik})}.
\end{aligned}$$

Since the length of $\mathcal{E}^{ik}$ is of the order of $\min(H_i,H_j)$, it can easily be shown that

$$\|\mathbf{r}_l\|^2_{L_2(\mathcal{E}^{ik})}\leq C\min(H_i,H_j)\ ,\quad l=1,2,3, \qquad (3.71)$$

with a constant C independent of H,h and $\mu_e^{(i)}$, cf. [55, (8.14)]. The shifted basis elements of $\mathbf{ker}\,(\varepsilon_P)$, cf. (2.17), lead to

$$\|\mathbf{r}_l\|^2_{L_2(\mathcal{E}^{ik})}\leq\int_{\mathcal{E}^{ik}}\frac{1}{H_\psi^2}CH_\psi^2\leq C\int_{\mathcal{E}^{ik}}1\ d\mathbf{x}=C|\mathcal{E}^{ik}|\leq C\min(H_i,H_j),$$

for $l=4,5,6$. Thus, we have

$$\|\mathbf{r}_l\|^2_{L_2(\mathcal{E}^{ik})}\leq C\min(H_i,H_j)\ ,\quad l=1,\ldots,6. \qquad (3.72)$$

We can proceed with all terms obtained so far as before and obtain

$$2\mu_e^{(i)}\left\|\mathbf{w}^{(i)}-\sum_{l=1}^{6} f_l^{\mathcal{F}^{ij}}(\mathbf{w}^{(i)})\mathbf{r}_l\right\|^2_{L_2(\mathcal{E}^{ik})}\leq C\mu_e^{(i)}\left(1+\log\left(\frac{H_i}{h_i}\right)\right)|\mathbf{w}^{(i)}|^2_{E_P(\partial\Omega_i)}$$

and in an analogous way

$$2\mu_e^{(j)} \left\| \mathbf{w}^{(j)} - \sum_{l=1}^{6} f_l^{\mathcal{F}^{ij}}(\mathbf{w}^{(j)})\mathbf{r}_l \right\|_{L_2(\mathcal{E}^{ik})}^2 \leq C\mu_e^{(j)} \left(1 + \log\left(\frac{H_j}{h_j}\right)\right) |\mathbf{w}^{(j)}|_{E_P(\partial\Omega_i)}^2 .$$

Combining this results with (3.70) gives

$$\begin{aligned} & \mu_e^{(i)} \|\delta_j^\dagger(\mathbf{w}^{(i)} - \mathbf{w}^{(j)})\|_{L_2(\mathcal{E}^{ik})}^2 \\ \leq\ & C\mu_e^{(i)} \left(1 + \log\left(\frac{H_i}{h_i}\right)\right) |\mathbf{w}^{(i)}|_{E_P(\partial\Omega_i)}^2 + C\mu_e^{(j)} \left(1 + \log\left(\frac{H_j}{h_j}\right)\right) |\mathbf{w}^{(j)}|_{E_P(\partial\Omega_i)}^2 . \square \end{aligned}$$

3.5 Some auxiliary lemmas

In this section some technical lemmas are provided which are needed in the convergence analysis. These results are borrowed from different other papers and most of them can be found in the book of Toselli and Widlund [89]. Here, they will be formulated using trace spaces on the subdomain boundaries, i.e., $H^{1/2}(\partial\Omega_i)$ instead of the space $H^1(\Omega_i)$ with the discrete harmonic extensions and we provide them for piecewise quadratic finite element spaces.

Lemma 12 is related to earlier lemmas for scalar functions and standard linear elasticity; see Dryja, Smith, and Widlund [24, Lemma 4.4], Klawonn and Widlund [55, Lemma 7.1] and also the book of Toselli and Widlund [89, Lemma 4.25]. Here, we present a new version for the rigid body modes of linear P-elasticity and piecewise quadratic finite element functions.

Lemma 12 *Let $\mathcal{F}^{ij}$ be the face common to Ω_i and Ω_j and let $\theta_{\mathcal{F}^{ij}}$ be the piecewise linear finite element function on the triangulation $\tau_{h/2}$ introduced in Section 3.4 that is equal to 1 at the nodal points on the face $\mathcal{F}^{ij} = \mathcal{F}^{ij}_{h/2}$ and vanishes on $(\partial\Omega_{i,h/2} \cup \partial\Omega_{j,h/2}) \setminus \mathcal{F}^{ij}_{h/2}$. In the interior of Ω_i and Ω_j, $\theta_{\mathcal{F}^{ij}}$ is assumed to be the discrete harmonic extension of the given values on the boundary. Furthermore, let $\mathbf{r} \in \{\mathbf{r}_1, \ldots, \mathbf{r}_6\}$ be a rigid body mode, cf. (2.17), with $\boldsymbol{\psi}$ being at most piecewise quadratic. Then*

$$|I^h(\theta_{\mathcal{F}^{ij}}\mathbf{r})|_{H^{1/2}(\partial\Omega_i)}^2 \leq C \left(1 + \log\left(\frac{H_i}{h_i}\right)\right) H_i .$$

Proof: From (3.37) and (3.38) follows

$$|I^h(\theta_{\mathcal{F}^{ij}}\mathbf{r})|_{H^{1/2}(\partial\Omega_i)}^2 \leq |I^h(\theta_{\mathcal{F}^{ij}}\mathbf{r})|_{H^1(\Omega_i)}^2 .$$

Since $\theta_{\mathcal{F}^{ij}}\mathbf{r}$ is at most piecewise cubic, we can follow the arguments given in [89, Lemma 3.9] and obtain for $\mathbf{r}^T = (r^{(1)}, r^{(2)}, r^{(3)})^T$ that

$$|I^h(\theta_{\mathcal{F}^{ij}}\mathbf{r})|_{H^1(\Omega_i)}^2 \leq C\, |\theta_{\mathcal{F}^{ij}}\mathbf{r}|_{H^1(\Omega_i)}^2 = \sum_{k=1}^{3} |\theta_{\mathcal{F}^{ij}} r^{(k)}|_{H^1(\Omega_i)}^2 ,$$

cf. [89, Lemma 4.31], by summing over the elements T of the triangulation. Thus, for $k = 1, 2, 3$, we have to estimate

$$\begin{aligned} |\theta_{\mathcal{F}^{ij}} r^{(k)}|^2_{H^1(\Omega_i)} &= \int_{\Omega_i} |(\nabla\theta_{\mathcal{F}^{ij}}) r^{(k)} + \theta_{\mathcal{F}^{ij}}(\nabla r^{(k)})|^2 \, dx \\ &\leq 2\left(\int_{\Omega_i} |\nabla\theta_{\mathcal{F}^{ij}}|^2 |r^{(k)}|^2 \, dx + \int_{\Omega_i} |\theta_{\mathcal{F}^{ij}}|^2 |\nabla r^{(k)}|^2 \, dx\right). \end{aligned} \quad (3.73)$$

For the first term in (3.73) we can use that the shifted version of the rigid body modes $\mathbf{r}$, cf. (2.17), are constructed such that $\|r^{(k)}\|_{L^\infty(\Omega_i)} \leq C$ with a constant C independent of H_i and h_i. Thus, we obtain

$$\begin{aligned} \int_{\Omega_i} |\nabla\theta_{\mathcal{F}^{ij}}|^2 |r^{(k)}|^2 \, dx \;\leq\; C|\theta_{\mathcal{F}^{ij}}|^2_{H^1(\Omega_i)} &\leq \tilde{C}\left(1 + \log\left(\frac{H_i}{\frac{h_i}{2}}\right)\right) H_i \\ &\leq (1 + \log(2))\tilde{C}\left(1 + \log\left(\frac{H_i}{h_i}\right)\right) H_i, \end{aligned}$$

where the penultimate inequality can be found in [89, Lemma 4.25].

The second term in (3.73) can be bounded by first representing the integral over Ω_i as the sum of the integrals over all elements $T \in \tau_h$ with $T \cap \Omega_i \neq \emptyset$. Then, we obtain

$$\int_{\Omega_i} |\theta_{\mathcal{F}^{ij}}|^2 |\nabla r^{(k)}|^2 \, dx = \sum_{T \subset \Omega_i} \int_T |\theta_{\mathcal{F}^{ij}}|^2 |\nabla r^{(k)}|^2 \, dx \leq \sum_{T \subset \Omega_i} \int_T |\nabla r^{(k)}|^2 \, dx,$$

where we use that $|\theta_{\mathcal{F}^{ij}}(x)| \leq 1$. Now we consider that $\mathbf{r}$ is a rigid body mode of P-elasticity, i.e.,

$$\mathbf{r}(\mathbf{x}) = \mathbf{r}_i(\mathbf{x}) = \tilde{\mathbf{r}}_i(\boldsymbol{\psi}(\mathbf{x})),$$

with $\tilde{\mathbf{r}}_i, i = 1, \ldots 6$, being the rigid body modes of standard linear elasticity. Thus, we have

$$\nabla_{\mathbf{x}}\mathbf{r}(\mathbf{x}) = (\nabla_{\mathbf{y}}\tilde{\mathbf{r}}_i(\mathbf{y}))\,(\nabla_{\mathbf{x}}\boldsymbol{\psi}(\mathbf{x})) = (\nabla_{\mathbf{y}}\tilde{\mathbf{r}}_i(\mathbf{y}))\, P^{-T} \;\text{ with }\; \mathbf{y} := \boldsymbol{\psi}(\mathbf{x}).$$

Since the $\tilde{\mathbf{r}}_i, i = 1 \ldots 6$, have elements which are at most linear functions their derivatives are either constant or zero. Hence, we obtain

$$\int_T |\nabla r^{(k)}|^2 \, dx \leq \hat{C}\; c_P^2 \int_T 1 \, d\mathbf{x} = \hat{C}\; c_P^2 |T|,$$

with c_P as defined in (3.23) and $|T|$ being the measure of the element T. Since $\log(\frac{H_i}{h_i})$ is positive, $|T| \leq h_i^3$, and $h_i < 1$, we have
$|T| \leq h_i^3 \leq h_i \leq H_i \leq H_i\left(1 + \log\left(\frac{H_i}{h_i}\right)\right)$.

Hence, we have

$$|I^h(\theta_{\mathcal{F}^{ij}}\mathbf{r})|^2_{H^{1/2}(\partial\Omega_i)} \le \max\{(1+\log(2))\tilde{C}, \hat{C}c_P^2\} H_i \left(1 + \log\left(\frac{H_i}{h_i}\right)\right). \qquad \square$$

We also need two additional results to estimate the contribution to our bounds from the edges of Ω_i. For the next lemma we refer to the same references as before [24, Lemma 4.7], and [89, Lemma 4.19].

Lemma 13 *Let $\theta_{\mathcal{E}^{ik}}$ be the linear function that is equal to 1 at the nodal points on the edge $\mathcal{E}^{ik}_{h/2}$ and vanishes on $(\partial\Omega_{i,h/2} \cup \partial\Omega_{j,h/2}) \setminus \mathcal{E}^{ik}_{h/2}$. Then, for all $u \in W^{(i)}$,*

$$|I^h(\theta_{\mathcal{E}^{ik}}u)|^2_{H^{1/2}(\partial\Omega_i)} \le C\|u\|^2_{L_2(\mathcal{E}^{ik})}.$$

Proof: As before we prove the estimate for the $H^1(\Omega_i)$-seminorm and obtain our result for the $H^{1/2}(\partial\Omega_i)$-seminorm using (3.37) and (3.38). Since $I^h(\theta_{\mathcal{E}^{ik}}u)$ is a finite element function in $\mathbf{W}^h$, we have

$$I^h(\theta_{\mathcal{E}^{ik}}u) = \sum_j (\theta_{\mathcal{E}^{ik}}u)(P_j)\ \boldsymbol{\phi}_j,$$

where P_j are the nodes of the triangulation and with $\boldsymbol{\phi}_j = (\phi_{j,q})$, $q = 1,2,3$, where $(\phi_{j,q})$ is the piecewise quadratic nodal basis function associated with P_j. Using Proposition 3.4.1 in [81] we can bound $|\phi_{j,q}|^2_{H^1(T)}$ as follows

$$ch_T \le |\phi_{j,q}|^2_{H^1(T)} \le Ch_T,$$

where the constants c and C depend on the $H^1(T_{\text{ref}})$-seminorms of the reference basis functions.

Let $T \in \tau_h, T \subset \bar{\Omega}_i$ be an element of the triangulation such that $\partial T \cap \mathcal{E}^{ik} \neq \emptyset$ is a straight line from a point $a \in \mathbb{R}^3$ to a point $b \in \mathbb{R}^3$. Then, for $\mathbf{u}^T = (u_1, u_2, u_3)^T$ and $q = 1,2,3$, we have

$$\begin{aligned}
|I^h(\theta_{\mathcal{E}^{ik}}u_q)|^2_{H^1(T)} &\le C\sum_{j=1}^{10} |(\theta_{\mathcal{E}^{ik}}u_q)(P_j)|^2 |\phi_{j,q}|^2_{H^1(T)} \\
&\le ch_T\left(u_q^2(a) + u_q^2(b) + u_q^2\left(\frac{a+b}{2}\right)\right) \\
&\le c\int_{\mathcal{E}^{ik}} |u_q(x)|^2\, dx \;=\; c\|u_q\|^2_{L_2(\mathcal{E}^{ik})}.
\end{aligned}$$

We obtain our result by summing over the elements belonging to the subdomain Ω_i and using (3.37) and (3.38). $\square$

We also need a Sobolev-type inequality for finite element functions.

Lemma 14 *Let $\mathcal{E}^{ik}$ be any edge of Ω_i that forms a part of the boundary of a face $\mathcal{F}^{ij} \subset \partial\Omega_i$. Then for all $\mathbf{u} \in \mathbf{W}^{(i)}$,*

$$\|u\|^2_{L_2(\mathcal{E}^{ik})} \leq C\left(1 + \log\left(\frac{H_i}{h_i}\right)\right)\left(|u|^2_{H^{1/2}(\partial\Omega_i)} + \frac{1}{H_i}\|u\|^2_{L_2(\partial\Omega_i)}\right).$$

Proof: For simplicity, we assume for the rest of the proof that u is a scalar finite element function. The result immediately carries over to the vector valued case by applying it component-by-component. To prove this lemma we first need a discrete Sobolev inequality in two dimensions. This estimate can be found in [13, Lemma (4.9.1)] for $\mathcal{P}_m$ Lagrange finite element functions. From [13, Lemma (4.9.1)], we have for a domain $\tilde{\Omega} \subset \mathrm{I\!R}^2$ with $\mathrm{diam}(\tilde{\Omega}) = H$

$$\|u\|^2_{L^\infty(\tilde{\Omega})} \leq C\left(1 + \log\left(\frac{H}{h}\right)\right)\|u\|^2_{H^1(\tilde{\Omega})},$$

for all $u \in \{v \in H^1(\tilde{\Omega}) : v \text{ piecewise in } \mathcal{P}_m\}$. With this estimate we can follow the line of arguments given in [89, Lemma 4.16], Bramble, Pasciak, and Schatz [11], and Bramble and Xu [12]. For convenience we assume that our edge $\mathcal{E}^{ik}$ is a straight line. Hence we can assume that $\mathcal{E}^{ik}$ can be described as $\{\mathbf{x} = (x, y, z) \in \mathrm{I\!R}^3 : x \in I \wedge y = f(x) \wedge z = g(x)\}$ with a real open interval I and linear functions f and g each mapping from $\mathrm{I\!R}$ to $\mathrm{I\!R}$. With this parametrization we have

$$\|u\|^2_{L_2(\mathcal{E}^{ik})} = \int_I |u(x, f(x), g(x))|^2 \, dx.$$

Hence, we can estimate $|u(x, f(x), g(x))|$ by its maximum over a two dimensional cross section of Ω_i denoted as $\Omega_{i,x}$ associated with a point $(x, f(x), g(x))$ for each x, and obtain

$$\|u\|^2_{L_2(\mathcal{E}^{ik})} \leq \int_I \|u\|^2_{L^\infty(\Omega_{i,x})} \, dx \leq \int_I \left(C\left(1 + \log\left(\frac{H_i}{h_i}\right)\right)\|u\|^2_{H^1(\Omega_{i,x})}\right) \, dx.$$

And since the integral over I combined with the integral over $\Omega_{i,x}$ leads to an integral over Ω_i we have

$$\|u\|^2_{L_2(\mathcal{E}^{ik})} \leq C\left(1 + \log\left(\frac{H_i}{h_i}\right)\right)\|u\|^2_{H^1(\Omega_i)}.$$

This argument holds for any function with the same trace and therefore, for the harmonic extension $\mathcal{H}u$ we obtain

$$\|u\|^2_{L_2(\mathcal{E}^{ik})} \leq C\left(1 + \log\left(\frac{H_i}{h_i}\right)\right)\|\mathcal{H}u\|^2_{H^1(\Omega_i)}$$

and we conclude by using (3.37), (3.38), and the fact that the harmonic extension has the least energy. □

The next lemma can also be found in the monograph by Toselli and Widlund [89, Lemma 4.28].

Lemma 15 *Let $\mathcal{V}^{il}$ be a vertex of a subdomain Ω_i and let $\mathbf{u} \in \mathbf{W}^{(i)}$. Then*

$$|u(\mathcal{V}^{il})\theta_{\mathcal{V}^{il}}|^2_{H^{1/2}(\partial\Omega_i)} \leq C\left(|u|^2_{H^{1/2}(\partial\Omega_i)} + \frac{1}{H_i}\|u\|^2_{L_2(\partial\Omega_i)}\right).$$

Proof: As in the proof of the previous lemma, we assume without restrictions that u is a scalar finite element function. From [89, (4.16)] we obtain for a finite element $T \in \tau_{h/2}$

$$\|u\|^2_{L^\infty(T)} \leq c\frac{1}{h_T}\|u\|^2_{H^1(T)}.$$

Using this estimate, we obtain

$$\begin{aligned} |u(\mathcal{V}^{il})\theta_{\mathcal{V}^{il}}|^2_{H^{1/2}(\partial\Omega_i)} &\leq |u(\mathcal{V}^{il})\theta_{\mathcal{V}^{il}}|^2_{H^1(\Omega_i)} \leq |u(\mathcal{V}^{il})|^2|\theta_{\mathcal{V}^{il}}|^2_{H^1(\Omega_i)} \\ &= \sum_{\substack{T\subset\bar{\Omega}_i \\ T\in\tau_{h/2}}} |u(\mathcal{V}^{il})|^2|\theta_{\mathcal{V}^{il}}|^2_{H^1(T)} \leq \sum_{\substack{T\subset\bar{\Omega}_i \\ T\in\tau_{h/2}}} c\frac{1}{h}\|u\|^2_{H^1(T)}|\theta_{\mathcal{V}^{il}}|^2_{H^1(T)}. \end{aligned}$$

It remains to estimate $|\theta_{\mathcal{V}^{il}}|^2_{H^1(\Omega_i)}$. The function $\theta_{\mathcal{V}^{il}}$ is linear and takes the value 1 in $\mathcal{V}^{il}$ and 0 in every other node. Its support is bounded by the volume of a tetrahedron and its gradient can be bounded by $\frac{2}{h}$. Hence, we obtain

$$|\theta_{\mathcal{V}^{il}}|^2_{H^1(T)} \leq c\frac{1}{h^2}h^3 = ch. \qquad \square$$

The following result can be found in Dryja, Smith, and Widlund [24, Lemma 4.5], Dryja [23, Lemma 3], and Toselli and Widlund [89, Lemma 4.24]. Here, we present a version for piecewise quadratic finite element functions. For this case, it can be proven by combining the arguments given in the proof of [89, Lemma 4.24] with the same element by element techniques as applied for the previous lemmas of this section.

Lemma 16 *Let $\theta_{\mathcal{F}^{ij}}$ be the function introduced in Lemma 12. For all $\mathbf{u} \in \mathbf{W}^{(\mathbf{i})}$,*

$$|I^h(\theta_{\mathcal{F}^{ij}}\mathbf{u})|^2_{H^{1/2}(\partial\Omega_i)} \leq C\left(1 + \log\left(\frac{H_i}{h_i}\right)\right)^2\left(|\mathbf{u}|^2_{H^{1/2}(\partial\Omega_i)} + \frac{1}{H_i}\|\mathbf{u}\|^2_{L_2(\partial\Omega_i)}\right).$$

3.6 Numerical results for P-elasticity

In this section we report on a series of computational experiments which are carried out to confirm numerically our theoretical findings. The computations were performed on a compute cluster consisting of 8 dual Opteron processor nodes with 2.2 GHz and 4 GB memory for each processor and a shared memory computer with 4 Opteron quad core processors with 2.5 GHz each and an overall memory of 128 GB. The algorithms are implemented in PETSc [5, 7, 6].

As for the staggered scheme the computations are carried out on the unit cube, i.e., $\Omega = [0,1]^3$. We discretized the unit cube as before; see Section 2.3. The material parameters are $E = 210$ and $\nu = 0.29$ which corresponds to $\mu_e \approx 81.4$ and $\lambda_e \approx 112.4$.

Since we use quadratic elements, additional points on the edges of the tetrahedra are introduced and the number of degrees of freedom for a subdomain can be calculated using $\frac{H}{h}$ by

$$3\left((2\cdot\frac{H}{h})^3 + (2\cdot\frac{H}{h}+1)^3\right), \tag{3.74}$$

here H is the diameter of the subdomain and h is the diameter of the elements of the subdomain.

The presentation of our results is divided into three subsections. First, we present results for the case which is completely covered by our analysis, i.e., $P^{-T} = \nabla\boldsymbol{\psi}$ where $\boldsymbol{\psi} : \mathbb{R}^3 \to \mathbb{R}^3$ is at most piecewise quadratic. The second subsection deals with the case $P^{-T} = \nabla\boldsymbol{\psi}$ when $\boldsymbol{\psi}$ can be an arbitrary differentiable function. In the last subsection, we present results for other cases when P^{-T} is not a gradient but P itself is. Two sets of experiments are carried out. For the first one the subdomain size is kept fixed, i.e., $\frac{H}{h} =$ const., and the number of subdomains, i.e., $\frac{1}{H}$, is increased. According to our theoretical estimate, cf. Theorem 4, we would expect that the condition number and thus the number of iterations is asymptotically bounded by a constant. In the second set of experiments the number of subdomains is kept fixed, i.e., $\frac{1}{H} =$ const., and the size of the subdomains, i.e., $\frac{H}{h}$, is increased. According to Theorem 4, we would expect the number of iterations to grow slowly and the condition number to grow as $O(\left(1+\log\left(\frac{H}{h}\right)\right)^2)$. Furthermore, if only vertex constraints are used, we know that we obtain a condition number estimate of the order of $O(H/h)$; see, e.g., Klawonn, Widlund, and Dryja [56] for a theoretical estimate, Klawonn, Rheinbach, and Widlund [53] and Farhat, Lesoinne, and Pierson [28] for numerical evidence. For our FETI-DP algorithms we consider five different sets of primal variables.

1. A set with only vertex constraints.

2. A set with edge average constraints in the interior of the cube.

3. A set with edge average constraints in the interior and on the Neumann boundary of the cube.

4. A set with vertex and interior edge average constraints.

5. A set with vertex constraints and edge average constraints in the interior and on the Neumann boundary.

3.6.1 Results for $P^{-T} = \nabla\boldsymbol{\psi}$ with $\boldsymbol{\psi}$ at most piecewise quadratic

In this section, we choose P^{-T} as the gradient of an at most piecewise quadratic function $\boldsymbol{\psi}$. This is the case covered by our theoretical estimates, cf. Chapter 3.4 and Section 3.3.1. Let us first introduce functions $\boldsymbol{\psi}_i : \mathbb{R}^3 \to \mathbb{R}^3$ which are at most quadratic polynomials in each of their components $\psi_i^{(j)}, j = 1, 2, 3$, then we define $P_i^{-T} = \nabla\boldsymbol{\psi}_i$. Here all six basis vectors of the kernel of the P-elasticity operator; see (2.16), are represented exactly by the finite element basis.

We provide the lower face of the cube, i.e., $\{(x, y, z)^T = \mathbf{x} \in \mathbb{R}^3 : z = 0\}$, with homogeneous Dirichlet boundary conditions. To provide the Dirichlet boundary with zero boundary data we choose the initial value of $\boldsymbol{\varphi}$ accordingly. This means that, for $z = 0$, we choose $\boldsymbol{\varphi}$ in accordance to the solution if it is known or near the solution if possible. In all other points the initial value for $\boldsymbol{\varphi}$ is the identity, i.e., $\boldsymbol{\varphi}(\mathbf{x}) = \mathbf{x}$ if $z \neq 0$. Note that we know the solution in advance when P is a gradient, i.e., there exists a function $\tilde{\boldsymbol{\psi}}$ such that $P = \nabla\tilde{\boldsymbol{\psi}}$. Then the solution $\boldsymbol{\varphi}$ is given by $\boldsymbol{\varphi} = \tilde{\boldsymbol{\psi}}$ since with this deformation our energy reduces to zero

$$\begin{aligned}
& \min_{(P,\boldsymbol{\varphi})} \int_\Omega \mu_e \|\mathrm{sym}(P^{-1}F_\nabla - \mathrm{Id}\,)\|_F^2 + \frac{\lambda_e}{2}\left(\mathrm{tr}(P^{-1}F_\nabla - \mathrm{Id}\,)\right)^2 \, d\mathbf{x} \\
= \; & \min_{(P,\boldsymbol{\varphi})} \int_\Omega \mu_e \|\mathrm{sym}((\nabla\tilde{\boldsymbol{\psi}})^{-1}(\nabla\boldsymbol{\varphi}) - \mathrm{Id}\,)\|_F^2 + \frac{\lambda_e}{2}\left(\mathrm{tr}((\nabla\tilde{\boldsymbol{\psi}})^{-1}(\nabla\boldsymbol{\varphi}) - \mathrm{Id}\,)\right)^2 \\
= \; & \min_{(P,\boldsymbol{\varphi})} \int_\Omega \mu_e \|\mathrm{sym}((\nabla\tilde{\boldsymbol{\psi}})^{-1}(\nabla\tilde{\boldsymbol{\psi}}) - \mathrm{Id}\,)\|_F^2 + \frac{\lambda_e}{2}\left(\mathrm{tr}((\nabla\tilde{\boldsymbol{\psi}})^{-1}(\nabla\tilde{\boldsymbol{\psi}}) - \mathrm{Id}\,)\right)^2 \\
= \; & \min_{(P,\boldsymbol{\varphi})} \int_\Omega \mu_e \|\mathrm{sym}(\mathrm{Id}\, - \mathrm{Id}\,)\|_F^2 + \frac{\lambda_e}{2}\left(\mathrm{tr}(\mathrm{Id}\, - \mathrm{Id}\,)\right)^2 \, d\mathbf{x} \\
= \; & 0.
\end{aligned}$$

Hence, we obtain the smallest energy for the solution $\boldsymbol{\varphi} = \tilde{\boldsymbol{\psi}}$. If P is not a gradient we do not know the solution in advance. In these cases we either choose Dirichlet boundary values with $\nabla\boldsymbol{\varphi}|_{\partial\Omega_D}$ approximately $P|_{\partial\Omega_D}$ or $\boldsymbol{\varphi}(\mathbf{x}) = \mathbf{x}$.

A first example is given by

$$\boldsymbol{\psi}_0(\mathbf{x}) = \begin{pmatrix} \frac{1}{2}x \\ y \\ 2x - 4y + 4z \end{pmatrix} \Rightarrow P_0^{-T} = \begin{pmatrix} \frac{1}{2} & 0 & 0 \\ 0 & 1 & 0 \\ 2 & -4 & 4 \end{pmatrix}.$$

Thus, we have

$$P_0 = \begin{pmatrix} 2 & 0 & -1 \\ 0 & 1 & 1 \\ 0 & 0 & \frac{1}{4} \end{pmatrix}$$

and from $P_0 = \nabla\boldsymbol{\varphi}_0$ follows

$$\boldsymbol{\varphi}_0 = \begin{pmatrix} 2x - z \\ y + z \\ \frac{1}{4}z \end{pmatrix};$$

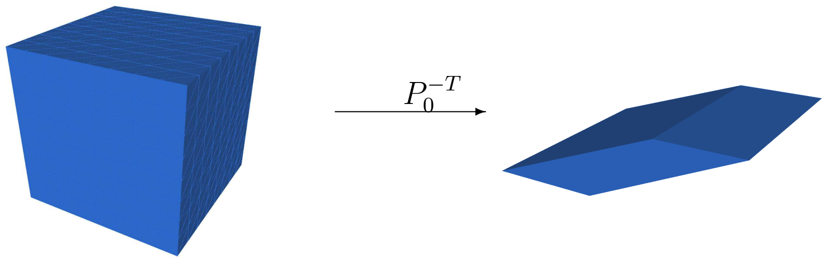

Figure 3.3: *Transformation induced by* $\boldsymbol{\varphi}_0$.

see also Figure 3.3.

We now perform computations using different sets of primal variables. We use the following notation

- d.o.f. = degrees of freedom
- d.o.f./dom = d.o.f. per subdomain
- N = number of subdomains
- c.p.s. = coarse problem size
- It = iterations
- $\lambda_{\max}$ = maximum eigenvalue

In Tables 3.1, 3.2, 3.3, 3.4, and 3.5 we present the results for P_0^{-T} with a fixed subdomain size, i.e., $\frac{1}{H}$ = const.. We present the maximum eigenvalue instead of the condition number since the minimum eigenvalue for the preconditioned FETI-DP matrix is, in accordance with the theory, almost exactly 1 in all experiments. The results in the tables match our theory, i.e., the condition number and the number of iterations are clearly asymptotically bounded. If we fix the number of subdomains instead and increase the size of the subdomains, i.e., increase $\frac{H}{h}$, see Figures 3.5, 3.6, 3.7, and 3.8, we obtain straight lines in plots of $\log(\frac{H}{h})$ versus $\sqrt{\lambda_{\max}}$. Thus, these experiments numerically confirm the quadratic-logarithmic dependence on $\frac{H}{h}$. Additionally, we present in Figure 3.4 the linear dependence of the maximum eigenvalue on the subdomain size in the case of only vertex constraints.

In fact, for several different constant matrices P we always observe condition numbers identical to those in Tables 3.1, 3.2, 3.3, 3.4, and 3.5.

Next, we choose P^{-T} as a linear function, i.e., P^{-T} is the gradient of a function consisting of at most piecewise quadratic polynomials. In these cases P is not

		$\frac{H}{h}=2$ 567 d.o.f./dom.			$\frac{H}{h}=3$ 1677 d.o.f./dom.			$\frac{H}{h}=4$ 3723 d.o.f./dom.		
N	c.p.s.	d.o.f.	It.	$\lambda_{\max}$	d.o.f.	It.	$\lambda_{\max}$	d.o.f.	It.	$\lambda_{\max}$
8	18	3723	40	14.31	11775	50	27.11	27027	55	41.50
27	84	11775	49	16.49	38073	67	31.37	88347	80	48.36
64	216	27027	50	17.16	88347	70	33.17	206115	86	51.55
125	432	51783	53	17.48	170373	73	34.20	398763	90	53.34
216	750	88347	54	17.71	291927	72	34.88	684723	90	54.50
343	1188	139023	53	17.89	460785	74	35.35	1082427	90	55.29
512	1764	206115	53	18.02	684723	75	35.69			
729	2496	291927	54	18.14	971517	75	35.95			
1000	3402	398763	54	18.22						
1331	4500	528927	54	18.29						
1728	5808	684723	55	18.35						
2197	7344	868455	55	18.40						

Table 3.1: $P^{-T} = \nabla \boldsymbol{\psi}_0$ *with vertex constraints.*

		$\frac{H}{h}=2$ 567 d.o.f./dom.			$\frac{H}{h}=3$ 1677 d.o.f./dom.			$\frac{H}{h}=4$ 3723 d.o.f./dom.		
N	c.p.s.	d.o.f.	It.	$\lambda_{\max}$	d.o.f.	It.	$\lambda_{\max}$	d.o.f.	It.	$\lambda_{\max}$
8	18	3723	34	12.34	11775	36	14.02	27027	36	15.37
27	108	11775	39	11.01	38073	41	12.23	88347	43	13.33
64	324	27027	39	9.69	88347	43	10.99	206115	44	12.19
125	720	51783	40	9.58	170373	43	10.84	398763	46	12.03
216	1350	88347	41	9.52	291927	43	10.79	684723	45	11.98
343	2268	139023	40	9.51	460785	43	10.77	1082427	45	11.96
512	3528	206115	39	9.51	684723	43	10.76			
729	5184	291927	39	9.51	971517	43	10.76			
1000	7290	398763	40	9.51						
1331	9900	528927	39	9.51						
1728	13068	684723	39	9.51						
2197	16848	868455	40	9.51						

Table 3.2: $P^{-T} = \nabla \boldsymbol{\psi}_0$ *with edge average constraints without boundary edges.*

		$\frac{H}{h}=2$ 567 d.o.f./dom.			$\frac{H}{h}=3$ 1677 d.o.f./dom.			$\frac{H}{h}=4$ 3723 d.o.f./dom.		
N	c.p.s.	d.o.f.	It.	$\lambda_{\max}$	d.o.f.	It.	$\lambda_{\max}$	d.o.f.	It.	$\lambda_{\max}$
8	78	3723	20	3.07	11775	23	3.93	27027	25	4.67
27	288	11775	23	3.40	38073	26	4.41	88347	29	5.27
64	684	27027	23	3.57	88347	27	4.66	206115	30	5.57
125	1320	51783	24	3.66	170373	28	4.79	398763	31	5.73
216	2250	88347	24	3.72	291927	28	4.86	684723	30	5.82
343	3528	139023	24	3.74	460785	28	4.92	1082427	31	5.88
512	5208	206115	23	3.76	684723	28	4.96			
729	7344	291927	24	3.79	971517	28	4.98			
1000	9990	398763	24	3.80						
1331	13200	528927	24	3.81						
1728	17028	684723	24	3.81						
2197	21528	868455	24	3.82						

Table 3.3: $P^{-T} = \nabla\boldsymbol{\psi}_0$ *with edge average constraints with boundary edges.*

		$\frac{H}{h}=2$ 567 d.o.f./dom.			$\frac{H}{h}=3$ 1677 d.o.f./dom.			$\frac{H}{h}=4$ 3723 d.o.f./dom.		
N	c.p.s.	d.o.f.	It.	$\lambda_{\max}$	d.o.f.	It.	$\lambda_{\max}$	d.o.f.	It.	$\lambda_{\max}$
8	36	3723	26	7.38	11775	30	9.45	27027	32	11.10
27	192	11775	29	6.49	38073	33	8.18	88347	36	9.56
64	540	27027	30	5.73	88347	34	7.13	206115	37	8.35
125	1152	51783	30	5.77	170373	34	7.20	398763	37	8.40
216	2100	88347	30	5.68	291927	33	7.11	684723	36	8.33
343	3456	139023	30	5.69	460785	33	7.11	1082427	36	8.33
512	5292	206115	29	5.68	684723	34	7.10			
729	7680	291927	30	5.68	971517	33	7.10			
1000	10692	398763	30	5.68						
1331	14400	528927	29	5.68						
1728	18876	684723	30	5.68						
2197	24192	868455	29	5.68						

Table 3.4: $P^{-T} = \nabla\boldsymbol{\psi}_0$ *with edge average constraints without boundary edges and with additional vertex constraints.*

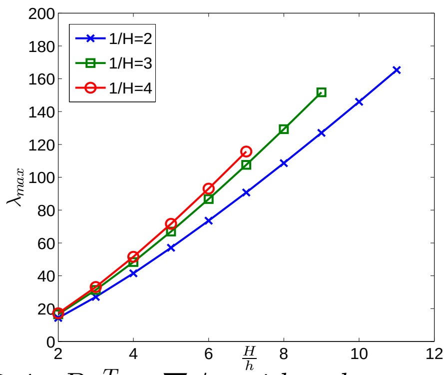

Figure 3.4: $P^{-T} = \nabla\psi_0$ *with only vertex constraints.*

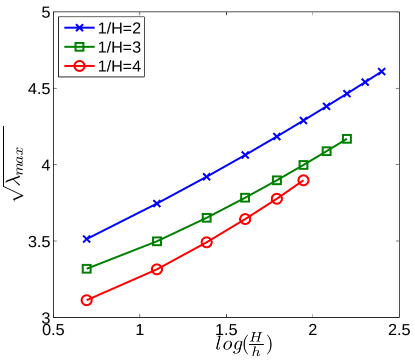

Figure 3.5: $P^{-T} = \nabla\psi_0$ *with edge average constraints without boundary edges.*

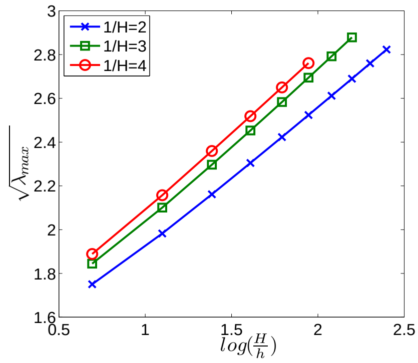

Figure 3.6: $P^{-T} = \nabla\psi_0$ *with edge average constraints with boundary edges.*

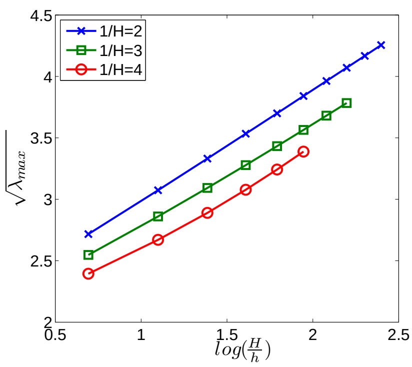

Figure 3.7: $P^{-T} = \nabla\psi_0$ *with edge average constraints without boundary edges and with additional vertex constraints.*

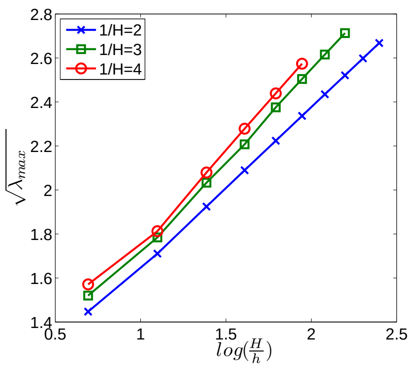

Figure 3.8: $P^{-T} = \nabla\psi_0$ *with edge average constraints with boundary edges and with additional vertex constraints.*

necessarily a gradient and therefore we do not know the solution in advance. As

		$\frac{H}{h}=2$ 567 d.o.f./dom.			$\frac{H}{h}=3$ 1677 d.o.f./dom.			$\frac{H}{h}=4$ 3723 d.o.f./dom.		
N	c.p.s.	d.o.f.	It.	$\lambda_{\max}$	d.o.f.	It.	$\lambda_{\max}$	d.o.f.	It.	$\lambda_{\max}$
8	96	3723	16	2.09	11775	21	2.93	27027	23	3.71
27	372	11775	18	2.31	38073	22	3.18	88347	26	4.13
64	900	27027	18	2.47	88347	22	3.29	206115	26	4.32
125	1752	51783	19	2.55	170373	23	3.35	398763	26	4.41
216	3000	88347	19	2.59	291927	22	3.39	684723	26	4.48
343	4716	139023	20	2.62	460785	23	3.42	1082427	27	4.51
512	6972	206115	19	2.64	684723	23	3.43			
729	9840	291927	19	2.66	971517	23	3.44			
1000	13392	398763	19	2.67						
1331	17700	528927	19	2.68						
1728	22836	684723	20	2.68						
2197	28872	868455	20	2.69						

Table 3.5: $P^{-T} = \nabla\boldsymbol{\psi}_0$ *with edge average constraints with boundary edges and additional vertex constraints.*

examples we consider

$$\boldsymbol{\psi}_1(\mathbf{x}) = \begin{pmatrix} x^2 - 2y + 3z \\ x - y^2 - \frac{1}{2}z \\ -x - y + \frac{1}{2}z^2 \end{pmatrix} \quad \Rightarrow \quad P_1^{-T} = \begin{pmatrix} 2x & -2 & 3 \\ 1 & -2y & - - \frac{1}{2} \\ -1 & -1 & z \end{pmatrix},$$

$$\boldsymbol{\psi}_2(\mathbf{x}) = \begin{pmatrix} x^2 + \frac{1}{3}y + 3z \\ x + y^2 \\ x^2 + 3z \end{pmatrix} \quad \Rightarrow \quad P_2^{-T} = \begin{pmatrix} 2x & \frac{1}{3} & 3 \\ 1 & 2y & 0 \\ 2x & 0 & 3 \end{pmatrix},$$

$$\boldsymbol{\psi}_3(\mathbf{x}) = \begin{pmatrix} 2x - \frac{1}{4}z^2 \\ \frac{3}{2}x^2 + 4y - \frac{1}{4}z \\ \frac{3}{2}x^2 + 4x - \frac{1}{8}z \end{pmatrix} \quad \Rightarrow \quad P_3^{-T} = \begin{pmatrix} 2 & 0 & -\frac{1}{2}z \\ 3x & 4 & -\frac{1}{4} \\ 3x & 4 & -\frac{1}{8} \end{pmatrix},$$

$$\boldsymbol{\psi}_4(\mathbf{x}) = \begin{pmatrix} x^2 - 3x + y \\ y^2 + 2y + z \\ \frac{1}{2}x + z^2 - 4z \end{pmatrix} \quad \Rightarrow \quad P_4^{-T} = \begin{pmatrix} 2x - 3 & 0 & \frac{1}{2} \\ 1 & 2y + 2 & 0 \\ 0 & 1 & 2z - 4 \end{pmatrix}.$$

In Tables 3.6, 3.7, 3.8, 3.9, 3.10, 3.11, 3.12, and 3.13 we present some of the results obtained for $\boldsymbol{\psi}_1$, $\boldsymbol{\psi}_2$, $\boldsymbol{\psi}_3$ and $\boldsymbol{\psi}_4$ in the case $\frac{H}{h} = \text{const}$. The results confirm the earlier observations.

Next, we increase $\frac{H}{h}$ while keeping the number of subdomains fixed. The results in Figures 3.11, 3.12, 3.13, 3.14, 3.15, 3.16, 3.17, and 3.18 match well with the theoretical estimates. It can be clearly seen that the square root of the maximum eigenvalue increases linearly with the logarithm of the subdomain size $\frac{H}{h}$ for edge average constraints. In the cases where we used vertex constraints we again obtained a linear relation between the subdomain size and the maximum

		$\frac{H}{h}=2$ 567 d.o.f./dom.			$\frac{H}{h}=3$ 1677 d.o.f./dom.			$\frac{H}{h}=4$ 3723 d.o.f./dom.		
N	c.p.s.	d.o.f.	It.	$\lambda_{\max}$	d.o.f.	It.	$\lambda_{\max}$	d.o.f.	It.	$\lambda_{\max}$
8	18	3723	43	15.19	11775	52	26.64	27027	58	40.49
27	84	11775	52	16.94	38073	70	31.42	88347	87	48.29
64	216	27027	54	17.33	88347	75	33.19	206115	94	51.52
125	432	51783	56	17.54	170373	78	34.23	398763	96	53.39
216	750	88347	56	17.74	291927	79	34.93	684723	99	54.62
343	1188	139023	57	17.91	460785	80	35.43	1082427	100	55.46
512	1764	206115	57	18.05	684723	81	35.79			
729	2496	291927	58	18.17	971517	82	36.07			
1000	3402	398763	58	18.26						
1331	4500	528927	58	18.33						
1728	5808	684723	58	18.39						
2197	7344	868455	59	18.44						

Table 3.6: $P^{-T} = \nabla\boldsymbol{\psi}_1$ *with vertex constraints.*

		$\frac{H}{h}=2$ 567 d.o.f./dom.			$\frac{H}{h}=3$ 1677 d.o.f./dom.			$\frac{H}{h}=4$ 3723 d.o.f./dom.		
N	c.p.s.	d.o.f.	It.	$\lambda_{\max}$	d.o.f.	It.	$\lambda_{\max}$	d.o.f.	It.	$\lambda_{\max}$
8	18	3723	36	15.73	11775	38	18.04	27027	41	19.94
27	108	11775	40	13.07	38073	45	14.83	88347	47	16.37
64	324	27027	41	11.80	88347	45	13.44	206115	48	14.86
125	720	51783	41	11.34	170373	44	12.90	398763	48	14.26
216	1350	88347	41	11.03	291927	45	12.54	684723	47	13.86
343	2268	139023	41	10.81	460785	45	12.28	1082427	47	13.58
512	3528	206115	41	10.64	684723	45	12.08			
729	5184	291927	41	10.50	971517	45	11.92			
1000	7290	398763	41	10.40						
1331	9900	528927	41	10.31						
1728	13068	684723	41	10.23						
2197	16848	868455	41	10.17						

Table 3.7: $P^{-T} = \nabla\boldsymbol{\psi}_1$ *with edge average constraints without boundary edges.*

		$\frac{H}{h}=2$ 567 d.o.f./dom.			$\frac{H}{h}=3$ 1677 d.o.f./dom.			$\frac{H}{h}=4$ 3723 d.o.f./dom.		
N	c.p.s.	d.o.f.	It.	$\lambda_{\max}$	d.o.f.	It.	$\lambda_{\max}$	d.o.f.	It.	$\lambda_{\max}$
8	18	3723	36	14.31	11775	39	16.14	27027	41	17.70
27	108	11775	41	12.36	38073	44	14.03	88347	46	15.53
64	324	27027	41	11.02	88347	44	12.57	206115	47	13.97
125	720	51783	41	10.48	170373	44	11.94	398763	47	13.28
216	1350	88347	41	10.22	291927	44	11.63	684723	47	12.92
343	2268	139023	41	10.07	460785	44	11.44	1082427	47	12.71
512	3528	206115	41	9.98	684723	44	11.33			
729	5184	291927	41	9.91	971517	44	11.25			
1000	7290	398763	41	9.87						
1331	9900	528927	41	9.83						
1728	13068	684723	41	9.79						
2197	16848	868455	41	9.77						

Table 3.8: $P^{-T} = \nabla\boldsymbol{\psi}_2$ *with edge average constraints without boundary edges.*

		$\frac{H}{h}=2$ 567 d.o.f./dom.			$\frac{H}{h}=3$ 1677 d.o.f./dom.			$\frac{H}{h}=4$ 3723 d.o.f./dom.		
N	c.p.s.	d.o.f.	It.	$\lambda_{\max}$	d.o.f.	It.	$\lambda_{\max}$	d.o.f.	It.	$\lambda_{\max}$
8	78	3723	21	3.14	11775	23	4.01	27027	25	4.76
27	288	11775	23	3.43	38073	27	4.44	88347	29	5.30
64	684	27027	23	3.58	88347	28	4.67	206115	31	5.58
125	1320	51783	24	3.66	170373	28	4.80	398763	31	5.74
216	2250	88347	24	3.71	291927	28	4.88	684723	31	5.83
343	3528	139023	24	3.75	460785	28	4.92	1082427	31	5.87
512	5208	206115	24	3.77	684723	28	4.96			
729	7344	291927	24	3.79	971517	28	4.98			
1000	9990	398763	24	3.80						
1331	13200	528927	24	3.80						
1728	17028	684723	24	3.82						
2197	21528	868455	24	3.81						

Table 3.9: $P^{-T} = \nabla\boldsymbol{\psi}_2$ *with edge average constraints with boundary edges.*

		$\frac{H}{h}=2$ 567 d.o.f./dom.			$\frac{H}{h}=3$ 1677 d.o.f./dom.			$\frac{H}{h}=4$ 3723 d.o.f./dom.		
N	c.p.s.	d.o.f.	It.	$\lambda_{\max}$	d.o.f.	It.	$\lambda_{\max}$	d.o.f.	It.	$\lambda_{\max}$
8	18	3723	43	14.46	11775	51	27.25	27027	59	41.68
27	84	11775	51	16.51	38073	70	31.40	88347	86	48.38
64	216	27027	54	17.16	88347	75	33.18	206115	94	51.55
125	432	51783	55	17.48	170373	77	34.20	398763	96	53.35
216	750	88347	56	17.71	291927	78	34.88	684723	98	54.51
343	1188	139023	57	17.89	460785	80	35.36	1082427	100	55.31
512	1764	206115	57	18.03	684723	80	35.70			
729	2496	291927	57	18.14	971517	81	35.96			
1000	3402	398763	58	18.23						
1331	4500	528927	58	18.30						
1728	5808	684723	58	18.35						
2197	7344	868455	58	18.40						

Table 3.10: $P^{-T} = \nabla \boldsymbol{\psi}_3$ *with vertex constraints.*

		$\frac{H}{h}=2$ 567 d.o.f./dom.			$\frac{H}{h}=3$ 1677 d.o.f./dom.			$\frac{H}{h}=4$ 3723 d.o.f./dom.		
N	c.p.s.	d.o.f.	It.	$\lambda_{\max}$	d.o.f.	It.	$\lambda_{\max}$	d.o.f.	It.	$\lambda_{\max}$
8	36	3723	27	7.41	11775	31	9.50	27027	34	11.18
27	192	11775	29	6.56	38073	34	8.29	88347	37	9.73
64	540	27027	30	5.88	88347	34	7.40	206115	37	9.72
125	1152	51783	30	5.85	170373	34	7.35	398763	37	8.63
216	2100	88347	30	5.79	291927	34	7.28	684723	37	8.56
343	3456	139023	30	5.78	460785	34	7.26	1082427	37	8.53
512	5292	206115	30	5.76	684723	34	7.24			
729	7680	291927	30	5.75	971517	34	7.22			
1000	10692	398763	30	5.75						
1331	14400	528927	30	5.74						
1728	18876	684723	30	5.73						
2197	24192	868455	30	5.73						

Table 3.11: $P^{-T} = \nabla \boldsymbol{\psi}_3$ *with edge average constraints without boundary edges and with additional vertex constraints.*

		$\frac{H}{h}=2$ 567 d.o.f./dom.			$\frac{H}{h}=3$ 1677 d.o.f./dom.			$\frac{H}{h}=4$ 3723 d.o.f./dom.		
N	c.p.s.	d.o.f.	It.	$\lambda_{\max}$	d.o.f.	It.	$\lambda_{\max}$	d.o.f.	It.	$\lambda_{\max}$
8	36	3723	28	9.15	11775	31	11.71	27027	35	13.80
27	192	11775	30	7.35	38073	35	9.18	88347	38	10.68
64	540	27027	31	6.59	88347	35	8.26	206115	38	9.66
125	1152	51783	31	6.37	170373	35	7.99	398763	38	9.35
216	2100	88347	31	6.22	291927	35	7.81	684723	38	9.15
343	3456	139023	31	6.12	460785	35	7.69	1082427	38	9.00
512	5292	206115	31	6.05	684723	35	7.59			
729	7680	291927	31	5.99	971517	35	7.52			
1000	10692	398763	31	5.94						
1331	14400	528927	31	5.90						
1728	18876	684723	31	5.87						
2197	24192	868455	31	5.85						

Table 3.12: $P^{-T} = \nabla \boldsymbol{\psi}_4$ *with edge average constraints without boundary edges and with additional vertex constraints.*

		$\frac{H}{h}=2$ 567 d.o.f./dom.			$\frac{H}{h}=3$ 1677 d.o.f./dom.			$\frac{H}{h}=4$ 3723 d.o.f./dom.		
N	c.p.s.	d.o.f.	It.	$\lambda_{\max}$	d.o.f.	It.	$\lambda_{\max}$	d.o.f.	It.	$\lambda_{\max}$
8	96	3723	16	2.12	11775	21	2.98	27027	24	3.78
27	372	11775	18	2.33	38073	22	3.20	88347	26	4.16
64	900	27027	18	2.48	88347	23	3.31	206115	27	4.34
125	1752	51783	19	2.55	170373	23	3.36	398763	27	4.41
216	3000	88347	19	2.60	291927	23	3.40	684723	27	4.48
343	4716	139023	19	2.63	460785	23	3.42	1082427	27	4.52
512	6972	206115	19	2.65	684723	23	3.43			
729	9840	291927	20	2.66	971517	23	3.44			
1000	13392	398763	20	2.67						
1331	17700	528927	20	2.68						
1728	22836	684723	20	2.69						
2197	28872	868455	20	2.69						

Table 3.13: $P^{-T} = \nabla \boldsymbol{\psi}_4$ *with edge average constraints with boundary edges and additional vertex constraints.*

eigenvalue; see Figures 3.9 and 3.10.

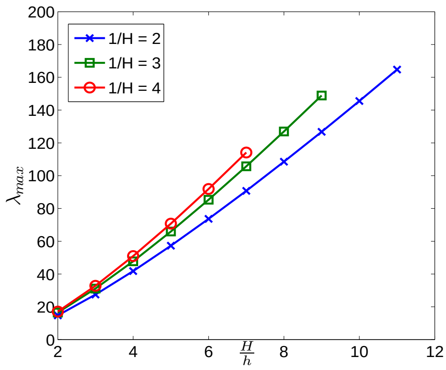

Figure 3.9: $P^{-T} = \nabla \boldsymbol{\psi}_2$ *with only vertex constraints.*

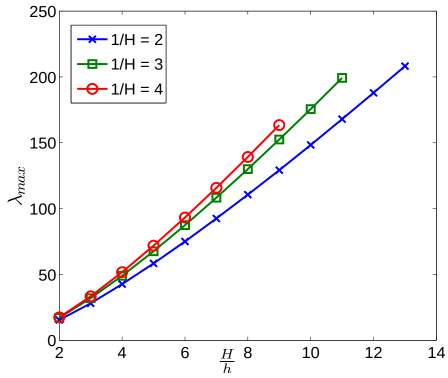

Figure 3.10: $P^{-T} = \nabla \boldsymbol{\psi}_4$ *with only vertex constraints.*

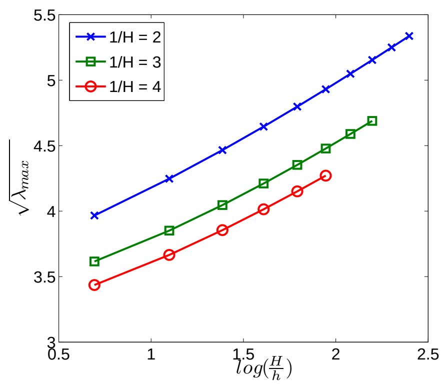

Figure 3.11: $P^{-T} = \nabla \boldsymbol{\psi}_1$ *with edge average constraints without boundary edges.*

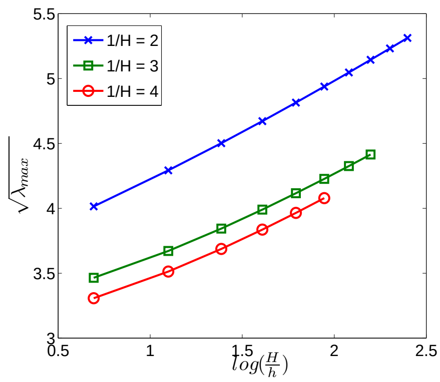

Figure 3.12: $P^{-T} = \nabla \boldsymbol{\psi}_4$ *with edge average constraints without boundary edges.*

3.6.2 Results for $P^{-T} = \nabla \boldsymbol{\psi}$

In this section we will present results for examples which do not completely match our assumptions made for our analysis in Section 3.4. The assumption that P^{-T} is the gradient of a function $\boldsymbol{\psi} : \mathbb{R}^3 \to \mathbb{R}^3$ will still be satisfied. The function $\boldsymbol{\psi}$ however does no longer consist of piecewise at most quadratic polynomials.

A special case, when only one entry of $\boldsymbol{\psi}$ is not a polynomial with at most degree 2, will also be considered. Note that for the case discussed here, the infinitesimal rotations $\mathbf{r}_4(\mathbf{x}), \mathbf{r}_5(\mathbf{x}), \mathbf{r}_6(\mathbf{x})$, see (2.16), may not be representable exactly in the finite element space. As a consequence, the dimension of the kernel of the stiffness matrix may be smaller than six. The dimension is at least three

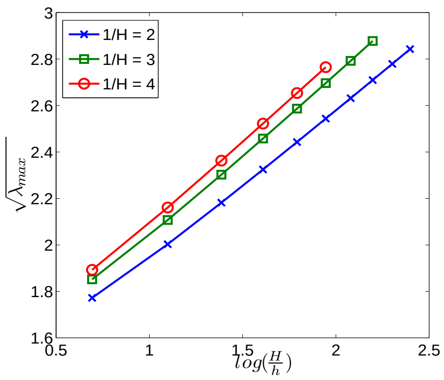

Figure 3.13: $P^{-T} = \nabla \boldsymbol{\psi}_2$ *with edge average constraints with boundary edges.*

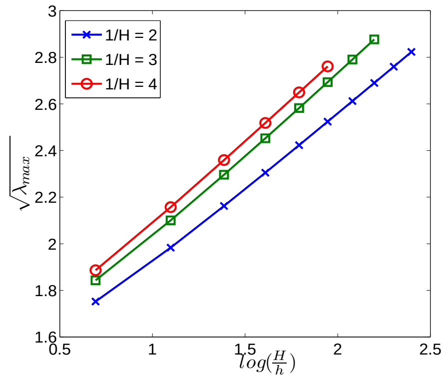

Figure 3.14: $P^{-T} = \nabla \boldsymbol{\psi}_3$ *with edge average constraints with boundary edges.*

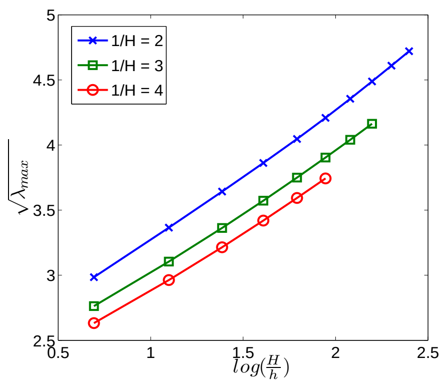

Figure 3.15: $P^{-T} = \nabla \boldsymbol{\psi}_1$ *with edge average constraints without boundary edges and with additional vertex constraints.*

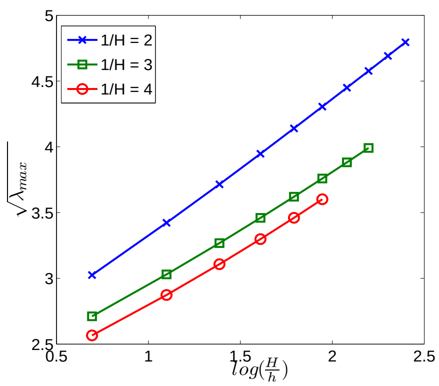

Figure 3.16: $P^{-T} = \nabla \boldsymbol{\psi}_4$ *with edge average constraints without boundary edges and with additional vertex constraints.*

since we can always represent exactly the translational basis vectors. But instead of the three zero eigenvalues associated with the three rotations we may have up to three additional positive eigenvalues. For example, in the case of $\boldsymbol{\psi}_6$ the basis vector $\tilde{\mathbf{r}}_4$ is a composition of $\psi_6^{(1)}$ and $\psi_6^{(2)}$ which are quadratic polynomials. Hence, numerically we have a four dimensional kernel in this case.

The examples in this section can be divided into two parts. First, we consider

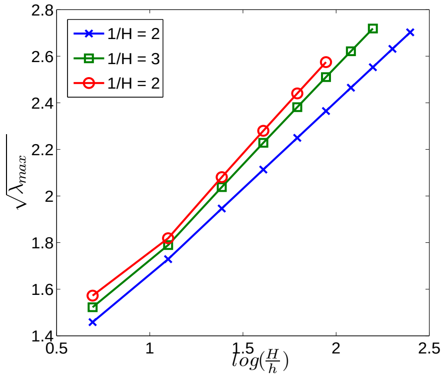

Figure 3.17: $P^{-T} = \nabla\boldsymbol{\psi}_1$ *with edge average constraints with boundary edges and with additional vertex constraints.*

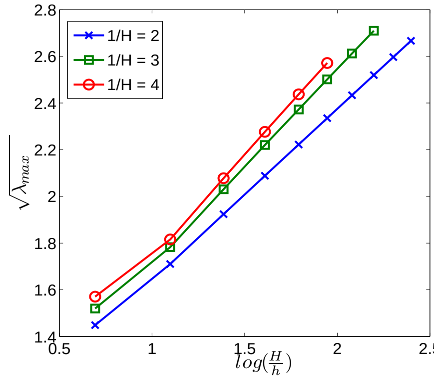

Figure 3.18: $P^{-T} = \nabla\boldsymbol{\psi}_3$ *with edge average constraints with boundary edges and with additional vertex constraints.*

the case when ψ consists of polynomials of different degrees, i.e.,

$$\boldsymbol{\psi}_5 = \begin{pmatrix} x^3 + y \\ x^3 + y + 2z \\ 3x + \frac{1}{9}z^3 \end{pmatrix} \quad \Rightarrow \quad P_5^{-T} = \begin{pmatrix} 3x^2 & 1 & 0 \\ 3x^2 & 1 & 2 \\ 3 & 0 & \frac{1}{3}z^2 \end{pmatrix},$$

$$\boldsymbol{\psi}_6 = \begin{pmatrix} x^2 + \frac{1}{2}y + 4z \\ x^2 + \frac{1}{2}y - 6z \\ -x + z^3 \end{pmatrix} \quad \Rightarrow \quad P_6^{-T} = \begin{pmatrix} 2x & \frac{1}{2} & 4 \\ 2x & \frac{1}{2} & -6 \\ -1 & 0 & 3z^2 \end{pmatrix},$$

$$\boldsymbol{\psi}_7 = \begin{pmatrix} x^3 - 9y + \frac{1}{3}z \\ 4x + 2y \\ x^3 - y + \frac{1}{3}z \end{pmatrix} \quad \Rightarrow \quad P_7^{-T} = \begin{pmatrix} 3x^2 & -9 & \frac{1}{3} \\ 4 & 2 & 0 \\ 3x^2 & -1 & \frac{1}{3} \end{pmatrix},$$

$$\boldsymbol{\psi}_8 = \begin{pmatrix} 4x + y^3 \\ \frac{2}{3}x^3 - 3y - \frac{1}{3}z^3 \\ x^3 + \frac{1}{3}z \end{pmatrix} \quad \Rightarrow \quad P_8^{-T} = \begin{pmatrix} 4 & 3y^2 & 0 \\ 2x^2 & -3 & -z^2 \\ 3x^2 & 0 & \frac{1}{3} \end{pmatrix},$$

and then we consider a function $\boldsymbol{\psi}$ which does not consist of polynomials

$$\psi_9 = \begin{pmatrix} ((1-h) + hx)\cos(2\pi y)\cos(\alpha + z(\beta - \alpha)) \\ ((1-h) + hx)\sin(2\pi y)\cos(\alpha + z(\beta - \alpha)) \\ ((1-h) + hx)\sin(\alpha + z(\beta - \alpha)) \end{pmatrix} =: \begin{pmatrix} A\cos(B)\cos(C) \\ A\sin(B)\cos(C) \\ A\sin(C) \end{pmatrix}$$

$$\Rightarrow P_9^{-T} = \begin{pmatrix} h\cos(B)cos(C) & -2\pi A\sin(B)cos(C) & -(\beta-\alpha)A\cos(B)\sin(C) \\ h\sin(B)cos(C) & 2\pi A\cos(B)cos(C) & -(\beta-\alpha)A\sin(B)\sin(C) \\ h\sin(C) & 0 & (\beta-\alpha)A\cos(C) \end{pmatrix}.$$

Here, we consider two different sets of variables h, α, and β. To the case with $h = \frac{1}{4}, \alpha = \frac{\pi}{8}$, and $\beta = \frac{\pi}{4}$ we will refer as $\boldsymbol{\psi}_{9.1}$ and to the example with $h = \frac{1}{8}, \alpha = \frac{\pi}{16}$, and $\beta = \frac{3\pi}{8}$ as $\boldsymbol{\psi}_{9.2}$.

		$\frac{H}{h}=2$ 567 d.o.f./dom.			$\frac{H}{h}=3$ 1677 d.o.f./dom.			$\frac{H}{h}=4$ 3723 d.o.f./dom.		
N	c.p.s.	d.o.f.	It.	$\lambda_{\max}$	d.o.f.	It.	$\lambda_{\max}$	d.o.f.	It.	$\lambda_{\max}$
8	78	3723	21	3.22	11775	23	4.10	27027	25	4.86
27	288	11775	23	3.48	38073	26	4.51	88347	29	5.38
64	684	27027	23	3.56	88347	27	4.71	206115	30	5.63
125	1320	51783	24	3.69	170373	28	4.82	398763	31	5.77
216	2250	88347	24	3.71	291927	28	4.89	684723	31	5.85
343	3528	139023	24	3.76	460785	28	4.94	1082427	31	5.91
512	5208	206115	24	3.77	684723	28	4.97			
729	7344	291927	24	3.80	971517	28	4.99			
1000	9990	398763	24	3.80						
1331	13200	528927	24	3.81						
1728	17028	684723	24	3.81						
2197	21528	868455	24	3.82						

Table 3.14: $P^{-T} = \nabla\psi_5$ *with edge average constraints with boundary edges.*

The results we obtained for for ψ_5, ψ_6, ψ_7, and ψ_8 differ only slightly from the ones presented in Section 3.6.1; see Tables 3.14, 3.15, 3.16, 3.17, 3.18, 3.19, 3.20, and 3.21. In some cases the asymptotic range seems to be reached later and the condition number seems to vary more. Although these experiments are not covered by the theory, numerically, the bound for the condition number still seems to hold, and the number of iterations is clearly bounded. Again, a linear dependence of the square root of the maximum eigenvalue on $\log(\frac{H}{h})$ can be observed numerically, see Figures 3.22, 3.21, 3.23, 3.24, 3.25, 3.26, 3.27, and 3.28, as well as the linear dependence on $\frac{H}{h}$ of the maximum eigenvalue in the case of only vertex constraints; see Figures 3.19 and 3.20.

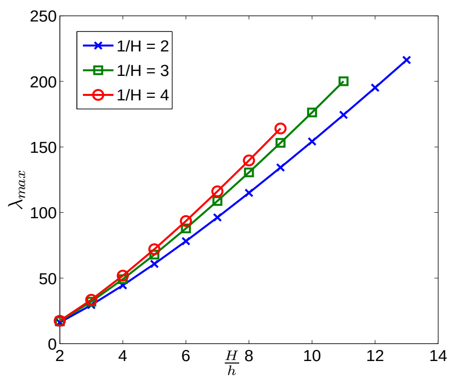

Figure 3.19: $P^{-T} = \nabla\psi_5$ *with only vertex constraints.*

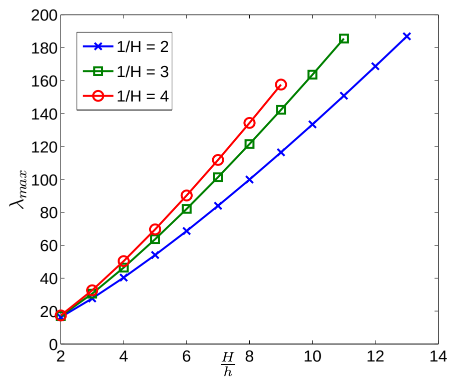

Figure 3.20: $P^{-T} = \nabla\psi_8$ *with only vertex constraints.*

		$\frac{H}{h}=2$ 567 d.o.f./dom.			$\frac{H}{h}=3$ 1677 d.o.f./dom.			$\frac{H}{h}=4$ 3723 d.o.f./dom.		
N	c.p.s.	d.o.f.	It.	$\lambda_{\max}$	d.o.f.	It.	$\lambda_{\max}$	d.o.f.	It.	$\lambda_{\max}$
8	36	3723	28	7.92	11775	32	10.48	27027	35	12.63
27	192	11775	30	7.16	38073	35	9.37	88347	38	11.26
64	540	27027	31	6.56	88347	35	8.57	206115	39	10.28
125	1152	51783	31	6.32	170373	35	8.22	398763	39	9.84
216	2100	88347	31	6.17	291927	35	7.99	684723	38	9.54
343	3456	139023	31	6.06	460785	35	7.82	1082427	38	9.32
512	5292	206115	31	5.97	684723	35	7.69			
729	7680	291927	31	5.90	971517	35	7.58			
1000	10692	398763	31	5.84						
1331	14400	528927	31	5.80						
1728	18876	684723	31	5.76						
2197	24192	868455	30	5.73						

Table 3.15: *$P^{-T}=\nabla\boldsymbol{\psi}_5$ with edge average constraints without boundary edges and with additional vertex constraints.*

		$\frac{H}{h}=2$ 567 d.o.f./dom.			$\frac{H}{h}=3$ 1677 d.o.f./dom.			$\frac{H}{h}=4$ 3723 d.o.f./dom.		
N	c.p.s.	d.o.f.	It.	$\lambda_{\max}$	d.o.f.	It.	$\lambda_{\max}$	d.o.f.	It.	$\lambda_{\max}$
8	18	3723	46	24.22	11775	59	39.40	27027	66	55.60
27	84	11775	54	19.35	38073	73	34.06	88347	89	50.80
64	216	27027	56	18.12	88347	77	33.67	206115	95	51.44
125	432	51783	57	17.84	170373	79	34.08	398763	98	52.57
216	750	88347	57	17.85	291927	80	34.55	684723	99	53.57
343	1188	139023	58	17.93	460785	81	34.97	1082427		54.39
512	1764	206115	58	18.02	684723	81	35.32			
729	2496	291927	58	18.10	971517	82	35.61			
1000	3402	398763	58	18.18						
1331	4500	528927	58	18.24						
1728	5808	684723	59	18.30						
2197	7344	868455	59	18.35						

Table 3.16: *$P^{-T}=\nabla\boldsymbol{\psi}_6$ with vertex constraints.*

		$\frac{H}{h}=2$ 567 d.o.f./dom.			$\frac{H}{h}=3$ 1677 d.o.f./dom.			$\frac{H}{h}=4$ 3723 d.o.f./dom.		
N	c.p.s.	d.o.f.	It.	$\lambda_{\max}$	d.o.f.	It.	$\lambda_{\max}$	d.o.f.	It.	$\lambda_{\max}$
8	96	3723	19	2.74	11775	22	3.64	27027	25	4.52
27	372	11775	19	2.63	38073	24	3.62	88347	27	4.58
64	900	27027	19	2.41	88347	24	3.49	206115	28	4.44
125	1752	51783	19	2.47	170373	23	3.44	398763	27	4.46
216	3000	88347	19	2.52	291927	23	3.44	684723	27	4.50
343	4716	139023	19	2.55	460785	23	3.45	1082427	27	4.53
512	6972	206115	19	2.57	684723	23	3.46	1610307	27	4.55
729	9840	291927	19	2.59	971517	23	3.46	2286795	27	4.56
1000	13392	398763	20	2.61	1328943	23	3.46			
1331	17700	528927	20	2.62	1764777	23	3.46			
1728	22836	684723	20	2.63						
2197	28872	868455	20	2.64						

Table 3.17: $P^{-T} = \nabla\boldsymbol{\psi}_6$ *with edge average constraints with boundary edges and additional vertex constraints.*

		$\frac{H}{h}=2$ 567 d.o.f./dom.			$\frac{H}{h}=3$ 1677 d.o.f./dom.			$\frac{H}{h}=4$ 3723 d.o.f./dom.		
N	c.p.s.	d.o.f.	It.	$\lambda_{\max}$	d.o.f.	It.	$\lambda_{\max}$	d.o.f.	It.	$\lambda_{\max}$
8	18	3723	43	65.10	11775	47	77.16	27027	52	86.67
27	108	11775	50	35.54	38073	54	40.50	88347	58	44.61
64	324	27027	50	25.75	88347	53	29.46	206115	56	32.55
125	720	51783	49	22.21	170373	52	25.39	398763	55	28.04
216	1350	88347	48	19.92	291927	51	22.76	684723	55	25.14
343	2268	139023	47	18.31	460785	51	20.91	1082427	54	23.11
512	3528	206115	46	17.12	684723	50	19.55			
729	5184	291927	46	16.20	971517	49	18.49			
1000	7290	398763	45	15.46						
1331	9900	528927	45	14.86						
1728	13068	684723	45	14.36						
2197	16848	868455	44	13.93						

Table 3.18: $P^{-T} = \nabla\boldsymbol{\psi}_7$ *with edge average constraints without boundary edges.*

		$\frac{H}{h}=2$ 567 d.o.f./dom.			$\frac{H}{h}=3$ 1677 d.o.f./dom.			$\frac{H}{h}=4$ 3723 d.o.f./dom.		
N	c.p.s.	d.o.f.	It.	$\lambda_{\max}$	d.o.f.	It.	$\lambda_{\max}$	d.o.f.	It.	$\lambda_{\max}$
8	96	3723	18	2.34	11775	22	3.60	27027	25	4.61
27	372	11775	19	2.36	38073	24	3.60	88347	28	4.66
64	900	27027	19	2.43	88347	24	3.49	206115	28	4.53
125	1752	51783	19	2.49	170373	24	3.47	398763	28	4.53
216	3000	88347	19	2.53	291927	24	3.47	684723	28	4.55
343	4716	139023	20	2.57	460785	24	3.47	1082427	28	4.57
512	6972	206115	20	2.59	684723	24	3.47			
729	9840	291927	20	2.61	971517	24	3.45			
1000	13392	398763	20	2.63						
1331	17700	528927	20	2.64						
1728	22836	684723	20	2.65						
2197	28872	868455	20	2.66						

Table 3.19: *$P^{-T} = \nabla \boldsymbol{\psi}_7$ with edge average constraints with boundary edges and additional vertex constraints.*

		$\frac{H}{h}=2$ 567 d.o.f./dom.			$\frac{H}{h}=3$ 1677 d.o.f./dom.			$\frac{H}{h}=4$ 3723 d.o.f./dom.		
N	c.p.s.	d.o.f.	It.	$\lambda_{\max}$	d.o.f.	It.	$\lambda_{\max}$	d.o.f.	It.	$\lambda_{\max}$
8	78	3723	22	4.23	11775	25	5.39	27027	28	6.37
27	288	11775	25	4.26	38073	28	5.50	88347	31	6.54
64	684	27027	25	4.09	88347	29	5.30	206115	32	6.33
125	1320	51783	25	3.96	170373	29	5.17	398763	32	6.19
216	2250	88347	24	3.90	291927	29	5.11	684723	32	6.12
343	3528	139023	24	3.87	460785	29	5.09	1082427	32	6.09
512	5208	206115	24	3.86	684723	29	5.08			
729	7344	291927	24	3.84	971517	28	5.06			
1000	9990	398763	24	3.85						
1331	13200	528927	24	3.83						
1728	17028	684723	24	3.85						
2197	21528	868455	24	3.82						

Table 3.20: *$P^{-T} = \nabla \boldsymbol{\psi}_8$ with edge average constraints including boundary edges.*

		$\frac{H}{h}=2$ 567 d.o.f./dom.			$\frac{H}{h}=3$ 1677 d.o.f./dom.			$\frac{H}{h}=4$ 3723 d.o.f./dom.		
N	c.p.s.	d.o.f.	It.	$\lambda_{\max}$	d.o.f.	It.	$\lambda_{\max}$	d.o.f.	It.	$\lambda_{\max}$
8	36	3723	30	9.49	11775	34	12.77	27027	37	16.02
27	192	11775	33	9.18	38073	38	12.60	88347	41	15.56
64	540	27027	33	8.90	88347	38	12.09	206115	42	14.82
125	1152	51783	33	8.66	170373	38	11.67	398763	42	14.23
216	2100	88347	33	8.40	291927	37	11.25	684723	41	13.67
343	3456	139023	33	8.17	460785	37	10.87	1082427	41	13.16
512	5292	206115	32	7.95	684723	37	10.53			
729	7680	291927	32	7.75	971517	37	10.23			
1000	10692	398763	32	7.58						
1331	14400	528927	32	7.43						
1728	18876	684723	31	7.30						
2197	24192	868455	31	7.18						

Table 3.21: $P^{-T} = \nabla\psi_8$ *with edge average constraints exclusive of boundary edges and additional vertex constraints.*

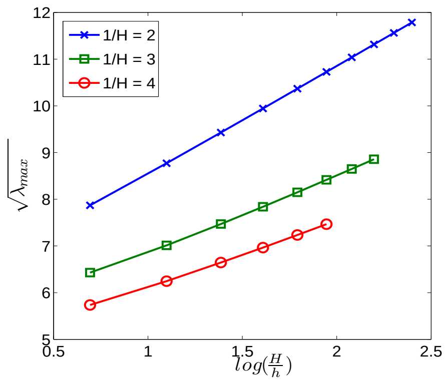

Figure 3.21: $P^{-T} = \nabla\psi_6$ *with edge average constraints without boundary edges.*

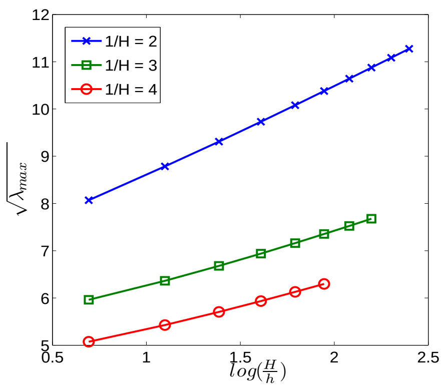

Figure 3.22: $P^{-T} = \nabla\psi_7$ *with edge average constraints without boundary edges.*

The results obtained for $\psi_{9.1}$ and $\psi_{9.2}$, for $\frac{H}{h}$ kept fixed, also match the theoretical expectations; cf. Tables 3.22, 3.23, 3.24, 3.25, 3.26 and 3.27.

In the case when $\frac{H}{h}$ is increased and the number of subdomains is kept fixed, the bound for the condition number still seems to hold; cf. Figures 3.29 and 3.30 for $\psi_{9.1}$ and Figures 3.31 and 3.32 for $\psi_{9.2}$. The slope for the case $\frac{1}{H} = 2$ in Figures 3.31 and 3.32 differs clearly from the cases $\frac{1}{H} = 3$ and $\frac{1}{H} = 4$. This suggests that the case $\frac{1}{H} = 2$ is still away from the asymptotic range with respect to the number of subdomains. The results for $\frac{1}{H} = 3$ and $\frac{1}{H} = 4$, i.e., $N = 27$ and $N = 64$ subdomains are then very similar. Again for only vertex constraints

		$\frac{H}{h}=2$ 567 d.o.f./dom.			$\frac{H}{h}=3$ 1677 d.o.f./dom.			$\frac{H}{h}=4$ 3723 d.o.f./dom.		
N	c.p.s.	d.o.f.	It.	$\lambda_{\max}$	d.o.f.	It.	$\lambda_{\max}$	d.o.f.	It.	$\lambda_{\max}$
8	18	3723	62	96.32	11775	79	234.54	27027	89	410.33
27	108	11775	86	114.24	38073	98	145.58	88347	110	182.68
64	324	27027	89	93.69	88347	102	111.02	206115	115	132.50
125	720	51783	87	75.26	170373	98	86.11	398763	111	99.89
216	1350	88347	84	63.79	291927	93	68.75	684723	105	78.85
343	2268	139023	83	60.37	460785	91	64.45	1082427	100	67.87
512	3528	206115	81	57.16	684723	88	61.21			
729	5184	291927	78	54.20	971517	84	58.30			
1000	7290	398763	75	51.46						
1331	9900	528927	74	48.92						
1728	13068	684723	71	46.57						
2197	16848	868455	69	44.38						

Table 3.22: *$P^{-T} = \nabla \boldsymbol{\psi}_{9.1}$ with edge average constraints without boundary edges.*

		$\frac{H}{h}=2$ 567 d.o.f./dom.			$\frac{H}{h}=3$ 1677 d.o.f./dom.			$\frac{H}{h}=4$ 3723 d.o.f./dom.		
N	c.p.s.	d.o.f.	It.	$\lambda_{\max}$	d.o.f.	It.	$\lambda_{\max}$	d.o.f.	It.	$\lambda_{\max}$
8	36	3723	38	13.34	11775	46	19.58	27027	53	25.31
27	192	11775	42	16.18	38073	50	16.28	88347	57	19.38
64	540	27027	43	14.54	88347	49	15.34	206115	55	18.23
125	1152	51783	44	13.59	170373	48	14.84	398763	53	17.49
216	2100	88347	44	12.89	291927	47	14.44	684723	52	16.87
343	3456	139023	43	12.24	460785	47	13.94	1082427	51	16.59
512	5292	206115	42	11.64	684723	47	13.46			
729	7680	291927	42	11.03	971517	46	12.96			
1000	10692	398763	42	10.48						
1331	14400	528927	41	9.95						
1728	18876	684723	40	9.51						
2197	24192	868455	39	9.32						

Table 3.23: *$P^{-T} = \nabla \boldsymbol{\psi}_{9.1}$ with edge average constraints without boundary edges and with additional vertex constraints.*

		$\frac{H}{h}=2$ 567 d.o.f./dom.			$\frac{H}{h}=3$ 1677 d.o.f./dom.			$\frac{H}{h}=4$ 3723 d.o.f./dom.		
N	c.p.s.	d.o.f.	It.	$\lambda_{\max}$	d.o.f.	It.	$\lambda_{\max}$	d.o.f.	It.	$\lambda_{\max}$
8	18	3723	73	239.95	11775	120	715.31	27027	156	1627.29
27	84	11775	104	217.96	38073	181	533.01	88347	244	982.77
64	216	27027	113	200.25	88347	197	485.51	206115	270	850.75
125	432	51783	117	188.09	170373	198	442.55	398763	273	748.23
216	750	88347	118	175.76	291927	194	404.37	684723	268	669.91
343	1188	139023	120	162.95	460785	189	366.07	1082427	258	596.44
512	1764	206115	120	150.32	684723	183	329.90			
729	2496	291927	120	138.38	971517	177	297.28			
1000	3402	398763	120	127.32						
1331	4500	528927	119	117.25						
1728	5808	684723	118	108.15						
2197	7344	868455	116	99.98						

Table 3.24: $P^{-T} = \nabla\boldsymbol{\psi}_{9.2}$ *with vertex constraints.*

		$\frac{H}{h}=2$ 567 d.o.f./dom.			$\frac{H}{h}=3$ 1677 d.o.f./dom.			$\frac{H}{h}=4$ 3723 d.o.f./dom.		
N	c.p.s.	d.o.f.	It.	$\lambda_{\max}$	d.o.f.	It.	$\lambda_{\max}$	d.o.f.	It.	$\lambda_{\max}$
8	18	3723	63	130.10	11775	80	334.83	27027	96	628.16
27	108	11775	86	108.46	38073	100	168.72	88347	117	215.07
64	324	27027	90	101.35	88347	105	137.65	206115	121	164.42
125	720	51783	92	95.61	170373	105	122.60	398763	121	142.83
216	1350	88347	92	88.63	291927	104	109.52	684723	120	125.47
343	2268	139023	90	81.38	460785	104	98.00	1082427	119	111.14
512	3528	206115	89	74.60	684723	102	88.28			
729	5184	291927	89	68.55	971517	100	80.15			
1000	7290	398763	86	63.25						
1331	9900	528927	85	58.63						
1728	13068	684723	85	54.63						
2197	16848	868455	84	51.27						

Table 3.25: $P^{-T} = \nabla\boldsymbol{\psi}_{9.2}$ *with edge average constraints without boundary edges.*

		$\frac{H}{h}=2$ 567 d.o.f./dom.			$\frac{H}{h}=3$ 1677 d.o.f./dom.			$\frac{H}{h}=4$ 3723 d.o.f./dom.		
N	c.p.s.	d.o.f.	It.	$\lambda_{\max}$	d.o.f.	It.	$\lambda_{\max}$	d.o.f.	It.	$\lambda_{\max}$
8	36	3723	39	13.31	11775	49	24.53	27027	60	36.24
27	192	11775	42	12.31	38073	53	15.87	88347	65	27.54
64	540	27027	42	11.41	88347	51	13.92	206115	66	27.28
125	1152	51783	42	10.59	170373	50	13.16	398763	64	24.27
216	2100	88347	42	9.91	291927	48	12.35	684723	61	21.07
343	3456	139023	41	9.40	460785	47	11.95	1082427	58	18.36
512	5292	206115	40	9.04	684723	47	11.56			
729	7680	291927	40	8.74	971517	46	11.56			
1000	10692	398763	39	8.56						
1331	14400	528927	39	8.39						
1728	18876	684723	39	8.35						
2197	24192	868455	38	8.37						

Table 3.26: $P^{-T} = \nabla \boldsymbol{\psi}_{9.2}$ *with edge average constraints without boundary edges and with additional vertex constraints.*

		$\frac{H}{h}=2$ 567 d.o.f./dom.			$\frac{H}{h}=3$ 1677 d.o.f./dom.			$\frac{H}{h}=4$ 3723 d.o.f./dom.		
N	c.p.s.	d.o.f.	It.	$\lambda_{\max}$	d.o.f.	It.	$\lambda_{\max}$	d.o.f.	It.	$\lambda_{\max}$
8	96	3723	34	7.62	11775	44	13.70	27027	52	16.53
27	372	11775	38	8.38	38073	51	14.58	88347	61	22.62
64	900	27027	38	8.23	88347	51	13.91	206115	61	21.21
125	1752	51783	38	8.03	170373	50	13.16	398763	58	18.30
216	3000	88347	37	7.67	291927	48	12.23	684723	54	15.39
343	4716	139023	36	7.31	460785	46	11.24	1082427	53	14.57
512	6972	206115	35	6.95	684723	44	10.39			
729	9840	291927	34	6.56	971517	43	9.85			
1000	13392	398763	33	6.20						
1331	17700	528927	32	5.86						
1728	22836	684723	31	5.55						
2197	28872	868455	30	5.25						

Table 3.27: $P^{-T} = \nabla \boldsymbol{\psi}_{9.2}$ *with edge average constraints with boundary edges and additional vertex constraints.*

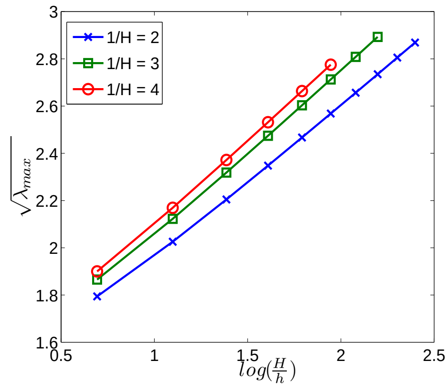

Figure 3.23: $P^{-T} = \nabla\psi_5$ *with edge average constraints with boundary edges.*

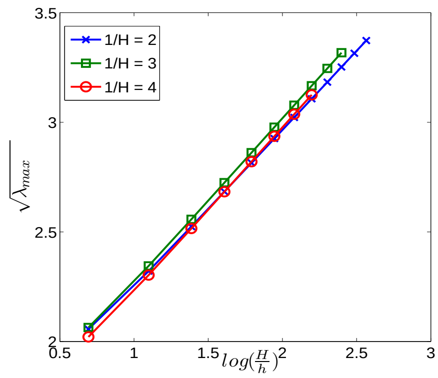

Figure 3.24: $P^{-T} = \nabla\psi_8$ *with edge average constraints with boundary edges.*

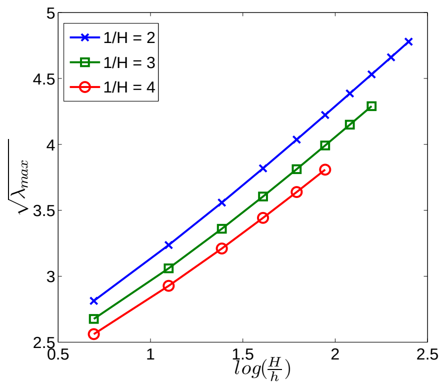

Figure 3.25: $P^{-T} = \nabla\psi_5$ *with edge average constraints without boundary edges and with additional vertex constraints.*

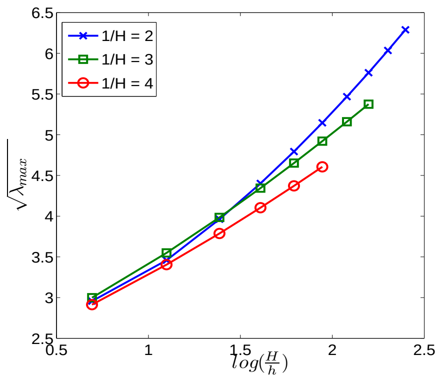

Figure 3.26: $P^{-T} = \nabla\psi_7$ *with edge average constraints without boundary edges and with additional vertex constraints.*

we obtain the linear relation between $\frac{H}{h}$ and $\lambda_{\max}$; see Figures 3.35 and 3.36.

Summarizing the results in this section we can state that the numerical results differ only slightly from the results obtained in Section 3.6.1 although the theory does not apply.

3.6.3 More general cases

Here, we will discuss results obtained for the case that P itself is a gradient, i.e., $P = \nabla\tilde{\psi}$. This has the advantage that the solution of the minimizing problem in φ is then given by $\varphi = \tilde{\psi}$; see Section 3.6.1 page 101. However, the examples in this section do not match the assumptions for our analysis, i.e., P^{-T} is not a gradient.

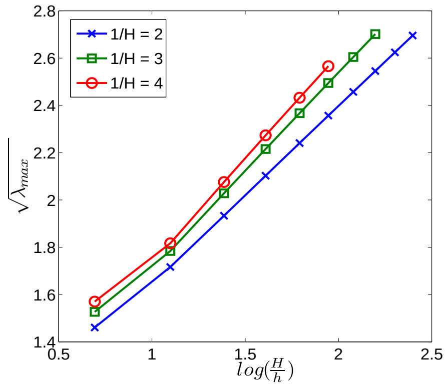

Figure 3.27: $P^{-T} = \nabla\boldsymbol{\psi}_5$ *with edge average constraints with boundary edges and with additional vertex constraints.*

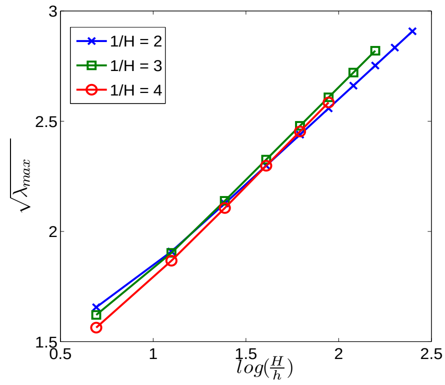

Figure 3.28: $P^{-T} = \nabla\boldsymbol{\psi}_6$ *with edge average constraints with boundary edges and with additional vertex constraints.*

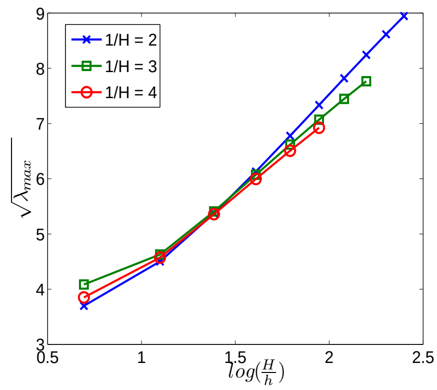

Figure 3.29: $P^{-T} = \nabla\boldsymbol{\psi}_{9.1}$ *with edge average constraints with boundary edges.*

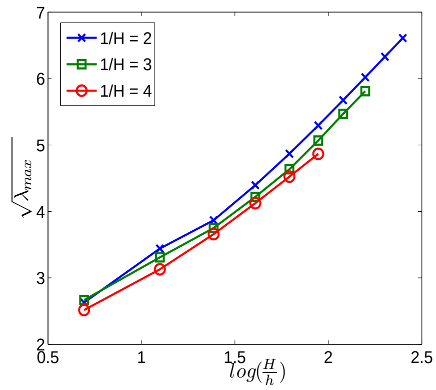

Figure 3.30: $P^{-T} = \nabla\boldsymbol{\psi}_{9.1}$ *with edge average constraints with boundary edges and with additional vertex constraints.*

The first example is constructed by the functions $\boldsymbol{\psi}_{9.1}$ and $\boldsymbol{\psi}_{9.2}$ introduced in Section 3.6.2, i.e., $\tilde{\boldsymbol{\psi}}_1 := \boldsymbol{\psi}_{9.1}$ and $\tilde{\boldsymbol{\psi}}_2 := \boldsymbol{\psi}_{9.2}$. These function transform the cube into a spherical dome with different thickness and angles if $P = \nabla\boldsymbol{\psi}_{9.1}$ or $P = \nabla\boldsymbol{\psi}_{9.2}$; see Figure 3.37. Here, in addition to the aforementioned Dirichlet boundary conditions we introduce further Dirichlet boundary conditions for the y-direction on $\{\mathbf{x} \in \mathbb{R}^3 : y \in \{0,1\}\}$ to prevent small gaps or element overlaps originating from inaccuracies in the numerical solutions.

Another example for $P = \nabla\tilde{\boldsymbol{\psi}}$ is given by $\tilde{\boldsymbol{\psi}}_3$

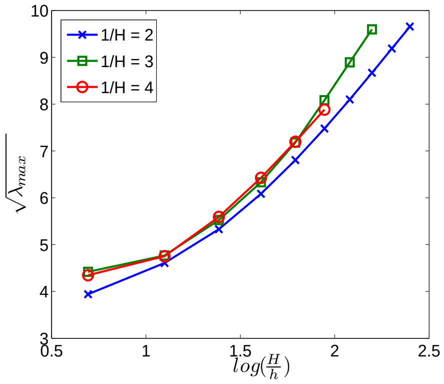

Figure 3.31: $P^{-T} = \nabla\boldsymbol{\psi}_{9.2}$ *with edge average constraints with boundary edges.*

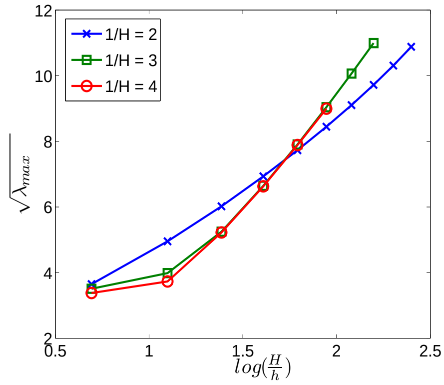

Figure 3.32: $P^{-T} = \nabla\boldsymbol{\psi}_{9.2}$ *with edge average constraints without edges and with additional vertex constraints.*

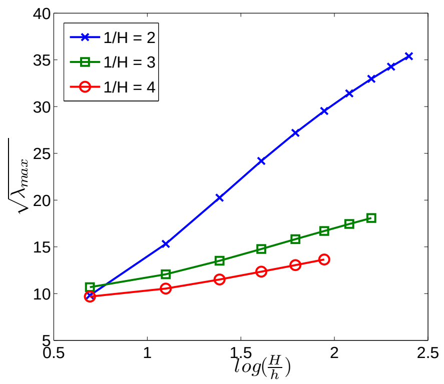

Figure 3.33: $P^{-T} = \nabla\boldsymbol{\psi}_{9.1}$ *with edge average constraints without boundary edges.*

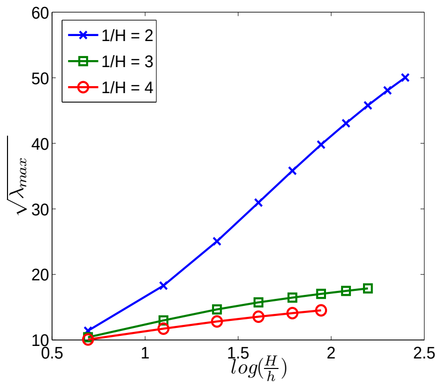

Figure 3.34: $P^{-T} = \nabla\boldsymbol{\psi}_{9.2}$ *with edge average constraints without boundary edges.*

$$
\begin{aligned}
\tilde{\boldsymbol{\psi}}_3(\mathbf{x}) &= \begin{pmatrix} x\cos(\frac{\pi}{2}z) - y\sin(\frac{\pi}{2}z) \\ x\sin(\frac{\pi}{2}z) + y\cos(\frac{\pi}{2}z) \\ z \end{pmatrix} \\
\Rightarrow \qquad P_3 &= \begin{pmatrix} \cos(\frac{\pi}{2}z) & -\sin(\frac{\pi}{2}z) & -\frac{\pi}{2}(x\sin(\frac{\pi}{2}z) + y\cos(\frac{\pi}{2}z)) \\ \sin(\frac{\pi}{2}z) & \cos(\frac{\pi}{2}z) & \frac{\pi}{2}(x\cos(\frac{\pi}{2}z) - y\sin(\frac{\pi}{2}z)) \\ 0 & 0 & 1 \end{pmatrix},
\end{aligned} \tag{3.75}
$$

which describes a linear increasing twist of the unit cube around the z-axis; see Figure 3.38.

The results for $P = \nabla\tilde{\boldsymbol{\psi}}_3$ in the case of a constant subdomain size match

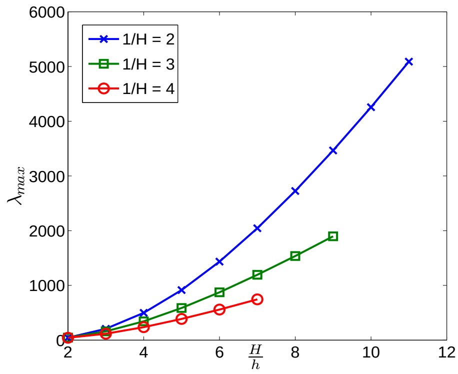

Figure 3.35: *$P^{-T} = \nabla \boldsymbol{\psi}_{9.1}$ with only vertex constraints.*

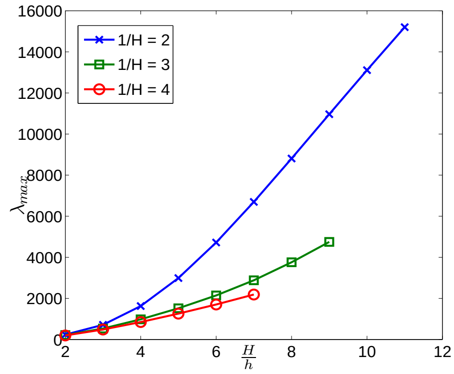

Figure 3.36: *$P^{-T} = \nabla \boldsymbol{\psi}_{9.2}$ with only vertex constraints.*

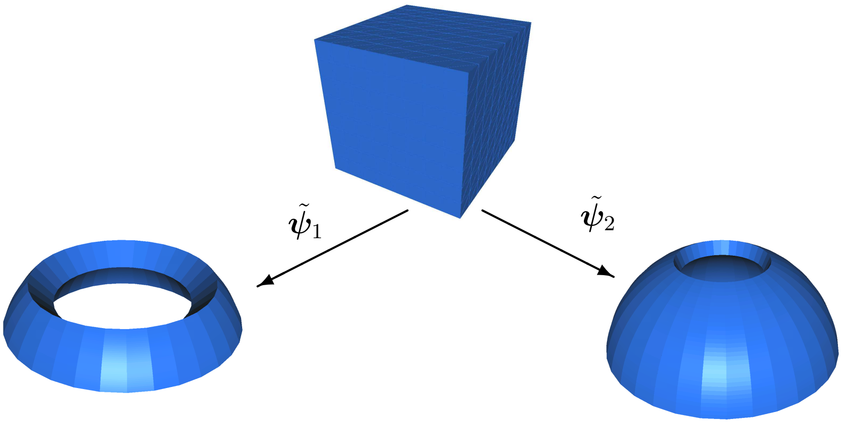

Figure 3.37: *Transformations induced by $\tilde{\boldsymbol{\psi}}_1$ and $\tilde{\boldsymbol{\psi}}_2$.*

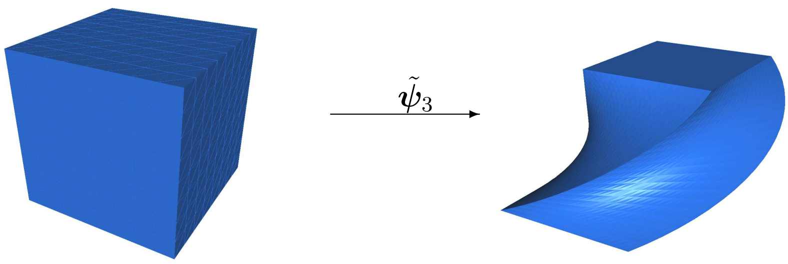

Figure 3.38: *Transformations induced by $\tilde{\boldsymbol{\psi}}_3$.*

the expectations from the theory in Section 3.4 even though the assumptions do not match. For growing $\frac{1}{H}$ and fixed $\frac{H}{h}$ the condition and iteration numbers are clearly bounded by a constant; cf. Tables 3.28, 3.29, and 3.30.

		$\frac{H}{h} = 2$ 567 d.o.f./dom.			$\frac{H}{h} = 3$ 1677 d.o.f./dom.			$\frac{H}{h} = 4$ 3723 d.o.f./dom.		
N	c.p.s.	d.o.f.	It.	$\lambda_{\max}$	d.o.f.	It.	$\lambda_{\max}$	d.o.f.	It.	$\lambda_{\max}$
8	18	3723	35	14.15	11775	36	17.51	27027	40	19.47
27	108	11775	41	13.01	38073	43	14.49	88347	45	15.82
64	324	27027	41	11.81	88347	44	13.17	206115	46	14.43
125	720	51783	40	11.26	170373	43	12.57	398763	46	13.80
216	1350	88347	41	10.90	291927	44	12.19	684723	46	13.41
343	2268	139023	41	10.65	460785	43	11.94	1082427	46	13.15
512	3528	206115	40	10.48	684723	43	11.75			
729	5184	291927	40	10.35	971517	43	11.61			
1000	7290	398763	40	10.24						
1331	9900	528927	40	10.16						
1728	13068	684723	40	10.10						
2197	16848	868455	40	10.04						

Table 3.28: $P = \nabla\tilde{\boldsymbol{\psi}}_3$ *with edge average constraints without boundary edges.*

		$\frac{H}{h} = 2$ 567 d.o.f./dom.			$\frac{H}{h} = 3$ 1677 d.o.f./dom.			$\frac{H}{h} = 4$ 3723 d.o.f./dom.		
N	c.p.s.	d.o.f.	It.	$\lambda_{\max}$	d.o.f.	It.	$\lambda_{\max}$	d.o.f.	It.	$\lambda_{\max}$
8	36	3723	27	7.48	11775	31	10.18	27027	34	12.37
27	192	11775	30	7.80	38073	34	9.81	88347	37	11.37
64	540	27027	31	6.82	88347	34	8.54	206115	37	9.92
125	1152	51783	31	6.53	170373	34	8.17	398763	37	9.50
216	2100	88347	31	6.22	291927	34	7.91	684723	37	9.21
343	3456	139023	31	6.20	460785	35	7.75	1082427	37	9.03
512	5292	206115	31	6.10	684723	34	7.62			
729	7680	291927	31	6.03	971517	34	7.53			
1000	10692	398763	31	5.97						
1331	14400	528927	31	5.93						
1728	18876	684723	31	5.91						
2197	24192	868455	31	5.90						

Table 3.29: $P = \nabla\tilde{\boldsymbol{\psi}}_3$ *with edge average constraints without boundary edges and with additional vertex constraints.*

For $\tilde{\boldsymbol{\psi}}_1$ and $\tilde{\boldsymbol{\psi}}_2$ we obtain similar results for fixed $\frac{H}{h}$; see Tables 3.31, 3.32, 3.33, 3.34, and 3.35, where the results are given for sets of primal variables which use edge averages or edge averages with combined vertex constraints.

In Figure 3.40 the behavior for an increasing $\frac{H}{h}$ is shown for $\tilde{\boldsymbol{\psi}}_1$ for the set of primal variables consisting of edge averages with boundary edges and combined with vertex constraints. In Figure 3.41 results are shown for $\tilde{\boldsymbol{\psi}}_2$. Further results

		$\frac{H}{h}=2$ 567 d.o.f./dom.			$\frac{H}{h}=3$ 1677 d.o.f./dom.			$\frac{H}{h}=4$ 3723 d.o.f./dom.		
N	c.p.s.	d.o.f.	It.	$\lambda_{\max}$	d.o.f.	It.	$\lambda_{\max}$	d.o.f.	It.	$\lambda_{\max}$
8	96	3723	16	2.09	11775	20	2.93	27027	22	3.72
27	372	11775	17	2.34	38073	21	3.18	88347	24	4.13
64	900	27027	18	2.49	88347	22	3.29	206115	25	4.32
125	1752	51783	18	2.56	170373	22	3.34	398763	26	4.42
216	3000	88347	19	2.60	291927	22	3.37	684723	26	4.43
343	4716	139023	19	2.63	460785	22	3.39	1082427	26	4.48
512	6972	206115	19	2.65	684723	22	3.41			
729	9840	291927	19	2.66	971517	22	3.39			
1000	13392	398763	19	2.67						
1331	17700	528927	19	2.68						
1728	22836	684723	19	2.69						
2197	28872	868455	19	2.69						

Table 3.30: *$P = \nabla\tilde{\psi}_3$ with edge average constraints with boundary edges and additional vertex constraints.*

		$\frac{H}{h}=2$ 567 d.o.f./dom.			$\frac{H}{h}=3$ 1677 d.o.f./dom.			$\frac{H}{h}=4$ 3723 d.o.f./dom.		
N	c.p.s.	d.o.f.	It.	$\lambda_{\max}$	d.o.f.	It.	$\lambda_{\max}$	d.o.f.	It.	$\lambda_{\max}$
8	34	3723	30	5.72	11775	37	10.29	27027	40	15.13
27	184	11775	34	8.79	38073	44	15.94	88347	52	24.71
64	522	27027	36	9.20	88347	48	16.73	206115	59	26.13
125	1120	51783	36	9.00	170373	49	15.34	398763	61	23.72
216	2050	88347	35	8.64	291927	48	14.12	684723	59	20.93
343	3384	139023	35	8.20	460785	47	12.61	1082427	57	18.24
512	5194	206115	34	7.79	684723	45	11.63			
729	7552	291927	34	7.43	971517	43	10.73			
1000	10530	398763	33	7.12						
1331	14200	528927	32	6.87						
1728	18634	684723	32	6.66						
2197	23904	868455	31	6.49						

Table 3.31: *$P = \nabla\tilde{\psi}_1$ with edge average constraints without boundary edges and with additional vertex constraints.*

		$\frac{H}{h}=2$ 567 d.o.f./dom.			$\frac{H}{h}=3$ 1677 d.o.f./dom.			$\frac{H}{h}=4$ 3723 d.o.f./dom.		
N	c.p.s.	d.o.f.	It.	$\lambda_{\max}$	d.o.f.	It.	$\lambda_{\max}$	d.o.f.	It.	$\lambda_{\max}$
8	70	3723	28	5.09	11775	33	7.53	27027	37	11.23
27	292	11775	30	5.67	38073	40	11.87	88347	47	19.00
64	738	27027	30	6.10	88347	43	12.74	206115	54	20.20
125	1480	51783	31	5.97	170373	44	12.19	398763	55	19.01
216	2590	88347	31	5.69	291927	44	11.57	684723	55	17.89
343	4140	139023	31	5.54	460785	44	10.96	1082427	54	16.82
512	6202	206115	30	5.36	684723	43	10.48			
729	8848	291927	30	5.21	971517	42	10.02			
1000	12150	398763	29	5.07						
1331	16180	528927	29	4.93						
1728	21010	684723	28	4.80						
2197	26712	868455	28	4.67						

Table 3.32: $P = \nabla\tilde{\psi}_1$ *with edge average constraints with boundary edges and additional vertex constraints.*

		$\frac{H}{h}=2$ 567 d.o.f./dom.			$\frac{H}{h}=3$ 1677 d.o.f./dom.			$\frac{H}{h}=4$ 3723 d.o.f./dom.		
N	c.p.s.	d.o.f.	It.	$\lambda_{\max}$	d.o.f.	It.	$\lambda_{\max}$	d.o.f.	It.	$\lambda_{\max}$
8	18	3723	41	17.01	11775	50	33.88	27027	54	49.96
27	108	11775	53	22.79	38073	69	51.27	88347	85	85.68
64	324	27027	57	20.57	88347	79	49.35	206115	99	87.07
125	720	51783	57	19.62	170373	82	46.29	398763	104	80.16
216	1350	88347	56	18.73	291927	85	43.73	684723	107	75.13
343	2268	139023	55	18.11	460785	83	41.43	1082427	108	70.72
512	3528	206115	55	17.39	684723	82	39.61			
729	5184	291927	54	16.80	971517	81	37.78			
1000	7290	398763	53	16.21						
1331	9900	528927	52	15.69						
1728	13068	684723	51	15.18						
2197	16848	868455	51	14.71						

Table 3.33: $P = \nabla\tilde{\psi}_2$ *with edge average constraints without boundary edges.*

		$\frac{H}{h}=2$ 567 d.o.f./dom.			$\frac{H}{h}=3$ 1677 d.o.f./dom.			$\frac{H}{h}=4$ 3723 d.o.f./dom.		
N	c.p.s.	d.o.f.	It.	$\lambda_{\max}$	d.o.f.	It.	$\lambda_{\max}$	d.o.f.	It.	$\lambda_{\max}$
8	54	3723	38	11.34	11775	44	20.67	27027	48	30.28
27	216	11775	48	17.01	38073	62	40.88	88347	73	67.66
64	540	27027	52	18.74	88347	72	44.85	206115	91	76.17
125	1080	51783	55	18.70	170373	76	44.31	398763	99	75.83
216	1890	88347	54	18.37	291927	82	42.78	684723	101	73.01
343	3024	139023	54	17.81	460785	81	40.97	1082427	105	69.90
512	4536	206115	54	17.25	684723	80	39.27			
729	6480	291927	53	16.68	971517	80	37.64			
1000	8910	398763	52	16.14						
1331	11880	528927	52	15.62						
1728	15444	684723	51	15.13						
2197	19656	868455	50	14.66						

Table 3.34: $P = \nabla\tilde{\boldsymbol{\psi}}_2$ *with edge average constraints with boundary edges.*

		$\frac{H}{h}=2$ 567 d.o.f./dom.			$\frac{H}{h}=3$ 1677 d.o.f./dom.			$\frac{H}{h}=4$ 3723 d.o.f./dom.		
N	c.p.s.	d.o.f.	It.	$\lambda_{\max}$	d.o.f.	It.	$\lambda_{\max}$	d.o.f.	It.	$\lambda_{\max}$
8	70	3723	29	5.26	11775	36	8.70	27027	41	13.19
27	292	11775	31	5.99	38073	42	12.41	88347	51	20.04
64	738	27027	32	6.28	88347	44	12.92	206115	57	20.73
125	1480	51783	32	6.13	170373	45	12.70	398763	58	20.80
216	2590	88347	32	6.04	291927	46	12.78	684723	58	20.59
343	4140	139023	31	6.06	460785	46	12.56	1082427	58	20.15
512	6202	206115	32	6.00	684723	46	12.42			
729	8848	291927	31	5.92	971517	46	12.29			
1000	12150	398763	31	5.91						
1331	16180	528927	31	5.85						
1728	21010	684723	31	5.78						
2197	26712	868455	31	5.73						

Table 3.35: $P = \nabla\tilde{\boldsymbol{\psi}}_2$ *with edge average constraints with boundary edges and additional vertex constraints.*

are presented in Figure 3.39 for only vertex constraints for $\tilde{\psi}_1$ and for a combined set of edge average constraints without boundary edges and additional vertex constraints for $\tilde{\psi}_2$ in Figure 3.41. The results are very similar to the ones obtained in the previous section.

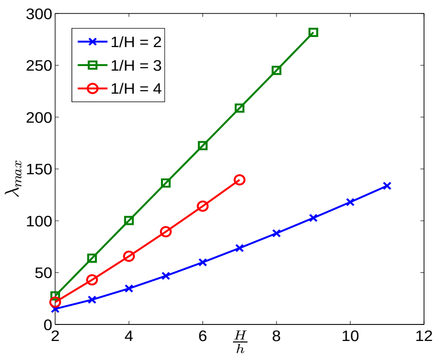

Figure 3.39: *$P = \nabla\tilde{\psi}_1$ with vertex constraints.*

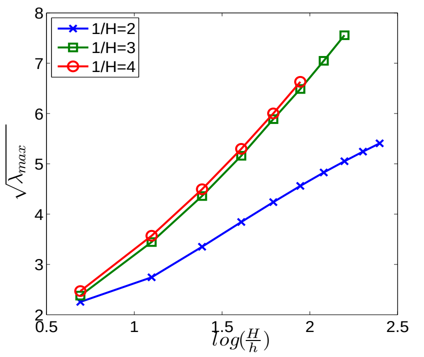

Figure 3.40: *$P = \nabla\tilde{\psi}_1$ with edge average constraints with boundary edges and with additional vertex constraints.*

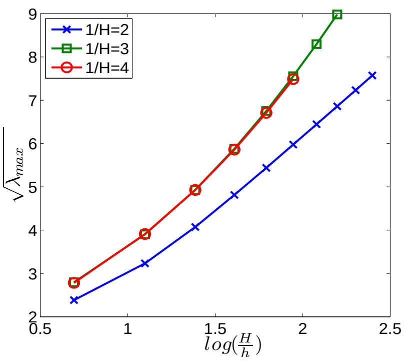

Figure 3.41: *$P = \nabla\tilde{\psi}_2$ edge average constraints without boundary edges and with additional vertex constraints.*

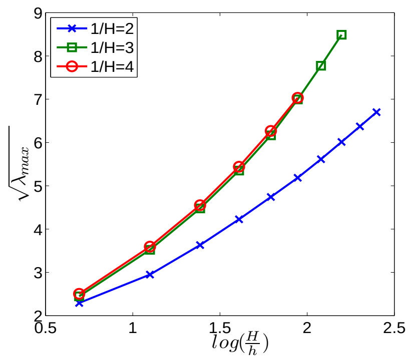

Figure 3.42: *$P = \nabla\tilde{\psi}_2$ with edge average constraints with boundary edges and with additional vertex constraints.*

See Figures 3.44, 3.45, 3.46, 3.47, and 3.48 for results for $\tilde{\psi}_3$ which are numerically in accordance with the theoretical findings although the theory does not apply.

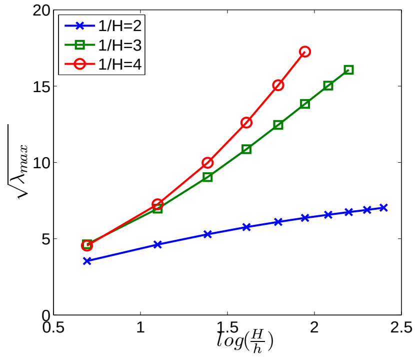

Figure 3.43: $P^{-T} = \nabla\tilde{\boldsymbol{\psi}}_1$ *with average constraints without boundary edges.*

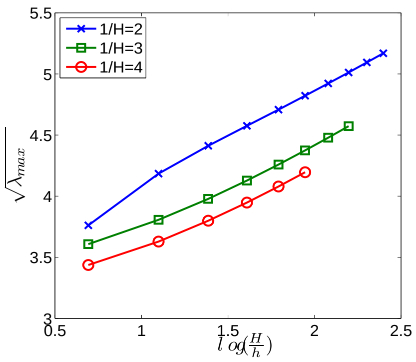

Figure 3.44: $P = \nabla\tilde{\boldsymbol{\psi}}_3$ *with edge average constraints without boundary edges.*

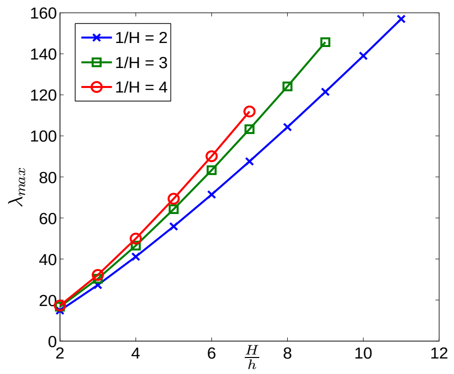

Figure 3.45: $P = \nabla\tilde{\psi}_3$ *with vertex constraints.*

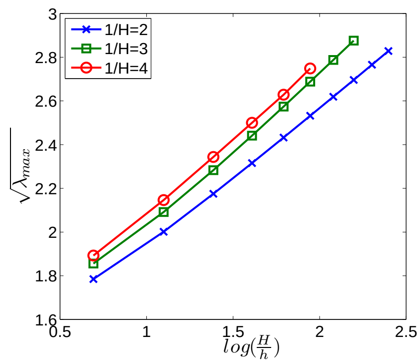

Figure 3.46: $P = \nabla\tilde{\psi}_3$ *with edge average constraints with boundary edges.*

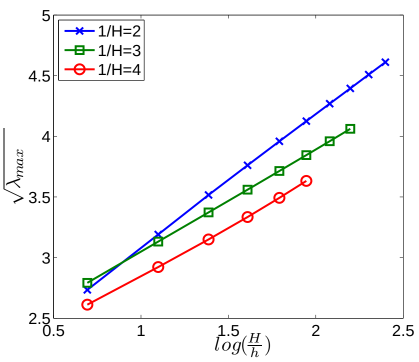

Figure 3.47: $P = \nabla\tilde{\psi}_3$ *with edge average constraints without boundary edges and with additional vertex constraints.*

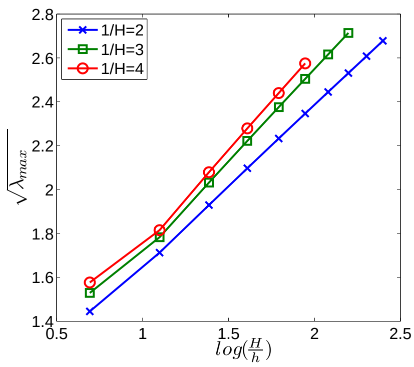

Figure 3.48: $P^{-T} = \nabla\tilde{\psi}_3$ *with edge average constraints with boundary edges and with additional vertex constraints.*

Bibliography

[1] Francisco Armero. Formulation and finite element implementation of a mutiplicative model of coupled poro-plasticity at finite strains under fully saturated conditions. *Comput. Methods Appl. Mech. Engrg.*, 171:205–241, 1999.

[2] Harm Askes, Irene Morata, and Elias C. Aifantis. Finite element analysis with staggered gradient elasticity. *Computers and Structures*, 86:1266–1279, 2008.

[3] Hédy Attouch, Jérôme Bolte, Patrick Redont, and Antoine Soubeyran. Alternating proximal algorithms for weakly coupled convex minimization problems. Applications to dynamical games and PDE's. *J. Convex Anal.*, 15(3):485–506, 2008.

[4] Hédy Attouch, Patrick Redont, and Antoine Soubeyran. A new class of alternating proximal minimization algorithms with costs-to-move. *SIAM J. Optim.*, 18(3):1061–1081, 2007.

[5] Satish Balay, Kris Buschelman, William D. Gropp, Dinesh Kaushik, Matt Knepley, Lois Curfman McInnes, Barry F. Smith, and Hong Zhang. PETSc users manual. Technical Report ANL-95/11 - Revision 2.2.3, Argonne National Laboratory, 2007.

[6] Satish Balay, Kris Buschelman, William D. Gropp, Dinesh Kaushik, Matthew G. Knepley, Lois Curfman McInnes, Barry F. Smith, and Hong Zhang. PETSc Web page, 2009. http://www.mcs.anl.gov/petsc.

[7] Satish Balay, William D. Gropp, Lois Curfman McInnes, and Barry F. Smith. Efficient management of parallelism in object oriented numerical software libraries. In E. Arge, A. M. Bruaset, and H. P. Langtangen, editors, *Modern Software Tools in Scientific Computing*, pages 163–202. Birkhäuser Press, 1997.

[8] Scott Bardenhagen and Nicolas Triantfyllidis. Derivation of higher order gradient continuum theories in 2,3-d nonlinear elasticity from periodic lattice models. *J. Mech. Phys. Solids*, 42(1):111–139, 1994.

[9] Petter E. Bjørstad and Olof B. Widlund. Iterative methods for the solution of elliptic problems on regions partitioned into substructures. *SIAM J. Numer. Anal.*, 23(no. 6):1093–1120, 1986.

[10] Dietrich Braess. *Finite Elemente, Theorie, schnelle Löser und Anwendungen in der Elastizitätstheorie.* Springer, 2003.

[11] James H. Bramble, Joseph E. Pasciak, and Alfred H. Schatz. The construction of preconditioners for elliptic problems by substructuring, IV. *Math. Comp.*, 53:1–24, 1989.

[12] James H. Bramble and Jinchao Xu. Some estimates for a weighted L^2 projection. *Math. Comp.*, 56(194):463–476, 1991.

[13] Susanne C. Brenner and L. Ridgway Scott. *The Mathematical Theory of Finite Element Methods.* Springer, Texts in Applied Mathematics 15, New York, second edition, 2002.

[14] Wolfgang Bunse and Angelika Bunse-Gerstner. *Numerische Lineare Algebra.* Teubner, Stuttgart, 1985.

[15] Gianfranco Capriz. *Continua with Microstructures.* Springer, Heidelberg, 1989.

[16] Philippe G. Ciarlet. *Mathematical Elasticity Volume I: Three–Dimensional Elasticity.* North-Holland, 1988.

[17] Michele Ciarletta and Dorin Ieşan. Some results in the dynamical theory of porous elastic bodies. *J. Elast.*, 50:3–14, 1998.

[18] Jean-Michel Cros. A preconditioner for the Schur complement domain decomposition method. In O. Widlund I. Herrera, D. Keyes and R. Yates, editors, *Domain Decomposition Methods in Science and Engineering*, pages 373–380. National Autonomous University of Mexico (UNAM), Mexico City, Mexico, ISBN 970-32-0859-2, 2003. Proceedings of the 14th International Conference on Domain Decomposition Methods in Science and Engineering; http://www.ddm.org/DD14.

[19] Hogenrich Damanik, Jaroslav Hron, Abderrahim Quazzia, and Stefan Turek. A monolithc FEM-multigrid solver for non-isothermal incompressible flow on general meshes. *J. Comp. Phy.*, 228:3869–3881, 2009.

[20] Timothy A. Davis. A column pre-ordering strategy for the unsymmetric-pattern multifrontal method. *ACM Transactions on Mathematical Software*, 30(2):165–195, June 2004.

[21] Rémy Dendievel, Samuel Forest, and Gilles R. Canova. An estimation of overall properties of heterogeneous Cosserat materials. In A. Bertram and F. Sidoroff, editors, *Mechanics of Materials with Intrinsic Length Scale: Physics, Experiments, Modelling and Applications.*, Journal Physique IV France 8, pages 111–118. EDP Sciences, France, 1998.

[22] Clark R. Dohrmann. A preconditioner for substructuring based on constrained energy minimization. *SIAM J. Sci. Comput.*, 25(1):246–258, 2003.

[23] Maksymilian Dryja. A method of domain decomposotion for three-dimensional finite element elliptic problem. In *First International Symposium on Domain Decomposition Methods for Partial Differential Equations (Paris 1987)*, pages 43–61. SIAM, Philadelphia, 1988.

[24] Maksymilian Dryja, Barry F. Smith, and Olof B. Widlund. Schwarz analysis of iterative substructuring algorithms for elliptic problems in three dimensions. *SIAM J. Numer. Anal.*, 31(6):1662–1694, 1994.

[25] A. Cemal Eringen. *Microcontinuum Field Theories.* Springer, Heidelberg, 1999.

[26] Patrick Amestoy et al. MUMPS 4.9.2. http://graal.ens-lyon.fr/MUMPS/.

[27] Charbel Farhat, Michel Lesoinne, Patrick LeTallec, Kendall H. Pierson, and Daniel J. Rixen. FETI-DP: A Dual-Primal unified FETI method - part I: A faster alternative to the two-level FETI method. *Internat. J. Numer. Methods Engrg.*, 2000.

[28] Charbel Farhat, Michel Lesoinne, and Kendall Pierson. A scalable dual-primal domain decomposition method. *Numer. Lin. Alg. Appl.*, 7:687–714, 2000.

[29] Charbel Farhat and Jan Mandel. The two-level FETI method for static and dynamic plate problems - part i: an optimal iterative solver for biharmonic systems. *Comput. Methods Appl. Mech. Engrg.*, 155:129–152, 1998.

[30] Charbel Farhat, Jan Mandel, and Francois-Xavier Roux. Optimal convergence properties of the FETI domain decomposition method. *Comput. Methods Appl. Mech. Engrg.*, 115:367–388, 1994.

[31] Charbel Farhat, Kendall H. Pierson, and Michel Lesoinne. The second generation of FETI methods and their application to the parallel solution of large-scale linear and geometrically nonlinear structural analysis problems. *Comput. Meth. Appl. Mech. Engrg*, 184:333–374, 2000.

[32] Charbel Farhat and François-Xavier Roux. Implicit parallel processing in structural mechanics. In J. Tinsley Oden, editor, *Computational Mechanics Advances*, volume 2 (1), pages 1–124. North-Holland, 1994.

[33] Charbel Farhat and Francois-Xavier Roux. A method of Finite Element Tearing and Interconnecting and its parallel solution algorithm. *Int. J. Numer. Meth. Engrg.*, 32:1205–1227, 1991.

[34] Samuel Forest. Mechanics of generalized continua: construction by homogenization. *J. Phys. IV France*, 8:Pr4–39–Pr4–48, 1998.

[35] Samuel Forest. Aufbau und Identifikation von Stoffgleichungen für höhere Kontinua mittels Homogenisierungsmethoden. *Technische Mechanik (Magdeburg)*, 19(4):297–306, 1999.

[36] Samuel Forest. An estimation of overall properties of heterogeneous Cosserat materials. In G.A. Maugin, editor, *Geometry, Continua and Microstructure.*, Travaux en Cours No. 60, pages 35–48. Hermann, Paris, France, 1999.

[37] Samuel Forest. Cosserat media. In *Encyclopedia of Materials: Science and Technology.*, pages 1715–1718. Elsevier, 2001.

[38] Samuel Forest, Fabrice Barbe, and Georges Cailletaud. Cosserat modelling of size effects in the mechanical behaviour of polycrystals and multi-phase materials. *Int. J. Solids Struct.*, 37:7105–7126, 2000.

[39] Samuel Forest, Georges Cailletaud, and Rainer Sievert. A Cosserat theory for elastoviscoplastic single crystals at finite deformation. *Arch. Mech.*, 49(4):705–736, 1997.

[40] Samuel Forest, Rémy Dendievel, and Gilles R. Canova. Estimating the overall properties of heterogeneous Cosserat materials. *Modelling Simul. Mater. Sci. Eng.*, 7:829–840, 1999.

[41] Samuel Forest and Karam Sab. Cosserat overall modeling of heterogeneous materials. *Mech. Res. Comm.*, 25(4):449–454, 1998.

[42] Samuel Forest and Rainer Sievert. Nonlinear microstrain theories. *Int. J. Solids Struct.*, 43:7224–7245, 2006.

[43] Elena F. Grekova and Gérard A. Maugin. Modelling of complex elastic crystals by means of multi-spin micromorphic media. *Internat. J. Engrg. Sci.*, 43(5-6):494–519, 2005.

[44] C. Britta Hirschberger, Ellen Kuhl, and Paul Steinmann. On deformational and configurational mechanics of micromorphic hyperelasticity - theory and computation. *Comput. Methods Appl. Mech. Engrg.*, 196(41-44):4027–4044, 2007.

[45] Gerhard A. Holzapfel. *Nonlinear Solid Mechanics. A continuum approach for engineering.* Wiley, Chichester, 2000.

[46] Dorin Ieşan. Some theorems in the theory of elastic materials with voids. *J. Elast.*, 15:215–224, 1985.

[47] Axel Klawonn, Patrizio Neff, Oliver Rheinbach, and Stefanie Vanis. FETI-DP domain decomposition methods for elasticity with structural changes: P-elasticity. Schriftenreihe der Fakultät für Mathematik, sm-e-706.pdf, Universität Duisburg-Essen, 2009.

[48] Axel Klawonn, Patrizio Neff, Oliver Rheinbach, and Stefanie Vanis. Solving geometrically exact micromorphic elasticity with a staggered algorithm. Schriftenreihe der Fakultät für Mathematik, sm-e-707.pdf, Universität Duisburg-Essen, 2009, to appear in GAMM-Mitteilungen 2010.

[49] Axel Klawonn, Luca F. Pavarino, and Oliver Rheinbach. Spectral element FETI-DP and BDDC preconditioners with multi-element subdomains. *Comput. Meth. Appl. Mech. Engrg.*, 198(3-4):511–523, 2008.

[50] Axel Klawonn and Oliver Rheinbach. A parallel implementation of Dual-Primal FETI methods for three dimensional linear elasticity using a transformation of basis. *SIAM J. Sci. Comput.*, 28(5):1886–1906, 2006.

[51] Axel Klawonn and Oliver Rheinbach. Inexact FETI-DP methods. *Internat. J. Numer. Methods Engrg.*, 69(2):284–307, 2007.

[52] Axel Klawonn and Oliver Rheinbach. Robust FETI-DP methods for heterogeneous three dimensional elasticity problems. *Comput. Methods Appl. Mech. Engrg.*, 196(8):1400–1414, 2007.

[53] Axel Klawonn, Oliver Rheinbach, and Olof B. Widlund. Some computational results for dual-primal FETI methods for elliptic problems in 3D. In Ralf Kornhuber, Ronald H. W. Hoppe, Jacques Périaux, Olivier Pironneau, Olof B. Widlund, and Jinchao Xu, editors, *Proceedings of the 15th international domain decomposition conference*, pages 361–368, Berlin, 2005. Springer LNCSE. Lect. Notes Comput. Sci. Eng.

[54] Axel Klawonn and Olof B. Widlund. FETI and Neumann–Neumann iterative substructuring methods: Connections and new results. *Comm. Pure Appl. Math.*, 54:57–90, January 2001.

[55] Axel Klawonn and Olof B. Widlund. Dual-Primal FETI methods for linear elasticity. *Comm. Pure Appl. Math.*, LIX:1523–1572, 2006.

[56] Axel Klawonn, Olof B. Widlund, and Maksymilian Dryja. Dual-Primal FETI methods for three-dimensional elliptic problems with heterogeneous coefficients. *SIAM J. Numer. Anal.*, 40, 159-179 2002.

[57] Axel Klawonn, Olof B. Widlund, and Maksymilian Dryja. Dual-Primal FETI methods with face constraints. In Luca F. Pavarino and Andrea Toselli, editors, *Recent developments in domain decomposition methods*, pages 27–40. Springer-Verlag, Lecture Notes in Computational Science and Engineering, Volume 23, 2002.

[58] Jing Li and Olof B. Widlund. FETI–DP, BDDC, and Block Cholesky Methods. *Internat. J. Numer. Methods Engrg.*, 66(2):250–271, 2006.

[59] Jan Mandel and Clark R. Dohrmann. Convergence of a balancing domain decomposition by constraints and energy minimization. *Numer. Linear Algebra Appl.*, 10:639–659, 2003.

[60] Jan Mandel, Clark R. Dohrmann, and Radek Tezaur. An algebraic theory for primal and dual substructuring methods by constraints. *Appl. Numer. Math.*, 54:167–193, 2005.

[61] Jan Mandel and Radek Tezaur. Convergence of a Substructuring Method with Lagrange Multipliers. *Numer. Math.*, 73:473–487, 1996.

[62] Jan Mandel and Radek Tezaur. On the convergence of a dual-primal substructuring method. *Numer. Math.*, 88:543–558, 2001.

[63] Paolo M. Mariano. Multifield Description of Microcracked Continua: A Local Model. *Math. Mech. Solids*, 3(2):183–200, 1998.

[64] Paolo M. Mariano. Influence of the material substructure on crack propagation: a unified treatment. *Proc. R. Soc. A*, 461:371–395, 2005.

[65] Paolo M. Mariano. Representation of material elements and geometry of substructural interaction. *Quaderni di Matematica*, 20:80–100, 2007.

[66] Paolo M. Mariano and Giuseppe Modica. Ground states in complex bodies. *ESAIM: COCV*, 15:377–402, 2009.

[67] Paolo M. Mariano and Furio L. Stazi. Strain localization in elastic microcracked bodies. *Comp. Meth. Appl. Mech. Engrg.*, 190:5657–5677, 2001.

[68] Paolo M. Mariano and Furio L. Stazi. Computational Aspects of the Mechanics of Complex Materials. *Arch. Comput. Meth. Engng.*, 12:391–478, 2005.

[69] Wolfgang Müller. *Numerische Analyse und parallele Simulation von nichtlinearen Cosserat-Modellen.* Dissertation in der Fakultät für Mathematik, electronic version available at http://digbib.ubka.uni-karlsruhe.de/volltexte/1000014838, Karlsruhe, 2009.

[70] Ingo Münch. *Ein geometrisch und materiell nichtlineares Cosserat-Modell - Theorie, Numerik und Anwendungmöglichkeiten.* PhD thesis, Universität Karlsruhe, Fakultät für Bauingenieur-, Geo- und Umweltwissenschaften, 2007. ISBN 978-3-935322-12-6, electronic version available at http://digbib.ubka.uni-karlsruhe.de/volltexte/1000007371.

[71] Patrizio Neff. On Korn's first inequality with nonconstant coefficients. *Proc. Roy. Soc. Edinb. A*, 132:221–243, 2002.

[72] Patrizio Neff. On material constants for micromorphic continua. In Y. Wang and K. Hutter, editors, *Trends in Applications of Mathematics to Mechanics*, STAMM Proceedings, Seeheim 2004, pages 337–348. Shaker Verlag, Aachen, 2005.

[73] Patrizio Neff. Existence of minimizers for a finite-strain micromorphic elastic solid. *Proc. Roy. Soc. Edinb. A*, 136:997–1012, 2006.

[74] Patrizio Neff. A finite-strain elastic-plastic Cosserat theory for polycrystals with grain rotations. *Int. J. Eng. Sci., DOI 10.1016/j.ijengsci.2006.04.002*, 44:574–594, 2006.

[75] Patrizio Neff, Krzysztof Chełmiński, and Hans-Dieter Alber. Notes on strain gradient plasticity. Finite strain covariant modelling and global existence in the infinitesimal rate-independent case. *Math. Mod. Meth. Appl. Sci. (M3AS)*, 19(2):1–40, 2009.

[76] Patrizio Neff and Samuel Forest. A geometrically exact micromorphic model for elastic metallic foams accounting for affine microstructure. Modelling, existence of minimizers, identification of moduli and computational results. *J. Elasticity*, 87:239–276, 2007.

[77] Patrizio Neff, Jena Jeong, and Hamidréza Ramezani. Subgrid interaction and micro-randomness - novel invariance requirements in infinitesimal gradient elasticity. *Int. J. Solids Struct.*, 46:4261–4276, 2009.

[78] Patrizio Neff, Antje Sydow, and Christian Wieners. Numerical approximation of incremental infinitesimal gradient plasticity. *Int. J. Num. Meth. Engrg.*, 77(3):414–436, 2009.

[79] Joachim A. Nitsche. On Korn's second inequality. *RAIRO Anal. Numér.*, 15:237–248, 1981.

[80] Waldemar Pompe. Korn's first inequality with variable coefficients and its generalizations. *Comment. Math. Univ. Carolinae*, 44,1:57–70, 2003.

[81] Alfio Quarteroni and Alberto Valli. *Numerical Approximation of Partial Differential Equations.* Springer Series in Computational Mathematics, 23. Springer, Berlin, 1991.

[82] Alfio Quarteroni and Alberto Valli. *Domain Decomposition Methods for Partial Differential Equations.* Oxford Science Publications, 1999.

[83] Véronique Rochus, Daniel J. Rixen, and Jean-Claude Golinval. Monolithic modeling of electro-mechanical coupling in micro-structures. *Int. J. Num. Meth. Engrg.*, 65:461–493, 2005.

[84] Michael Růžička. *Nichlineare Funktionalanalysis.* Springer, Heidelberg, 2004.

[85] Walter Rudin. *Real and complex analysis.* Higher Mathematics. McGraw-Hill, second edition, 1974.

[86] Joachim Schöberl. NETGEN 4.0. http://www.hpfem.jku.at/netgen/.

[87] Joachim Schöberl. NETGEN - An advancing front 2D/3D-mesh generator based on abstract rules. *Computing and Visualization in Science*, 1(1):41–52, 1997.

[88] Barry F. Smith, Petter E. Bjørstad, and William Gropp. *Domain Decomposition: Parallel Multilevel Methods for Elliptic Partial Differential Equations.* Cambridge University Press, 1996.

[89] Andrea Toselli and Olof Widlund. *Domain Decomposition Methods - Algorithms and Theory*, volume 34 of *Springer Series in Computational Mathematics.* Springer, 2004.

[90] Franck J. Vernerey, Wing Kam Liu, and Brian Moran. Multi-scale micromorphic theory for hierarchical materials. *J. Mech. Phys. Solids*, 55(12):2603–2651, 2007.

[91] Franck J. Vernerey, Wing Kam Liu, Brian Moran, and Gregory Olson. A micromorphic model for the multiple scale failure of heterogeneous materials. *J. Mech. Phys. Solids*, 56(4):1320–1347, 2008.

[92] Olof B. Widlund. An extension theorem for finite element spaces with three applications. In *Proceedings of the Second GAMM-Seminar, Kiel January 1986. Notes on Numerical Fluid Mechanics*, pages 110–122. 16. Friedr. Vieweg und Sohn, Braunschweig/Wiesbaden, 1987.

[93] Gil Ho Yoon and Ole Sigmund. A monolithic approach for topology optimization of electrostatically actuated devices. *Comput. Methods Appl. Mech. Engrg.*, 197:4062–4075, 2008.